THE ROLE OF LIPID DROPLET PROTEIN PERILIPIN2 IN LIPID METABOLISM AND INFLAMMATION

By

Charles Najt

A DISSERTATION

Submitted to
Michigan State University
in partial fulfillment of the requirements
for the degree of

Biochemistry and Molecular Biology - Doctor of Philosophy

2016

ABSTRACT

THE ROLE OF LIPID DROPLET PROTEIN PERILIPIN2 IN LIPID METABOLISM AND INFLAMMATION

By

Charles Najt

Perturbations in lipid droplet function have been implicated in promoting several diseases including type-2 diabetes, atherosclerosis, and cardiovascular disease, yet few studies have focused on the role of lipid droplets and associated proteins in the regulation of inflammation. The most abundant lipid droplet protein in liver, Perilipin 2 (Plin2), has been shown to promote lipid accumulation, lipid droplet proliferation, and to augment inflammation in macrophages, yet the current approaches used to study Plin2 are generally descriptive and lack details on the mechanism of action. The objective of this study is to establish a mechanistic link between Plin2's action on the lipid droplet and the onset of lipid-based inflammation by examining recombinant Plin2, overexpression-Plin2 cells, and Plin2 liver-specific knockout mice in the context of hepatic steatosis and inflammation.

Using molecular modeling, fluorescence binding, circular dichroic, and FRET techniques, we demonstrated that Plin2 contains a lipid binding site that consists of a 4-helix bundle and unique α/β domain. We found that Plin2 residues 119−251 are critical for highest affinity lipid binding. Both stearic acid and cholesterol interact favorably with the Plin2 cleft formed by conserved residues in helix α6 and adjacent strands within the 4-helix bundle. Findings that Plin2 contains specific domains responsible for Plin2−lipid interactions and binding are significant because it suggests a mechanism by which Plin2 may retain pro-inflammatory lipids on the lipid droplet surface to promote

inflammation. To support this hypothesis we treated cells with LPS to induce inflammation. Using a novel technique that traps eicosanoids at the site of synthesis, we found that Plin2-coated lipid droplets are the site of PGE_2 production. These findings are consistent with our results showing that Plin2 actively recruits COX2 to the lipid droplet surface promoting eicosanoid biosynthesis. Taken together, our findings indicate that Plin2 may exert a significant role in COX-mediated inflammation through direct interactions on the lipid droplet surface.

To establish Plin2's inflammatory effect *in vivo* we challenged Plin2 liver-specific knockout mice and their respective wild type controls with a methionine-choline-deficient (MCD) diet to induce a NASH phenotype of increased hepatic steatosis, inflammation, and fibrosis. Results on liver weights, body weights, fat tissue mass, and histology in wild type and Plin2 null mice fed the MCD diet revealed signs of hepatic steatosis, fibrosis, and inflammation however; these effects were blunted in the Plin2 null mice. Levels of PC and VLDL were unchanged and hepatic steatosis was reduced by hepatic ablation of Plin2 due in part to an increase in remodeling of PE to PC via the enzyme phosphatidylethanolamine methyl transferase (PEMT). We also found that Plin2 ablation influences the hepatic miRNA-biome. Two of the miRNAs affected by Plin2 ablation (miRNAs-1894 and -711) were predicted to target genes associated with eicosanoid biosynthesis and inflammation. Luciferase reporter assays and Western blotting demonstrated that miRNAs-1894 and -711 directly target COX1, COX2, and human PTGIS and inhibit protein expression of the target genes. Overall, results from several studies indicate that Plin2 may play a key role in the development of inflammation and inflammation-related diseases.

“You’re braver than you believe, stronger than you seem, and smarter than you think.”
-A.A. Milne

ACKNOWLEDGMENTS

Achieving a PhD and surviving the graduate school experience would not be possible without the moral and academic support of a multitude of people. I owe many more thanks than are possible here, and I am forever grateful to all those who have helped me through the years. I have grown both scientifically and personally and will look back on this time with fond memories.

To my advisor Dr. Barbara Atshaves, you took a chance bringing me in as a biochemistry research training program (BRTP) student five years ago. Then again by taking me in as a graduate student just a short while after I started out, but we made it! I cannot express how grateful I am for your mentorship, and encouragement. You have had great faith in my ability and pushed hard for me to be at my best even when I doubted I could achieve success. None of what I have accomplished as a graduate student or as a researcher would be possible without your help and guiding hand. Thank you for letting me aim high, take on way more than I should, and for teaching me how to achieve anything I set my mind to; thank you! I will always remember the lessons you have taught me and pass them on to students I have the opportunity to mentor. I also need to extend a thank you to Dr. Avery McIntosh whose presence, while brief, made a large impact in my technical understanding, and reminded me that cross disciplinary research is paramount for success.

To Dr. Laurie Kaguni, I need to thank you for your trust and encouragement as it was through your BRTP program that I was able to start down the path that ultimately led to my PhD in biochemistry. You reached out to me as a young undergraduate and encouraged my enrolment in the BRTP and graduate program. You allowed me to travel

to Finland and to participate in FINMiT, an experience that I will never forget. I also need to thank Dr. Susan Conrad for allowing me to rotate in her lab and then continuing to provide support via proof reading, ideas, and moral support. You have provided an outsiders look at everything I have done and helped steer me back to reality when I strayed from the path. I have come to greatly appreciate your thoughts and suggestions on all matters, which have led me in the right direction even when the going got tough.

To Dr. Charlie Hoogstraten, you have been a great advisor throughout my nine-years at Michigan State (can you really believe that, nine-years!). You were my undergraduate teacher, counselor, and academic advisor always willing to meet and help out a naïve undergraduate student, which I am grateful for. I am also extremely blessed that after 4 years of advising me as an undergraduate, you didn't even flinch when I asked you to join my graduate committee. You were wonderful to teach with and I consider myself lucky to have been part of your BMB 461 class from the students' side and the teaching side. From a teaching point of view I also need to thank Dr. Neil Bowlby, who like Dr. Hoogstraten had the opportunity to teach and mentor me via BMB 471; thank you!

To Dr. Susanne Hoffmann-Benning, it has been an honor to be a part of your lipids graduate level class, to TA for you in BMB 200, and to participate in the genetics mini-symposium that you and Dr. Atshaves set-up. I learned a great deal from the class and had the opportunity to meet my post-doctorate advisor through the mini-symposium; thank you!

To Dr. Chengfeng Yang and members of the Yang lab, I would not have been able to tackle the miRNA aspect of my thesis without your insight and know-how. You

provided me with cells, reagents, protocols, encouragement, and all around moral support. The work I was able to achieve in the miRNA field is thanks to you, and I am forever grateful.

To our collaborators Dr. Daniel Jones, Dr. Todd Lytic, and Dr. Sandra O'Reilly, much of what I have achieved experimentally would not be possible without your guidance, training, and help. For the technical assistance of Mohammad Aljazi, Ken Moon, Kelly Fader, Sandra Olenic, Brendan Kelly, Raghav Jain, and Brandon Oswald all your hard work was much appreciated.

Last but not least, I would also like to extend a thank you to my friends and classmates Laura Schroeder, Bryan Lenneman, Meredith Frie, Michael Steury, Michael McAndrew, Kelly Fader, and Brock Humphries, for their encouragement and frequent visits with me to Crunchies, HopCat and El Azteco. You guys are the best!

TABLE OF CONTENTS

LIST OF TABLES

LIST OF FIGURES

KEY TO ABBREVIATIONS

Plin, Perilipin

ADRP, adipose differentiation-related protein

TIP47, tail-interacting protein 47

PAT, Perilipin/ADRP/TIP47

ACBP, acylCoA binding protein

NBD-cholesterol,[22-(N-(7-nitrobenz-2-oxa-1,3-diazol-4-yl)amino)-23,24-bisnor-5-cholen-3b-ol]

NBD-stearate, 12-N-methyl-(7-nitrobenz-2-oxa-1,3-diazo)aminostearic acid

PDB, Protein Data Bank

HDL, high density lipoproteins

VLDL, very low density lipoproteins

FRET, fluorescence resonance energy transfer

NASH, nonalcoholic steatohepatitis

MCD, methionine choline deficient diet

PC, phosphatidylcholine

SMS, sphingomyelin synthase

PLA2, phospholipase A2

PE, phosphatidylethanolamine

PEMT, phosphatidylethanolamine N-methyltransferase

COX2, Prostaglandin-endoperoxide synthase 2

IL-6, interleukin 6

TNFα, tumor necrosis factor α

IL-1β, interleukin 1β

CHOP, C/EBP homologous protein

NAFLD, nonalcoholic fatty liver disease

CASP1, caspase-1

LIMSA, Lipid Mass Spectrum Analysis

PCA, principle component analysis

WAT, white adipose tissue

PERK, eukaryotic translation initiation factor 2-α kinase 3

TLR4, toll-like receptor 4

LDL, low density lipoproteins

Chol, cholesterol

CE, cholesteryl esters

DG, diglycerides

FA, fatty acids

Cer, ceramides

PG phosphatidylglycerol

PS, phosphatidylserine

PI, phosphatidylinositol

UNSAT, unsaturated fatty acid

SAT, saturated fatty acid

PUFA, poly-unsaturated fatty acid

MUFA, mono-unsaturated fatty acid

CCT, phosphate cytidyltransferase 1

ACOX1, acyl-coenzyme A oxidase 1

CPT1α, carnitine palmitoyltransferase 1 α

FASN, fatty acid synthase

ACS, Acyl-coenzyme A synthase

SCD1, sterol-coenzyme A desaturase

MGAT, monoglycerol O-acyltransferase 1

DGAT1, diacylglycerol O-acyltransferase 1

DGAT2, diacylglycerol O-acyltransferase 2

MTTP, microsomal triacylglycerol transfer protein

HSL, hormone sensitive lipase

ATGL, adipose triglyceride lipase

ACC, Acyl-coenzyme A carboxylase

ASO, anti-sense oligonucleotide

SAMe, S-adenosylmethionine

NLRP3, PYD domains-containing protein 3

GNMT, glycine N-methyltransferase

miRNA, microRNA

UTR, untranslated region

PGH, prostaglandin hydroperoxide

LPS, Lipopolysaacharides

COX1, Prostaglandin-endoperoxide synthase 1

5-LO, arachidonate 5-lipoxygenase

15-LO arachidonate 15-lipoxygenase

FLAP, arachidonate 5-lipoxygenase-activating protein

LTC_4, leukotriene C4

MCP-1, monocyte chemoattractant protein-1

PTGIS, prostacyclin synthase

PPAR, peroxisome-proliferator activated preceptor

RXR, retinoid X receptor

NFκB, nuclear factor kappa-light-chain-enhancer of activated B cells

STAT1 signal transducer and activator of transcription 1

Bexa, bexartene

Rosi, rosiglitazone

KLA, kdo2-lipid A

CHAPTER 1:

INTRODUCTION

INTRODUCTION

The ability to utilize and store neutral lipids is evolutionarily conserved and reflects the importance of efficient lipid management for survival (*1, 2*). When chronic over-nutrition occurs, the body and its tissues are saturated with excess lipids, leading to disruptions in lipid homeostasis and key cellular functions. Excess lipid storage in tissue leads to chronic inflammation involving increased cytokine production that can give rise to several disease states including cardiovascular disease, atherosclerosis, type-2 diabetes, and non-alcoholic steatohepatitis (NASH) (*3-9*). It is clear that the accumulation of excess lipids causes an inflammatory response, yet little is known regarding the underlying mechanism involved. The work presented in this thesis focuses on the lipid droplet protein Perilipin2 (Plin2) and the role it plays in inflammation. What follows is a brief overview of lipid droplet biology; intracellular lipid metabolism; an introduction into lipid droplet associated proteins; and finally how miRNAs play a role in mediating lipid metabolism.

LIPID DROPLETS

Originally considered passive bags of fat, lipid droplets are now understood to be complex, dynamic organelles that play a central role in energy metabolism, membrane synthesis, and production of lipid-derived molecules such as lipoproteins, bile salts, hormones, eicosanoids, and prostaglandins (*10-13*). Lipid droplets are thought to develop as budding vesicles in the endoplasmic reticulum (ER) lipid bilayer, where enzymes involved in lipid synthesis and lipolysis deposit neutral lipids between the bilayer leaflets (*14-19*). During the maturation process, the lipid droplet structure forms

a neutral lipid core surrounded by a phospholipid monolayer embedded with proteins. Lipid droplet associated proteins play a critical role in regulating the balance between lipid storage and lipid utilization, yet the vast majority of this regulatory network remains unknown. Interestingly, factors such as intracellular and extracellular stresses trigger lipid droplet formation (*20-24*). In particular, inflammation dramatically increases lipid droplet formation and eicosanoid production at the lipid droplet surface (*11, 20, 25, 26*). The lipid droplet formation under extracellular and intracellular signals reflects a role for lipid droplets and their associated proteins in processes not directly related to lipid metabolism, leading to a link between lipid droplets and pathologies. Indeed, with lipid droplets implicated in a variety of critical cellular processes related to cell homeostasis and disease progression, an understanding of the organelle and its associated proteins is paramount to developing new therapeutic targets.

Multiple enzymatic reactions contribute to lipid droplet assembly. Activated fatty acids produced by Acyl-CoA synthase (ACS) are essential for the initial formation of triglycerides (TG) found in the neutral lipid core of lipid droplets as indicated by studies that show inhibition of ACS by Triacsin C significantly reduces TG synthesis and completely inhibits the formation of lipid droplets promoted by fatty acid treatment (*16, 27-29*). ACS activity also modulates the cellular AMP/ATP ratio indicating ACS influences metabolic signaling via AMP kinases (*29-31*). By modulating the AMP/ATP ratio, ACS acts as a critical sensor of the energy state in the cell, thus determining lipid storage lipid droplets. In addition, ACS proteins form complexes with other ER-associated proteins and potentially organize micro-domains within the ER membrane (*18, 19, 32*). This complex of neutral lipid synthesis enzymes likely increases the

efficiency of neutral lipid production mediating the initial stages of lipid droplet formation (*18*). In addition, the ACS derived complexes have been shown to include diacylglycerol acyl-transferase 1/2 (DGAT1/2), acetyl-CoA acetyltransferase 1/2 (ACAT1/2) and other lipid droplet associated proteins including Spartan (*18, 19, 33-36*). An outline of the initial stages of lipid droplet formation is shown in Figure 1.

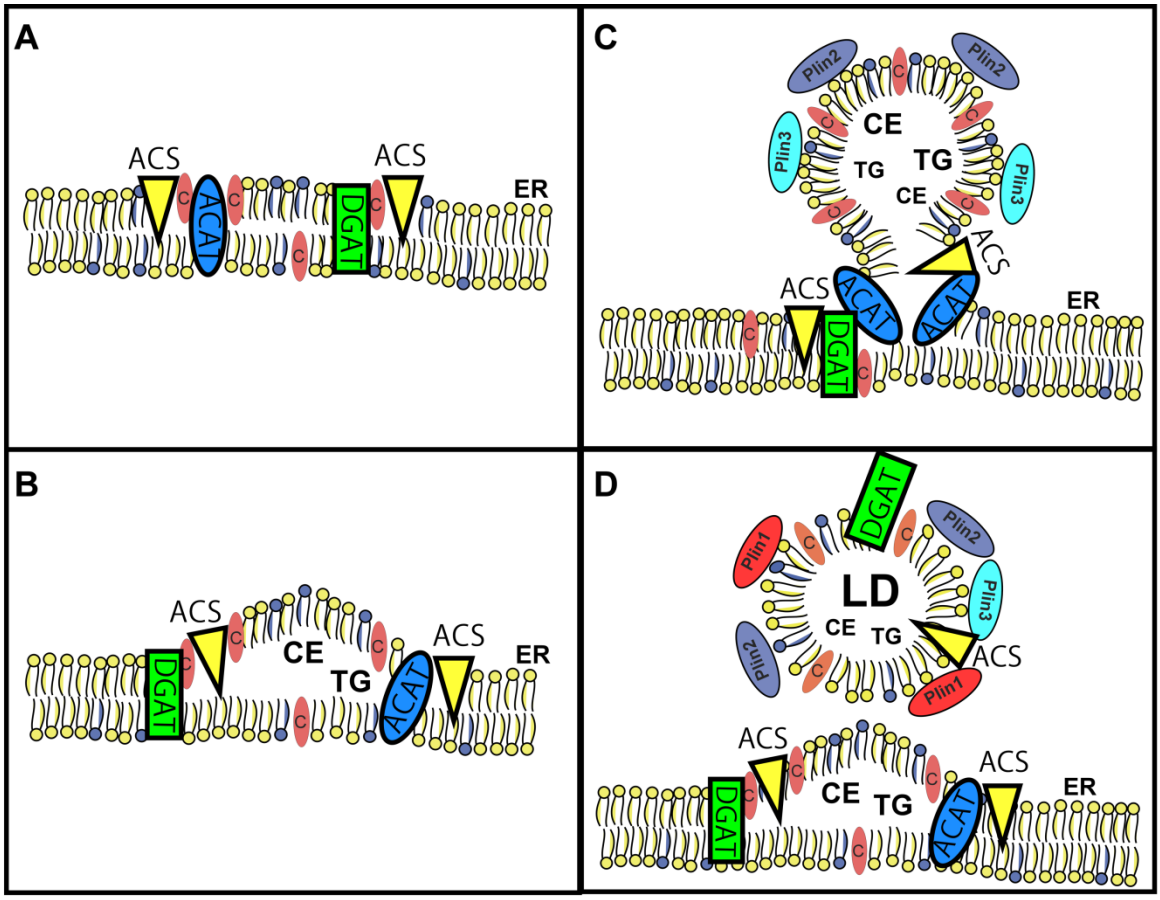

Figure 1. Schematic representation of lipid droplet biogenesis. (A) Neutral lipid synthesis enzymes form complexes in the ER membrane, promoting the efficiency of neutral lipid synthesis. ACS is thought to play an important role in the initial complex formation. (B) During neutral lipid synthesis, TG and CE are deposited between the two ER leaflets causing a local bulging or swelling. The initial accumulation of lipids will move laterally through the ER membrane until the lipids are dispersed or a nucleation event occurs. (C) Nucleation marks the onset of lipid droplet biogenesis and is classified by the recruitment of Plin3. Shortly after the appearance of Plin3 at the nucleation site, Plin2 targets the naïve lipid droplet stabilizing the structure and increasing lipid loading. (D) Once the lipid droplet reaches a sufficient size, the lipid droplet is thought to release from the ER and function as an independent organelle. If the lipid droplet continues to grow, Plin2 and Plin3 will be replaced on the lipid droplet surface by Plin1.

NEUTRAL LIPID SYNTHESIS AND STORAGE IN LIPID DROPLETS

The most abundant neutral lipids in lipid droplets are triacylglycerols (TG) and cholesterol esters, with sterol esters more prevalent in yeast and *Drosophila (37)*. Neutral lipids are synthesized by enzymes permanently or transiently located in the ER (*37*) and also on the lipid droplet surface (*16, 18, 38*). The classical model of de novo TG synthesis occurs in four reactions catalyzed by members of the glycerol-3-phosphate *O*-acyltransferase (GAPT), 1-acylglycerol-3-phosphate *O*-acyltransferase (AGAPT), phosphatidic acid phosphatase (PAP)/lipin, and DGAT enzyme families(*16, 33, 39-44*). A diagram of neutral lipid synthesis is found in Figure 2. The final step in this pathway is the esterification of diacylglycerol into triacylglycerol conducted by DGAT1 and DGAT2 which accounts for nearly all TG synthesis in mouse cells. When neutral lipid storage is promoted, the enzymes initially located on or in the ER become segregated, with some remaining in the ER and others accumulating on the lipid droplet surface. GPAT4, AGPAT3, PAP, and DGAT2 localize on lipid droplets in flies and mammals while Gat1p, Gt2p, Pah1P, and Dga1p are found on yeast lipid droplets (*14-16, 45-47*). While not completely understood, transmembrane proteins also target to lipid droplets and embed in a phospholipid monolayer, a process thought to occur through membrane bridges or by early embedding in naïve lipid droplets formed from the ER (*1, 18, 19, 48*). In addition to TG, diacylglycerol is also present in lipid droplets. In newly formed lipid droplets, diacylglycerol generates membrane curvature, replacing phospholipids such as phosphatidylcholine (PC) to provide a platform for protein binding (*49-51*). This last point is critical, as targeting of membrane expansion proteins and other lipid droplet associated proteins require the presence of diacylglycerol to target to

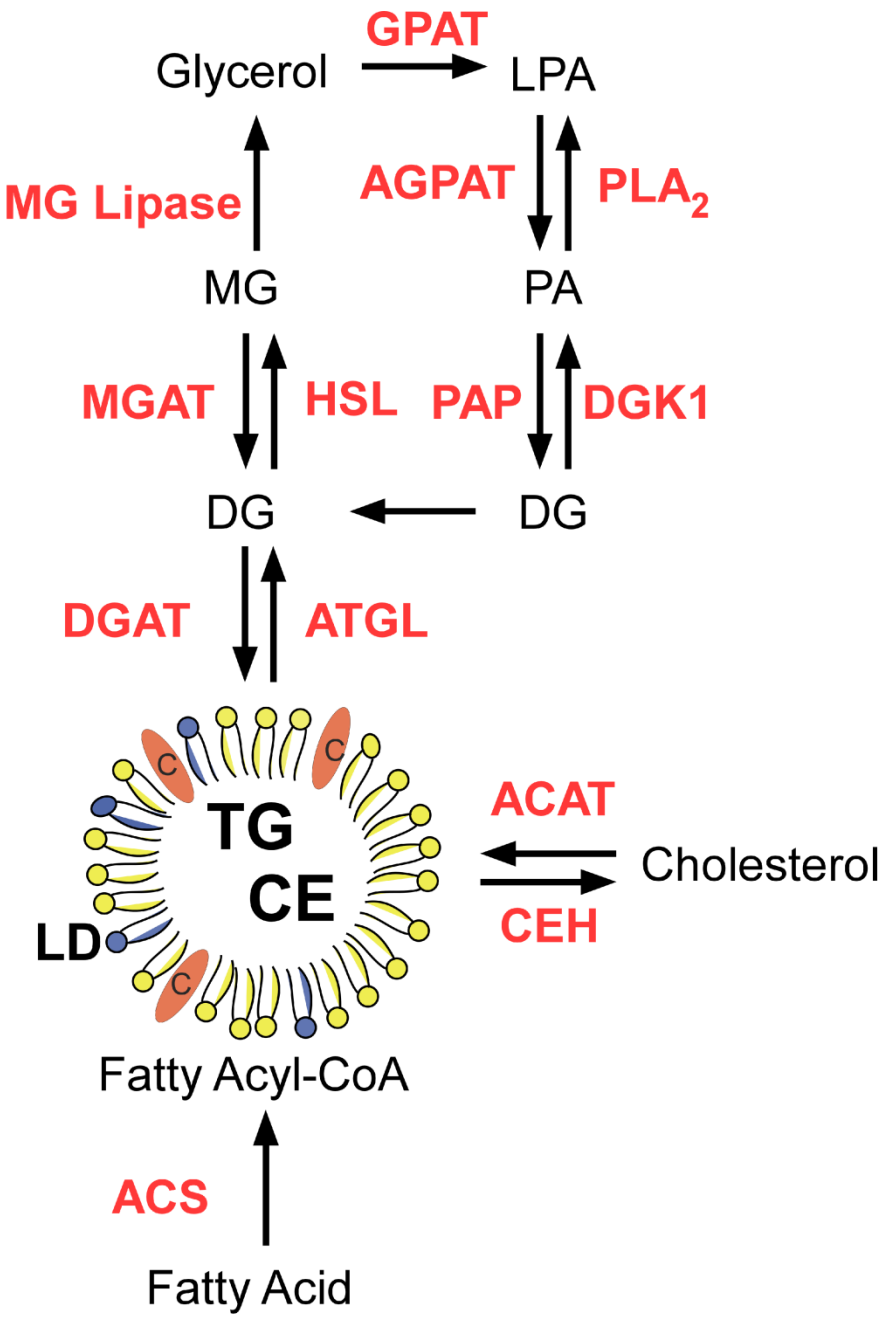

Figure 2. Neutral lipid metabolism and lipid droplet formation. Lipid droplet biogenesis requires the coordination of fatty acid activation by ACS and de novo synthesis of TG and cholesterol esters. The enzymes and lipid intermediates involved in these pathways are indicated in red and black letters, respectively.

lipid droplets. Lipid droplets also contain a significant amount of cholesterol and cholesterol esters, especially in macrophages and steroidogenic cells under conditions of atherosclerosis (*14, 16, 52-55*). The synthesis of cholesterol esters is mediated by acyl-CoA:cholesterol *O*-acyltransferase (ACAT1 and ACAT2) on the ER (*39, 56*). Lipid droplets store cholesterol and cholesterol esters through the incorporation of cholesterol esters into small-naïve lipid droplets budding from the ER.

LIPOLYSIS OF NEUTRAL LIPIDS IN LIPID DROPLETS

Lipolysis of TG occurs when fatty acids are released from the glycerol backbone. Lipolysis generates fatty acids for β-oxidation and energy production, yet recent studies have highlighted the importance of lipolytic intermediates in the synthesis of phospholipids, cholesterol esters, and signaling molecules (*57-61*). The initial step of TG hydrolysis is carried out by adipose triacylglycerol lipase (ATGL) which releases a single fatty acid to produce DG (*62-65*). Hormone-sensitive lipase (HSL) removes a second fatty acid to produce monoglyceride (MG) (*63, 66-68*). The final step of TG breakdown is performed by monoglyceride lipase (MGL) which releases a third fatty acid and glycerol (*15, 16*). Under basal lipolytic conditions, lipases ATGL and HSL are cytosolic bound. Comparative gene identification-58 (CGI-58), the co-activator of ATGL, localizes to the lipid droplet and is held in place by Perilipin 1 (Plin1), the major lipid droplet protein in white adipose tissue (WAT) (*68-80*). Plin1 also interacts with A-kinase anchor protein (AKAP) to tether and regulate PKA type 1 and type 2 subunits at the lipid droplet surface, preventing lipolytic activation (*65, 71, 76, 78, 80-82*). Upon β-adrenergic stimulation, Plin1 and HSL are phosphorylated by PKA (*65, 68, 71, 76, 78, 83*).

Conformational changes in Plin1 by phosphorylation and recruitment of HSL cause the release of CGI58. ATGL binds CGI58 in the cytosol causing the two proteins to translocate to the lipid droplet surface and lipolysis is activated. It is important to note that other lipid droplet associated proteins including Plin2 and Plin3 have no known lipolytic activities (*64, 72, 84-87*). However, it has been suggested that Plin2 limits ATGL binding to lipid droplets, yet no direct interactions between the two proteins have been observed. Interestingly, chaperone mediated autophagy (CMA) was shown to degrade Plin2 and Plin3 under starvation conditions thus allowing ATGL and HSL to bind to the lipid droplet surface. Alternative methods for lipid release have recently been reported (*87, 88*). In these studies Plin2 interacted with heat-shock protein-70 (HSP-70) and PMAK phosphorylase which phosphorylates the complex targeting Plin2 and Plin3 for degradation (*87, 88*). The absence of Plin2 and Plin3 allows ATGL and HSL mediated lipolysis to occur or macro-autophagy proteins to consume large portions of the lipid droplet rapidly (*87, 88*). In a similar manner, release of cholesterol from the neutral lipid core has been described via two hydrolytic pathways. The first pathway involves the association of cholesterol ester hydrolase (CEH) to the lipid droplet surface where it hydrolyzes cholesterol esters into free cholesterol and the second involves lysosomal fusion with the lipid droplet via a lysosomal acid lipase which results in release of cholesterol. An overview of lipid droplet lipolytic pathways is outlined in Figure 3.

About 95% of the biologically available energy stored in TG resides in the fatty acid moieties, making them critical components in maintaining cellular energy production. β-oxidation occurring in the mitochondria releases the stored energy in the fatty acids. Enzymes involved in this process include acyl-CoA synthetase (ACS), acyl-CoA

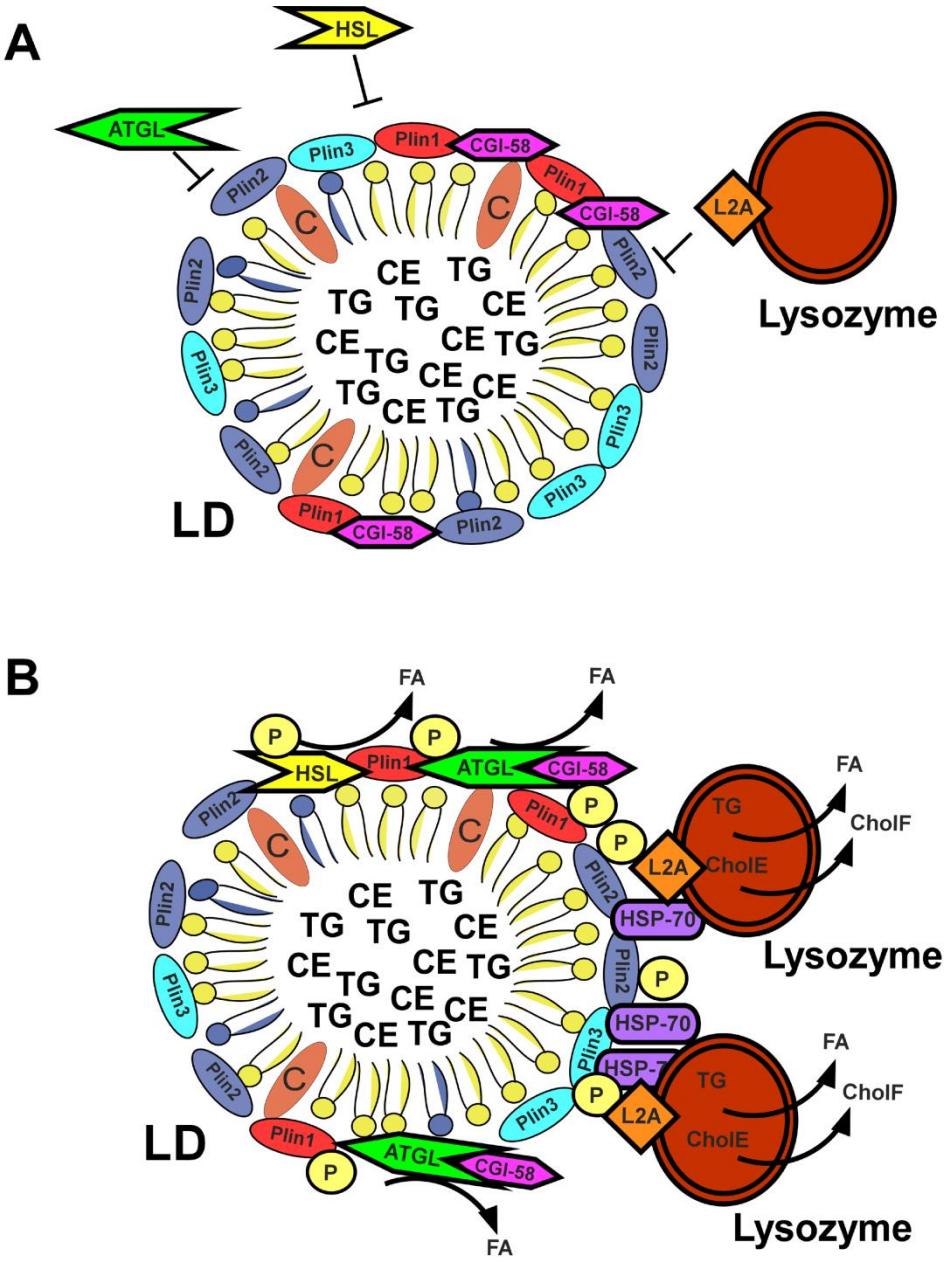

Figure 3. Schematic of lipid droplet based lipolysis. (A) Under basal conditions, lipid droplets are coated by Plin1, Plin2 and Plin3. Lipolysis is inhibited by both the retention of retention of CGI-58 by Plin1, and Plin2/Plin3 mediated inhibition of blocking ATGL and HSL binding to the lipid droplet membrane. (B) Upon stimulation, removal and degradation of Plin2 and Plin3 by CMA permits ATGL and HSL access to the lipid core. The targeting of Plin2 and Plin3 by CMA is mediated by HSP-70, which sequesters PMAK to the lipid droplet surface and results in subsequent phosphorylation of Plin2. Another phosphorylase, PKA, phosphorylates Plin1 releasing CGI-58 further recruiting ATGL to the lipid droplet surface

dehydrogenase, enoyl-CoA hydratase, β–hydroxyacyl-CoA dehydrogenase, and acyl-CoA acetyltransferase. These enzymes are relevant in the current thesis since expression levels of several were influenced in cells and mice with altered Plin2 expression.

PHOSPHOLIPID MEMBRANE EXPANSION IN LIPID DROPLETS

Lipid droplet expansion occurs through phospholipid remodeling and synthesis via two pathways: the Kennedy pathway (also known as the CDP-choline pathway) and the Land's Cycle (*16, 51, 89*). Both pathways are involved in PC synthesis, the major phospholipid comprising 50-60% of total phospholipid content in cells. In the Kennedy pathway, exogenous choline is taken into the cell and phosphorylated via choline kinase producing phosphor-choline (*16, 90-93*). Phosphor-choline is then activated by the addition of CTP, a reaction that is catalyzed by the rate-limiting enzymes CTP:phosphor-choline cytidylyltransferase (CCT) to form CDP-choline. The final step of the pathway takes the CDP-choline and adds it onto a DG backbone thereby producing PC (*91, 94, 95*). This last step is catalyzed by CDP-cholinephosphotransferase (CDT). It is through this pathway that lipid droplets expand. Deposition of TG in the lipid droplet core either by TG storage in the lipid droplet or *de novo* synthesis of TG on the lipid droplet surface increases the size and depletes the relative amount of PC in the phospholipid monolayer (*51, 90*). As DG and phosphatidic acid become enriched at the lipid droplet surface, CCT is able to translocate from the nucleus and bind to the lipid droplet monolayer. This translocation and binding action activates the enzyme. While

CCT localizes to the lipid droplet, choline kinase and CDT do not, indicating that CCT is the rate limiting enzyme for lipid droplet expansion and lipid storage(*51, 90*).

In the liver, PC can also be produced independent of CCT by either the Lands cycle or the phosphatidylethanolamine methyltransferase (PEMT) pathway (*96-100*). The Lands cycle utilizes lysophosphatidycholine acyltransfease (LPACT) by combining a lysophosphocholine with an acyl-CoA (*25, 89, 101-103*), two molecules that can be produced on the lipid droplet surface by phospholipase A2 and acyl-CoA synthase, respectively. In the PEMT pathway, PE is converted to PC through three sequential methylations of PE by PEMT using methionine-derived substrates (SAMe) (*96, 97*). An overview of lipid droplet phospholipid metabolism can be seen in Figure 4. In the current thesis, we investigate the significance of PEMT-mediated PC production in Plin2 liver-specific knockout mice, the details of which will be discussed in Chapter 4.

LIPID DROPLET ASSOCIATED PROTEINS

The lipid droplet proteome has been extensively studied across a wide array of organisms and cell types. Proteomic analysis of lipid droplets isolated from lipolytically stimulated 3T3-L1 cells indicated a diverse group of proteins associated with the lipid droplet surface (*46, 104-108*). This included proteins involved in lipid metabolism as well as structural proteins, and the traditional Perilipin family members. For example, HSL, lanosterol synthase, NADP-dependent steroid dehydrogenase-like protein, ACS, 17-β-Hydroxysteroid dehydrogenase, and CGI-58 were identified in lipid droplet preparations under basal condition (*45*). Intriguingly, a dramatic shift in the lipid droplet associated proteins was observed under lipolytic stimulation (*45*). ACS3 and 4 and two short-

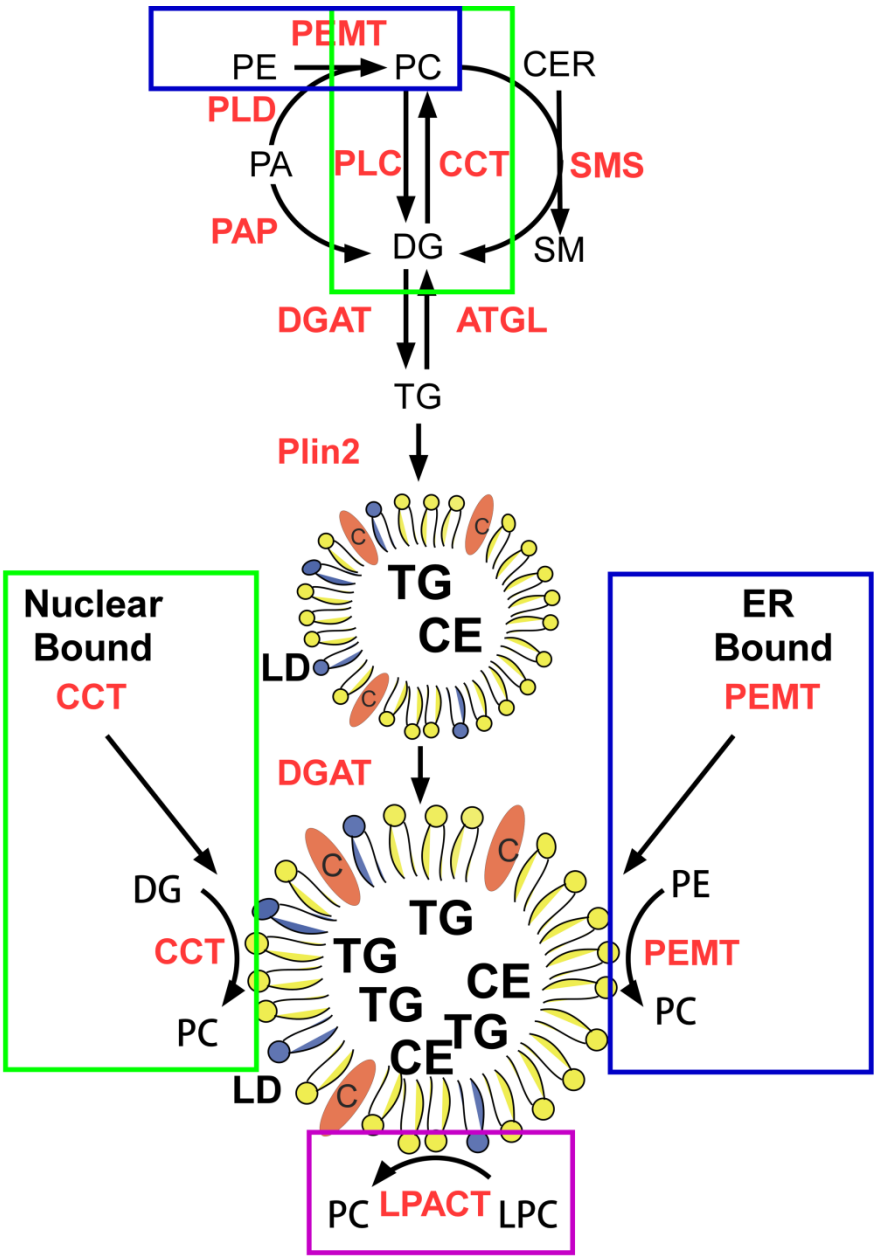

Figure 4. Phospholipid metabolism and lipid droplet expansion. Lipid droplet expansion due to increased neutral lipid storage requires a significant amount of phospholipids. The main phospholipid in the lipid droplet monolayer is PC. Phospholipid metabolic enzymes are in red while the intermediates are in black. The Kennedy pathway is highlighted by the green box, while the PEMT and Lands cycle are highlighted in blue and purple, respectively.

chain reductase/dehydrogenases were identified on lipid droplets from lipolytically stimulated cells. In addition, several Rab GTPases, tumor protein D54, and mitochondrial associated proteins such as pyruvate carboxylase, and prohibitin were identified in lipid droplets under lipolytic stimulation (*45, 46, 104, 105*). These results indicated that lipid droplets contain specific structural proteins as well as lipid metabolic enzymes that undergo structural reorganization in response to lipolysis. In support of these findings, additional proteomic studies with lipid droplets isolated from mice found 48 proteins that were increased, and 53 proteins that were decreased, on lipid droplets due to high-fat feeding (*104*). Many proteins involved in fatty acid catabolism or xenobiotic metabolism were enriched in lipid droplet fractions following high-fat feeding whereas glucose metabolism and liver X receptor or retinoid X receptor activated proteins were decreased (*104*). Taken together, proteomic analysis of lipid droplets provided insights into the unique biological functions of hepatic lipid droplets under normal and altered metabolic conditions.

Another outcome of the proteomic screens was the discovery that the cell death-inducing DFFA-like effector (CIDE) family of proteins targets lipid droplets (*109*). The CIDE family of proteins includes CIDEA, CIDEB, and CIDEC (also known as FSP-27) (*110-114*). CIDE proteins promote cell death when upregulated, however they are also associated with the lipid droplet membrane. While the exact function of these proteins in lipid droplet biology is unclear, studies suggest CIDEA affects lipid metabolism as knockout mice showed a lean phenotype with decreased adiposity, decreased leptin, and increased lipolysis and fatty acid oxidation (*109, 111*). CIDEB knockout mice exhibited a similar phenotype to CIDEA mice however, CIDEB knockout resulted in

increased hepatic insulin sensitivity (*110*). This was manifested by increased IRS-1 and AKT2 phosphorylation under insulin stimulation (*110*). In addition, CIDEB null mice showed a significant decrease in lipogenesis via downregulation of SREBP1c (*110, 115*). CIDEC (FSP-27) knockout mice showed altered lipid metabolism by increasing lipolysis similar to CIDEB knockout mice. The major phenotypical difference between the CIDEC and the CIDEB was in the case of CIDEC, a direct role in mitochondrial β-oxidation was observed (*112-114, 116, 117*). Suggesting the CIDEC not only had a role in lipid droplet biology, but also mitochondrial function. In support of this, WAT tissue in CIDEC knockout mice took on several aspects of brown adipose tissue with increased mitochondrial volume and activity indicating CIDEC (*112*).

ER, membrane trafficking, and signaling proteins have also been identified to target lipid droplets (*53, 118*). Some of these include members of the Rab family of small GTPases as well as the Caveolins and Cavins (*37, 53, 105, 119-122*). The targeting of Caveolins to the lipid droplet appears to be a regulated process in the sequestration of cholesterol (*53*) and fatty acids (*123*). When cells were lipid loaded with cholesterol or fatty acids prior to induction of lipolysis, Caveolin 1 was found to target to the lipid droplet (*53*). Similar to lipid raft structures induced by Caveolin in the plasma membrane, Caveolin 1 was found in lipid raft like domains on the lipid droplet phospholipid monolayer (*124, 125*). In the lipid raft like domains isolated from lipid droplets, Caveolin-1 and Flotilin were present along with lipolytic enzymes such as ATGL, HSL, and phospho-Plin1 (*124*). The presence of the lipolytic enzymes in these domains indicated lipid raft complexes of lipolytic enzymes that likely increase the

efficiency of lipolysis and lipid release. In addition, SRB1 co-localization with Caveolin-1 on lipid droplets indicated a direct role for caveolin in cholesterol storage (*126, 127*).

Recently, proteins of the hypoxia-inducible protein (HIG) family of proteins have also been discovered to have roles in lipid droplet biology (*128-131*). HIG2 is a target of the hypoxia-inducible factor 1 (HIF1), and co-localizes with Plin2 and Plin3 on the lipid droplet surface (*129, 131*). In addition, HIG2 targeting lipid droplets is induced under HIF1 activation (*130*). This is significant as recent work demonstrates Plin2 expression is promoted by HIF1-α binding to an enhancer region in the promoter region of Plin2, linking HIG2 and Plin2 to hepatic hypoxia (*132-134*).

The proteome "signature" for lipid droplets also consistently includes at least one member of the Perilipin (Plin) family of proteins. This family is defined by an N-terminal sequence known as the PAT-domain (*135-137*). The mammalian genome encodes five Plin genes and additional mRNA splice variants with individual tissue-dependent expression patterns (*135, 137*). The five Plin variants are Plin1, Plin2 (also known as ADRP, ADFP, and adipophilin), Plin3 (previously TIP-47), Plin4 (previously S3-12), and Plin5 (previously LSDP5, OXPAT, MLDP, and PAT1). Homologous regions between the Plin proteins are outlined in Figure 5. Each Plin protein is thought to have a distinct role, but several of the functions remain unclear. The best-characterized Plin protein, Plin1, controls lipolysis by recruiting or preventing access of lipases on lipid droplets. Under basal lipolytic conditions, lipases ATGL and HSL are cytosolic bound. Comparative gene identification-58 (CGI-58), the co-activator of ATGL, localizes to the lipid droplet, and is held in place by Plin1, the major lipid droplet protein in WAT (*78*). Plin1 also interacts with A-kinase anchor protein (AKAP) to tether and regulate PKA type 1 and

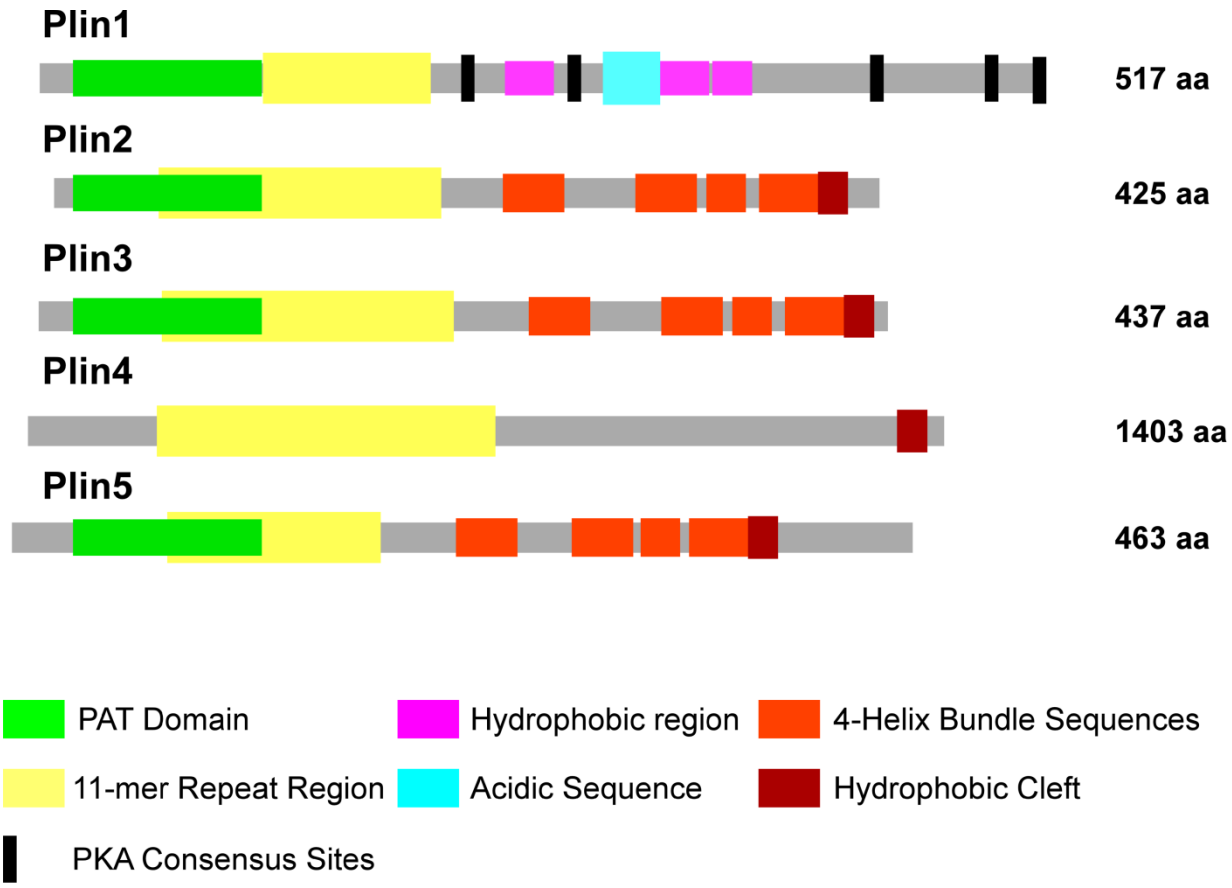

Figure 5. Schematic diagram of the structural features of the Perilipin family of proteins. The N termini of Plin1, Plin2, Plin3, and Plin5 but not Plin4 contain 100 amino acid (aa) sequences that are highly conserved between members of the family (denoted at green box). Overlapping with these sequences are stretches of amino acids that create a secondary structure known as 11-mer repeats that consist of amphipathic helices (designates at light yellow box). Following the putative 11-mer repeats, sequences of Plin3 fold into a four helix bundle with a hydrophobic made up of a unique α/β domain (orange and red boxes, respectively). Both Plin2 and Plin5 share these sequences and are modeled to contain similar three-dimensional structures. In contrast, Plin1 has three sequences of moderate hydrophobicity (pink boxes) and a highly acid region (bright blue) in its C-terminal region.

type 2 subunits at the lipid droplet surface, preventing lipolytic activation (*65, 68, 76, 78*). Upon β-adrenergic stimulation, Plin1 and HSL are phosphorylated by PKA. Conformational changes in Plin1 by phosphorylation and recruitment of HSL cause the release of CGI58 (*62, 78*). ATGL binds CGI58 in the cytosol causing the two proteins to translocate to the lipid droplet surface and lipolysis is activated.

It has been suggested that Plin2 also plays a role in lipolysis however, the protein has no known lipolytic activity (*57, 64, 138*). Plin2 acts by limiting ATGL binding to lipid droplets in a non-interactive mechanism between the two proteins (*64, 139*). Plin2 has also been implicated in lipid droplet formation (*140, 141*), LPS induced lipid droplet formation (*20, 142, 143*), and VLDL assembly (*144, 145*). A more in-depth review of Plin2 literature can be found below. With regard to Plin3, in mammalian cells the protein is recruited to the ER during lipid droplet biogenesis by recognition of the initial accumulation of diacylglycerol. The protein's presence at the onset of lipid droplet formation suggests that Plin3 regulates efficient lipid droplet formation (*16*). While Plin2 and Plin3 are ubiquitously expressed, many organisms do not have a Plin3 orthologue. For example, certain insect cells types do not express Plin3 (*16*). This suggests alternative mechanisms of lipid droplet formation or functional compensation between the Plin proteins occurs (*146*). Plin3 has also been shown to inhibit lipolytic enzymes, reducing lipid droplet lipid catabolism (*87, 138, 146, 147*). Under starvation conditions, Plin3 is targeted for chaperone mediated autophagy, thereby increasing *in vivo* lipolysis of lipid droplets via ATGL (*87, 88*).

To date, little is known regarding the function of Plin4. Originally discovered as a gene upregulated by PPARγ during adipocyte differentiation, it is expressed at low

levels in heart and skeletal muscle and is completely absent in brown adipose tissue (BAT) and liver (*16, 28, 148-150*). Structurally, Plin4 has a unique feature in that approximately two-thirds of Plin4 are comprised of tandem repeats of an 11-residue motif shared between Plin2, Plin3 and Plin5 (*135, 137*). Excluding the 11-residue repeat, Plin4 displays a more divergent carboxyl and amino terminus than Plin2, Plin3 and Plin5. In cultured adipocytes, Plin4 is in the cytosol. Upon lipid loading, Plin4 co-localizes with nascent lipid droplets, rapidly packaging TG (*137, 148, 151*). These results suggest Plin4 functions as a regulated protein that associates with lipid droplets when there is a need for lipid storage in lipid droplets.

In contrast to Plin4, the Plin5 gene is highly expressed in oxidative tissues including heart, skeletal muscle, BAT and liver (*148, 152-154*). Consistent with this, Plin5 was shown to increase fatty acid uptake, decrease lipolysis, and increase fatty acid oxidation (*152*). These studies support divergent roles for Plin5 in both lipid storage and lipid oxidation (*139, 155, 156*). In other work with hepatocytes, skeletal muscle, and cardiomyocytes Plin5 was shown to protect against lipotoxic stress by regulating lipolysis (*153, 154, 157*). Plin5 expression increases in response to fatty acid exposure, which is likely due to the activation of PPAR α and δ (*152*). Plin5 also interacts with ATGL, HSL, and CGI-58 to prevent uncontrolled lipolysis and modulates the regulation of Plin1 and ATGL/HSL to increase β-oxidation efficiency (*139, 153-156*). Metabolic regulation by Plin5 is apparent in endurance trained athletes where increased lipid droplets and Plin5 expression are often observed (*158*). In these individuals, Plin5 was proposed to regulate release of fatty acids from lipid droplets to provide long term energy stores during extensive exercise (*158, 159*).

PERILIPIN 2

Plin2 (also known as adipose differentiation-related protein, ADRP, ADHP, or adipophilin) was first identified by Serrero et al in 1992, as an mRNA transcript induced during adipocyte differentiation (*160*). The gene encoding Plin2 spans 14kb and contains 8 exons and 7 introns (*160, 161*). The gene produces a 48 kDa protein that contains an N-terminal PAT domain, 11-mer repeat region, and a unique α/β domain coupled to a 4-helix bundle whose functions are outlined in Chapter 3 of this thesis. Studies to elucidate the function of Plin2 have included gain- and loss-of-function experiments in cells and mice. Although the experimental systems and designs have varied from study to study, the primary function of Plin2 appears to be in neutral lipid accumulation in lipid droplets (*84, 140, 143, 162-165*). While recent work indicates Plin2's role on the lipid droplet surface may also include the recruitment or displacement of enzymes under different metabolic conditions, the mechanism of action remains unclear. In this section of Chapter 1, an in-depth summary of the work previously performed will be covered as well as areas of current research.

Overexpression of Plin2 has been associated with expansion of lipid droplet pools and increased cellular TG (*1, 17, 166*). For example, over-expression of the green fluorescent protein (GFP)-Plin2 fusion protein in 3T3-L1 cells resulted in increased TG content even when cells were cultured in depleted serum (*140*). The increase in cellular TG content was thought to be a result of Plin2 blocking access of lipases and other proteins targeting the lipid droplet (*64, 166*). Since no direct interaction between Plin2 and the two lipid droplet TG lipases, ATGL and HSL, has been characterized, the mechanism by which Plin2 prevents lipolysis remains unknown (*64, 138*). However, it

has been proposed that Plin2 binding to the lipid droplet surface induces phospholipid crowding in the lipid droplet monolayer (*64, 167*). The crowding effect produces localized phospholipid rich and phospholipid poor areas (*64, 167*). In doing so, proteins that rely on hydrophobic interactions are able to bind to the phospholipid rich regions while enzymes requiring the phospholipid polar head groups are not able to target the phospholipid poor regions. Thus, Plin2 interactions with the phospholipid monolayer determine the ability of proteins to target the lipid droplet and may deny access to other proteins in the areas in which it binds. This area of research is ongoing as Plin2 has been shown to change its confirmation when bound to a membrane and/or when it is post-translationally modified (*88*), indicating its interactions with the phospholipid monolayer may be altered.

In support of Plin2's function in regulating protein recruitment to the lipid droplet surface, recent studies have demonstrated that Plin2 coats smaller, more metabolically active lipid droplets whereas Plin1, the homolog responsible for regulating lipolytic enzymatic activity, coats large mature lipid droplets (*82*). Plin2 when not bound to lipid droplets is targeted for degradation via the ubiquitin proteasome pathway (*35, 168*). Addition of a fusion tag such as CFP, GFP, or FLAG-tag on the N-terminal region of the protein negates proteasomal degradation of Plin2 (*168*). Creation of N-terminal mutants highlighted a sequence in the PAT domain responsible for ubiquitination, mutation of which resulted in a non-degradable version Plin2. Recent work has indicated that Plin2 can be degraded on the lipid droplet surface via chaperone-mediated autophagy (CMA) (*87, 88*). The latter process involves a newly discovered phospho-Plin2 which is dependent on HSP70 interaction with AMPK (*88*). In cells lacking the required CMA

enzymes, Plin2 levels remain constant even when unbound to lipid droplets. These findings are significant as CMA degradation of Plin2 is critical for lipolytic turnover of lipid droplets lacking Plin1 (as seen in hepatic lipid droplets) (*73*). Without CMA mediated autophagy lipid droplets continue to retain lipids causing the onset of steatosis (*87, 88*).

There are several Plin2 deficient and Plin2 knockout models that were originally derived to study the effect of Plin2 ablation on adipose tissue development and lipolytic activity. The first Plin2 null mouse was described by Larry Chan and was globally deficient in full-length Plin2 (*169*). The Chan Plin2 deficient mouse displayed normal adipocyte and adipose tissue differentiation and function, as assessed by histology, adipocyte markers, TG mass, and basal/stimulated lipolysis (*169*). The mice also exhibited normal plasma lipids, glucose, and insulin levels, yet there was a substantial decrease in hepatic neutral lipid content. The overall reduction in liver TG was not explained by reduced fatty acid uptake or increased β-oxidation in these mice (*169*) yet Plin2 deficiency also prevented hepatic steatosis by high fat feeding (*144*). There was also no sign of reduced lipogenesis or lipogenic enzyme activity however, there was increased micro-vesicle formation (*144, 169*). These micro-vesicles were originally thought to be smaller lipid droplets, but they contained a significant amount of MTTP, the rate limiting enzyme in VLDL formation (*144, 169*). It was later proposed in Plin2 deficient mice cross bred with $Lep^{Obe/Obe}$ mice that the small, MTTP-TG rich micro-vesicles fed directly into VLDL production, thereby secreting TG from the liver and preventing hepatic steatosis (*144, 169*). Interpretation of these data was complicated as an amino-terminal truncation of Plin2 was found in lactating mammary tissue that

partially replaced the functions of full-length Plin2 in lipid droplet formation and secretion (*170*). In an attempt to clarify the Chan Plin2 deficient studies, Plin2 antisense oligonucleotides were used to knockdown Plin2 in $Lep^{Obe/Obe}$ and high-fat fed obese mice (*164, 171, 172*). In these two mouse models, Plin2 levels were decreased between 40-65% (*171, 172*). While a significant amount of Plin2 expression remained, both antisense mouse models exhibited changes in lipid and glucose metabolism (*164, 171, 172*). Similar to the Chan deficient mice, antisense Plin2 knockdown mice showed decreased hepatic TG content and were again protected against diet induced hepatic steatosis (*164, 171, 172*). In contrast to the Chan mouse, antisense Plin2 knockdown mice exhibited decreased lipogenic genes rather than increased lipolysis and increased TG export as VLDL (*171, 172*). The hepatic TG changes were accompanied by improved insulin sensitivity and glucose tolerance, as well as reduced body fat. The link between Plin2 and VLDL secretion was supported by cell-based studies of hepatoma cell lines. In hepatoma and primary rat hepatocytes, increased expression of Plin2 partitioned TG into lipid storage, thereby reducing secretion of TG as VLDL (*145*). Conversely, silencing of Plin2 via siRNA resulted in reduced lipid droplets, increased β-oxidation, lipolysis, and increased secretion of apoB-VLDL particles (*145*). Interestingly, a genetic variation in the Plin2 gene causing a serine to proline mutation (Ser251Pro) resulted in dysregulation of plasma lipid and lipoprotein profiles in humans, possibly due to disruption of helical structure within a putative lipid binding site (*86, 173*). A depiction of Plin2's role in lipid droplet biology and lipid trafficking is outline in Figure 6.

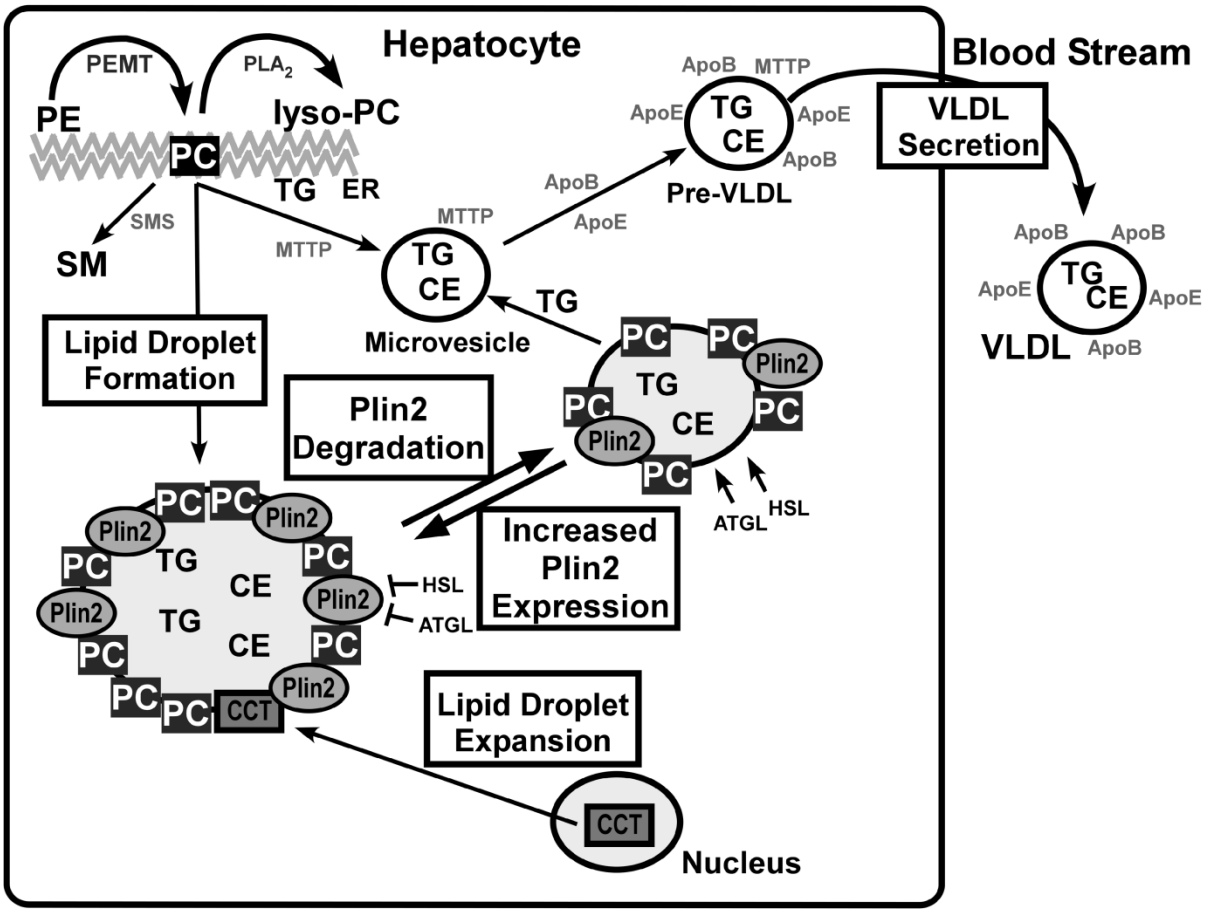

Figure 6. Schematic diagram illustrating lipid droplet formation, VLDL secretion, and lipid droplet expansion. Lipid droplet formation: Phospholipids and triglycerides synthesized at the ER form naïve lipid droplets. Lipid droplet expansion: Increased neutral lipid storage in lipid droplets causes a relative decrease in the amount of phospholipids in the monolayer. To restore the levels of phospholipids, phospholipid synthesis enzymes such as CCT translocate to the lipid droplet surface. Decreased Plin2 expression: Lack of Plin2 results in formation of smaller lipid droplets and production of MTTP-rich microsomes that are precursors of pre-VLDL and VLDL particles. VLDL secretion: Partially lipidated ApoB100 containing microsomes constitute naive VLDL particles in the ER. MTTP transfers triglycerides and phospholipids to the nascent VLDL to form pre-VLDL that are stabilized by ApoE.

Until 2013 the two Plin2 deficient mouse models remained the only viable options for work with Plin2 in an *in vivo* setting. After that, three additional Plin2 mouse models were reported. McManaman et al described a true Plin2 global knockout mouse that again prevented hepatic steatosis, but also protected mice from adipose tissue inflammation (*174*). While the study did not clarify the mechanism behind decreased hepatic TG content, an increase in PPAR-α and PPAR-γ was observed indicating lipolytic and β-oxidation gene activation (*174*). The second mouse model involving Plin2 was a Plin2-glycine N-methyltransferase (GNMT) double knockout. The ablation of Plin2 in this model relieved hepatic steatosis and inflammation present in the single GNMT knockout model (*175*). Interestingly, the decrease in hepatic steatosis and inflammation was attributed to an increase in PE being remodeled to form PC (*175*). By maintaining PC in the hepatic tissue of the Plin2 GNMT mice, VLDL secretion of TG was maintained, thus relieving the hepatic steatosis and inflammation found in the single knockout mouse (*175, 176*). A third Plin2 knock out mouse model was described in 2016 that was a liver specific Plin2 null mouse the details of which will be discussed in Chapter 4.

Plin2 expression is also associated with lipid accumulation and inflammation in macrophages, foam cells, and eosinophils where it is proposed to participate in eicosanoid and prostaglandin production (*4, 5, 10-13, 143*). Macrophages play an important role in the development and progression of atherosclerosis. An early event in atherosclerosis is the accumulation of lipids in lipid droplets where increased Plin2 expression is observed (*3, 4*). This effect can be induced in *ex vivo* experiments with LPS, oxidized LDL (oxLDL), or acetylated LDL treatment that leads to increased lipid

loading, lipid droplets, and Plin2 (*26, 143, 177, 178*). In addition, Plin2 mRNA is upregulated in human atherosclerotic plaques as compared to lesion-free areas in the same artery (*177*). Knockdown of Plin2 in macrophage models of atherosclerosis reversed lipid droplet formation and lipid loading along with inflammation markers such as TNFα, IL-6, and MCP-1 (*179*). Plin2 knockdown also increased lipid efflux from atherosclerotic plaques, reversing the damage done to mice by oxLDL treatment (*177*). In macrophages induced with LPS, oxLDL, or acetylated LDL, lipid droplets coated by Plin2 were shown to be the site of PGE_2, PGH_2, PGD_2, 5 HETE, 15-HETE, and TXA_2 propagating the inflammation response (*10, 180-185*).

Given the accumulating *in vivo* and *ex vivo* evidence that Plin2 facilitates lipid accumulation in liver and macrophages, it is increasingly important to understand the factors that regulate is expression and function. It has been shown that Plin2 gene expression is controlled by nuclear hormone receptors PPARα, PPARγ, and RXR in hepatocytes and PPARβ/δ in keratinocytes (*149, 165, 186*). PPAR response elements (PPRE) mapped in both the mouse and human to Plin2 promoter regions indicate PPARs induce Plin2 mRNA under a variety of conditions *(149, 165)*. These findings are significant because basal and anti-inflammatory conditions are associated with PPAR control of lipid metabolism enzymes. Under inflammatory conditions, displacement of PPARγ by p65 promoted increased expression of Plin2 (*20, 165*), COX2 (*25*), and TNFα (*187*) under inflammation conditions (*142*). Consistent with this, mice injected with LPS exhibited increased hepatic lipid accumulation and expression of Plin2 while expression of PPARα, RXR, and PPARγ were decreased (*142*). Moreover, enzymes involved in fatty acid synthesis and oxidation including fatty acid synthase, enoyl-CoA hydratase,

stearoylCoA desaturase, acyl-CoA dehydrogenase, acetyl-CoA carboxylase, and carnitine palmitoyl-transferase 1 that are direct targets of PPARα, RXR, and PPARγ were also decreased following LPS-induced inflammation (*142*). A closer examination of the cross talk between PPARs and p65 in keratinocytes demonstrated *in vivo* that p65/RelA repression of PPARδ in TNF-α stimulated cells increased lipid accumulation, Plin2, and cytokine expression (*188*) through a mechanism involving histone deacetylases (*188*). In contrast direct interactions of PPARγ with the p65 RelA region caused p65 to undergo ubiquitination and degradation, resulting in termination of NFκB signaling (*142, 188*).

LIPID DROPLETS AND MICRO-RNA REGULATION

MicroRNAs (miRNAs) are short endogenous RNA sequences consisting of 18-22 nucleotides that regulate gene expression by repressing or targeting mRNAs for degradation. An overview of how miRNAs are transcribed and processed to maturity is outlined in Figure 7. Currently, there are more than 2000 confirmed miRNAs encoded by various intergenic, intronic or exonic sequences in the human genome. It is estimated that these 2000 miRNAs target up to 60% of all human genes. These findings are significant as deregulation of miRNAs has been associated with altered lipid and glucose metabolism, oxidative stress, inflammation, fibrosis, and end stage liver disease. In addition, diet-induced obesity in mice results in approximately 6% of total miRNAs being differentially expressed. As a result of their influence, miRNAs have emerged as novel biomarkers and potential therapeutic targets. In terms of lipid droplet

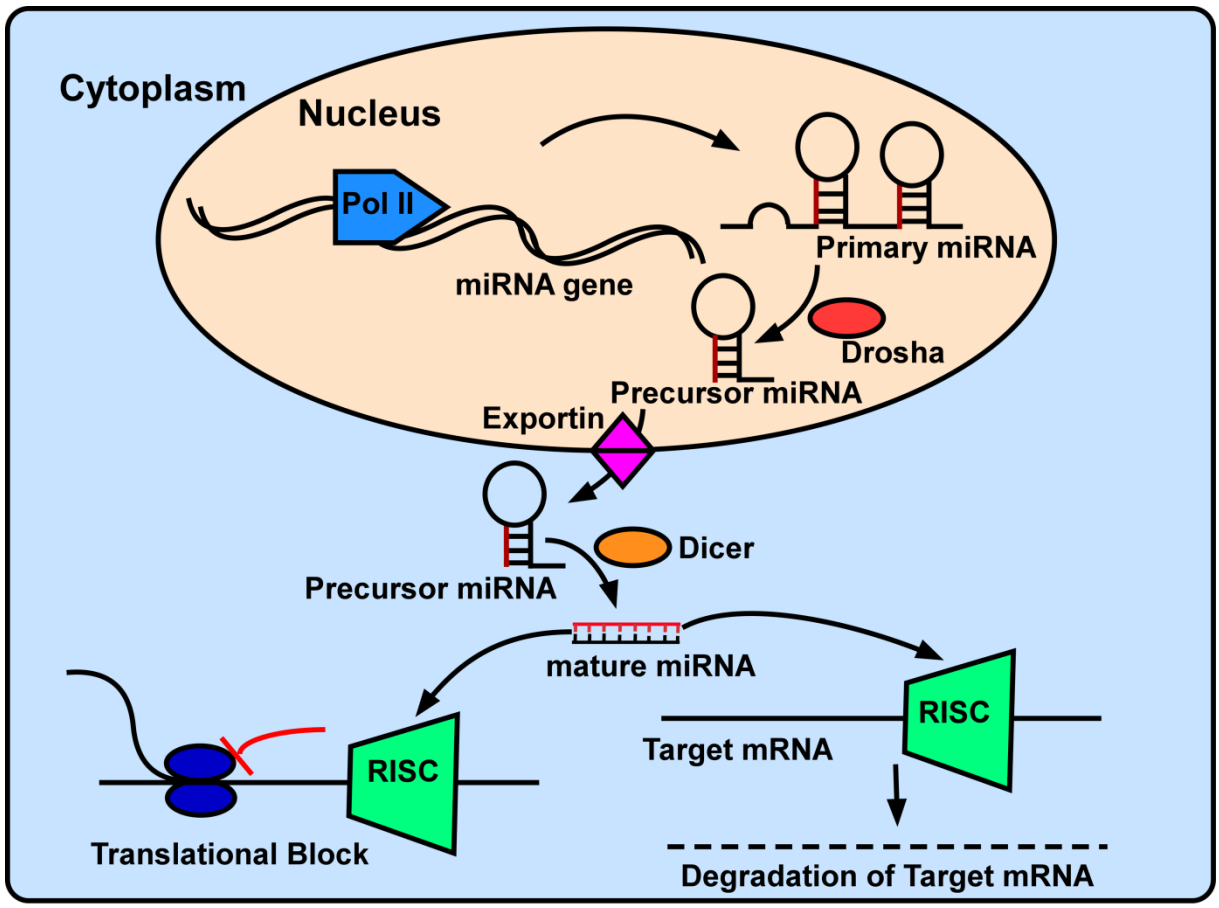

Figure 7. Biogenesis of miRNA. Transcription of miRNA is carried out by RNA Pol II in the nucleus. The initial transcript, known as the primary miRNA, contains hair-pin structures. The primary sequence is processed by Drosha creating the precursor miRNA. This precursor miRNA consists of a single hair-pin structure which can be exported to the cytoplasm by Exportin. In the cytoplasm, the precursor miRNA undergoes additional processing by Dicer. Dicer removes the hair-pin structure, creating double stranded mature miRNA 18-22 nucleotides in length. The mature miRNA duplex is unwound and loaded into the RISK complex which will target the 3'-UTR of mRNA. miRNA exert there gene regulator function via one of two pathways; translational blocking or mRNA degradation.

biology and Plin2, overexpression of miRNAs -215, -96, -124, -122, and -489 in primary mouse hepatocytes led to increased Plin2 levels and increased lipid droplet size and number (*30*). Conversely, cells overexpressing miRNAs –let7d, let7e, let7g, and -148a exhibited decreased Plin2 levels and cellular triglyceride content (*30*). In addition, miRNA-122 has been reported to stimulate the production of lipid droplets and cholesterol-rich caveolae, while inhibition of the miRNA increases lipolysis resulting in smaller lipid droplets. In another study, inhibition of PPARδ by miRNA-9 in M1 macrophages led to upregulation of Plin2, STAT1, and TNFα when cells were treated with LPS to induce inflammation (*31*). miRNA-155 was shown to modify the inflammatory capacity of macrophages by increasing lipid loading and promoting the formation of lipid droplet derived foam cells (*189*). THP-1 macrophages stimulated with oxLDL showed increased expression of miRNA-150, along with increased lipid loading and atherosclerosis (*101*). This work supported studies challenging miRNA-150 knockout mice with a high fat diet. The mice exhibited increased fat accumulation and decreased glucose tolerance and insulin sensitivity, along with increased expression of pro-inflammatory cytokines in adipose tissue (*143*). Studies with miRNA-21 showed increased expression when macrophages were treated with LPS to induce inflammation (*103*). When miRNA-21 was overexpressed by transfection, increased lipid accumulation and formation of lipid-laden foam cells was observed which was reversed when expression of miRNA-21 was silenced (*103*). Plin2 was not measured in these studies, however the close association of Plin2 with foam cell formation has been extensively reported (*3-5, 177*) and was likely part of the process. In the current thesis

we examine the effect of Plin2 ablation on miRNAs and discuss the results in depth in a later chapter.

CONCLUSION

Developing therapeutic strategies to treat the increasing number of obesity related diseases is dependent on identifying potential protein targets of intervention. Lipid droplets and their associated proteins play a critical role in maintaining lipid homeostasis and perturbations in their function dramatically impact human health. Therefore lipid droplets and their associated proteins are potential targets for the next generation of therapeutics. Plin2, a prominent hepatic lipid droplet protein that is associated with lipid accumulation (*64, 141, 166, 190*) and inflammation (*179, 191*) represents a significant target despite minimal information regarding its mechanism of action. Results outlined in the current thesis are expected to elucidate how Plin2's role in lipid droplet biology. Moreover, our goal was to identify Plin2's mechanism in promoting steatosis, inflammation, fibrosis, and cirrhosis. This contribution is significant because it represents the first steps towards reaching the ultimate goal of treating and curing obesity-driven diseases.

REFERENCES

REFERENCES

1. Walther, T. C., and Farese, R. (2012) Lipid droplets and cellular lipid metabolism, *Annu Rev Biochem 81*, 28.21-28.28.

2. Murphy, D. (2012) The dynamic roles of intracellular lipid droplets: from archaea to mammals, *Protoplasm 249*, 541-585.

3. Tangirala, R. K., Jerome, W. G., Jones, N. L., Small, D. M., Johnson, W. J., Glick, J. M., Mahlberg, F. H., and Rothblat, G. H. (1994) Formation of cholesterol monohydrate crystals in macrophage-derived foam cells, *J Lipid Res 35*, 93-104.

4. Llorent-Cortes, V., Royo, T., Juan-Babot, O., and Badimon, L. (2007) Adipocyte differentiation-related protein is induced by LRP1-mediated aggregated LDL internalization in human vascular smooth muscle cells and macrophages, *J Lipid Res 48*, 2133-2140.

5. Weibel, G. L., Joshi, M. R., Wei, C., Bates, S. R., Blair, I. A., and Rothblat, G. H. (2009) Lipoxygenase-1 associates with neutral lipid droplets in macrophage foam cells: evidence of lipid droplet metabolism, *J Lipid Res 50*, 2371-2376.

6. Day, C. P., and James, O. F. (1998) Steatohepatitis: a tale of two 'hits'?, *Gastroenterology 114*, 842-845.

7. Day, C. P. (2002) Pathogenesis of steatohepatitis., *Best Pract Res Clin Gastroenterol 16*, 663-678.

8. Wasmuth, H. E., Zaldivar, M. M., Beraza, N., and Trautwein, C. (2007) Of mice and NASH-from fat to inflammation and fibrosis, *Drug discov Today:Disease Models 4*, 25-30.

9. Anstee, Q. M., Targher, G., and Day, C. P. (2013) Progression of NAFLD to diabetes mellitus, cardiovascular disease or cirrhosis, *Natl Rev Gastroenterol Hepatol 10* 330-344.

10. Bozza, P. T., Yu, W., Penrose, J. F., Morgan, E. S., Dvorak, A. M., and Weller, P. F. (1997) Eosinophil lipid bodies: specific, inducible intracellular sites for enhanced eicosanoid formation., *J Exp Med 186*, 909-920.

11. Agarwal, S., Reddy, G. V., and Reddanna, P. (2009) Eicosanoids in inflammation and cancer: the role of COX-2, *Expert Review of Clinical Immunology 5*, 145-165.

12. Bozza, P. T., Baker-Abreu, I., Navarro-Xavier, R. A., and Bandeira-Melo, C. (2011) Lipid body function in eicosanoid synthesis: an update., *Prostaglandins Leukot Essent Fatty Acids 85*, 205-213.

13. Bandeira-Melo, C., Weller, P. F., and Bozza, P. T. (2011) Identifying intracellular sites of eicosanoid lipid mediator synthesis with EicosaCell assays, *Methods Mol Biol 717*, 277-289.

14. Martin, S., and Parton, R. G. (2006) Lipid droplets: A unified view of a dynamic organelle, *Nat Rev Mol Cell Biol 7*, 373-378.

15. Fujimoto, T., and Parton, R. G. (2011) Not just fat: The structure and function of the lipid droplet, *Cold Spring Harb Perspect Biol 3*, a004838.

16. Pol, A., Gross, S. P., and Parton, R. G. (2014) Review: biogenesis of the multifunctional lipid droplet: lipids, proteins, and sites, *J Cell Biol 204*, 635-646.

17. Farese, R. V., and Walther, T. C. (2009) Lipid droplets finally get a little R-E-S-P-E-C-T, *Cell 139*.

18. Wilfling, F., Wang, H., Haas, J., Krahmer, N., Bould, T., Uchida, A., Cheng, J.-X., Graham, M. J., Christiano, R., Frohlich, F., Liu, X., Buhman, K., Coleman, R., Bewersdorf, J., Farese, R., and Walther, T. (2013) Triacylglycerol synthesis enzymes mediate lipid droplet growth by relocalizing from the ER to lipid droplets., *Devel Cell 24*, 384-399.

19. Wilfling, F., Thiam, A., Olarte, M.-J., Wang, J., Beck, R., Gould, T., Allgeyer, E., Pincer, F., Bewersdorf, J., Farese, R., and Walther, T. (2014) Arf/COP1 machinery acts directly on lipid droplets and enables their connection to the ER for protein targeting, *eLife 3*, e01607 DOI: 01610.07554/eLife.01607.

20. Khatchadourian, A., Bourque, S., Richard, V., Titorenko, V., and Maysinger, D. (2012) Dynamics and regulation of lipid droplet formation in lipopolysaccharide (LPS)-stimulated microglia, *Biochimica et Biophysica Acta 1821*, 607-617.

21. Hope, R. G., Murphy, D., and McLauchlan, J. (2002) The domains required to direct core proteins of Hepatitis C virus and GB Virus-B to lipid droplets share common features with plant oleosin proteins, *J Biol Chem 277*, 4261-4270.

22. Shi, S. T., Polyak, S. J., Hong, T., Taylor, D., Gretch, D. R., and Lai, M. M. C. (2002) Hepatitis C virus NS5A colocalizes with the core protein on lipid droplets and interacts with apolipoproteins, *Virology 292*, 198-210.

23. Cheng, A., Chan, H., Leung, W., To, K., Go, M., Chan, L., Liew, C., and Sung, J. (2004) Expression of HBx and COX-2 in chronic hepatitits B, cirrhosis and

hepatocellular carcinoma:implication of HBx in up-regulation of COX-2., *Mod Pathol 17*, 1169-1179.

24. Cermelli, S., Ruggieri, A., Marrero, J., Ioannou, G., and Beretta, L. (2011) Circulating microRNAs in patients with chronic hepatitis C and non-alcoholic fatty liver disease., *PLoS One 6*, e23937.

25. Lands, W. (1958) Metabolism of glycerolipides; a comparison of lecithin and triglyceride synthesis, *J Biol Chem 231*, 883-888.

26. Rajala, M. W., and Scherer, P. E. (2003) The Adipocyte-at the crossroads of energy homeostasis, inflammation, and atherosclerosis, *Endocrinology 144*, 3765-3773.

27. Igal, R. A., and Coleman, R. A. (1996) Acylglycerol recycling from triacylglycerol to phospholipid, not lipase activity, is defective in neutral lipid storage disease fibroblasts, *J Biol Chem 271*, 16644-16651.

28. Dalen, K. T., Dahl, T., Holter, E., Arntsen, B., Londos, C., Sztalryd, C., and Nebb, H. I. (2007) LSDP5 is a PAT protein specifically expressed in fatty acid oxidizing tissues, *Biochimica et Biophysica Acta (BBA) - Molecular and Cell Biology of Lipids 1771*, 210-227.

29. Kassan, A., Herms, A., Fernández-Vidal, A., Bosch, M., Schieber, N. L., Reddy, B. J. N., Fajardo, A., Gelabert-Baldrich, M., Tebar, F., Enrich, C., Gross, S. P., Parton, R. G., and Pol, A. (2013) Acyl-CoA synthetase 3 promotes lipid droplet biogenesis in ER microdomains, *The Journal of Cell Biology 203*, 985-1001.

30. Doege, H., and Stahl, A. (2006) Protein-Mediated Fatty Acid Uptake: Novel Insights from In Vivo Models, *Physiology 21*, 259-268.

31. Ellis, J. M., Frahm, J. L., Li, L. O., and Coleman, R. A. (2010) Acyl-coenzyme A synthetases in metabolic control, *Current Opinion in Lipidology 21*, 212-217.

32. Rao, G. A., and Johnston, J. M. (1966) Purification and properties of triglyceride synthetase from the intestinal mucosa, *Biochimica et Biophysica Acta (BBA) - Lipids and Lipid Metabolism 125*, 465-473.

33. Xu, N., Zhang, S. O., Cole, R. A., McKinney, S. A., Guo, F., Haas, J. T., Bobba, S., Farese, R. V., and Mak, H. Y. (2012) The FATP1–DGAT2 complex facilitates lipid droplet expansion at the ER–lipid droplet interface, *The Journal of Cell Biology 198*, 895-911.

34. Eastman, S. W., Yassaee, M., and Bieniasz, P. D. (2009) A role for ubiquitin ligases and Spartin/SPG20 in lipid droplet turnover, *The Journal of Cell Biology 184*, 881-894.

35. Klemm, E. J., Spooner, E., and Ploegh, H. L. (2011) Dual Role of Ancient Ubiquitous Protein 1 (AUP1) in Lipid Droplet Accumulation and Endoplasmic Reticulum (ER) Protein Quality Control, *Journal of Biological Chemistry 286*, 37602-37614.

36. Milewska, M., McRedmond, J., and Byrne, P. C. (2009) Identification of novel spartin-interactors shows spartin is a multifunctional protein, *Journal of Neurochemistry 111*, 1022-1030.

37. Ost, A., Ortegren, U., Gustavsson, J., Nystrom, F. H., and Stralfors, P. (2005) Triacylglycerol is synthesized in a specific subclass of caveolae in primary adipocytes, *J Biol Chem 280*, 5-8.

38. Harris, C., Haas, J., Streeper, R., Stone, S., Kumari, M., Yang, K., Han, X., Brownell, N., Gross, R., Zechner, R., and Farese, R. (2011) DGAT enzymes are required for triacylglycerol synthesis and lipid droplets in adipocytes., *J Lipid Res 52*, 657-667.

39. Chang, T., Li, B.-L., Chang, C., and Urano, Y. (2009) Acyl-coenzyme A:cholesterol acyltransferases, *Am J Phys Endocrinol Metab 297*, E1-E9.

40. Yen, C.-L., Sonte, S., Koliwad, S., Harris, C., and Farese, R. (2008) DGAT enyzmes and triacylglycerol biosynthesis, *J Lipid Res 49*, 2293-2301.

41. Shi, S., and Cheng, D. (2009) Beyond triglyceride synthesis: the dynamic functional roles of MGAT and DGAT enzymes in energy metabolism, *Am J Physiol Endocrinol Metab 297*, E10-E18.

42. Wang, S., Lee, D., Gong, N., Schwerbrock, N., Mashek, D., Gonzalez-Baro, M., Stapleton, C., Li, L., Lewin, T., and Coleman, R. (2007) Cloning and functional characterization of a novel mitochondrial N-ethymaleimide-sensitive glycerol-3-phosphate acyltransferase (GPAT2), *Arch Biochem Biophys 465*, 347-358.

43. Gimeno, R., and Cao, J. (2008) Mammalian glycerol-3-phosphate acyltransferases: new genes for an old activity., *J Lipid Res 49*, 2079-2088.

44. Wendel, A., Lewin, T., and Coleman, R. (2009) Glycerol-3-phosphate acytransferases: Rate limiting enzymes of triacylglycerol biosynthesis, *Biochim Biophys Acta 1791*, 501-506.

45. Brasaemle, D., Bolios, G., Shapiro, L., and Wang, R. (2004) Proteomic analysis of proteins associated with lipid droplets of basal and lipolytically stimulated 3T3-L1 adipocytes, *J Biol Chem 279*, 46835-46842.

46. Yang, L., Ding, Y., Chen, Y., Zhang, S., Huo, C., Wang, Y., Yu, J., Zhang, P., Na, H., Zhang, H., Ma, Y., and Liu, P. (2012) The proteomics of lipid droplets: structure, dynamics, and function of the organelle conserved from bacteria to humans., *J Lipid Res 53*, 1245-1253.

47. Currie, E., Guo, X., Christiano, R., Chitraju, C., Kory, N., Harrison, K., Haas, J., Walther, T., and Farese, R. (2014) High confidence proteomic analysis of yeast LDs identifies addtional droplet proteins and reveals connections to dolichol synthesis and sterol acetylation, *J Lipid Res 55*, 1465-1477.

48. Wilfling, F., Wang, H., Haas, Joel T., Krahmer, N., Gould, Travis J., Uchida, A., Cheng, J.-X., Graham, M., Christiano, R., Fröhlich, F., Liu, X., Buhman, Kimberly K., Coleman, Rosalind A., Bewersdorf, J., Farese, Robert V., Jr., and Walther, Tobias C. Triacylglycerol Synthesis Enzymes Mediate Lipid Droplet Growth by Relocalizing from the ER to Lipid Droplets, *Developmental cell 24*, 384-399.

49. Chen, J.-S., Greenberg, A. S., and Wang, S.-M. (2002) Oleic acid-induced PKC isozyme translocation in RAW 264.7 macrophages, *Journal of Cellular Biochemistry 86*, 784-791.

50. Toker, A. (2005) The biology and biochemistry of diacylglycerol signalling, *EMBO rep 6*, 310-314.

51. Krahmer, N., Guo, Y., Wilfling, F., Hilger, M., Lingrell, S., Heger, K., Newman, H., Schmidt-Supprian, M., Vance, D., Mann, M., Farese, R., and Walther, T. (2011) Phosphatidylcholine synthesis for lipid droplet expansion is mediated by localized activation of CTP:Phosphocholine cytidylyltransferease, *Cell Metab 14*, 504-515.

52. Shekelle, R. B., Shryock, A. M., Lepper, O. P., Stamler, J., Liu, S., and Raynor, W. J. (1981) Diet, serum cholesterol, and death from coronary heart disease. The Western Electric study, *New Eng J Med 304*, 65-70.

53. Pol, A., Martin, S., Fernandez, M. A., Ingelmo-Torres, M., Ferguson, C., Enrich, C., and Parton, R. G. (2005) Cholesterol and fatty acids regulate dynamic caveolin trafficking through the Golgi complex and between the cell surface and lipid bodies, *Mol Biol Cell 16*, 2091-2105.

54. McIntosh, A. L., Storey, S. M., and Atshaves, B. P. (2010) Intracellular lipid droplets contain dynamic pools of sphingomyelin: ADRP binds phospholipids with high affinity, *Lipids 45*, 465-477. PMCID: PMC3065392

55. London, L., Kumar, A., Wall, R., Casey, P., O'Sullivan, O., Shanahan, F., Hill, C., Cotter, P., Fitzgerald, G., Ross, R., Caplice, N., and Stanton, C. (2014) Exopolysaccharide-producing probiotic Lactobacilli reduce serum cholesterol and modify enteric microbiota in ApoE-deficient mice., *J Nutr 144*, 1956-1962.

56. Chang, C., Dong, R., Miyazaki, A., Sakashita, N., Zhang, Y., Liu, J., Guo, M., Li, B.-L., and Chang, T.-Y. (2006) Human Acyl-CoA:cholesterol Acyltransferease (ACAT) and its potential as a target for pharmaceutical intervention against atherosclerosis, *Acta Biochimica et Biophysica Sinica 38*, 151-156.

57. Lafontan, M., and Langin, D. (2009) Lipolysis and lipid mobilization in human adipose tissue, *Prog Lipid Res 48*, 275-297.

58. Ahmadian, M., Duncan, R. E., and Sul, H. S. (2009) The skinny on fat: lipolysis and fatty acid utilization in adipocytes, *Trends Endocrin Metab 20*, 424-428.

59. Zimmerman, R., Lass, A., Haemmerle, G., and Zechner, R. (2009) Fate of fat: The role of adipose triglyceride lipase in lipolysis, *Biochim Biophys Acta 1791*, 494-500.

60. Brasaemle, D. L. (2010) Lipolysis control: The plot thickens, *Cell Metab 11*, 173-174.

61. Zechner, R., Zimmerman, R., Eichmann, T., Kohlwein, S., Haemmerle, G., Lass, A., and Madeo, F. (2012) Fat Signals- Lipases and lipolysis in lipid metabolism and signaling, *Cell Metab 15*, 279-291.

62. Lass, A., Zimmermann, R., Haemmerle, G., Riederer, M., Schoiswohl, G., Schweiger, M., Kienesberger, P., Strauss, J. G., Gorkiewicz, G., and Zechner, R. (2006) Adipose triglyceride lipase-mediated lipolysis of cellular fat stores is activated by CGI-58 and defective in Chanarin-Dorfman Syndrome, *Cell Metabolism 3*, 309-319.

63. Schweiger, M., Schreiber, R., Haemmerle, G., Lass, A., Fledelius, C., Jacobsen, P., Tomqvist, H., Zechner, R., and Zimmermann, R. (2006) Adipose triglyceride lipase and hormone-sensitive lipase are the major enzymes in adipose tissue triacylglycerol catabolism, *J Biol Chem 281*, 40236-40241.

64. Listenberger, L. L., Ostermeyer-Fay, A. G., Goldberg, E. B., Brown, W. J., and Brown, D. A. (2007) Adipocyte differentiation-related protein reduces the lipid droplet association of adipose triglyceride lipase and slows triacyglycerol turnover, *J Lipid Res 48*, 2751-2761.

65. Miyoshi, H., Perfield, J. W., Souza, S. C., Shen, W. J., Zhang, H. H., Stancheva, Z. S., Kraemer, F. B., Obin, M. S., and Greenberg, A. S. (2007) Control of adipose triglyceride lipase action by serine 517 of perilipin A globally regulates protein kinase A-stimulated lipolysis in adipocytes, *J.Biol.Chem. 282*, 996-1002.

66. Brasaemle, D. L., Levin, D. M., Adler-Wailes, D. C., and Londos, C. (2000) The lipolytic stimulation of 3T3-L1 adipocytes promotes the translocation of hormone-

sensitive lipase to the surfaces of lipid droplets, *Biochim.Biophy.Acta 1483*, 251-262.

67. Grober, J., Lucas, S., Sorhede-Winzell, M., Zaghini, M., Mairal, A., Contreras, J., Besnard, P., Holm, C., and Langin, D. (2003) Hormone-sensitive lipase is a cholesterol esterase of the intestinal mucosa, *J Biol Chem 278*, 6510-6515.

68. Miyoshi, H., Souza, S. C., Zhang, H. H., Strissel, K. J., Christoffolete, M. A., Kovsan, J., Rudich, A., Kraemer, F. B., Bianco, A. C., Obin, M. S., and Greenberg, A. S. (2006) Perilipin promotes hormone-sensitive lipase-mediated adipocyte lipolysis via phosphorylation-dependent and -independent mechanisms, *J.Biol.Chem. 281*, 15837-15844.

69. Greenberg, A. S. (1993) Isolation of cDNAs for perilipins A and B:sequence and expression of lipid droplet-associated proteins of adipocytes, *Proc.Natl.Acad Sci USA 90*, 12035-12039.

70. Servetnick, D. A., Brasaemle, D. L., Gruia-Gray, J., Kimmel, A. R., Wolff, J., and Londos, C. (1995) Perilipins are associated with cholesteryl ester droplets in steroidogenic adrenal cortical and leydig cells, *J.Biol.Chem. 270*, 16970-16973.

71. Souza, A. C., de Vargas, L. M., Yamamoto, M. T., Lien, P., Franciosa, M. D., Moss, L. G., and Greenberg, A. S. (1998) Overexpression of perilipin A and B blocks the ability of tumor necrosis factor alpha to increase lipolysis in 3T3-L1 adipocytes, *J.Biol.Chem. 273*, 24665-24669.

72. Londos, C., Brasaemle, D. L., Schultz, C. J., Segrest, J. P., and Kimmel, A. R. (1999) Perilipins, ADRP, and other proteins that associate with intracellular neutral lipid droplets in animal cells, *Cell Dev Biol 10*, 51-58.

73. Martinez-Botas, J., Anderson, J. B., Tessier, D., Lapillonne, A., Chang, B. H., Quast, M. J., Gorenstein, D., Chen, K. H., and Chan, L. (2000) Absence of perilipin results in leanness and reverses obesity in Lepr dbdb mice, *Nature Genetics 26*, 474-479.

74. Tansey, J. T., Sztalryd, C., Gruia-Gray, J., Roush, D. L., Zee, J. V., Gavrilova, O., Reitman, M. L., Deng, C. X., Li, C., Kimmel, A. R., and Londos, C. (2002) Perilipin ablation results in a lean mouse with aberrant adipocyte lipolysis, enhanced leptin production, and resistance to diet-induced obesity, *Proc Natl Acad Sci USA 98*, 6494-6499.

75. Garcia, A., Sekowski, A., Subramanian, V., and Brasaemle, D. (2003) The central domain is required to target and anchor Perilipin A to lipid droplets, *J Biol Chem 278*, 625-635.

76. Tansey, J. T., Huml, A. M., Vogt, R., Davis, K. E., Jones, J. M., Fraser, K. A., Brasaemle, D. L., Kimmel, A. R., and Londos, C. (2003) Functional studies on native and mutated forms of perilipins. A role in protein kinase A-mediated lipolysis of triacylglycerols in Chinese hamster ovary cells, *J Biol Chem 278*, 8401-8406.

77. Subramanian, V., Garcia, A., Sekowski, A., and Brasaemle, D. L. (2004) Hydrophobic sequences target and anchor perilipin A to lipid droplets., *J Lipid Res 45*, 1983-1991.

78. Subramanian, V., Rothenberg, A., Gomez, C., Cohen, A., Garcia, A., Bhattacharyya, S., Shapiro, L., Dolios, G., Wang, R., Lisanti, M., and Brasaemle, D. (2004) Perilipin A mediates the reversible binding of CGI-58 to lipid droplets in 3T3-L1 adipocytes, *J Biol Chem 279*, 42062-42071.

79. Brasaemle, D. L. (2007) The perilipin family of stuctural lipid droplet proteins:stabilization of lipid droplets and control of lipolyis, *J Lipid Res 48*, 2547-2559.

80. Granneman, J. G., Moore, H. P. H., Krishnamoorthy, R., and Rathod, M. (2009) Perilipin control lipolysis by regulating the interactions of AB-hydrolase containing 5 (Abhd5) and adipose triglyceride lipase (Atgl), *J Biol Chem 284*, 34538-34544.

81. Brasaemle, D. L., Subramanian, V., Garcia, A., Marcinkiewicz, A., and Rothenberg, A. (2009) Perilipin A and the control of triacylglycerol metabolism, *Mol Cell Biochem 326*, 15-21.

82. Sun, Z., Gong, J., Wu, H., Xu, W., Wu, L., Xu, D., Gao, J., Wu, J. W., Yang, H., Yang, M., and Li, P. (2013) Perilipin 1 promotes unilocular lipid droplet formation through the activation of FSP27 in adipocytes., *Nature Commun 4*, 1594.

83. Aboulaich, N., Vener, A. V., and Stralfors, P. (2006) Hormonal control of reversible translocation of perilipin B to the plasma membrane in primary human adipocytes, *J Biol Chem 281*, 11446-11449.

84. Gao, J., and Serrero, G. (1999) Adipose differentiation related protein (ADRP) expressed in transfected COS-7 cells selectively stimulates long chain fatty acid uptake, *J Biol Chem 274*, 16825-16830.

85. Ehrenborg, E., Aminoff, A., Perman, J., Mannila, M. N., Magne, J., Neville, M., Karpe, F., and Boren, J. (2012) A missense polymorphism in perilipin 2 (Plin2) disrupts an α-helix, affects the lipolysis, and is associated with reduced plasma triglyceride concentration in humans., *FASEB meeting: Metabolic consequences of the storage of neutral lipids. July 22-27*.

86. Magne, J., Aminoff, A., Sundelin, J., Mannila, M. N., Gustafsson, P., Hultenby, K., Wernerson, A., Bauer, G., Listenberger, L. L., Neville, M., Karpe, F., Boren, J., and Ehrenborg, E. (2013) The minor allele of the missense polymorphism Ser251Pro in perilipin 2 (PLIN2) disrupts an α-helix, affect lipolysis, and is associated with reduced plasma tryglyceride concentration in humans, *FASEB J 27*, 3090-3099.

87. Kaushik, S., and Cuervo, A. (2015) Degradation of lipid droplet-associated proteins by chaperone-mediated autophagy facilitates lipolysis., *Nature Cell Biol 17*, 759-770.

88. Kaushik, S., and Cuervo, A. M. (2016) AMPK-dependent phosphorylation of lipid droplet protein PLIN2 triggers its degradation by CMA, *Autophagy 12*, 432-438.

89. Lands, W. E. M. (2000) Stories about acyl chains, *Biochimica et Biophysica Acta (BBA) - Molecular and Cell Biology of Lipids 1483*, 1-14.

90. Payne, F., Lim, K., Girousse, A., Brown, R., Kory, N., Robbins, A., Xue, Y., Sleigh, A., Cochran, E., Adams, C., Dev Borman, A., Russel-Jones, D., BGorden, P., Semple, R., Saudek, V., O'Rahilly, S., Walther, T., Barroso, I., and Savage, D. (2014) Mutations disrupting the Kennedy phophatidylcholine pathway in humans with congenital lipodystrophy and fatty liver disease., *PNAS 111*, 8901-8906.

91. HENNEBERRY, A. L., and McMASTER, C. R. (1999) Cloning and expression of a human choline/ethanolaminephosphotransferase: synthesis of phosphatidylcholine and phosphatidylethanolamine, *Biochemical Journal 339*, 291-298.

92. Kennedy, E. P., and Weiss, S. B. (1956) THE FUNCTION OF CYTIDINE COENZYMES IN THE BIOSYNTHESIS OF PHOSPHOLIPIDES, *Journal of Biological Chemistry 222*, 193-214.

93. Kent, C. (1995) Eukaryotic Phospholipid Biosynthesis, *Annual Review of Biochemistry 64*, 315-343.

94. Hjelmstad, R. H., Morash, S. C., McMaster, C. R., and Bell, R. M. (1994) Chimeric enzymes. Structure-function analysis of segments of sn-1,2-diacylglycerol choline- and ethanolaminephosphotransferases, *Journal of Biological Chemistry 269*, 20995-21002.

95. Henneberry, A. L., Wistow, G., and McMaster, C. R. (2000) Cloning, Genomic Organization, and Characterization of a Human Cholinephosphotransferase, *Journal of Biological Chemistry 275*, 29808-29815.

96. Vance, D. E. (2013) Physiological roles of phosphatidylethanolamine N-methyltransferase, *Biochimica et Biophysica Acta (BBA) - Molecular and Cell Biology of Lipids 1831*, 626-632.

97. du Vigneaud, V., Cohn, M., Chandler, J. P., Schenck, J. R., and Simmonds, S. (1974) The Utilization of the Methyl Group of Methionine in the Biological Synthesis of Choline and Creatine, *Nutrition Reviews 32*, 144-146.

98. STETTEN Jr, D. (1941) Biological relationships of choline, ethanolamine, and related compounds, *Journal of Biological Chemistry 140*, 143-152.

99. Bremer, J., Figard, P. H., and Greenberg, D. M. (1960) The biosynthesis of choline and its relation to phospholipid metabolism, *Biochimica et Biophysica Acta 43*, 477-488.

100. Bremer, J., and Greenberg, D. M. (1961) Methyl transfering enzyme system of microsomes in the biosynthesis of lecithin (phosphatidylcholine), *Biochimica et Biophysica Acta 46*, 205-216.

101. Nakanishi, H., Shindou, H., Hishikawa, D., Harayama, T., Ogasawara, R., Suwabe, A., Taguchi, R., and Shimizu, T. (2006) Cloning and characterization of mouse lung-type acyl-CoA: lysophosphatidylcholine acyltransferase 1 (LPCAT1) Expression in alveolar type II cells and possible involvement in surfactant production, *Journal of Biological Chemistry 281*, 20140-20147.

102. Soupene, E., and Kuypers, F. A. (2008) Mammalian long-chain acyl-CoA synthetases., *Exp Biol Med 233*, 507-521.

103. Soupene, E., and Kuypers, F. A. (2012) Phosphatidylcholine formation by LPCAT1 is regulated by Ca2+ and the redox status of the cell, *BMC biochemistry 13*, 8.

104. Khan, S. A., Wollaston-Hayden, E. E., Markowski, T. W., Higgins, L., and Mashek, D. G. (2015) Quantitative analysis of the murine lipid droplet-associated proteome during diet-induced hepatic steatosis, *Journal of Lipid Research 56*, 2260-2272.

105. Bartz, R., Zehmer, J. K., Zhu, M., Chen, Y., Serrero, G., Zhao, Y., and Liu, P. (2007) Dynamic activity of Lipid droplets: Protein phosphorylation and GTP-mediated protein translocation, *J Proteome Res 6*, 3256-3265.

106. Xie, X., Yi, Z., Bowen, B., Wolf, C., Flynn, C. R., Sinha, S., Mandarino, L. J., and Meyer, C. (2010) Characterization of the human adipocyte proteome and reproducibility of protein abundance by one-dimensional gel electrophoresis and HPLC-ESI-MS/MS, *J Proteome Res 9*, 4521-4534.

107. Zhang, H., Wang, Y., Li, J., Yu, J., Pu, J., Li, L., Zhang, H., Zhang, S., Peng, G. Y., F., and Liu, J. (2011) Proteome of skeletal muscle lipid droplet reveals association with mitochondria and apolipoprotein A-I, *J Proteome Res 10*, 4757-4768.

108. Forster, L. J., de Hoog, C. L., and Mann, M. (2003) Unbiased quantitative proteomics of lipid rafts reveals high specificity for signaling factors, *Proceedings of the National Academy of Sciences of the United States of America 100*, 5813-5818.

109. Lin, S.-C., and Li, P. (2004) CIDE-A, a novel link between brown adipose tissue and obesity, *Trends in molecular medicine 10*, 434-439.

110. Li, J., Ye, J., Xue, B., Qi, J., Zhang, J., Zhou, Z., Li, Q., Wen, Z., and Li, P. (2007) Cideb regulates diet-induced obesity, liver steatosis, and insulin sensitivity by controlling lipogenesis and fatty acid oxidation, *Diabetes 56*, 2523-2532.

111. Puri, V., Ranjit, S., Konda, S., Nicoloro, S. M. C., Straubharr, J., Chawla, A., Chouinard, M., Lin, C., Burkart, A., Corvera, S., Perugini, R. A., and Czech, M. P. (2011) Cidea is associated with lipid droplets and insulin sensitivity in humans. , *Proc Natl Acad Sci USA 105*, 7833-7838.

112. Toh SY, Gong J, Du G, Li JZ, Yang S, Ye J, Yao H, Zhang Y, Xue B, Li Q, Yang H, Wen Z, and P, L. (2008) Up-regulation of mitochondrial activity and acquirement of brown adipose tissue-like property in the white adipose tissue of FSP27 deficient mice., *PLoS ONE 3*, e2890.

113. Puri, V., Virbasius, J. V., Guilherme, A., and Czech, M. P. (2008) RNAi screens reveal novel metabolic regulators:RIP140, MAP4k4, and the lipid droplet asociated fat specific protein (FSP) 27., *Act Physiol 192*, 103-115.

114. Nishino, N., Tamori, Y., Tateya, S., Kawaguchi, T., Shibakusa, T., Mizunova, W., Inoue, K., Kitazawa, R., Matusuki, Y., Hiramatsu, R., Masubuchi, S., Omachi, A., Kumura, K., Siaito, M., Amo, T., Ohta, S., Yamaguchi, T., Osumi, T., Cheng, J., Fujimoto, T., Nakao, H., Nakao, K., Aiba, A., Okamura, H., Fushiki, T., and Kasuga, M. (2008) FSP27 contributes to efficient energy storage in murine white adipocytes by promoting the formation of unilocular lipid droplets., *J Clin Invest 118*, 2808-2821.

115. Gong, J., Sun, Z., and Li, P. (2009) CIDE proteins and metabolic disorders, *Current Opinion in Lipidology 20*, 121-126.

116. Jambunathan S, Yin J, Khan W, Tamori Y, and Puri V. (2011) FSP27 promotes lipid droplet clustering and then fusion to regulate triglyceride accumulation, *PLoS ONE 6*, e28614.

117. Gong, J., Sun, Z., Wu, L., Xu, W., Schieber, N., Xu, D., Shui, G., Yang, H., Parton, R. G., and Li , P. (2011) FSP27 promotes lipid droplet growth by lipid exchange and transfer at lipid droplet contact sites., *J Cell Biol 195*, 953-963.

118. Pilch, P. F., and Liu, L. (2011) Fat caves: caveolae, lipid trafficking and lipid metabolism in adipocytes, *Trends in endocrinology and metabolism: TEM 22*, 318-324.

119. Schnitzer, J. E., Oh, P., and McIntosh, D. P. (1996) Role of GTP hydrolysis in fission of caveolae directly from plasma membranes, *Science 274*, 239-242.

120. Blouin, C., Le Lay, S., Eberl, A., Kofeler, H., Guerrera, I., Klein, C., Le Liepvre, X., Lasnier, F., Bourron, O., Gautier, J.-F., Ferre, P., hajduch, E., and Dugail, I. (2010) Lipid droplet analysis in caveolin-deficient adipocytes: alterations in surface phopholipid composition and maturation defects., *J Lipid Res 51*, 945-956.

121. Boscher, C., and Nabi, I. R. (2012) Caveolin-1: role in cell signaling, *Advances in experimental medicine and biology 729*, 29-50.

122. Martin, S. (2013) Caveolae, lipid droplets, and adipose tissue biology: pathophysiological aspects., *Horm Mol Biol Clin Investig 15*, 11-18.

123. Trigatti, B. L., Anderson, R. G., and Gerber, G. E. (1999) Identification of caveolin-1 as a fatty acid binding protein, *Biochemical and biophysical research communications 255*, 34-39.

124. Storey, S. M., McIntosh, A. L., Senthivinayagam, S., Moon, K. C., and Atshaves, B. P. (2011) The phospholipid monolayer associated with perilipin-enriched lipid droplets is a highly organized rigid membrane structure, *Am J Physiol Endocrinol Metab 301*, E991-E1003. PMCID: PMC3213997.

125. (2014) Metabolism: Caveolae influence lipid droplet storage in adipocytes via expression of caveolin-1 and cavins, *Nat Rev Endocrinol 10*, 512-512.

126. Smart, E. J., and van der Westhuyzen, D. R. (1998) Scavenger receptors, caveolae, caveolin, and cholesterol trafficking, In *Intracellular Cholesterol Trafficking* (Chang, T. Y., and Freeman, D. A., Eds.), pp 253-272, Kluwer Academic Publishers, Boston.

127. Silver, D. (2004) SRB1 and protein-protein interactions in hepatic high density lipoprotein metabolism, *Rev Endocr Metab Disord 5*, 327-333.

128. DiStefano, M. T., Danai, L. V., Roth Flach, R. J., Chawla, A., Pedersen, D. J., Guilherme, A., and Czech, M. P. (2015) The Lipid Droplet Protein Hypoxia-

inducible Gene 2 Promotes Hepatic Triglyceride Deposition by Inhibiting Lipolysis, *Journal of Biological Chemistry 290*, 15175-15184.

129. Gimm, T., Wiese, M., Teschemacher, B., Deggerich, A., Schödel, J., Knaup, K. X., Hackenbeck, T., Hellerbrand, C., Amann, K., Wiesener, M. S., Höning, S., Eckardt, K.-U., and Warnecke, C. (2010) Hypoxia-inducible protein 2 is a novel lipid droplet protein and a specific target gene of hypoxia-inducible factor-1, *The FASEB Journal 24*, 4443-4458.

130. Rankin, E. B., Rha, J., Selak, M. A., Unger, T. L., Keith, B., Liu, Q., and Haase, V. H. (2009) Hypoxia-Inducible Factor 2 Regulates Hepatic Lipid Metabolism, *Molecular and cellular biology 29*, 4527-4538.

131. Qu, A., Taylor, M., Xue, X., Matsubara, T., Metzger, D., Chambon, P., Gonzalez, F. J., and Shah, Y. M. (2011) Hypoxia-inducible transcription factor 2α promotes steatohepatitis through augmenting lipid accumulation, inflammation, and fibrosis, *Hepatology 54*, 472-483.

132. Shen, G., Ning, N., Zhao, X., Liu, X. I., Wang, G., Wang, T., Zhao, R. A. N., Yang, C., Wang, D., Gong, P., Shen, Y. A. N., Sun, Y., Zhao, X., Jin, Y., Yang, W., He, Y. A. N., Zhang, L. E. I., Jin, X., and Li, X. (2015) Adipose differentiation-related protein is not involved in hypoxia inducible factor-1-induced lipid accumulation under hypoxia, *Molecular Medicine Reports 12*, 8055-8061.

133. Qiu, B., Ackerman, D., Sanchez, D. J., Li, B., Ochocki, J. D., Grazioli, A., Bobrovnikova-Marjon, E., Diehl, J. A., Keith, B., and Simon, M. C. (2015) HIF2α-Dependent Lipid Storage Promotes Endoplasmic Reticulum Homeostasis in Clear-Cell Renal Cell Carcinoma, *Cancer Discovery 5*, 652-667.

134. Pereira, E. R., Frudd, K., Awad, W., and Hendershot, L. M. (2013) ER stress and hypoxia response pathways interact to potentiate HIF-1 transcriptional activity on targets like VEGF, *Journal of Biological Chemistry*.

135. Robenek, H., Robenek, M. J., and Troyer, D. (2005) PAT family proteins pervade lipid droplet cores, *J Lipid Res 46*, 1331-1338.

136. Robenek, H., Robenek, M. J., Buers, I., Lorkowski, S., Hofnagel, O., Troyer, D., and Severs, N. J. (2005) Lipid droplets gain PAT family proteins by interaction with specialized plasma membrane domains, *J Biol Chem 280*, 26330-26338.

137. Bickel, P. E., Tansey, J. T., and Welte, M. A. (2009) PAT proteins, an ancient family of lipid droplet proteins that regulate cellular lipid stores, *Biochim Biophys Acta 1791*, 419-440.

138. Patel, S., Yang, W., Kozusko, K., Saudek, V., and Savage, D. (2014) Perilipins 2 and 3 lack a carboxy-terminal domain present in perilipin1 involved in

sequestering ABHD5 and supressing basal lipolysis, *Proc Natl Acad Sci USA 111*, 9163-9168.

139. Wang, H., Sreenevasan, U., Hu, H., Saladino, A., Polster, B. M., Lund, L. M., Gong, D. W., Stanley, W. A., and Sztalryd, C. (2011) Perilipin 5, a lipid droplet-associated protein, provides physical and metabolic linkage to mitochondria, *J Lipid Res 52*, 2159-2168.

140. Imamura, M., Inoguchi, T., Ikuyma, S., Taniguchi, S., Kobayashi, K., Nakashima, N., and Nawata, H. (2002) ADRP stimulates lipid accumulation and lipid droplet formation in murine fibroblasts, *Am J Physiol Endocrinol Metab 283*, E775-E783.

141. Fukushima, M., Enjoji, M., Kohjima, M., Sugimoto, R., Ohta, S., Kotoh, K., Kuniyoshi, M., Kobayashi, K., Imamura, M., Inoguchi, T., Nakamuta, M., and Nawata, H. (2005) Adipose differentiation related protein induces lipid accumulation and lipid droplet formation in hepatic stellate cells, *In Vitro Cell Dev Biol Anim 41*, 321-324.

142. Ohhira, M., Motomura, W., Fukuda, M., Yoshizaki, T., Takahashi, N., Tanno, S., Wakamiya, N., Kohgo, Y., Kumei, S., and Okumura, T. (2007) Lipopolysaccharide induces adipose differentiation-related protein expression and lipid accumulation in the liver through inhibition of fatty acid oxidation in mice, *Journal of Gastroenterology 42*, 969-978.

143. Wang, J., Si, Y., Wu, C., Sun, L., Ma, Y., Ge, A., and Li, B. (2012) Lipopolysaccharide promotes lipid accumulation in human adventitial fibroblasts via TLR4-NF-κB pathway, *Lipids in Health and Disease 11*, 139-139.

144. Chang, B. H., Li, L., Saha, P., and Chan, L. (2010) Absence of adipose differentiation related protein upregulates hepatic VLDL secretion, relieves hepatosteatosis, and improves whole body insulin resistance in leptin-deficient mice, *J Lipid Res 51*, 2132-2142.

145. Magnusson, B., Asp, L., Bostrom, P., Ruiz, M., Stillemark-Billton, P., Linden, D., Boren, J., and Olofsson, S. (2006) Adipocyte differentiation-related protein promotes fatty acid storage in cytosolic triglycerides and inhibits secretion of very low-dnesity lipoproteins, *Arterio Throm Vasc Biol 26*, 1566-1571.

146. Miura, S., Gan, J. w., Brzostowski, J., Parisi, M. J., Schultz, C. J., Londos, C., Oliver, B., and Kimmel, A. R. (2002) Functional conservation for lipid storage droplet association among perilipin, ADRP, and TIP47 (PAT)-related proteins in mammals, Drosophila, and dictyostelium, *J Biol Chem 277*, 32253-32257.

147. Bulankina, A., Deggerich, A., Wenzel, D., Mutenda, K., Wittmann, J., Rudolph, M., Burger, K., and Honing, S. (2009) TIP47 functions in the biogenesis of lipid droplets., *J Cell Biol 185*, 641-655.

148. Chen, W., Chang, B., Wu, X., Li, L., Sleeman, M., and Chan, L. (2013) Inactivation of Plin4 downregulates Plin5 and reduces cardiac lipid accumulation in mice., *Am J Physiol Endocrinol Metab 304*, E770-E779.

149. Dalen, K. T., Ulven, S. M., Arnsten, B. M., Solaas, K., and Nebb, H. I. (2006) PPARalpha activators and fasting induce the expression of adipose differentiation-related protein in liver, *J Lipid Res 47*, 931-943.

150. Brasaemle DL, and NE, W. (2012) Packaging of fat: An evolving model of lipid droplet assembly and expansion, *J Biol Chem 287*, 2273-2279.

151. Kimmel, A. R., Brasaemle, D. L., McAndrews-Hill, M., Sztalryd, C., and Londos, C. (2010) Adoption of PERILIPIN as a unifying nomenclature for the mammalian PAT-family of intracellular lipid storage droplet proteins, *J Lipid Res 51*, 468-471.

152. Wolins, N., Quaynor, B., Skinner, J., Tzekov, A., Croce, M., Gropler, M., Varma, V., Yao-Borengasser, A., Rasouli, N., Kern, P., Finck, B., and Bickel, P. (2006) OXPAT/PAT-1 is a PPAR-induced lipid droplet protein that promotes fatty acid utilization, *Diabetes 55*, 3418-3428.

153. Granneman, J. G., Moore, H. P., Mottillo, E. P., Zhu, Z., and Zhou, L. (2011) Interactions of perilipin-5 (plin5) with adipose triglyceride lipase, *J Biol Chem 286*, 5126-5135.

154. Bosma, M., Sparks, L., Hooiveld, G. J., Jorgensen, J. A., Houten, S. M., Schrauwen, P., Kersten, S., and Hesselink, M. K. (2013) Overexpression of Plin5 in skeletal muscle promotes oxidative gene expression and intrayocellular lipid content without compromising insulin sensitivity, *Biochim Biophys Acta 1831*, 844-852.

155. Kurmoto, K., Okamura, T., Yamaguchi, T., Nakamura, T. Y., Wakabayashi, S., Morinaga, H., Nomura, M., Yanase, T., Otsu, K., Usuda, N., Matsumura, S., Inoeu, K., Fushiki, T., Kojima, Y., Hashimoto, T., Sakai, F., Hirose, F., and Osumi, T. (2012) Perilipin 5, a lipid droplet-binding protein, protects heart from oxidative burden by sequestering fatty acid from excessive oxidation., *J Biol Chem 287*, 23852-23863.

156. Wang, C., Zhao, Y., Gao, X., Li, L., Yuan, Y., Liu, F., Zhang, L., Wu, J., Hu, P., Zhang, X., Gu, Y., Xu, Y., Li, Z., Zhang, H., and Ye, J. (2014) Perilipin 5 improves hepatic lipotoxicity by inhibiting lipolysis, *Hepatology In Press*.

157. Minnaard, R., Scrauwen, P., Schaart, G., Jorgensen, J. A., Lenaers, E., Mensink, M., and Hesselink, M. K. C. (2009) Adipocyte differentiation-related protein and OXPAT in rat and human skeletal muscle: Involvement in lipid accumulation and type 2 diabetes mellitus, *J Clin Endocrinol Metab 94*, 4077-4085.

158. Mohktar, R. A. M., Montgomery, M. K., Murphy, R. M., and Watt, M. J. (2016) Perilipin 5 is dispensable for normal substrate metabolism and in the adaptation of skeletal muscle to exercise training, *American Journal of Physiology - Endocrinology and Metabolism*.

159. Ramos, S. V., Turnbull, P. C., MacPherson, R. E. K., LeBlanc, P. J., Ward, W. E., and Peters, S. J. (2015) Changes in mitochondrial perilipin 3 and perilipin 5 protein content in rat skeletal muscle following endurance training and acute stimulated contraction, *Experimental Physiology 100*, 450-462.

160. Jiang, H. P., and Serrero, G. (1992) Isolation and characterization of a full-length cDNA coding for an adipose differentiation-related protein, *Proc Natl Acad Sci USA 89*, 7856-7860.

161. Jiang, H.-P., Harris, S., and Serrero, G. (1992) Molecular cloning of a differentiation-related mRNA in the adipogenic cell line 1246, *Cell Growth Diff 3*, 21-30.

162. Brasaemle, D. L., Barber, T., Wolins, N., Serrero, G., Blanchette-Mackie, E. J., and Londos, C. (1997) Adipose differentiation-related protein is an ubiquitously expressed lipid storage droplet-associated protein, *J Lipid Res 38*, 2249-2263.

163. Gao, G., Ye, H., and Serrero, G. (2000) Stimulation of adipose differentiation related protein (ADRP) expression in adipocyte precursors by long-chain fatty acids, *J Cellular Physiol 182*, 297-302.

164. Varela, G. M., Antwi, D. A., Dhir, R., Yin, X., Singhal, N. S., Graham, M. J., Crook, R. M., and Ahima, R. S. (2008) Inhibition of ADRP prevents diet-induced insulin resistance, *Am J Physiol Gastro Liver Physiol 295*, G621-G628.

165. Fan, B., Ikuyama, S., Gu, J. Q., Oyama, J., Wei, P., Inoguchi, T., and Nishimura, J. (2009) Oleic acid-induced ADRP expression requires both AP-1 and PPAR response elements, and is reduced by psycnogenol through mRNA degradation in NMuLi liver cells, *Am J Physiol Endocrinol Metab 297*, E112-E123.

166. Larigauderie, G., Cuaz-Perolin, C., Younes, A. B., Furman, C., Lasselin, C., Copin, C., Jaye, M., Fuchart, J. C., and Rouis, M. (2006) Adipophilin increases triglyceride storage in human macrophages by simulation of biosynthesis and inhibition of beta-oxidation, *FEBS J 273*, 3498-3510.

167. Sletten, A., Seline, A., Rudd, A., Logsdon, M., and Listenberger, L. L. (2014) Surface features of the lipid droplet mediate perilipin 2 localization, *Biochemical and biophysical research communications 452*, 422-427.

168. Xu, G., Sztalryd, C., Lu, X., Tansey, J. T., Gan, J., Dorward, H., Kimmel, A. R., and Londos, C. (2005) Post-translational regulation of adipose differentiation-related protein by the ubiquitin/proteasome pathway, *J Biol Chem 280*, 42841-42847.

169. Chang, B. H., Li, L., Paul, A., Taniguchi, S., Nannegari, V., Heird, W. C., and Chan, L. (2006) Protection against fatty liver but normal adipogenesis in mice lacking adipose differentiation-related protein, *Mol Cell Biol 26*, 1063-1076.

170. Russell, T. D., Palmer, C. A., Orlicky, D. J., Bales, E. S., Chang, B.-J., Chan, L., and McManaman, J. L. (2008) Mammary glands of adipophilin-null mice produce an animo-terminally truncated form of adipophilin that mediates milk lipid droplet formation and secretion, *J Lipid Res 49*, 206-216.

171. Imai, Y., Varela, G. M., Jackson, M. B., Graham, M. J., Crook, R. M., and Ahima, R. S. (2007) Reduction of hepatosteatosis and lipid levels by an adipose differentiation-related protein antisense oligonuceotide, *Am J Physiol Gastro Liver Physiol 295*, G621-G628.

172. Imai, Y., Boyle, S., Varela, G., Caron, E., Yin, X., Dhir, R., Dhir, R., Graham, M., and Ahima, R. (2012) Effects of perilipin 2 antisense oligonucleotide treatment on hepatic lipid metabolism and gene expression, *Physiol Genomics 44*, 1125-1131.

173. Fajutrao Valles, S. (2014) The Effects of the Plin2 Ser251Pro Polymorphism on Plasma Lipid Profiles of 3164 Individuals, *The British Conference of Undergraduate Research 2014, University of Nottingham*,

174. McManaman, J. L., Bales, E. S., Orlicky, D. J., Jackson, M. B., MacLean, P. S., Cain, S., Crunk, A. E., Mansur, A., Graham, C. E., Bowman, T. A., and Greenberg, A. S. (2013) Perilipin-2 null mice are protected against diet-induced obesity, adipose inflammation and fatty liver disease, *J Lipid Res 54*, 1346-1359.

175. Martinez-Una, M., Varela-Rey, M., Cano, A., Fernandez-Ares, L., Beraza, N., Aurrekoetxea, I., Martinez-Arranz, I., Garcia-Rodriguez, J. L., Buque, X., Mestre, D., Luka, Z., Wagner, C., Alonso, C., Finnell, R. H., Lu, S. C., Martinez-Chantar, M. L., Aspichueta, P., and Mato, J. M. (2013) Excess S-adenosylmethionine reroutes phosphatidylethanolamine towards phosphatidylcholine and triglyceride synthesis., *Hepatology 58*, 1296-1305.

176. Martinez-Una, M., Varela-Rey, M., Mestre, D., Fernandez-Ares, L., Fresnedo, O., Fernandez-Ramos, D., Gutierrez-de Juan, V., Martin-Guerrero, I., Garcia-Orad, A., Luka, Z., Wagner, C., Lu, S., Garcia-Monzon, C., Finnell, R. H., Aurrekoetxea, I., Buque, X., Martinez-Chantar, M. L., Mato, J. M., and Aspichueta, P. (2015) S-Adenosylmethionine increases circulating ver-low-density lipoprotein clearance in non-alcoholic fatty liver disease, *J Hepatol 62*, 673-681.

177. Paul, A., Chang, B., Li, L., Yechoor, V., and Chan, L. (2008) Deficiency of adipose differentiation-related protein impairs foam cell formation and protects against atherosclerosis, *Circ Res 102*, 1492-1501.

178. Kucukazman, M., Ata, N., Yavuz, B., Dal, K., Sen, O., Deveci, O., Agladioglu, K., Yeniova, A., Nazliqul, Y., and Ertugrul, D. (2013) Evaluation of early atherosclerosis markers in patients with nonalcoholic fatty liver disease, *Eur J Gastroenterol Hepatol 25*, 147-151.

179. Chen, F. L., Yang, Z. H., Wang, X. C., Liu, Y., Yang, Y. H., Li, L. X., Liang, W. C., Zhou, W. B., and Hu, R. M. (2010) Adipophilin affects the expression of TNFα, MCP-1, and IL-6 in THP-1 macrophages, *Mol Cell Biochem 337*, 193-199.

180. Dvorak, A. M., Dvorak, H. F., Peters, S. P., Shulman, E. S., MacGlashan, D. W., Pyne, K., Harvey, S. V., Galli, S., and Lichtenstein, L. M. (1983) Lipid Bodies: cytoplasmic organelles important to arachidonate metabolism in macrophages and mast cells, *J of Immunol 131*, 2965-2976.

181. Vierira-de-Abreu, A., Assis, E. F., Gomes, S., Castro-Farla-Neto, H., Weller, P. F., Bandeira-Melo, C., and Bozza, P. T. (2005) Allergic challenge-ellicited lipid bodies compartmentalize in vivo leukotriene C4 synthesis within eosinophils, *Am J Respir Cell Mol Biol 33*, 254-261.

182. Accioly, M. T., Pacheco, P., Maya-Monterio, C. M., Carrossini, N., Robbs, B. K., Oliveira, S. S., Kaufmann, C., Morgado-Diaz, J. A., Bozza, P. T., and Viola, J. P. (2008) Lipid bodies are reservoirs of cyclooxygenase-2 and sites of prostaglandin-E2 synthesis in colon cancer cells., *Cancer Res 68*, 1732-1740.

183. Feng, L., Xia, Y., Garcia, G., Hwang, D., and Wilson, C. (1995) Involvement of reactive oxygen intermediates in cyclooxygenase-2 expression induced by interleuken-1, tumor necrosis factor-α and lipopolysaccharide, *J Clin Invest 95*, 1669-1675.

184. Leahy, K., Ornberg, R., Wang, Y., Zweifel, B., Koki, A., and Masferrer, J. (2002) Cyclooxygenase-2 inhibition by celecoxib reduces proliferation and induces apoptosis in angiogenic endothelial cells in vivo, *Cancer Res 62*, 625-631.

185. Mohammed, N., Abd El-Aleem, S., El-Hafiz, H., and MaMahon, R. (2004) Distribution of constitutive (COX-1) and inducible (COX-2) cyclooxygenase in postviral human liver cirrhosis: a possible role for COX-2 in the pathogenesis of liver cirrhosis., *J Clin Pathol 57*, 350-354.

186. Edvardsson, U., Ljungberg, A., Linden, D., Peilot-Sjogren, H., Ahnmark, A., and Oscarsson, J. (2006) PPAR activation increases triglyceride mass and adipose differentiation-related protein in hepatocyte, *Journal of Lipid Research 47*, 329-340.

187. Xiong, A., Yang, Z., Shen, Y., Zhou, J., and Shen, Q. (2014) Transcription factor STAT3 as a novel target for cancer prevention, *Cancers 6*, 926-957.

188. Aarenstrup, L., Flindt, E. N., Otkjaer, K., Kirkegaard, M., Andersen, J. S., and Kristiansen, K. (2008) HDAC Activity Is Required for p65/RelA-Dependent Repression of PPARδ-Mediated Transactivation in Human Keratinocytes, *Journal of Investigative Dermatology 128*, 1095-1106.

189. Nazari-Jahantigh, M., Wei, Y., Noels, H., Akhtar, S., Zhou, Z., Koenen, R. R., Heyll, K., Gremse, F., Keiessling, F., Grommes, J., Weber, C., and Schober, A. (2012) MicroRNA-155 promotes atherosclerosis by repressing Bcl6 in macrophages., *J Clin Invest 122*, 190-202.

190. McIntosh AL, Senthivinayagam S, Moon KC, Gupta S, Lwande JS, Murphy CC, Storey S, and Atshaves BP. (2012) Direct interaction of ADRP with lipids on the surface of lipid droplets: A live cell FRET analysis., *Am J Physiol Cell Physiol 303*, C728-742.

191. Fujii, H., Ikura, Y., Arimoto, J., Sugioka, K., Lezzoni, J. C., Park, S. H., Naruko, T., Itabe, H., Kawada, N., Caldwell, S. H., and Ueda, M. (2009) Expression of Perilipin and Adipohilin in Nonalcoholic Fatty Liver Disease; Relevance to Oxidative Injury and Hepatocyte Ballooning., *J Atheroscler Thromb 16*, 1893-1901.

CHAPTER 2:

HYPOTHESIS, SPECIFIC AIMS, AND SIGNIFICANCE

OVERVIEW

The leading cause of liver disease in the United States is nonalcoholic fatty liver disease (NAFLD), a clinical continuum from reversible steatosis, characterized by excess hepatic TG storage in lipid droplets to the more life-threatening nonalcoholic steatohepatitis (NASH) that predisposes to irreversible liver fibrosis, cirrhosis, and hepatocarcinoma. What drives the disease forward from fatty liver to hepatic inflammation is poorly understood; however recent studies have shown that obesity produces low-grade chronic inflammation in response to over nutrition. Despite the correlation between the metabolic state and inflammation, the lack of mechanistic details represents a critical oversight as the limited knowledge impedes development of novel targets for therapy. The most abundant hepatic lipid droplet protein, Plin2, has been associated with increased lipid storage, lipid droplet proliferation, insulin resistance,[5,6] and has been found to line ballooned hepatocytes of NAFLD patients.[7] Together, these findings suggest Plin2 may play a role in NAFLD or inflammation related disorders. The objective of this thesis was to establish a direct link between Plin2 and inflammation based metabolic diseases. By completing the work outlined in the listed specific aims, we have provided compelling evidence that Plin2 promotes COX-mediated inflammation through high-affinity interactions with pro-inflammatory lipids and direct interactions with COX2. Plin2 mitigates COX1 and COX2 expression post-transcriptionally by altering the levels of miRNAs that target COX1 and COX2. Ablation of Plin2 in hepatic tissue blunted the onset of hepatic steatosis and inflammation through a PEMT-mediated mechanism. Plin2 ablation in mice also resulted in decreased expression of the inflammation markers COX2, TNFα, IL-1β, and

IL-6. What follows is the global hypothesis on which the thesis is based, along with the specific aims that were used to test the hypothesis.

HYPOTHESIS

Plin2 interactions with lipids are promoted through high affinity binding within specific sites of the protein. These interactions stimulate inflammation under conditions of lipid excess by promoting binding to, and regulation of pro-inflammatory lipids, proteins, and miRNAs.

SPECIFIC AIMS

In order to test the hypothesis, recombinant Plin2 protein, Plin2-overexpression cells, and Plin2 knockout mouse models were used in the following Specific Aims:

1: Identify and characterize the lipid binding site of Plin2.

2: Determine the effect of Plin2 ablation on lipid accumulation and inflammation.

3: Determine the effect of altered Plin2 expression on microRNA regulation.

SIGNIFICANCE

Developing therapeutic strategies to treat the increasing number of obesity related diseases is dependent on identifying potential protein targets of intervention. Lipid droplets and their associated proteins play a critical role in maintaining lipid homeostasis and perturbations in their function dramatically impact human health. Therefore lipid droplets and their associated proteins are desirable targets for the next generation of therapeutics. Our work to establish the effect of Plin2 on lipid metabolism

represents a comprehensive examination of the physiological relevance of Plin2. The work outlined in the following chapters supports a role for Plin2 not only as a lipid droplet surface coat protein but also as a key regulator of lipid metabolism and inflammation. This contribution is significant because it represents the first steps towards reaching the ultimate goal of treating and curing obesity related diseases.

CHAPTER 3:

STRUCTURAL AND FUNCTIONAL ASSESSMENT OF PERILIPIN 2 LIPID BINDING DOMAIN(S)

Published: Biochemistry. 53: 7051-7066.

Title: Structural and Functional Assessment of Perilipin 2 Lipid Binding Domain(s)

Authors: Charles P. Najt, Joel S. Lwande, Avery L. McIntosh, Subramanian Senthivinayagam, Shipra Gupta, Leslie A. Kuhn, and Barbara P. Atshaves

ABSTRACT

Although Perilipin 2 (Plin2) has been shown to bind lipids with high affinity, the Plin2 lipid binding site has yet to be defined. This is of interest since Plin2's affinity for lipids has been suggested to be important for lipid droplet biogenesis and intracellular triacylglycerol accumulation. To define these regions, mouse Plin2 and several deletion mutants expressed as recombinant proteins and in mammalian cells were assessed by molecular modeling, fluorescence binding, circular dichroic, and FRET techniques to identify the structural and functional requirements for lipid binding. Major findings of this study indicate: 1) The N-terminal PAT domain does not bind cholesterol or stearic acid; 2) Plin2 residues 119-251, containing helix α4, the α–β domain, and part of helix α6 form a Plin3-like cleft found to be important for highest affinity lipid binding; 3) Both stearic acid and cholesterol interact favorably with the Plin2 cleft formed by conserved residues in helix α6 and adjacent strands, which is common to all the active lipid-binding constructs; and 4) Discrete targeting of the Plin2 mutants to lipid droplets supports Plin2 containing two independent, non-overlapping lipid droplet targeting domains in its central and C-terminal sequences. Thus, the current work reveals specific domains responsible for Plin2-lipid interactions that involve the protein's lipid binding and targeting functions.

INTRODUCTION

The lipid droplet protein perilipin 2 (Plin2, also known as adipose differentiation-related protein, ADRP, or adipophilin) has been shown to play a key role in lipid droplet formation, (*1*) intracellular triglyceride accumulation, (*1-4*) and to bind lipids with high affinity, (*5-8*) yet little is known about the structure or location of its lipid binding site(s).

This represents a significant gap in knowledge since there is evidence that Plin2's binding capacity may influence several lipid parameters including fatty acid uptake, (*9*) HDL-mediated cholesterol uptake/efflux, (*8, 10*) and VLDL content in mouse models of obesity (*11*). In fact, a genetic variation in the *Plin2* gene causing a serine to proline mutation (Ser251Pro) results in dysregulation of plasma lipid and lipoprotein profiles in humans, (*12*) possibly due to disruption of helical structure within a putative lipid binding site. As part of the Plin (or PAT, for *p*erilipin/*A*DRP/*T*IP47) family of lipid droplet targeting proteins which includes Plin1/perilipin, Plin2/ADRP, Plin3/TIP47, Plin4/S3-12, and Plin5/OXPAT, Plin2 shares high sequence homology with members of the group (*13*). With Plin1 (*14*) and other lipid droplet-associated proteins such as caveolins, (*15*) the targeting and anchoring of proteins depends on targeting signals in the form of hydrophobic sequences. These signals are not however, conserved in Plin2, (*14*) suggesting different lipid droplet targeting mechanisms exist among lipid droplet associated proteins. In support of this, Plin2 contains two lipid droplet targeting domains that are not hydrophobic in nature (*16, 17*). These domains are non-overlapping suggesting that targeting of Plin2 to lipid droplets is controlled by the tertiary structure in which contributing residues are brought together to form the targeting signal (*16, 17*). Likewise, the lipid binding site of Plin2 may also be defined by the tertiary structure of the protein and may not be easily described by a linear sequence motif. In keeping with this, there is evidence that binding of cholesterol and other lipids by membrane proteins often occurs in grooves between helices and involves conserved spatial motifs (*18-21*). Based on sequence similarity (*22*) and predicted structure, (*16, 17*) several conserved regions within Plin2 have the potential to bind lipids including: 1) a highly conserved N-

terminal hydrophobic domain (residues 1-115) known as the PAT domain (*22, 23*) that is involved in lipid droplet stabilization, lipid accumulation, and proteasomal degradation of Plin2; (*23, 24*) 2) the N-terminal 11-mer repeating domain located within residues 103-215 (*25, 26*) that is believed to participate with part of the C-terminal domain to regulate secretion of milk lipids by forming an adaptive link between lipid droplets and the plasma membrane; (*27*) 3) two predicted lipid droplet targeting domains in the middle and C-terminal regions of the protein; (*16, 17*) and 4) a C-terminal α-β domain and a 4-helix bundle domain reminiscent of the LDL receptor binding domain of apolipoprotein E (*25*). The last structure was predicted based on homology between Plin2 and the known crystal structure of the closely related Plin3 (*25*). In Plin3, the α-β domain and 4-helix bundle fold together into an L-shape, forming a cleft (13 Å at its widest, 18 Å long, and 10 Å deep) with several hydrophobic residues and a deep polar pocket of sufficient size to accommodate lipid ligands and interact with their polar groups. Since Plin2 and Plin3 share 42% overall sequence identity throughout and 35% identity in the C-terminal region (NCBI BLAST), substantial structural similarity is expected. In fact, a comprehensive study has shown that sequences with at least 25% identity over at least 80 residues have backbone structures that overlay closely (*28*). Recently, a structural model was presented for Plin2 based on sequence similarity to the known 3-dimensional structures of Plin3, apolipoprotein A1, the signal receiver domain of a putative luxo repressor protein, and dihydroorotate reductase (*29*). Work presented here supports that an apolipophorin-like N-terminal domain and a Plin3-like C-terminal domain together can account for the overall tertiary fold of Plin2. Others have noted structural similarities between apolipoproteins and the N-terminal domain of Plin

proteins (*25*). Both contain 11-mer repeats (located within helix α4 and the α–β domain in Plin2) that are found in other lipid- or membrane-associated proteins including phosphate cytidyltransferases and synucleins, (*30*) suggesting these domains may serve as lipid interacting sites in these proteins. In support of these findings, others have shown that structure predictions of 11-mer repeats, such as those described in the N-terminal regions of Plin2 and Plin3, do not produce stable helical entities in proteins such as synucleins (*31, 32*) and only adopt a helical structure upon interaction of lipid ligands or lipid membranes (*33*). Interestingly Bulankina et al demonstrated that the 11-mer repeat region in Plin3 interacted with lipid droplet membranes through residues 87-198 (*34*). Moreover, it was suggested that Plin3 adopts a distinct N-terminal and C-terminal structure that extends upon membrane interaction to accommodate the lipid structure and cause lipid reorganization (*34*). Thus, despite structural similarities between Plin2 and Plin3, differences in the N-terminal and C-terminal regions contribute to the distinct functions of the proteins.

The present investigation was undertaken to examine the structure and location of the Plin2 lipid binding site(s) within conserved domains by characterizing Plin2 and several deletion mutants using molecular modeling, fluorescence binding, circular dichroism, and FRET techniques. Evidence is provided that lipid binding by Plin2 does not require the full-length protein, but instead employs residues from two helical bundle domains for highest affinity lipid binding and targeting to lipid droplets, activities that are dependent on strong Plin2-lipid or Plin2-membrane interactions. Crucial residues within these domains are 119-251, a region that contains helix α4, the α–β domain (α5, β3), and part of helix α6, included in the cleft region. Residues within ConSurf analysis

shows that surface-exposed residues within the cleft are highly conserved and likely to be functionally important. Furthermore, flexible docking of stearic acid and cholesterol into this region indicates favorable interactions with both ligands and the cleft formed from a polar pocket with surrounding hydrophobic residues. Since mutations in this region of Plin2 resulted in dysregulation of plasma lipid and lipoprotein profiles in humans, (*12*) study of the functional importance of this area is warranted.

MATERIALS AND METHODS

MATERIALS

Cholesterol and stearic acid were purchased from Sigma (St. Louis, MO). NBD-Cholesterol and NBD-stearic acid were obtained from Molecular Probes (Eugene, OR). Expression vector pQE9-His was purchased from Addgene (Cambridge, MA). CFP-fusion protein expression vector pECFP-N1 was purchased from BD Biosciences (BD Biosciences Clontech, Palo Alto, CA). Ni-NTA resin and M15 cells for protein expression were obtained from Qiagen (Chatsworth, CA). Rabbit anti-Plin2 polyclonal anti-body was prepared as described (*35*). Lipofectamine 2000 was purchased from Life Technologies-Invitrogen (Carlsbad, CA).

BUFFERS

Buffer A contained 50 mM Na_2HPO_4 (pH 8.0), 300 mM NaCl, and protease inhibitors (1 tablet per 50ml). Buffer B contained 20 mM Tris-HCl (pH 7.9), 100 mM Na_2HPO_4, 500 mM NaCl and 20 mM imidazole and 6M guanidine hydrochloride. Buffer C contained 20 mM Tris-HCl (pH 7.9), 500 mM NaCl, 20 mM imidazole, and 6 M urea. Buffer D was Buffer C at pH = 5.9. Buffer E was 10 mM Tris-HCl (pH 7.5), and 150 mM NaCl. Buffer F contained

PBS, 2 mM EDTA, 10 mM DTT, and protease inhibitors. Buffer G contained PBS, 10 mM DTT, 0.1% SDS and 10% glycerol. Buffer H was PBS, 10 mM DTT and 2 M urea. Buffer I was Buffer H in 8 M urea. Buffer J was Buffer E at pH 8.3 plus 20mM imidazole. Buffer K was Buffer J at pH 7.5. Buffer L was Buffer E plus 50mM EDTA.

PLASMIDS

The full coding sequence of mouse Plin2 cDNA was cloned into pQE9-His vector (Origene, Rockville, MD) following standard procedures. Unique restriction sites *Bam*HI and *Hin*dIII were introduced by PCR amplification with the following forward and reverse primers: Plin2-forward, 5'-CAC GGA TCC ATG GCA GCA GCA GTA GTA GAT CCG CAA C -3'and Plin2-reverse, 5'-GTG AAG CTT TTA CTG AGC TTT GAC CTC-3'. The forward primer was designed with a silent mutation where guanine was replaced by adenine in the Plin2 sequence to remove a *Bam*HI site located within the first 18 bp of the Plin2 gene. By cloning Plin2 cDNA into the pQE9-His vector, an N-terminal His-Tagged fusion protein was formed upon expression that allowed recombinant protein to be purified using Ni-NTA based affinity chromatography. Expression plasmids for the deletion mutants were generated from the above construct by site-directed mutagenesis as described elsewhere (*36*) using the following primers: Plin2-C1 forward, 5'-CAT CAC GGA TCC ATG ACG ACT ACC ATG GCT GGA GCC-3'; Plin2-C1 reverse, 5'-AGC CAT GGT AGT CGT CAT GGA TCC GTG ATG GTG ATG-3'; Plin2-C2 forward, 5'-CAT CAC GGA TCC ATG GTC CAC CTG ATT GAA TTC GCC-3'; Plin2-C2 reverse, 5'-TTC AAT CAG GTG GAC CAT GGA TCC GTG ATG GTG ATG-3'; Plin2-N1 forward, 5'-GAT GTG ACG ACT TAA AAG CTT AAT TAG CTG AGC-3'; Plin2-N1 reverse, 5'-

CTA ATT AAG CTT TTA AGT CGT CAC ATC CTT CGC-3'; Plin2-N2 forward, 5'-ACC ATT TCT CAG CTC TAA AAG CTT AAT TAG CTG AGC-3'; Plin2-N2 reverse, 5'-CTA ATT AAG CTT TTA GAG CTG AGA AAT GGT CTC CTG-3'. Plin2-I was made using Plin2-C1 as the template DNA and the primers used for creating Plin2-N2. The resulting plasmids were sequenced to ensure fidelity and identity.

EXPRESSION AND PURIFICATION OF RECOMBINANT PROTEINS IN ESCHERICHIA COLI CELLS

Recombinant Plin2 and the deletion mutants were purified as previously described with some modifications (*5*). Briefly, proteins were overexpressed in *E. coli* host strain M15 and grown at 37 ^{o}C in 1 liter cultures containing 2X-YT medium with 100 µg/mL ampicillin until OD_{600} = 0.8, followed by induction with IPTG (1 mM). After 1 hour, cells were harvested by centrifugation (4 ^{o}C for 30 min at 3500 g). For purification of Plin2, Plin2-I, Plin2-N1, and Plin2-N2, pelleted cells were resuspended in Buffer A then sonicated. Lysates were centrifuged at 4 ^{o}C for 15 min at 25000 g and the pellet was solubilized in Buffer B and applied to a Ni-NTA column equilibrated in Buffer B. The column was sequentially washed with buffers B, C and D, and E. The protein was eluted using Buffer L and then checked for purity by SDS-PAGE analysis. For deletion mutants Plin2-C1 and Plin2-C2, the pelleted cells were resuspended in Buffer F, sonicated, and centrifuged at 4 ^{o}C for 15 min at 25000 g. The resulting pellet was washed 2x each with buffers G and H, solubilized in Buffer I, and centrifuged at 4 ^{o}C for 15 min at 25000 g. The supernatant was then sequentially dialyzed against PBS containing 10 mM DTT in decreasing concentrations of urea (6 M, 5 M, and 4 M urea). The protein in 4 M urea was then loaded onto a Ni-NTA column equilibrated in Buffer J. The column was then

sequentially washed with the buffers J and K, and then eluted with Buffer L. Analysis by SDS-PAGE and Western blotting as described in (*4*) allowed assignment of protein purity.

PLIN2 STRUCTURAL PREDICTION AND ANALYSIS

The Hopp and Woods hydropathy analysis method (*37*) (web server: http://www.vivo.colostate.edu/molkit/hydropathy/index.html) was used to predict hydrophilic and hydrophobic segments within Plin2 based on a hydrophilicity index assigned to the amino acids, averaged over six successive residues. The PAT domain and two lipid droplet targeting domains in Plin2 were previously described (*17, 24, 26*). The secondary structure of Plin2 was predicted by the PredictProtein server at http://www.predictprotein.org (*38*). This method has greater than 72% accuracy, on average, in assigning α-helical, β-strand (extended) or loop conformation to protein residues. Secondary structural predictions of the Plin2 N-terminal region (residues 1-171) were consistent with further analysis by PSIPRED (*39, 40*), SAM (*41*), and SABLE2 (*42*). Based on their significant (35%) sequence identity, the Plin2 C-terminal domain structure was modeled by homology to the structure of residues 209-431 in Plin3 (*25*) from Protein Data Bank entry 1SZI (*43*) by using Modeller (*44, 45*), as implemented in the ModWeb webserver (salilab.org/modweb). Given the absence of close homologs of known structure to the Plin2 N-terminal region, this sequence was submitted for analysis by the Pcons fold recognition web server (http://pcons.net/) to identify the 3-dimensional structural fold providing the most compatible amino acid environments and secondary structures. By comparing the top-scoring predictions from

eleven different 3-dimensional modeling methods (Pcons, Pmodeller, PconsM, blast, forte, fugue, hhpred2, nfold, rpsblast, sam-t02 and sam-t08), Pcons selected the structural model for the N-terminal Plin2 region showing the highest degree of structural consensus among the results. The degree of amino acid conservation within 38 homologs of the C-terminal domain of ADRP was assessed by ConSurf (http://consurf.tau.ac.il/), which automatically detects homologs, performs multiple sequence alignment, and maps amino acid conservation values onto the structure (*46, 47*). Molecular graphics figures were rendered using PYMOL (Schrödinger, LLC) (*35*). Stearic acid interactions with the modeled Plin2 C-terminal domain were assessed by extracting the 3-dimensional structure of stearic acid from the PDB X-ray structure 1HMT (*48*). Partial charges were assigned to its atoms with Molcharge v. 1.3.1 software from OpenEye Scientific Software (http://www.eyesopen.com; Santa Fe, NM). Low-energy (favorable) flexible conformations of highly flexible stearic acid were then generated by using Omega2 v. 2.3.2 (also from OpenEye Scientific Software). Similarly, the 3-dimensional structure of cholesterol (residue 3001D) was extracted from PDB entry 3KDP (*49*). Partial charges were assigned with Molcharge, and low-energy conformations of the cholesterol hydrophobic tail were sampled with Omega2. The stearic acid and cholesterol conformers were evaluated for their ability to interact favorably with the conserved cleft in the 3-dimensional model of the C-terminal domain structure of Plin2 by using SLIDE version 3.3.5 software to dock each conformer of stearic acid or cholesterol into the cleft between the α-β domain and 4-helix bundle, and selecting the orientation and conformation with the most favorable predicted $\Delta G_{binding}$ to

Plin2, as assessed by SLIDE AffiScore. SLIDE models side-chain flexibility in both molecules during docking (*50*).

CELLS CULTURE AND TRANSFECTIONS

Mouse L cell fibroblasts expressing CFP-labeled Plin2 and the deletion mutants were generated as described (*4*) using mammalian expression vector pECFP-N1 and unique restriction sites (*Xho*I, *Kpn*I) introduced by PCR. Resulting expression plasmids were sequenced to verify identity and fidelity and then stably transfected into L cells using Lipofectamine 2000 from Life Technologies (Grand Island, NY) according to the manufacturer's instructions. Clones surviving selection with G418 were cell-sorted for strong CFP signal under sterile conditions using an INFLUX cell sorter (BD scientific, Palo Alto, CA) and screened by Western blot analysis and fluorescence imaging to ensure stable expression of CFP-labeled protein. Mock transfectants (clones transfected with vector DNA without insert) were generated in parallel and were designated as controls.

UREA DENATURATION STUDIES

To show the effects of protein unfolding on Plin2 tryptophan residues, protein-denaturation studies in the presence of urea were performed as described (*51*). In brief, the intrinsic tryptophan fluorescence (excitation 295 nm, emission 300 to 400 nm) of three Plin2 tryptophans located at positions 283, 286, and 398 was collected using a Cary Eclipse fluorescence spectrophotometer (Varian, Walnut Creek, CA) at constant temperature (25^0C) before and after addition of increasing amounts of urea (up 6 M) to

Plin2 (100nM) in 10 mM NaH_2PO_4, pH 7.5. Samples were allowed to equilibrate 2 minutes after addition of each urea aliquot. Data was corrected for background scatter originating from the buffer and analyzed to graphically show the tryptophan fluorescence spectrum at increasing urea concentrations and the percent fluorescence remaining after each addition.

INTRINSIC TRYPTOPHAN FLUORESCENCE BINDING STUDIES

The binding of cholesterol and stearic acid to Plin2 was examined by measuring the fluorescence quenching of Plin2 tryptophan residues after addition of ligand as described (*52, 53*). In brief, the intrinsic tryptophan fluorescence of Plin2 (100 nM in 10 mM NaH_2PO_4, pH 7.5) was monitored from 300 to 400 nm after excitation at 295 nm (to minimize interference from Plin2 tyrosine fluorescence) both before and after addition of increasing increments of cholesterol, stearic acid, arachidonic acid, and docosahexaenoic acid (up to 100 nM) using a Cary Eclipse fluorescence spectrophotometer. Data was corrected for background scatter originating from the buffer and increasing ligand without protein present. The intrinsic tryptophan fluorescence in the presence of different concentrations of ligand was plotted as the maximum fluorescence difference ($\Delta F = F_o - F$) vs. ligand concentration to yield a saturation curve where F and F_o were the measured fluorescence emission intensity of the protein solution in the presence and absence of ligand, respectively. The dissociation constant K_d was determined from the double reciprocal plot of the saturation curve. Linear regression of 1/[1-(F/Fmax)] versus [ligand]/(F/Fmax) yielded a slope = 1/ K_d and ordinate intercept = nE_o/ K_d where F represented fluorescence

intensity at a given concentration of ligand, Fmax was the maximal fluorescence, [ligand] was the ligand concentration, E_o was the protein concentration, and n equaled the number of ligand binding sites.

NBD-LABELED LIGAND BINDING ASSAYS

Since not all of the deletion mutations contained tryptophan residues, a fluorescent ligand binding assay was developed using NBD-Cholesterol and NBD-stearic acid as described (*5-8*). In brief, NBD-labeled lipids were added incrementally (0-300 nM) to proteins (Plin2 and Plin2 deletion mutants) at 100 nM in phosphate buffer (10 mM, pH 7.5). Samples were allowed to mix 2-5 min after each addition before exciting at 469 nm. Fluorescence emission spectra were recorded from 490 to 600 nm and integrated. Data was corrected for both background scatter originating from the buffer and increasing ligand without protein present. A saturation curve developed by plotting fluorescence intensities vs. ligand concentration and the double reciprocal plot of this curve allowed determination of K_d as discussed previously.

CO-LOCALIZATION STUDIES

To show the ability of Plin2 and the deletion mutants to target to lipid droplets, co-localization studies were performed as described (*4, 35*) with cells expressing full length Plin2 or one of the deletion constructs. Cells seeded at a density of 50,000 cells/well in 4-well chamber slides (EZ Slide, Millipore, Billerica, MA) were treated overnight with oleic acid (100µM) 4-5 hrs after plating. After 16 hrs, cells were incubated with NBD-Cholesterol (2µM) for 2 hours, then fixed in 3.7% formaldehyde for 20 min at room

temperature followed by washing (3x) with PBS. The cells were then blocked with 2% BSA and incubated with rabbit anti-CFP antibody (1:50) for 1 hr at room temperature. Since the transfected cells express CFP-labeled proteins (as described above), anti-CFP was used in place of anti-Plin2 to discriminate endogenous Plin2 from the transfected mutant proteins. After extensive washing, cells were incubated with Cy5 labeled anti-rabbit secondary antibody (1:100) in 2% BSA for 1 hr. Cells were washed with PBS and mounted with coverslips using fluorogel mounting medium (Electron Microscopy Science, Hatfield, PA). As a control, cells were also labeled with the Cy5-labeled secondary antibody alone. Images were acquired sequentially on an Olympus FluoView 1000 Laser Scanning Confocal Microscope (Olympus Inc, Center Valley, CA) equipped with an IX81 automated inverted microscope and operated with Fluoview software. Fluorescence emission was detected using 488 nm excitation and 500/100 band path emission filter for NBD-Cholesterol (green channel) and 635 nm excitation with a 725/30 band path filter for the Cy5 emission (red channel). To minimize photobleaching, samples were exposed to the light source for minimal time periods. Image files were analyzed using Metamorph software (West Chester, PA). Images derived from the red and green channels were combined and appeared as yellow to orange where superimposition of images derived from the red and green channels overlapped.

FLUORESCENCE RESONANCE ENERGY TRANSFER MICROSCOPY

Acceptor photobleaching experiments were performed as previously described (*4, 54*) on cells labeled as described above by measuring the fluorescence emission of the NBD donor through the 500/100 nm filter upon excitation at 488nm both before and

after photobleaching of the Cy5-acceptor excited at 635nm. Control experiments were performed to limit interference from non-specific fluorescence including: 1) Imaging non-labeled cells to determine auto-fluorescence in the green channel (NBD) while maintaining maximum dynamic range; 2) Adjusting the gain and black levels in the red channel after excitation at 635nm to limit fluorescence bleed-through into the green channel; 3) Photobleaching NBD-labeled donor cells without Cy5 present to check for non-specific fluorescent increases in the donor channel to ensure that the donor intensity was not affected by bleaching the cells; and 4) Leaving one or two cells unbleached during the FRET experiment to serve as in-field bleaching control. To calculate the FRET efficiency (*E*), representing the efficiency of energy transfer between donor and acceptor, the following equation was used: $E = 1-(I_{DA}/I_D)$ where I_{DA} is donor fluorescence intensity before acceptor photobleaching and I_D is the donor fluorescence intensity after acceptor photobleaching. An average *E* value was calculated from the NBD fluorescence emission increase after photobleaching. The intermolecular distance *R* between NBD-label and the Cy5-labeled Plin2 was calculated from the equation $R = R_0(1/E-1)^{(1/6)}$, where *E* was experimentally determined and R_o was the Förster radius for the NBD-Cy5 FRET pair (56 Å). Since accurate determination within the cellular environment of parameters of the probes (e.g. donor quantum yield, acceptor extinction coefficient, and dipole orientation factor between donor/acceptor pair) involved in the calculation of R_0 is difficult, interaction distances (*R*) were also presented in terms of R_0, with R_0 <75 Å such that κ^2 <4 (*55*).

CIRCULAR DICHROIC ANALYSIS OF SECONDARY STRUCTURE

The far UV circular dichroic (CD) spectra of each protein was measured in phosphate buffer (10 mM NaH_2PO_4, pH 7.5 with 10 mM NaCl) in the presence and absence of ligand (cholesterol or stearic acid) to a final concentration of 5 µM. Experiments were performed at 25ºC in a 1 mm path length cuvette using a JASCO J-815 CD spectrometer (JASCO Analytical Instruments, Easton, MD). Experiments with ligand were allowed to incubate for 2-5 min prior to each scan to allow maximal protein-ligand interaction. CD spectra were recorded from 270 to 190 nm at a scan rate of 50 nm/minute with a time constant of 1 s and bandwidth of 2 nm. For each experiment, 10 iterations were performed in triplicate. Secondary structure analysis was carried out using the CDSSTR analysis program (*56*) with results reported as percentages of regular α-helices, distorted α-helices, regular β-strands, distorted β-strands, turns and unordered structures. In a separate experiment, measurements on purified recombinant Plin2 were performed at 5ºC, 25ºC, and 40ºC to determine the dependence of secondary structure on temperature.

STATISTICS

All values were expressed as the means ± SE. Statistical analyses were performed using Student's t test or one-way ANOVA with Newman Keuls posthoc test (GraphPad Prism, San Diego, CA) to determine statistical significance. Values with $P < 0.05$ or less were considered significant.

RESULTS

PREDICTION OF PLIN2 SECONDARY STRUCTURE AND CONSERVED DOMAINS

To understand how ligand binding relates to structure, the secondary structure of Plin2 was predicted using several prediction programs including PredictProtein, (*38*) PSIPRED, (*39, 40*) SAM, (*41*) and SABLE2 (*42*). Results from these programs indicated that the secondary structure of Plin2 is mostly α-helical in nature (9 α-helices) with 5 β strands inter-connected by random coils (Fig. 8A). The Plin2 N-terminal region contains 2 β-strands (β1, β2) and 4 α-helices (α1, α2, α3, and α4). Based on homology to the C-terminal domain of the crystal structure of Plin3, the Plin2 C-terminal region is predicted to contain an α–β domain (α5, β3), a 4-helix bundle (α6- α9), and 2 β–strands (β4, β5) that together form a deep cleft that is conserved in the perilipin family and large enough to bind lipids (*25*). In addition, several conserved regions have been identified within Plin2 including a highly conserved hydrophobic domain within the N-terminal region (residues 1-115) known as the PAT domain (Fig. 8B), which was shown to participate in

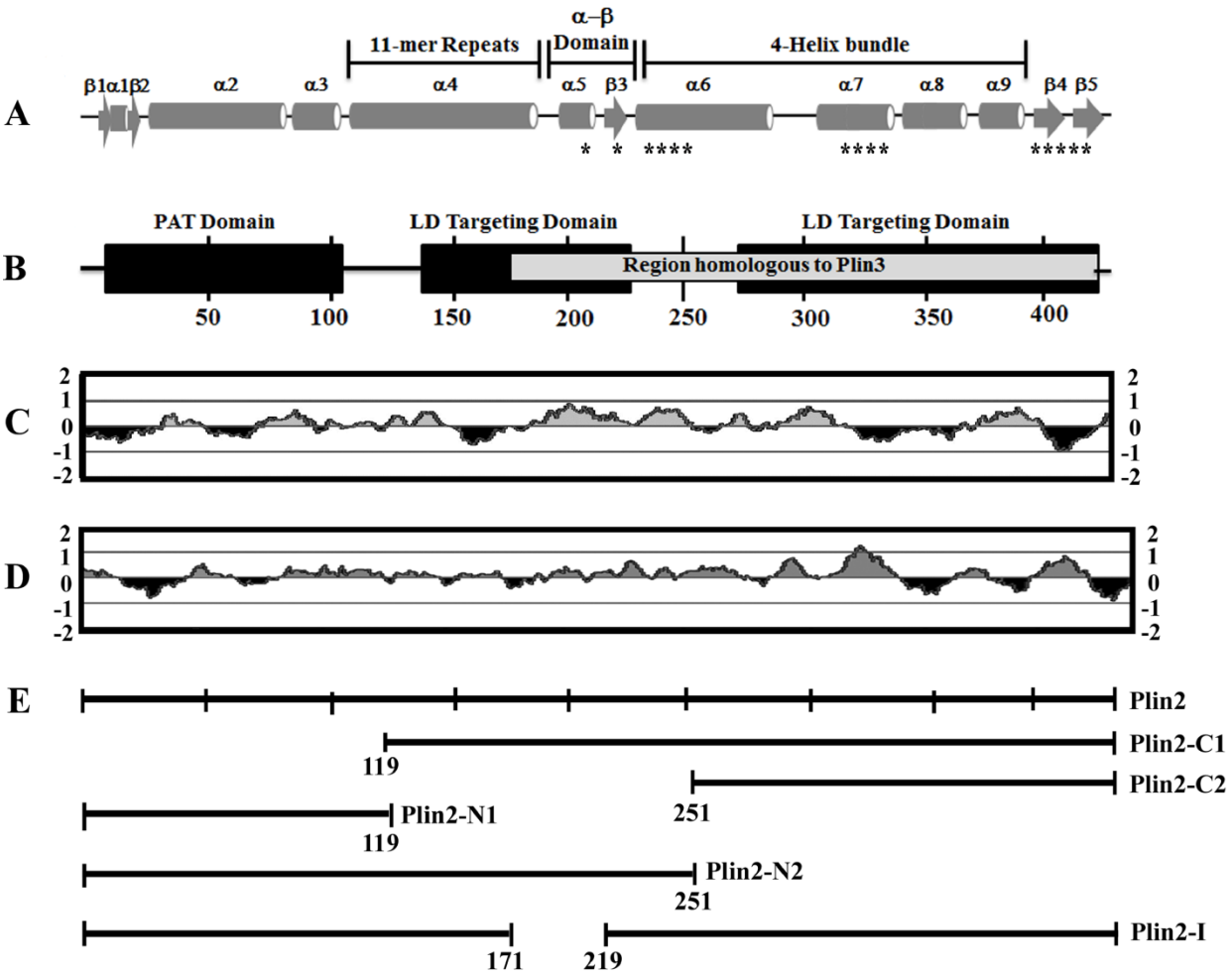

Figure 8. Predicted secondary structure and conserved domains of Plin2. Based on prediction software (SABLE2, SAM and PsiPRED) and the known X-ray crystal structure of the homologous Plin3 protein, the predicted structure of Plin2 (A) contains 9 α-helices and 5 small β strands inter-connected by random coils and unordered structure. Several regions of interest include the PAT domain (B), 11-mer repeat region (A), two lipid droplet (LD) targeting domains (B), and the C-terminal area containing an α/β domain (A) and 4 Helix bundle (A) that together formed a cleft region. Residues that line the cleft (indicated by *) include: Val-203, Tyr-215, Ala-233, Arg-236, Val-237, Ala-240, Thr-325, Val-326, Asn-329, Gln-331, Trp-398, Leu-399, Val-400, Pro-402 and Phe-403. Hopp-Woods hydrophilicity plots for Plin2 (C) and Plin3 (D) were generated using a server at the Colorado State University (http://www.vivo.colostate.edu/molkit/hydropathy/index.html) to provide predicted hydrophilic (lines above zero) and hydrophobic regions (below zero) within the proteins. Line diagrams of Plin2 and the deletion mutants (E) include full length Plin2 (containing amino acid residues 1-425); Plin2-C1 (residues 119-425); Plin2-C2 (residues 251-425); Plin2-N1 (residues 1-119); and Plin2-N2 (residues 1-251); and Plin2-I (residues1-171 and 219-425).

the stabilization and accumulation of lipid droplets and to determine proteasomal degradation of Plin2; (*22-24*) an 11-mer repeating unit of unknown function within residues 103-215 (Fig. 8A); and two lipid droplet targeting domains (*16, 17*) located in the middle and C-terminal regions (Fig. 8B) that participated with part of the C-terminal domain to regulate secretion of milk lipids (*13, 27*). Alternating patterns of hydrophobic/hydrophilic segments are observed in Plin2 (Fig. 8C) and Plin3 (Fig. 8D) over the N-terminal PAT domain and 11-mer repeat region from patterns of hydrophobicity predicted using the method of Hopp and Woods (*37*). In keeping with the high degree of homology shared between these proteins, similar hydrophobic characteristics were observed for both Plin2 and Plin3. Large segments of hydrophobic sequence conducive to membrane targeting were not observed with either protein, suggesting that regions within the protein come together spatially to form larger recognition surfaces for hydrophobic ligands including the membrane itself.

To assess the lipid binding affinities of these regions, Plin2 and several Plin2 deletion mutants that contain select regions within Plin2 with the potential to bind lipids were expressed in *E. coli* and purified as recombinant proteins. The deletion mutants included regions containing the PAT domain, (*23*) one or two of the lipid droplet targeting domains, (*16, 22*) or the central alpha/beta domain residues near the cleft in the C-terminal region (*25*) (Fig. 8E).

EFFECT OF UREA AND TEMPERATURE ON PLIN2 STRUCTURE: INTRINSIC TRYPTOPHAN FLUORESCENCE QUENCHING AND CD ANALYSIS

Recombinant full length Plin2 protein was overexpressed and purified as described in the Methods section (Fig. 9). To determine if the recombinant Plin2 protein was conformational and functionally intact, two distinct experiments were performed. First, to show the effects of protein unfolding, Plin2 was titered against increasing amounts of urea, up to 6 M. Protein unfolding was monitored via tryptophan fluorescence, as described in (*51*) and in the Methods section. Tryptophan fluorescence, in contrast to tyrosine fluorescence, is sensitive to solvent polarity, therefore it can be used as a measure of protein folding (*55*). Plin2 contains three tryptophan residues in the C-terminal region at positions 283, 286, and 398. More importantly, the tryptophan residues are located in the 4-helix bundle of the predicted binding region of the protein. Analysis of the Plin2 tryptophan fluorescence emission collected from 300 nm to 400 nm showed the refolded full length Plin2 protein exhibited a typical emission spectra with maxima at 327 nm (Fig. 10A), indicating a blue-shift relative to tryptophan in water where the fluorescence maximum is 348 nm (*57*). Addition of increasing concentrations of urea (up to 6 M) resulted in fluorescence quenching of one or more of the three tryptophan residues (Fig. 10A). A red-shift in the emission maxima to 332 nm at 4.6 M urea was observed, indicating increased exposure of the residues to the hydrophilic solvent. At 6 M urea, only 22% of the initial tryptophan fluorescence remained indicating substantial exposure of the tryptophan residues to the solvent. It is this 78% decrease in

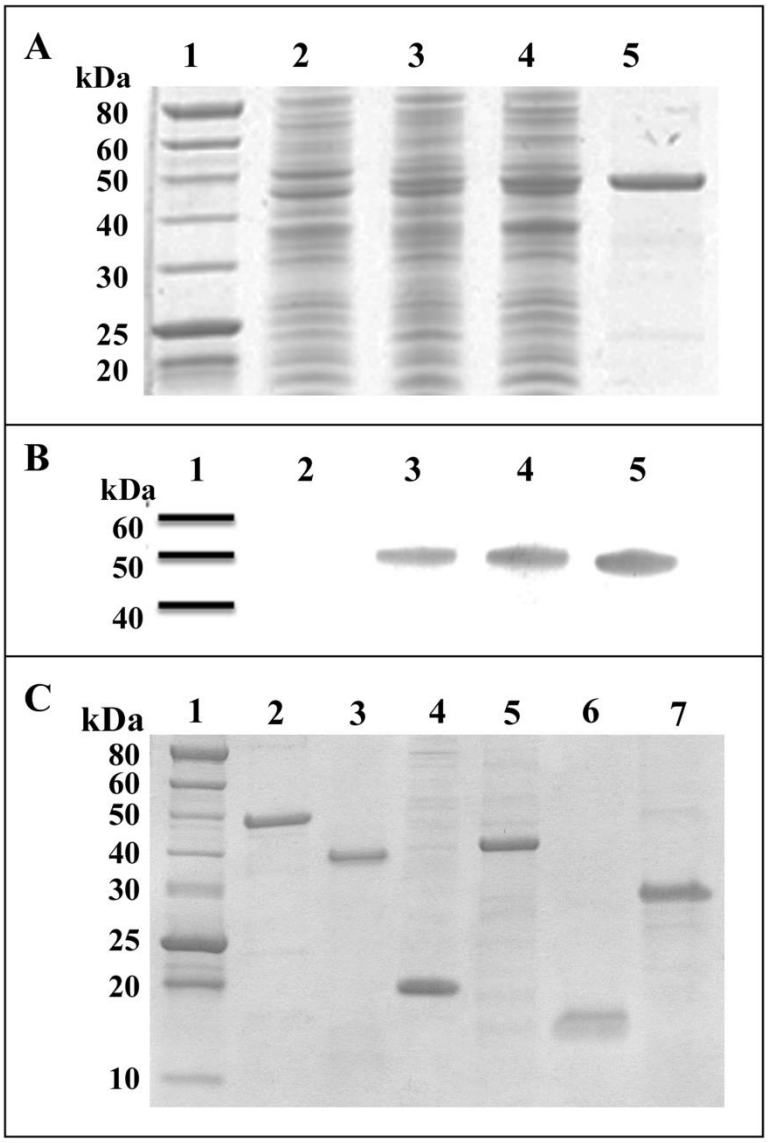

Figure 9. Expression and purification of recombinant Plin2. Purification of recombinant full length Plin2 protein was shown on a 10% Tricine-PAGE gel (A) loaded as follows: lane 1, molecular weight marker; lane 2, un-induced cells; lane 3, cells after 1 hour of induction with IPTG (1mM); lane 4, cells pelleted and washed; and lane 5, purified Plin2. A Western blot (B) run in parallel was loaded as indicated above and probed with polyclonal anti-Plin2. A 10% Tricine-PAGE gel showing the purified deletion mutants (C) was loaded as follows: lane 1, molecular weight marker; lane 2, Plin2 (48 kDa); lane 3, Plin2-C1 (35.5 kDa); lane 4, Plin2-C2 (20.8 kDa); lane 5, Plin2-I2 (42.5 kDa); lane 6, Plin2-N1 (13.7 kDa); and lane 7, Plin2-N2 (28.4 kDa).

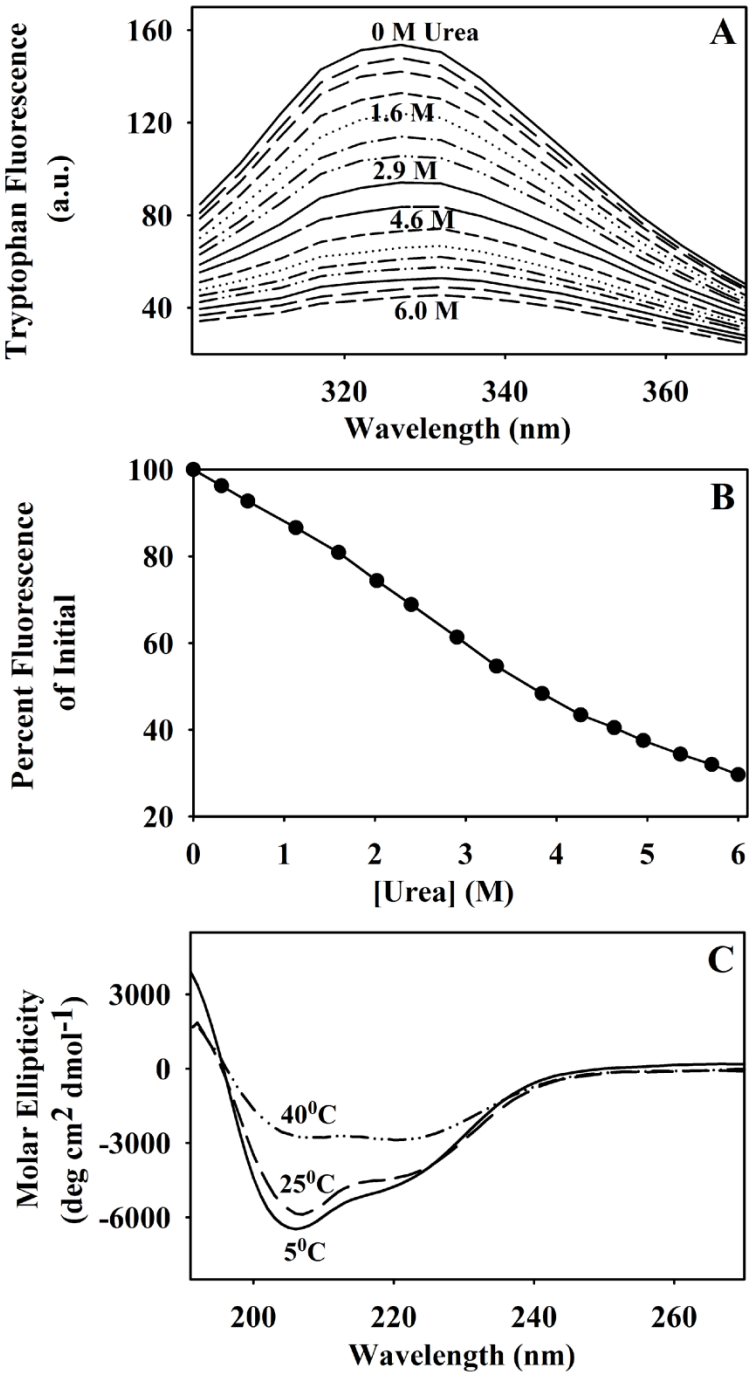

Figure 10. Tryptophan fluorescence (total and percent of initial) upon urea denaturation and circular dichroism of Plin2 as a function of temperature. Protein-denaturation studies were performed by addition of increasing aliquots of urea (0-6.0M) to recombinant Plin2. The tryptophan emission spectra (A) upon excitation at 280 nm and percent fluorescence of initial (B) was determined to show the overall effect of solvent polarity upon protein stability. Exposure of tryptophan residues to solvent upon denaturation resulted in decreased fluorescence due to quenching of residues. The effect of temperature on Plin2 secondary structure was determined by circular dichroism (C) to show Plin2 unfolding at temperatures above 40°C.

tryptophan fluorescence and red shift that is indicative of denaturation of the refolded protein (Fig. 10B).

Second, to show the effects of protein unfolding on Plin2 secondary structure, changes in the CD spectra at increasing temperatures was examined. At room temperature (25^0C) recombinant Plin2 exhibited a double minimum at ~208 and 222 nm signifying substantial amounts of α-helices were present (Fig. 10C). However, the molar ellipticity at 208 nm was lower than at 222 nm suggesting a subtle influence of random coils and β-sheets. Upon lowering the temperature to 5^0C, the minima at 208 nm and 222 nm were intensified, consistent with slower conformational transitions and enhanced resolution. In contrast, at 40^0C the protein began losing its secondary structure as the peak intensities approached zero molar ellipticity (Fig. 10C). Results from these studies indicated that Plin2 tryptophans in the refolded protein were sensitive to urea denaturation. Moreover, CD analysis of the secondary structure of the refolded protein was consistent with predictions and exhibited enhanced resolution at lower temperatures but destabilization when temperatures were increased above room temperature.

TRYPTOPHAN QUENCHING BINDING STUDIES: FULL LENGTH PLIN2 BINDS CHOLESTEROL, STEARIC ACID, ARACHIDONIC ACID, AND DOCOSAHEXAENOIC ACID (DHA) WITH HIGH AFFINITY

The binding affinities of full length Plin2 for cholesterol, stearic acid, arachidonic acid, and DHA were determined by measuring changes in the intrinsic tryptophan fluorescence of Plin2 upon ligand addition as described in the Methods section.

Fluorescence quenching of one or more of the three tryptophan residues located in the C-terminal 4-helix bundle resulted in a decrease in fluorescence signal intensity when ligand was added. It should also be noted that in some cases binding of ligand can increase tryptophan fluorescence. In situations where an increase is observed, the tryptophan residues become embedded in a hydrophobic environment either by directly interacting with the lipid residue or by a conformational change in which the reverse of tryptophan quenching occurs. Since addition of the lipid ligand was seen to cause conformational changes in Plin2, the decrease in tryptophan fluorescence upon lipid binding in the present work is thought to arise from the exposure of tryptophans to water. Saturable binding curves for cholesterol (Fig. 11A), stearic acid (Fig. 11B), arachidonic acid (Fig. 11C), and DHA (Fig. 11D) were observed and the dissociation constant K_d determined for each ligand to reveal K_d values of 7 $\pm$ 1 nM, 80 $\pm$ 9 nM, 22 $\pm$ 1 nM, and 46 $\pm$ 6 nM, respectively at a single site that was not necessarily the same for each ligand. Thus, Plin2 exhibited very high affinity for cholesterol and less so for the saturated fatty acid stearic acid, consistent with values obtained from previous studies (*5, 6, 8*). High affinity binding was also observed with the polyunsaturated fatty acids arachidonic acid (20:4n-6) and DHA (22:6n-3), indicating that the purified recombinant Plin2 protein contained an active ligand binding site for these lipids.

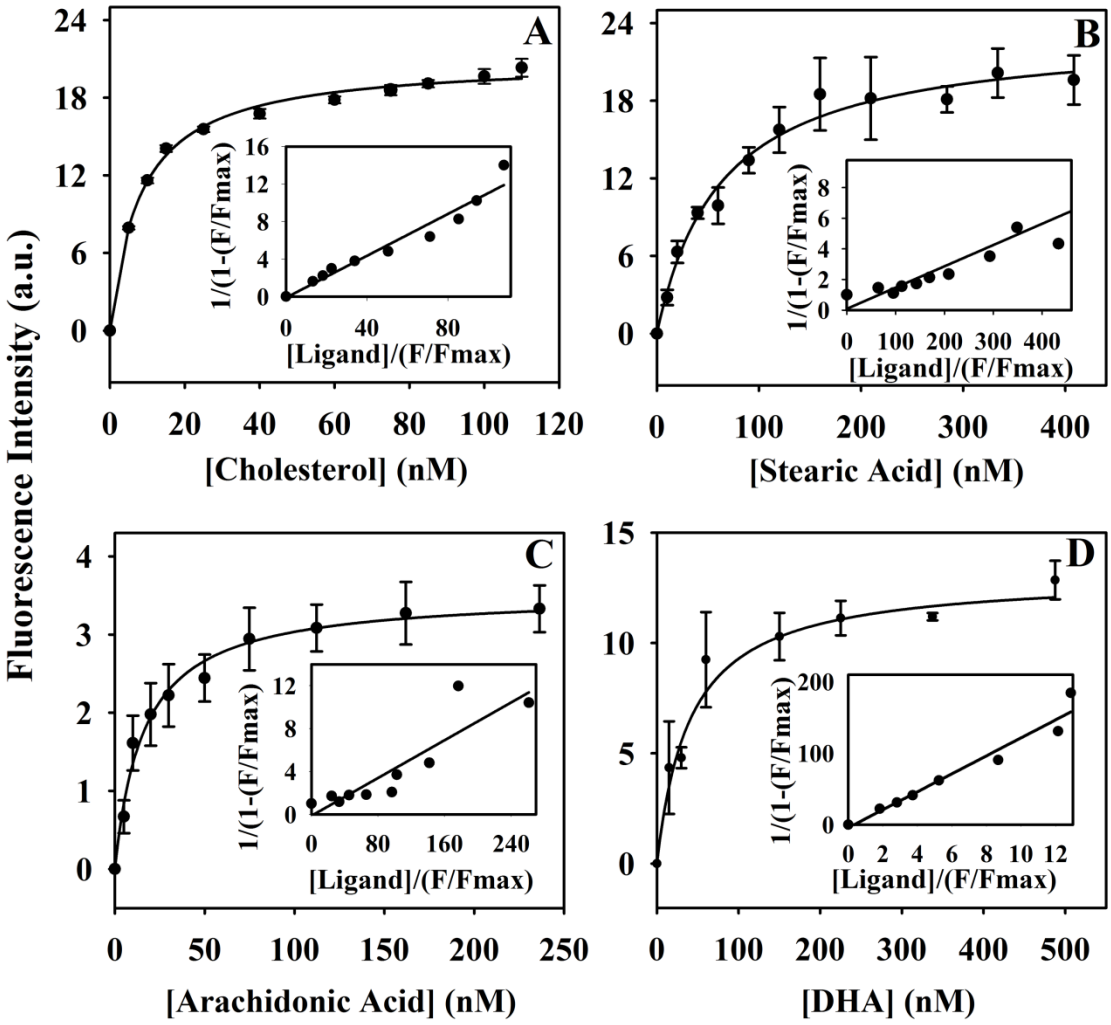

Figure 11. Tryptophan quenching binding assays. The Plin2 binding affinity for cholesterol (A), stearic acid (B), arachidonic acid (C), and DHA (D) was determined when titered with increasing amounts of ligand (1-120 nM) using a quenching of tryptophan fluorescence assay as described in the Experimental section. Inset, a linear plot of 1/(1–F/Fmax) versus [ligand]/(F/Fmax) allowed determination of the dissociation constant Kd where the slope of the line = 1/ Kd and the ordinate intercept = nEo/ Kd and F represented fluorescence intensity at a given concentration of ligand, Fmax was the maximal fluorescence, [ligand] was the ligand concentration, Eo was the protein concentration, and n equaled the number of binding sites. Analysis of multiple curves yielded Kd of 7 ± 1 nM, 80 ± 9 nM, 22 ± 1 nM, and 46 ± 6 nM for cholesterol, stearic acid, arachidonic acid, and DHA, respectively.

NBD-LABELED BINDING STUDIES: PLIN2 AND DELETION MUTANTS BIND CHOLESTEROL AND STEARIC ACID WITH SELECTIVE AFFINITY

Recombinant Plin2 deletion mutants were overexpressed and purified as described in the Methods section (Fig. 9). To establish the ability of Plin2 and the deletion mutants to bind lipids such as cholesterol and stearic acid, NBD-labeled lipid binding assay were performed as previously described (*5-8*). The NBD-fluorophore in NBD-lipids was sensitive to environmental hydrophobicity and therefore provided a useful tool to determine ligand binding affinity. NBD-cholesterol showed minimal fluorescence in aqueous buffer with an emission maximum (λmax) equal to 545nm. Addition of Plin2 or the deletion mutant proteins resulted in increased fluorescence with shifts in λmax to blue wavelengths (0-5 nm) indicating binding of the probe to a site increasingly more hydrophobic than the aqueous buffer (Table 1). With full length Plin2, K_d = 11 $\pm$ 2 nM (Table 1), in keeping with results from the tryptophan quenching studies (Fig. 11A) and with previous reports (*5, 8*). In comparison, deletion mutants Plin2-C1 (Fig. 12B), Plin2-I (Fig. 12F), Plin2-N2 (Fig. 12E), and Plin2-C2 (Fig. 12C) showed significantly less affinity for NBD-cholesterol (Table 1). Most interestingly, deletion mutant Plin2-N1 (Fig. 12D) did not bind NBD-cholesterol, showing little to no increase in fluorescence over the buffer control. This last result indicated that the cholesterol binding site for Plin2 did not reside within the PAT domain.

In similar fashion, the full length protein bound NBD-stearic acid with K_d = 121 $\pm$ 12 nM. These results were comparable to the higher affinity observed (K_d = 80 $\pm$ 9 nM) with

Table 1. Cholesterol and stearic acid binding to Plin2 and the deletion mutants.

	NBD-Cholesterol		NBD-Stearic Acid	
Protein	K_d (nM)	λmax (nm)	K_d (nM)	λmax (nm)
Plin2	11 ± 2	543	121 ± 12	544
Plin2-C1	48 ± 3*,@	540	69 ± 7*,@	538
Plin2-C2	98 ± 10*	545	160 ± 3*	544
Plin2-N1	ND	548	ND	545
Plin2-N2	50 ± 6*,@	543	92 ± 14@	547
Plin2-I	34 ± 4*,@	540	90 ± 7@	540

The dissociation constant (K_d) and emission maximum (λmax) of Plin2 and the deletion mutants for NBD-labeled cholesterol and stearic acid were determined using a fluorescent lipid binding assay as described in the Materials and Methods section. Values represent the mean ± SE (n=3-4). (*) indicates $P \leq 0.05$ as compared to full length Plin2. (@) indicates $P \leq 0.05$ as compared to Plin2-C2. ND indicates no detectable binding was observed.

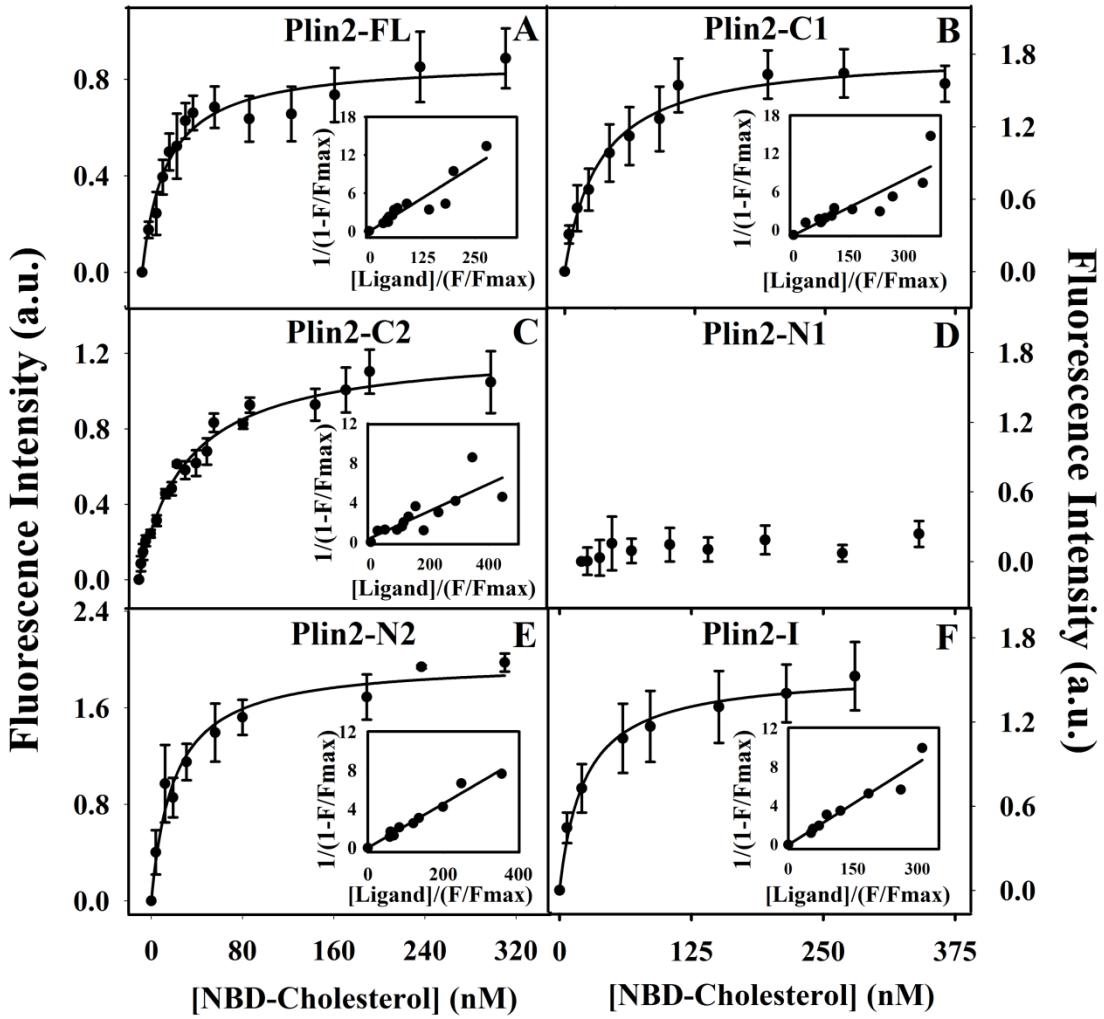

Figure 12. Titration of Plin2 and the deletion mutant proteins with NBD-Cholesterol. The binding affinities of Plin2 (A), Plin2-C1 (B), Plin2-C2 (C), Plin2-N1 (D), Plin2-N2 (E), and Plin2-I (F) for NBD-Cholesterol were determined using a fluorescence binding assay. The titration of the recombinant proteins with NBD-Cholesterol was followed by an increase in fluorescence (excitation 480 nm, emission 540 nm). The data representing the mean ± SE of three independent measurements was fit to a single binding site model as described in the Experimental section. Inset, a linear plot of 1/(1–F/Fmax) versus [ligand]/(F/Fmax) was used to determine the Kd as previously described where F represented fluorescence intensity at a given concentration of ligand, Fmax was the maximal fluorescence, and [ligand] was the ligand concentration.

unlabeled stearic acid in the tryptophan quenching study (Fig. 11B). Likely, the decrease in affinity observed with the labeled ligand was due to the NBD group and its position within the binding pocket. However, despite the differences in K_d values between the labeled and unlabeled ligands, both bound with affinities consistent with results from previous reports (*5, 6*). NBD-lipid binding studies were also performed with acyl CoA binding protein (ACBP), a cytosolic lipid binding protein that exclusively binds long-chain fatty acyl CoA (*58*) but not cholesterol or fatty acids (*59*). When increasing concentrations of NBD-lipids were added to ACBP in solution, no increase in fluorescence was observed after background subtraction, indicating that ACBP did not bind either lipid (data not shown). These results support the specificity of Plin2 for NBD-labeled lipids.

INTRACELLULAR TARGETING AND FRET ANALYSIS

The extent of Plin2/lipid interactions on the lipid droplet surface were determined in a series of experiments using NBD-labeled cholesterol in colocalization and FRET assays. First, co-labeling of NBD-cholesterol with Cy5-labeled Plin2 overexpressed in L cells was accomplished as described in the Methods section and repeated with each deletion mutant. Simultaneous acquisition of multiple confocal images of NBD-cholesterol co-labeled with Cy5-proteins revealed the following: 1) Plin2 (Fig. 13A) and Plin2-I (Fig. 13F) expression cells showed increased numbers of lipid droplets as compared to the control (data not shown) and other mutant expression cell lines. Likewise, these expression cells showed full targeting to the lipid droplet surface.

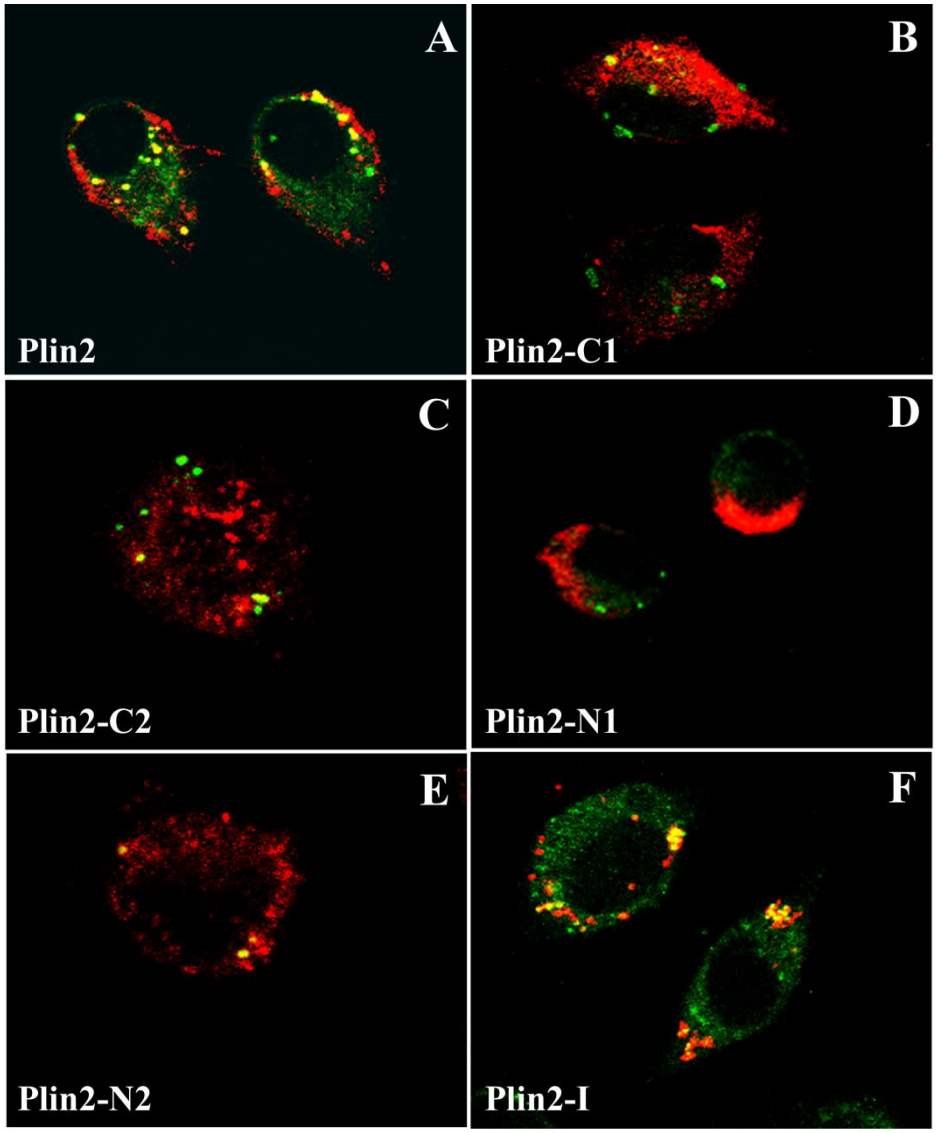

Figure 13. Confocal microscopy colocalization of NBD-Cholesterol and Cy5-labeled cells expressing Plin2 and the deletion mutants. Colocalization experiments of NBD-Cholesterol and Cy5-labeled L cells overexpressing Plin2 (A), Plin2-C1 (B), Plin2-C2 (C), Plin2-N1 (D), Plin2-N2 (E), or Plin2-I (F) were performed as described in the Methods section. Images were acquired sequentially and fluorescence emission was detected upon 488 nm excitation and 500/100 band path emission filter for NBD-Cholesterol (green channel) and 635 nm excitation with a 725/30 band path filter for the Cy5 emission (red channel). Images derived from the red and green channels were combined and appeared as yellow to orange where superimposition of images derived from the red and green channels overlapped.

2) Plin2-C1 (Fig. 13B) and Plin2-C2 (Fig. 13C) expressing cells exhibited partial targeting to lipid droplets, resulting in diminished lipid droplet number as compared to cells expressing full length protein or Plin2-I. 3) Plin2-N2 (Fig. 13E) also showed partial lipid droplet targeting but diminished number of lipid droplets as compared Plin2-C1 or -C2 expression cells. 4) In contrast, Plin2-N1 (Fig. 13D) showed no targeting and the least amount of lipid droplets. These results suggested that Plin2 lipid droplet targeting was closely related to the amount of lipid droplets produced. Second, in expression clones that targeted to lipid droplets, FRET analysis was performed as described in previous work (*4, 54*) to ascertain if the Cy5-labeled proteins and the NBD-cholesterol (ligand) are in close proximity for binding. With appropriate choice of fluorescent probes, FRET detects direct interactions at the molecular level when the donor and acceptor are in within distances of 10-100 Å. FRET was observed between NBD-Cholesterol (donor) and Cy5-labeled Plin2 (acceptor) by measuring the amount of increase in donor intensity after acceptor photobleaching. The calculation of the FRET efficiency (*E*), a measure of the extent of probe overlap, was determined as 25 $\pm$ 5 (Table 2), values consistent with efficient overlap of electronic states and direct interaction of NBD-cholesterol and Plin2 on the lipid droplet surface. The FRET efficiency represents a mean interaction distance of 1.20 R_0. Using the calculated Förster radius, R_0 = 56Å, the mean interaction distance was calculated to equal 67 $\pm$ 4 Å, indicating close proximity (Table 2). In similar fashion, FRET was performed with NBD-cholesterol and the Cy5-labeled deletion mutants to show FRET occurred between the NBD-labeled ligand and the following deletion mutants: Plin2-C1, Plin2-C2, and Plin2-I with *R* values ranging from 85-96 Å (Table 2). No FRET was observed with

Table 2. Intracellular targeting and FRET analysis of Plin2 and the deletion mutants in transfected L cells.

Protein	Intracellular Targeting	*E* (%)	*R*(*R*$_0$)	*R* (Å)
Plin2	LD	25 ± 5	1.20R_0	67 ± 4
Plin2-C1	LD, Cytosol	7 ± 1	1.54R_0	86 ± 4
Plin2-C2	LD, Cytosol	13 ± 3	1.37R_0	77 ± 4
Plin2-N1	Cytosol	ND	ND	ND
Plin2-N2	LD, Cytosol	ND	ND	ND
Plin2-I	LD	9 ± 1	1.47R_0	82 ± 4

Intracellular targeting, FRET efficiencies *E*, and distance *R* between Cy5-labeled Plin2 deletion proteins and NBD-cholesterol were determined as described in the Materials and Methods section. FRET was not detected (ND) in Plin2-N1 or Plin2-N2 expression cells. Values reflect mean ± SE from n≥20 lipid droplets (LD) from 20-30 cells. Intracellular targeting indicated localization sites of Cy5-Plin2 (red) and NBD-Cholesterol (green) where yellow-to-orange indicated colocalization of the probes.

Plin2-N1 or Plin2-N2. Taken together, these findings were consistent with results from the binding studies and indicated that Plin2 and several of the deletion mutants directly interacted with NBD-Cholesterol on the lipid droplet surface.

CIRCULAR DICHROIC ANALYSIS OF ADRP AND DELETION MUTANTS

To further examine how structure affects function, the secondary structures of Plin2 and the deletion mutants were analyzed by circular dichroism (CD) both with and without ligand (cholesterol and stearic acid). In absence of ligand, the CD spectrum for full length Plin2 (Fig. 14A, solid line) showed a double minimum at ~208 and 222 nm signifying the presence of substantial amounts of α-helices. The molar ellipticity was slightly lower at 208 nm than at 222 nm however, indicating a significant amount of unordered structure or random coil. A similar trend was visible in the spectra for Plin2-N1 and Plin2-N2 before addition of ligand (Fig. 14D and 14E, solid lines). In contrast, the CD spectra for deletion mutants Plin2-C1, Plin2-C2 and Plin2-I (Fig. 14B, 14C and 14F, solid lines) showed a fairly well balanced molar ellipticity at both wavelengths along with a strong positive peak at 190nm-200nm, indicating that these mutants had less unordered structure and retained strong α-helical character. These results were supported when the data was analyzed using CDSSTR software. Quantitative analysis of multiple CD spectra revealed that deletion mutants Plin2-C1, Plin2-C2 and Plin2-I exhibited the lowest proportion of unordered structure (29%, 29%, and 31%, respectively) and high α-helicity (Table 3). Similar results were shown by SELCON2 analysis (data not shown).

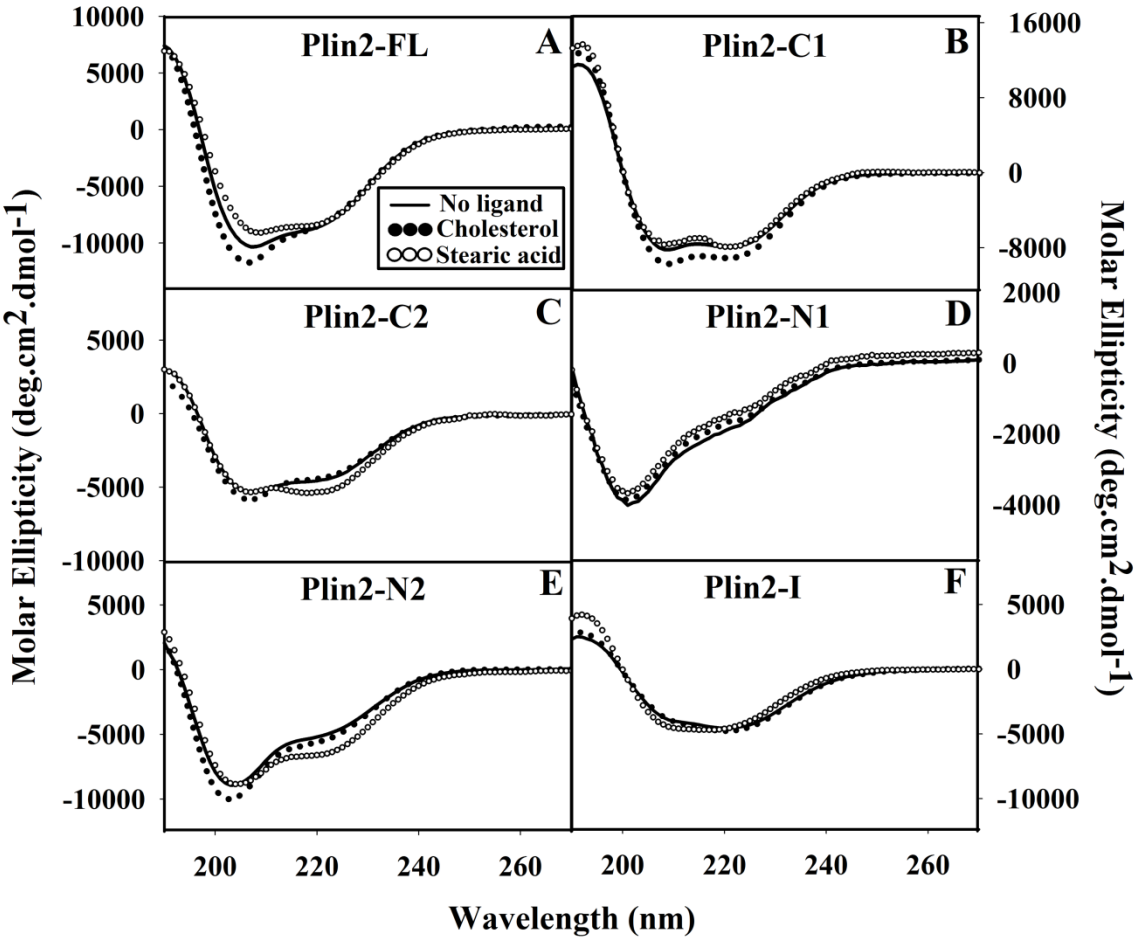

Figure 14. Circular dichroic analysis of Plin2 and the deletion mutants. Far ultraviolet (UV) circular dichroic (CD) spectra of Plin2 (A), Plin2-C1 (B), Plin2-C2 (C), Plin2-N1 (D), Plin2-N2 (E), and Plin2-I (F) was shown in the presence or absence of ligand (cholesterol or stearic acid, 5 μM). Solid line indicates protein without ligand. Spectral trace designated by closed circles indicates protein incubated with cholesterol; open circle indicates protein incubated with stearic acid. Each spectrum represents an average of ten scans repeated in triplicate.

Further analysis of the secondary structure of Plin2 showed that Plin2 contained 21.8% α-helices and 24.5% β-strands based on analysis by CDSSTR analysis (Table 3) with similar results observed with SELCON3 analysis (data not shown). A comparison of the secondary structure of Plin2 to that of each deletion mutant showed that Plin2-C1 and Plin2-C2 had a higher percentage of α-helices (regular and distorted) than Plin2. These results were consistent with secondary structure predictions (Fig. 8A) since Plin2-C1 contained the 4-helix bundle (α6, α7, α8, α9) and Plin2-C2 contained α7, α8, α9, giving them the highest α-helical percentage within the group. In contrast, the other three deletion mutants; Plin2-I, Plin2-N1, and Plin2-N2 exhibited less α-helical structure than full length Plin2 based on both methods of analysis with results showing a respective 16.4%, 10.5%, and 16.5% α-helical structure (regular and distorted). The percentage of β-sheets (regular and distorted) was also significantly higher in Plin2 (24.5%) when compared to Plin2-C1 (11.5%) and Plin2-C2 (19.1%) but significantly less than Plin2-I (30.2%), Plin2-N1 (40%), or Plin2-N2 (27.2%). Results from CDSSTR analysis showed that Plin2 had significantly more β-turns (21.8%) than Plin2-C2 (19.1%) but less than Plin2-N2 (23.4%). There were no significant differences between Plin2-C1, Plin2-I (19.3%) and Plin2-N1. In summary, in the absence of ligand, the C-terminal region of Plin2 (residues 119-436) exhibited a strong α-helical character with less unordered structure as compared to the full length protein or mutants containing the N-terminal region (residues 1-119). Alternatively, the N-terminal region of the protein contained significantly more unordered structure than the C-terminal region.

Table 3. Predicted secondary structures of Plin2 and the deletion mutants in the presence and absence of cholesterol and stearic acid.

		Secondary Structure (%)					
		H(r)	**H(d)**	**S(r)**	**S(d)**	**Turns**	**Unrd**
Plin2	(-)Ligand	10.3±0.1	11.5±0.2	15.0±0.1	9.5±0.1	21.8±0.1	31.7±0.1
	(+)Chol	12.05±0.4**	11.7±0.3	15.3±0.1	9.4±0.1	21.5±0.4	31.1±0.2
	(+)STA	9.9±0.1**	11.1±0.2	15.0±0.3	9.9±0.1**	21.9±0.1	32.2±0.2
Plin2-C1	(-)Ligand	21.3±0.2*	19.6±0.6*	6.1±0.6*	5.4±0.4*	19.1±1	28.0±0.5*
	(+)Chol	27.7±0.2**	23.6±0.2**	5.0±0.1	4.9±0.1	18.2±0.2	26.9±0.2
	(+)STA	18.3±0.2**	18.3±0.2	7.0±0.6	6.5±0.1	20.9±0.8	29.2±0.4
Plin2-C2	(-)Ligand	18.6±0.1*	14.2 ± 0.1*	11.2±0.1*	7.9±0.1*	19.1±0.1*	29.1±0.1*
	(+)Chol	19.6±0.4	13.4±0.1**	11.3±0.7	8.1±0.1	19.1±0.5	29.7±0.2
	(+)STA	18.8±0.1	14.1±0.1	11.3±0.1	8.0±0.1	19.0±0.2	28.6±0.1**
Plin2-I	(-)Ligand	7.5±0.2*	8.9±0.1*	19.0±0.2*	11.2±0.1*	21.9±0.1	30.6±0.1*
	(+)Chol	6.3±0.1**	9.1±0.1	19.4±0.1	11.2±0.1	21.8±0.1	30.9±0.2
	(+)STA	6.9±0.1	8.5±0.1**	19.9±0.1**	11.6±0.1**	22.1±0.1	30.3±0.1
Plin2-N1	(-)Ligand	0.8±0.5*	2.5±0.8*	26±3*	14±1*	27±2	30±4
	(+)Chol	0.4±0.1	3.8±0.2	26.5±0.7	12.5±0.1	22.1±0.6	33.8±0.2
	(+)STA	0.1±0.1	3.6±0.4	25.7±0.2	12.4±0.1	24±1	32±1
Plin2-N2	(-)Ligand	6.5±0.1*	10.0±0.2*	16.5±0.1*	10.7±0.1*	23.4±0.1*	33.0±0.2*
	(+)Chol	5.2±0.4**	7.1±0.4**	18.1±0.3**	11.0±0.2	23±1	33±1
	(+)STA	6.9±0.2	10.4±0.1	16.1±0.1**	10.6±0.1	23.5±0.2	32.6±0.2

All conditions were as described in the Materials and Methods section. Values represent the mean ± SE (10 iterations/run performed in triplicate) analyzed by CDSSTR. H(r) indicates regular α-helices; H(d), distorted α-helices; S(r), regular β-sheets; S(d), distorted β-sheets; Unrd, unordered structures. Chol refers to cholesterol and STA to stearic acid. (*) indicates $P \leq 0.05$ as compared to Plin2 without ligand. (**) indicates $P \leq 0.05$ as compared to each protein in the absence of ligand.

The effect of ligand binding on secondary structure was also examined. The addition of cholesterol (Fig. 14A, closed circles) and stearic acid (Fig. 14A, open circles) altered the shape of the CD spectrum of full length Plin2, intensifying the minima at 208 nm with cholesterol but diminishing the peak when stearic acid was present. These alterations were reflected by significant changes in the percent composition of α–helical structures where an increase and decrease respectively, were observed when cholesterol and stearic acid were added to the protein. With the deletion mutants, subtle changes in the CD spectra were also observed upon addition of ligands. As with the full length protein, the CD spectrum of Plin2-C1 showed a significant increase in the intensity of the 208 nm minimum when cholesterol was added but a significant decrease upon addition of stearic acid, reflecting significant increases in both disordered helices and unordered structures while decreasing the percentage of β-sheets (Fig. 14B, Table 3). Subtle conformational changes in the CD spectra were also observed with Plin2-C2, Plin2-I, and Plin2-N2 upon ligand addition, reflecting significant changes in percentage of α-helices and β-sheets based on CDSSTR analysis (Table 3). All three mutants exhibited significant decreases in α-helical structure when cholesterol was added, concomitant with significant increases in β-sheet and unordered structure (Table 3). In summary, the CD results were consistent with the predicted secondary structure (Fig. 8) and indicated that several of the proteins were sensitive to ligand binding. Lack of conformational change upon ligand binding with deletion mutant Plin2-N1 was consistent with results from the binding studies which indicated that this mutant did not bind cholesterol or stearic acid. Interestingly, the decrease in signal, along with the increase in unordered structure upon addition of stearate was indicative of a more flexible binding pocket that

does not enhance the secondary structure of Plin2. Conversely, addition of cholesterol enhanced CD signal and increased the percentage of α–helical character. This increase in structured secondary structure suggests that binding of cholesterol was dependent on a defined secondary structure.

THE TERTIARY STRUCTURE OF THE PLIN2 C-TERMINAL DOMAIN DEFINES A CLEFT THAT CAN INTERACT FAVORABLY WITH STEARIC ACID AND CHOLESTEROL

The tertiary structure of Plin2 (Fig. 15A) was modeled by using two comparative modeling approaches. Homology modeling by Modeller (*44*) (web server: http://salilab.org/modweb) was employed for the C-terminal domain based on its sequence similarity to Plin3, since this technique provides the most accurate structural models. Modeller constructed a homology model of the structure of C-terminal residues 190-409 of murine Plin2 (Fig. 15A) based on its alignment with murine Plin3 (also known as TIP47) with 38% sequence identity, well above the 25% threshold required for confident homology modeling (*28*). In the absence of a structural template with high enough sequence similarity to the N-terminal region of Plin2 to allow homology modeling, the next most accurate approach, fold recognition, was used. This approach defines the best-matching structural template in the Protein Data Bank (PDB) based on the compatibility of the query sequence with the primary and secondary structure of the NMR or crystal structure being evaluated as a template, and the favorability of the 3-dimensional chemical interactions of each residue with its neighbors when modeled using that particular 3-D structure. The Pcons.net (http://pcons.net) server was used to model residues 1-171 of murine Plin2 based on the consensus of predicted structures

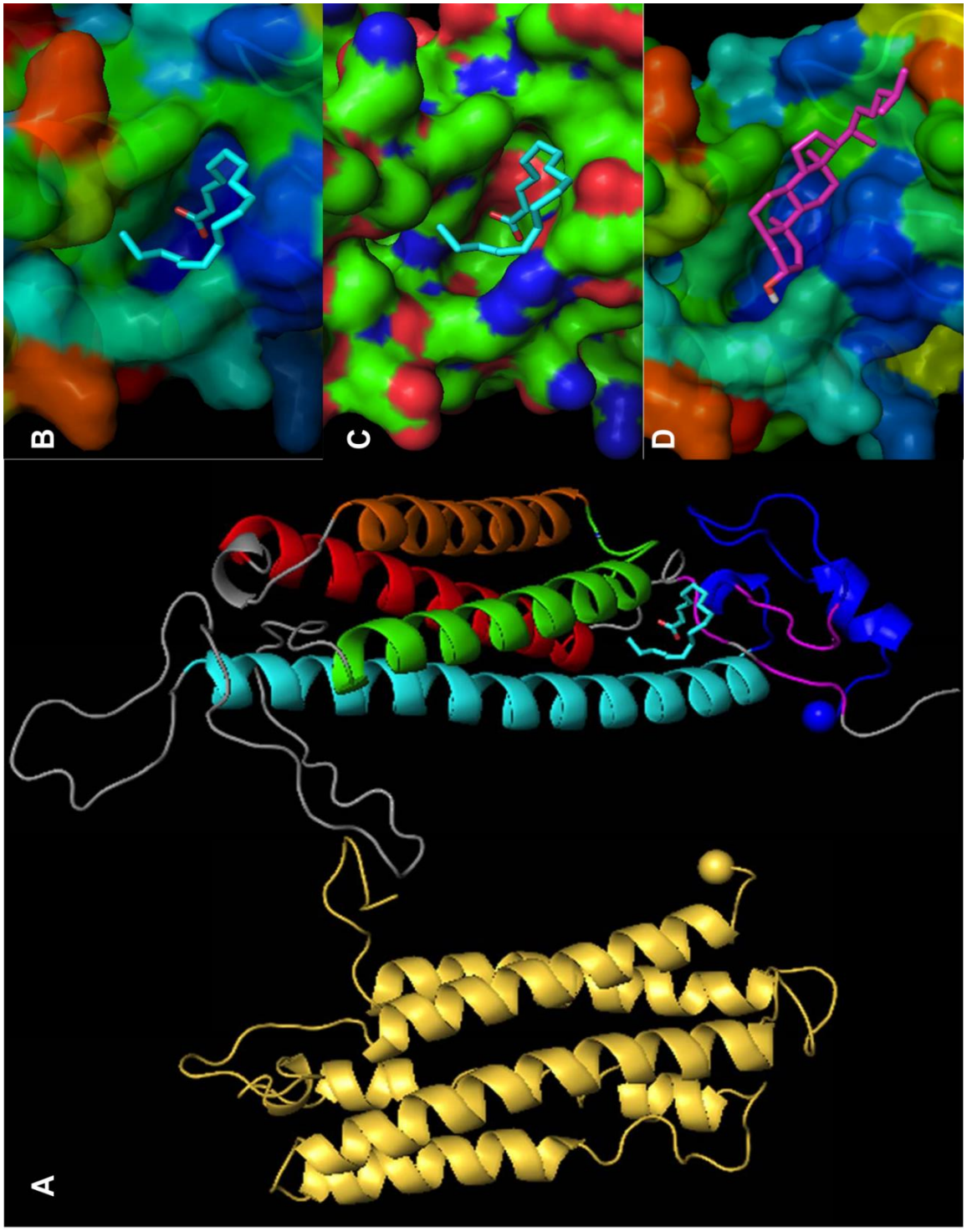

Figure 15. Plin2 has an apophorin-like N-terminal domain and a Plin3-like C-terminal domain containing a potential lipid binding cleft.

Figure 15. (cont'd). The N-terminal domain structure of Plin2 (residues 1-171; shown in yellow ribbons) was modeled using the nfold fold recognition server via Pcons, based on the high degree of Plin2 sequence and secondary structural compatibility with the 3-dimensional structure of apolipophorin III (PDB entry 1AEP) and this model's consensus with the top-scoring results from 11 other fold recognition predictions for the N-terminal Plin2 sequence, all of which are alpha-helical bundles. This structure contains 5 helices connected by turns in a compact bundle. This model for the N-terminal 171 residues of Plin2 received a Pcons consensus score of 0.77, indicating a high degree of shared features with the top-scoring models from the different fold recognition methods. A value of 0.77 corresponds to 98% sensitivity (meaning 98% of the proteins of similar fold are predicted correctly) and 94% specificity (meaning that 94% of proteins with dissimilar folds will not be incorrectly assigned as similar in fold). The homology model of the C-terminal domain of Plin2 appears to the right in panel (A), based on its 38% sequence identity with the crystal structure of the corresponding region in Plin3 (residues 191-437, PDB entry 1SZI). The structure contains a 4-helix bundle (cyan, green, orange and red helices), which together with an α-β domain (blue, magenta and light grey) form the cleft. Stearic acid (the U-shaped light blue-colored stick figure, with carboxylate oxygens in red) is shown positioned in this cleft, based on the most energetically favorable binding mode predicted by SLIDE (48). Cleft residues include Val203, Tyr215, Ala233, Arg236, Val237, Ala240, Thr325, Val326, Asn329, Gln331, Trp398, Leu399, Val400, Pro402 and Phe403. (B) ConSurf analysis of residue conservation in the perilipin family, color-mapped onto the surface of the Plin2 C-terminal domain. The position of the cleft is indicated by the predicted binding mode for stearic acid (light blue stick figure). Dark blue to green surface indicates the most highly and next most highly conserved residues in perilipins mapped onto the Plin2 structure, and yellow to red indicate increasingly low conservation. (C) Atom-colored surface representation of the same region in Plin2 (green for carbon, blue for nitrogen, and red for oxygen atoms). Hydrogen-bonding atoms are found deep in the cleft ringed by hydrophobic surface, positioned such that they can bridge to the predicted position of the carboxylate group in stearic acid. (D) Predicted most favorable mode of cholesterol binding (pink tubes) with the conserved cleft of Plin2, shown with surface colored by residue conservation (as in panel B, above).

from 11 different fold recognition methods. Of the 10 highest-consensus structural models provided by Pcons, two corresponded to functionally relevant apolipoprotein structures that form compact α-helical bundles: apolipophorin III (PDB entry 1AEP, residues A6-A158); (*60*) and apoliprotein A-I (PDB entry 2A01, residues A44-A187 (*61*). The apolipophorin-based model for Plin2 was chosen based on having higher sequence identity (20%, relative to 10% sequence identity for apolipoprotein A-I). Additionally, the matched region of Plin2 corresponds to the entire helical bundle structure of apolipophorin, including a fifth, irregular helix, as shown in yellow in Fig. 15A. This model is consistent with previous studies suggesting N-terminal domain homology with apolipoproteins (*25, 27*). Together, the N-terminal apolipophorin (left side of Fig. 15A) and C-terminal Plin3-based structural model (right side of Fig. 15A) cover all but the 18 linking residues between the two domains and the 16 C-terminal residues of Plin2, which could not be modeled due to lack of homology. A close sequence match in the PDB was found for 13 of the 18 linking residues in Plin2 (VDNAITKSELLVD) which match residues A136-A153 in PDB entry 1E6B (VNNAITKGFTALEKLLVN), forming an alpha helix (*62*). The central residues FTAL in this known structure are an insertion corresponding to a full turn of helix not found in the Plin2 sequence. Though the matching sequence comes from a glutathione S-transferase, which is unlikely to be a functional homolog of Plin2, an exact match of 9/13 residues between these two peptides means they are statistically likely to fold the same, as an alpha helix as previously described (*28*). Thus, the C-terminus (yellow sphere at bottom center of Fig. 15A) of the apolipophorin-like domain and the N-terminus (blue sphere) of the Plin3 domain may well be connected by a helical linker. The model presented here is

consistent with the solution based structures for Plin3 described by Hynson et al., who show the Plin3 C-terminal domain as one-half of an elongated structure (*33*). Their volumetric profile is consistent with end-to-end packing of the N-terminal and C-terminal domains in the Plin3 solution structure.

ConSurf multiple-sequence alignment of 38 diverse proteins in the Plin family yielded conservation values for each residue, which were color-mapped onto the surface of the Plin2 C-terminal domain structure and defined a cleft region (Fig. 15B). In the model, blue identified highly conserved residues with a gradient towards green, yellow, orange and red indicating decreasing chemical conservation. The Plin2 model was also colored by atom type, with blue for nitrogen atoms, green for carbon, and red for oxygen atoms (Fig. 15C). In both models the most favorable mode of stearic acid interaction with the cleft was predicted by SLIDE molecular docking (*50*) to reveal 5,613 favorable conformers of stearic acid generated by Omega2, including protein side-chain and ligand single-bond rotations for steric complementarity between stearic acid and Plin2. The result was an orientation of stearic acid and conformation of Plin2 side chains that yielded a favorable predicted $\Delta G_{binding}$ (-7.5 kcal/mol). The resulting orientation of stearic acid matches a highly conserved surface patch in Plin2 (blue region, Fig. 15B), as well as placing the terminal carboxylate group of stearic acid within favorable distance of conserved hydrogen-bonding groups, including the Arg236 guanidinium on helix α6, the side-chain amines of Asn329 (helix α6) and Trp398 (β4), and the main-chain nitrogen of Gly401 (β4), all absolutely conserved between Plin2 and Plin3. Since some of the deletion mutants (e.g., Plin2-N2 or Plin2-C2) remove several residues contributing to the cleft, the stearic acid binding orientation would likely differ in those

cases. In fact, Plin2-C2 most likely retains lipid binding ability despite lack of key structural features of the cleft domain (helix α4, the $\alpha-\beta$ domain, and part of helix α6) due to retention of interacting residues including Asn329, Trp398 (β4), and Gly401. Docking of cholesterol into the same cleft (Fig. 15D) resulted in greater predicted affinity of binding (-9.6 kcal/mol) relative to steric acid. Cholesterol formed interactions with several residues including Val205, Phe208, Val211, the aliphatic part of Lys213, and Tyr217 in the α-β domain, Thr325 and Val328 in helix α7, and Pro402 in strand β4. Hydrophobic contacts were also made with the collar region created by the conserved residues identified in Plin3 (*25*). Since these residues are conserved between Plin2 and Plin3, similar lipid interactions are also possible in Plin3.

DISCUSSION

Previous studies demonstrated that Plin2 binds lipids with high affinity (*4-8*) and is involved in lipid droplet formation, (*1*) triacylglycerol accumulation, (*1-4*) fatty acid uptake, (*9*) and lipoprotein regulation (*8, 12*). Despite these findings, little is known regarding the structural and functional requirements of Plin2-lipid interactions that facilitate these processes. To address this issue, truncated Plin2 mutants were designed to contain one or more predicted domains conserved among the Plin protein family to identify structural motifs required for Plin2 lipid binding. Studies herein provide the following new insights. First, the N-terminal PAT domain is not involved in lipid binding since the Plin2-N1 mutant (containing the PAT domain) showed no evidence of binding lipids. These results are consistent with earlier studies that give evidence the PAT domain is involved in other roles including lipid droplet stabilization, lipid

accumulation, and proteasomal degradation of Plin2 (*24*). Second, Plin2 residues 119-251, containing helix α4, the α–β domain, and part of helix α6 form a Plin3-like cleft found to be important for highest affinity lipid binding. This follows from findings that mutants containing residues 119-251 (Plin2-C1 and Plin2-N2) showed the highest affinity for cholesterol and stearic acid ligands, while those lacking these residues exhibited the least (Plin2-C2) or no (Plin2-N1) lipid binding. With Plin2-C2, NBD-stearate and NBD-cholesterol binding decreased up to 9-fold when compared to the full length protein and more than 3-fold when compared to Plin2-C1, resulting in a protein that still targeted to lipid droplets but with the lowest affinity of all the mutants that showed binding. Results finding residues 119-251 important to binding are not surprising, since the region includes structures found in the X-ray crystal of Plin3 that form a cleft of sufficient size to accommodate lipid ligands (*25*). In addition, other work shows that the region of Plin2 within residues 119-426 is able to fold and function independently from the rest of the protein (*27*). Some of the residues within the cleft region however, are not entirely essential for lipid binding since removal of the α-β domain (residues 171-219) resulted in a mutant (Plin2-I) with similar binding affinity to that of the full length protein. It should also be noted that affinities for the two ligands (cholesterol and stearic acid) were distinctly different. For example, Plin2-I showed a 3-fold decrease in NBD-cholesterol binding as compared to the full length protein, but with NBD-stearic acid no significant change in binding was observed. The results suggest that Plin2 has slightly different determinants for cholesterol and stearic acid binding. For instance, the proposed lipid binding site in the C-terminal domain (Fig. 15) has some shared interactions for cholesterol and stearic acid binding, but different footprints due

to the different chemical structures of the individual ligands. Consistent with this, Plin2 is known to support binding to an array of lipids with diverse structures such as phospholipids, sphingomyelin, cholesterol, and fatty acids (*5-8*). In the present study, we show for the first time that Plin2 binds polyunsaturated fatty acids including arachidonic acid, a ω6 fatty acid that is precursor to several families of pro-inflammatory eicosanoid lipid mediators, and DHA, a ω3 fatty acid associated with anti-inflammatory benefits, with high affinity (K_d = 22 ± 1 nM and 46 ± 6 nM, respectively). These results suggest that lipid droplets may act as physiological stores for essential fatty acids. In addition, since Plin2 binds arachidonic acid with 2.1-fold higher affinity than DHA and close to 4-fold higher affinity than stearic acid, these findings support Plin2 selectively sequestering proinflammatory fatty acids to the lipid droplet surface. Consistent with this, arachidonic acid-derived eicosanoids have been detected on lipid droplets that colocalize with Plin2. Discrete targeting of the Plin2 mutants to lipid droplets was also demonstrated. Deletion mutants Plin2-N1, containing residues 1-119 (the PAT domain) and Plin2-N2, comprised of residues 1-251 (the PAT domain, helix α4, α5–β3 domain, part of helix α6) did not target to lipid droplets or show FRET interactions, consistent with earlier work demonstrating that N-terminal deletion mutants containing residues 1-131 were not found on lipid droplets (*16, 17*). Addition of 52 residues to the PAT domain salvaged targeting ability in previous studies, (*16, 17*) suggesting the presence of a lipid droplet targeting domain in the central region of the protein. With regard to C-terminal mutants, both Plin2-C1 (containing residues 119-426) and Plin2-C2 (residues 251-426) targeted to lipid droplets, consistent with previous reports (*16, 17*). However, removal of residues 154-174 in other studies (*16*) showed lack of targeting while exclusion of

residues 172-218 in the present work resulted in a protein that targeted lipid droplets and interacted with NBD-cholesterol in FRET assays. Despite some inconsistencies between reports, these results reinforce the idea that Plin2 contains two independent, non-overlapping targeting domains in its internal and C-terminal sequence that need consideration of the tertiary structure to understand their structure. Likewise, the fluorescence binding data supported that the ligand binding site of Plin2 is not dictated by a linear structural motif within the primary sequence. Much like the regions required for lipid droplet targeting, domains involved in forming the lipid binding pocket of the protein come from non-contiguous parts of the protein. This motivated the modeling of Plin2 tertiary structure to understand how these regions organize into functional lipid binding and targeting domains. The tertiary structure of Plin2 was modelled using Modeller and Pcons, also providing insights into the differences in ligand binding affinities among the mutant proteins. Comparative modeling revealed the Plin2 tertiary structure contained an apolipophorin III-like N-terminal domain and a TIP47-like C-terminal domain, which were linked by 18 residues. Consistent with earlier predictions and X-ray crystal data for the most similar proteins, the modeled N-terminal domain is likely to form an α-helical bundle, (*26, 27*) while the C-terminal domain contained a highly conserved cleft formed from the union of the $\alpha-\beta$ domain and the 4-helix bundle with high homology to the corresponding crystal structure of this region in Plin3 (*25*). ConSurf multiple-sequence alignment identified highly conserved residues within the Plin family which localize to the cleft. SLIDE molecular docking (*50*) revealed favorable conformers of stearic acid and cholesterol interaction in the cleft region. Key residues predicted to interact with stearic acid included Trp398, Gly401, and two residues in helix

α6, Arg236 and Asn329 that are conserved between Plin2 and Plin3, suggesting conservation of function. Cholesterol formed interactions with several residues in the same region as stearic acid including Val205, Phe208, Val211, Lys213, and Tyr217. However, cholesterol also interacted with residues Thr325 and Val328 in helix α7, and Pro402 in strand β4 near the C-terminal end of the protein. Orientations of stearic acid and cholesterol within the cleft were favored energetically, with cholesterol predicted to have greater affinity of binding relative to stearic acid ($\Delta G_{binding}$ of -9.6 kcal/mol versus -7.5 kcal/mol). These results were consistent with experimental binding results that showed Plin2 bound NBD-cholesterol with higher affinity than NBD-stearic acid. Deletion mutants that remove residues contributing to the cleft (e.g. Plin2-I) would also be expected to differ in binding interactions and affinity, as was observed with the experimental data demonstrating higher affinity for stearic acid than cholesterol with deletion mutant Plin2-I and decreased affinity for cholesterol when compared to the full length protein. Moreover, Plin2-C2 is missing some structures that form the cleft domain but retention of several interacting residues (Asn329, Trp398, Gly401, Thr325, Val328, and Pro402) likely contributes to its ability to bind both stearic acid and cholesterol, although at decreased affinity. These results support that the predicted cleft in the C-terminal region of Plin2 favorably binds lipids.

Structural changes induced by mutation or ligand addition were also examined. Plin2 in the absence of ligand was significantly helical. However, the percentage of helical content doubled in the Plin-C1 and Plin-C2 mutants, in which the N-terminal domain and part or all of the α-β domain were absent, suggesting that the C-terminal region is much more strongly helical than the N-terminal region. These trends were preserved in the

presence of both cholesterol and stearic acid, suggesting that ligand binding does not dissolve or nucleate helical structure in Plin2. Consistent with these findings, Hynson et al showed that the C-terminal region of the homologous Plin3 protein was mostly α-helical with little β–strand content (*33*). In addition, the Plin3 N-terminal was found to increase the percentage of amino acid residues forming β-strand, turns, and random coil (*33*). CD analysis of the Plin2 N-terminal region showed similar results; despite the sequence-based prediction of predominantly helical structure for the N-terminal half of the protein. One interpretation of these results is that the N-terminal helices are less stable and fluctuate more without the presence of lipid ligand or membrane. Indeed, studies with the Plin3 protein show the N-terminal region is highly elongated in solution, suggesting that Plin3 N-terminus becomes a highly structured domain upon interaction with lipids or membrane (*33*). However, the Plin2 N-terminal domain may interact differently and these domain orientations could also change when associated with a lipid droplet. It should be noted that conformational change in another lipid droplet protein, Plin1 occurs upon hyperphosphorylation, allowing access to lipids in the droplet (*63-66*). This raises the question as to whether the C-terminal domain of Plin2, containing the suggested binding site for stearic acid and cholesterol, is likely to undergo a large-scale rearrangement upon interacting with lipid droplets. Amphipathic alpha-helical bundles with tightly packed hydrophobic cores, like that found in Plin2, are not typically observed to alter conformation significantly due to the considerable energy it would take to disrupt the extensive favorable hydrophobic interactions within the core. Even the highly hydrophobic helical bundles in integral membrane proteins like cytochrome c oxidase typically only show coupled motion of helices rather than any

reorganization of interfaces (*67*). Viral fusion with host membranes has been shown in some cases to depend on the formation of helical bundles as a rate-limiting step (*68*). The same phenomenon has been observed for Hsp12 stress proteins, which are unfolded in the cytosol and then adopt helical conformation upon interaction with the membrane (*69*). Because the helical bundles in Plin2 have polar surfaces, however, it is hard to imagine any configuration or rearrangement in which they could be favorably buried inside a lipid milieu. Thus, association could be with the surface of the lipid droplet, through interaction with polar headgroups, or by a tethering mechanism. Indeed this was shown through a series of experiments by McManaman et al in which the polar surface of the helical bundles targeted to membranes in non-ionic solutions and were displaced as salt was added (*27*). These results further support that the 4-helix bundle in the C-terminus of Plin2 can interacts with polar head groups of the lipid droplet thereby binding and sequestering lipids.

Lipid droplet targeting was also associated with maintenance of the helical regions in both the N- and C-terminal helical bundles, as evidenced by Plin2 and Plin2-I being fully targeted to lipid droplets, while the other mutants were partially or fully targeted to the cytoplasm. Fluorescence binding and FRET results with labeled cholesterol support strong interactions between cholesterol and the native Plin2 structure, with weaker interactions with Plin2-C1, Plin2-C2, Plin2-I, and Plin2-N2 constructs. No evidence for cholesterol (or stearic acid) interaction with Plin2-N1 was detected. These results support the crucial role of the C-terminal helical bundle region of Plin2 that is homologous to Plin3 for binding lipids; this region contains the conserved cleft. Other recent reports support the functional importance of the Plin family's C-terminal regions

(*70, 71*). The C-terminal region of Plin1 contains a C-terminal region, implicated in binding AB-hydrolase domain containing-5 (ABHD5), a cofactor that prevents the activation of adipose tissue triacylglycerol lipase. Patel *et al.* (*70*) demonstrated that fusing the carboxyl terminal region of Plin1 to the amino terminus of Plin2 was sufficient to stabilize ABHD5 and suppress basal lipolysis. For Plin5, Sztalryd *et al.* (*71*) demonstrated that fusing the carboxyl terminal region of Plin5 to Plin2 generated a protein that was able to recruit lipid droplets to mitochondria, whereas Plin2 by itself did not. Our work supports specific lipid binding as a function for the C-terminal region in Plin2.

In summary, the modeled tertiary structure for Plin2 highlighted the structural and functional features necessary for ligand binding and lipid droplet targeting. The PAT domain was not required for lipid binding or lipid droplet targeting; removal of this domain resulted in C-terminal mutants with high affinity for lipids. Crucial elements contained within residues 119-251 in the C-terminal region include the central α–β domain, along with the conserved end of helix $\alpha 6$, which form part of the cleft region. Removal of these residues decreased binding with cholesterol and stearic acid ligands several-fold. Evidence of the functional relevance of this region was recently provided in studies with a human Plin2 variant where a serine to proline mutation at residue 251 caused individuals with the minor allele to exhibit decreased plasma triglyceride and decreased VLDL levels (*12*). Structurally, the mutation would be predicted to disrupt helix $\alpha 6$. In the present work, both cholesterol and stearic acid were shown through molecular docking experiments to interact favorably with a cleft formed by conserved

residues within the C-terminal region, including helix $\alpha 6$. Furthermore, the modeled interactions together with the mutant construct binding studies suggest that this conserved cleft is a site of favorable lipid interaction for both cholesterol and stearic acid.

REFERENCES

REFERENCES

1. Fukushima, M., Enjoji, M., Kohjima, M., Sugimoto, R., Ohta, S., Kotoh, K., Kuniyoshi, M., Kobayashi, K., Imamura, M., Inoguchi, T., Nakamuta, M., and Nawata, H. (2005) Adipose differentiation related protein induces lipid accumulation and lipid droplet formation in hepatic stellate cells, *In Vitro Cell Dev Biol Anim 41*, 321-324.

2. Larigauderie, G., Cuaz-Perolin, C., Younes, A. B., Furman, C., Lasselin, C., Copin, C., Jaye, M., Fuchart, J. C., and Rouis, M. (2006) Adipophilin increases triglyceride storage in human macrophages by simulation of biosynthesis and inhibition of beta-oxidation, *FEBS J 273*, 3498-3510.

3. Listenberger, L. L., Ostermeyer-Fay, A. G., Goldberg, E. B., Brown, W. J., and Brown, D. A. (2007) Adipocyte differentiation-related protein reduces the lipid droplet association of adipose triglyceride lipase and slows triacyglycerol turnover, *J Lipid Res 48*, 2751-2761.

4. McIntosh AL, Senthivinayagam S, Moon KC, Gupta S, Lwande JS, Murphy CC, Storey S, and Atshaves BP. (2012) Direct interaction of ADRP with lipids on the surface of lipid droplets: A live cell FRET analysis., *Am J Physiol Cell Physiol 303*, C728-742.

5. Serrero, G., Frolov, A., Schroeder, F., Tanaka, K., and Gelhaar, L. (2000) Adipose differentiation related protein. Expression, purification of recombinant protein in E. coli and characterization of its fatty acid binding properties, *Biochim Biophys Acta 1488*, 245-254.

6. Atshaves, B. P., Storey, S. M., McIntosh, A. L., Peterscu, A. D., Lyuksyutova, O. I., Greenberg, A. S., and Schroeder, F. (2001) Sterol carrier protein 2 expression modulates protein and lipid composition of lipid droplets, *J Biol Chem 276*, 25324-25335.

7. McIntosh, A. L., Storey, S. M., and Atshaves, B. P. (2010) Intracellular lipid droplets contain dynamic pools of sphingomyelin: ADRP binds phopholipids with high affinity, *Lipids 45*, 465-477.

8. Frolov, A., Petrescu, A., Atshaves, B. P., So, P. T. C., Gratton, E., Serrero, G., and Schroeder, F. (2000) High density lipoprotein mediated cholesterol uptake and targeting to lipid droplets in intact L-cell fibroblasts, *J Biol Chem 275*, 12769-12780. .

9. Gao, J., and Serrero, G. (1999) Adipose differentiation related protein (ADRP) expressed in transfected COS-7 cells selectively stimulates long chain fatty acid uptake, *J Biol Chem 274*, 16825-16830.

10. Atshaves, B. P., Starodub, O., McIntosh, A. L., Roths, J. B., Kier, A. B., and Schroeder, F. (2000) Sterol carrier protein-2 alters HDL-mediated cholesterol efflux, *J Biol Chem 275*, 36852-36861.

11. Chang, B. H., Li, L., Saha, P., and Chan, L. (2010) Absence of adipose differentiation related protein upregulates hepatic VLDL secretion, relieves hepatosteatosis, and improves whole body insulin resistance in leptin-deficient mice, *J Lipid Res 51*, 2132-2142.

12. Magne, J., Aminoff, A., Sundelin, J., Mannila, M. N., Gustafsson, P., Hultenby, K., Wernerson, A., Bauer, G., Listenberger, L. L., Neville, M., Karpe, F., Boren, J., and Ehrenborg, E. (2013) The minor allele of the missense polymorphism Ser251Pro in perilipin 2 (PLIN2) disrupts an a-helix, affect lipolysis, and is associated with reduced plasma tryglyceride concentration in humans, *FASEB J 27*, 3090-3099.

13. Brasaemle, D. L., Subramanian, V., Garcia, A., Marcinkiewicz, A., and Rothenberg, A. (2009) Perilipin A and the control of triacylglycerol metabolism, *Mol Cell Biochem 326*, 15-21.

14. Subramanian, V., Garcia, A., Sekowski, A., and Brasaemle, D. L. (2004) Hydrophobic sequences target and anchor perilipin A to lipid droplets., *J Lipid Res 45*, 1983-1991.

15. Fujimoto, T., Kogo, H., Ishiguro, K., Tauchi, K., and Nomura, R. (2001) Caveolin-2 is targeted to lipid droplets, a new membrane domain in the cell, *J.Cell.Biol. 152*, 1079-1085.

16. Nakamura, N., and Fujimoto, T. (2003) Adipose differentiation-related protein has two independent domains for targeting to lipid droplets, *Biochem Biophys Res Comm 306*, 333-338.

17. Targett-Adams, P., Chambers, D., Gledhill, S., Hope, R. G., Coy, J. F., Girod, A., and McLauchlan, J. (2003) Live cell analysis and targeting of the lipid droplet-binding adipocyte differentiation-related protein, *J Biol Chem 278*, 15998-16007.

18. Wiener, M. (2005) A census of ordered lipids and detergents in X-ray crystal structures of integral membrane proteins, In *Protein-Lipid Interactions: From Membrane Domains to Cellular Networks* (Tamm, L., Ed.), Wiley-VCH Verlag GmbH & Co, New York.

19. Qin, L., Sharpe, M., Garavito, R., and Ferguson-Miller, S. (2007) Conserved lipid-binding sites in membrane proteins: a focus on cytochrome c oxidase, *Current Opinion in Structural Biology 17*, 444-450.

20. Hanson, M., Cherezov, V., Roth, C., Griffith, M., Jaakola, V.-P., Chien, E., Valasquez, J., Kuhn, P., and Stevens, R. (2008) A specifc cholesterol binding site is established by the 2.8 A structure of human b_2-adrenergic receptor in an alternate crystal form., *Structure 16*, 897-905.

21. Adamian, L., Naveed, H., and Liang, J. (2011) Lipid-binding surfaces of membrane proteins:Evidence from evolutionary and structural analysis, *Biochem Biophys Acta 1808*, 1092-1102.

22. Garcia, A., Sekowski, A., Subramanian, V., and Brasaemle, D. (2003) The central domain is required to target and anchor Perilipin A to lipid droplets, *J Biol Chem 278*, 625-635.

23. Miura, S., Gan, J. w., Brzostowski, J., Parisi, M. J., Schultz, C. J., Londos, C., Oliver, B., and Kimmel, A. R. (2002) Functional conservation for lipid storage droplet association among perilipin, ADRP, and TIP47 (PAT)-related proteins in mammals, Drosophila, and dictyostelium, *J Biol Chem 277*, 32253-32257.

24. Orlicky, D. J., DeGala, G., Greenwood, C., Bales, E. S., Russell, T. D., and McManaman, J. L. (2008) Multiple function encoded by the N-terminal PAT domain of adipophilin, *J Cell Science 121*, 2921-2929.

25. Hickenbottom, S. J., Kimmel, A. R., Londos, C., and Hurley, J. H. (2004) Structure of a lipid droplet protein: The PAT family member TIP47, *Structure 12*, 1199-1207.

26. McManaman, J. L., Zabaronick, W., Schaack, J., and Orlicky, D. J. (2003) Lipid droplet targeting domains of adipophilin, *J Lipid Res 44*, 668-673.

27. Chong, B. M., Russell, T. D., Schaack, J., Orlicky, D. J., Reigan, P., Ladinsky, M., and McManaman, J. L. (2011) The adipophilin C terminus is a self-folding membrane binding domain that is important for milk lipid secretion, *J Biol Chem 286*, 23254-23265.

28. Sander, C., and Schneider, R. (1991) Database of homology-derived protein structure and the structureal meaning of sequence alignment., *Protein: Structure, Function, and Genetics 9*, 56-68.

29. Chong, B. M., Reigan, P., Mayle-Combs, K. D., Orlicky, D. J., and McManaman, J. L. (2011) Determinants of adipophilin function in milk lipid formation and secretion, *Trends Endocrin Metab 22*, 211-217.

30. Bussell, R., and Eliezer, D. (2003) A strucutral and functional role for 11-mer repeats in alpha-synuclein and other exchangeable lipid binding proteins., *J Mol Biol 329*, 763-778.

31. Davidson, W., Jonas, A., Clayton, E., and George, J. (1998) Stabilization of a-synuclein secondary structure upon binding to synthetic membranes, *J Biol Chem 273*, 9443-9449.

32. Eliezer, D., Kutluay, E., Bussell, R., and Browne, G. (2001) Conformational properties of a-synuclein, *J Mol Biol 307*, 1061-1073.

33. Hynson, R., Jeffries, C., Trewhella, J., and Cocklin, S. (2012) Solution structure studies of monomeric human TIP47/perilipin-3 reveal a highly extended conformation, *Proteins 80*, 2046-2055.

34. Bulankina, A., Deggerich, A., Wenzel, D., Mutenda, K., Wittmann, J., Rudolph, M., Burger, K., and Honing, S. (2009) TIP47 functions in the biogenesis of lipid droplets., *J Cell Biol 185*, 641-655.

35. Atshaves, B. P., Petrescu, A. D., Starodub, O., Roths, J. B., Kier, A. B., and Schroeder, F. (1999) Expression and intracellular processing of the 58 KDa SCP-x/3-oxoacyl-CoA thiolase in transfected mouse L cells, *J Lipid Res 40*, 610-622.

36. Hansson, M. D., Rzeznicka, K., Rosenback, M., Hansson, M., and Sirijovski, N. (2008) PCR-mediated deletion of plasmid DNA., *Anal Biochem 375*, 373-375.

37. Hopp, T. P., and Woods, K. R. (1981) Prediction of protein antigenic determinants from amino acid sequences., *Proc Natl Acad Sci USA 78*, 3824.

38. Rost, B., and Sander, C. (1994) Combing evolutionary information and neural networks to predict protein secondary structure., *Proteins 19*, 55-72.

39. Jones, D. T. (1999) Protein secondary structure prediction basedo on position-specific scoring matrices., *J Mol Biol 292*, 195-202.

40. McGuffin, L. J., Bryson, K., and Jones, D. T. (2000) The PSIPRED protein structure prediction server, *Bioinformatics 16*, 404-405.

41. Karplus, K., Karchin, R., Barrett, C., Tu, S., Cline, M., Diekhans, M., Grate, L., Casper, J., and Hughey, R. (2001) What is the value added by human intervention in protein structure prediction?, *Proteins: Struct Funct Genet Suppl 5*, 86-91.

42. Adamczak, R., Porollo, A., and Meller, J. (2005) Combining prediction of secondary structure and solvent accessibility in proteins., *Proteins: Struct Funct Genet 59*, 467-475.

43. Bernstein, F., Koetzle, T., Williams, G., Meyer, E., Brice, M., Rodgers, J., Kennard, O., Shimanouchi, T., and Tasumi, M. (1977) The protein data bank: A computer-based archival file for macromolecular structures., *Eur J Biochem 80*, 319-324.

44. Marti-Renom, M. A., Stuart, A., Fiser, A., Sanchez, R., Melo, F., and Sali, A. (2000) Comparative protein structure modeling of genes and genomes, *Annu Rev Biophys Biomol Struct 29*, 291-325.

45. Eswar, N., Mari-Renom, M. A., Webb, B., Madhusudhan, M. S., Eramian, D., Shen, M., Pieper, U., and Sali, A. (2006) Comparative protein structure modeling with MODELLER, *Curr Protocols Bioinform Supl 15*, 5.6.1-5.6.30.

46. Landau, M., Mayrose, I., Rosenberg, Y., Glaser, F., Martz, E., Pupko, T., and Ben-Tal, N. (2005) Con/Surf 2005: The projection of evolutionary conservation scores of residues on protein structures., *Nucleic Acids Res. 33*.

47. Glaser, F., Pupko, T., Paz, I., Bell, R. E., Bechor, D., Martz, E., and Ben-Tal, N. (2003) ConSurf: Identification of functional regions in proteins by surface-mapping of phylogenetic information., *Bioinformatics 19*, 163-164.

48. Young, A., Scapin, G., Kromminga, A., Patel, S., Veerkamp, J., and Sacchettini, J. (1994) Structural studies on human muscle fatty acid binding at 1.4 A resolution: binding interactions with three C18 fatty acids., *Structure 2*, 523-534.

49. Morth, J., Pedersen, P., Toustrup-Jensen, M., Sorensen, T., Petersen, J., Andersen, J., Vilsen, B., and Nissen, P. (2007) Crystal structure of the sodium-potassium pump., *Nature 450*, 1043-1049.

50. Zavodszky, M. I., Sanschagrin, P. C., Korde, R. S., and Kuhn, L. A. (2002) Distilling the essential features of a protein surface for improving protein-ligand docking, scoring and virtual screening., *J Comp-aided Mol Design 16*, 883-902.

51. Thumser, A. E. A., and Wilton, D. C. (1994) Characterization of binding and structural properties of rat liver fatty-acid-binding protein using tryptophan mutants, *Biochem J 300*, 827-833.

52. Rawel, H., Frey, S., Meidtner, K., Kroll, J., and Schweigert, F. (2006) Determining the binding affinities of phenolic compounds to proteins by quenching of the intrinsic tryptophan fluorescence, *Mol Nutr Food Res 50*, 705-713.

53. Hostetler, H., Kier, A., and Schroeder, F. (2006) Very-long-chain and branched-chain fatty acyl-CoAs are high affinity ligands for the peroxisome proliferatror-activated receptor a (PPARa), *Biochemistry 45*, 7669-7681.

54. Senthivinayagam, S., McIntosh, A. L., Moon, K. C., and Atshaves, B. P. (2013) Plin2 inhibitis cellular glucose uptake through interactions with SNAP23, a SNARE complex protein, *PLoS ONE 8*, e73696. doi: 73610.71371/journal.pone.0073696.

55. Lakowicz, J. (1999) *Principles of Fluorescence Spectroscopy*, Kluwer Academic/Plenum Publishers, New York.

56. Sreerama, N., and Woody, R. W. (2000) Estimation of protein secondary structure from circular dichroism spectra: comparison of CONTIN, SELCON, and CDSSTR methods with an expanded reference set, *Anal Biochem 287*, 252-260.

57. Teale, F., and Weber, G. (1957) Ultraviolet flurescence of the aromatic amino acids, *Biochem J 65*, 476-482.

58. Frolov, A., and Schroeder, F. (1998) Acyl coenzyme A binding protein. Conformational sensitivity to long chain fatty acyl-CoA, *J Biol Chem 273*, 11049-11055.

59. Frolov, A., and Schroeder, F. (1998) Acyl Coenyme A Binding Protein, *The Journal of Biological Chemistry 273*, 11049-11055.

60. Breiter, D. R., Kanost, M. R., Benning, M. M., Wesenberg, G., Law, J. H., Wells, M. A., Rayment, I., and Holden, H. M. (1991) Molecular structure of an apolipoprotein determined at 2.5-A resolution, *Biochemistry 30*, 603.

61. Ajees, A. A., Anantharamaiah, G. M., Mishra, V. K., Hussain, M. M., and Murthy, K. H. M. (2006) Crystal structure of human apolipoprotein A-I: Insights into its protective effect against cardiovascular diseases., *Proc Natl Acad Sci USA 103*, 2126.

62. Dixon, T., Edwards, D., Cole, D., and Lapthorn, A. (2001) The structure of a zeta class glutathione S-transferase from Arabidopsis thaliana: characterisation of a GST with novel active-site architecture and a putative role in tyrosine catabolism., *J Mol Biol 308*, 949-962.

63. Choi, S., Tucker, D., Gross, D., Easton, R., DiPilato, L., Dean, A., Monks, B., and Brnbaum, M. (2010) Insulin regulates adipocyte lipolysis via an Akt-independent signaling pathway, *Mol Cell Biol 30*, 5009-5020.

64. Brasaemle, D., Bolios, G., Shapiro, L., and Wang, R. (2004) Proteomic analysis of proteins associated with lipid droplets of basal and lipolytically stimulated 3T3-L1 adipocytes, *J Biol Chem 279*, 46835-46842.

65. Brasaemle, D. L., Levin, D. M., Adler-Wailes, D. C., and Londos, C. (2000) The lipolytic stimulation of 3T3-L1 adipocytes promotes the translocation of hormone-

sensitive lipase to the surfaces of lipid droplets, *Biochim.Biophy.Acta 1483*, 251-262.

66. Tansey, J. T., Huml, A. M., Vogt, R., Davis, K. E., Jones, J. M., Fraser, K. A., Brasaemle, D. L., Kimmel, A. R., and Londos, C. (2003) Functional studies on native and mutated forms of perilipins. A role in protein kinase A-mediated lipolysis of triacylglycerols in Chinese hamster ovary cells, *J Biol Chem 278*, 8401-8406.

67. Buhrow, L., Ferguson-Miller, S., and Kuhn, L. (2012) From static structure to living protein:Computational prediction and validation of cytochrome c oxidase flexibility., *Biophys J 102*, 2158-2166.

68. Melikyan, G., Markosyan, R., Hemmati, H., Delmedico, M., Lambert, D., and Cohen, F. (2000) Evidence that the transition of HIV-1 Gp41 into a six-helix bundle, not the bundle configuration, induces membrane fusion., *J Cell Biol 151*, 413-424.

69. Welker, S., Rudolph, B., Frenzel, E., Hagn, F., Liebisch, G., Schmitz, G., Scheuring, J., Kerth, A., Blume, A., Weinkauf, S., Haslbeck, M., Kessler, H., and Buchner, J. (2010) Hsp12 is an intrinsically unstructured stress protein that folds upon membrane association and modulates membrane function., *Mol Cell 39*, 507-520.

70. Patel, S., Yang, W., Kozusko, K., Saudek, V., and Savage, D. (2014) Perilipins 2 and 3 lack a carboxy-terminal domain present in perilipin1 involved in sequestering ABHD5 and supressing basal lipolysis, *Proc Natl Acad Sci USA 111*, 9163-9168.

71. Wang, H., Sreenevasan, U., Hu, H., Saladino, A., Polster, B. M., Lund, L. M., Gong, D. W., Stanley, W. A., and Sztalryd, C. (2011) Perilipin 5, a lipid droplet-associated protein, provides physical and metabolic linkage to mitochondria, *J Lipid Res 52*, 2159-2168.

CHAPTER 4:

LIVER-SPECIFIC LOSS OF PERILIPIN 2 ALLEVIATES DIET-INDUCED HEPATIC STEATOSIS, INFLAMMATION, AND FIBROSIS

Published: American Journal of Physiology: Gastrointestrology and Liver Physiology. 2016 210:726-738
Title: Liver-specific Loss of Perilipin 2 Alleviates Diet-Induced Hepatic Steatosis, Inflammation, and Fibrosis
Authors: Charles P. Najt, Subramanian Senthivinayagam, Mohammad B. Aljazi, Kelly A. Fader, Sandra D. Olenic, Julienne R.L. Brock, Todd A. Lydic, A. Daniel Jones, and Barbara P. Atshaves

ABSTRACT

Hepatic inflammation and fibrosis are key elements in the pathogenesis of nonalcoholic steatohepatitis (NASH), a progressive liver disease initiated by excess hepatic lipid accumulation. Lipid droplet protein Perilipin 2 (Plin2) alleviates dietary-induced hepatic steatosis when globally ablated, however its role in the progression of NASH remains unknown. To investigate this further, we challenged Plin2 liver-specific knockout mice (designated L-KO) and their respective wild type (WT) controls with a methionine-choline-deficient (MCD) diet for 15 days to induce a NASH phenotype of increased hepatic triglyceride levels through impaired phosphatidylcholine (PC) synthesis and VLDL secretion. Results on liver weights, body weights, fat tissue mass, and histology in WT and L-KO mice fed the MCD diet revealed signs of hepatic steatosis, fibrosis, and inflammation; however these effects were blunted in L-KO mice. In addition, levels of PC and VLDL were unchanged and hepatic steatosis was reduced in L-KO mice fed the MCD diet, due in part to an increase in remodeling of PE to PC via the enzyme PEMT. These mice also exhibited decreased hepatic expression of pro-inflammatory markers COX2, IL-6, TNFα, IL-1β and reduced expression of ER stress proteins C/EBP homologous protein (CHOP) and cleaved caspase-1. Taken together, these results suggest Plin2 liver-specific ablation alleviates diet-induced hepatic steatosis and inflammation via a PEMT-mediated mechanism that involves compensatory changes in proteins involved in phospholipid remodeling, inflammation, and ER stress that work to alleviate diet-induced NASH. Overall, these findings support a role for Plin2 as a target for NASH therapy.

INTRODUCTION

In parallel to obesity trends, nonalcoholic fatty liver disease (NAFLD) is on the rise, with one person in three potentially affected in the United States. NAFLD covers a spectrum of conditions including benign steatosis where excess triglycerides are stored in hepatic lipid droplets, to the more serious nonalcoholic steatohepatitis (NASH), fibrosis, and cirrhosis. Approximately 35% of individuals who have hepatic steatosis will progress to NASH (*1-3*), yet factors driving the process forward remain unclear. A "two-hit" model by Day and James proposes a first hit of excess hepatic lipids leaves the liver more vulnerable to multiple second hits of oxidative stress, mitochondrial dysfunction, and lipid peroxidation (*4, 5*) that increase production of proinflammatory cytokines, influx of inflammatory cells, collagen deposition leading to fibrosis, hallmarks of the NASH phenotype (*6-8*). However, while numerous studies have defined the molecular and physiological changes that occur in the progression of NASH, it remains unclear what role hepatic lipid droplets and associated proteins play in promoting the disease process. Notably, several proinflammatory metabolites and enzymes that initiate inflammation reside on the surface of lipid droplets (*9-11*). More importantly, the most abundant lipid droplet protein in the liver, Perilipin 2 (Plin2) is associated with promoting two key features of NASH, i.e., lipid accumulation and inflammation (*12-17*), yet the role of Plin2 in the progression of NASH remains unclear.

Plin2 is part of the perilipin family of proteins that are closely related through sequence homology and affinity for lipid droplets. Members include Plin1 (formerly known as perilipin), Plin2 (ADRP, adipophilin), Plin3 (TIP-47), Plin4 (S3-12), and Plin5 (OXPAT) (*18*). Plin1 and Plin2 are constitutively located on the lipid droplet surface

while Plins 3, 4, and 5 can be found in both cytosolic and lipid droplet compartments (*19-22*). Plin1 is the most widely studied lipid droplet protein but hepatic expression is low. When NASH is present however, both Plin1 and Plin2 are up-regulated and differentially targeted; Plin1 was found on larger lipid droplets in the liver while Plin2 targeted inflamed ballooned hepatocytes (*14*). This alternate targeting is significant since Plin1 acts to repress lipolysis by inhibiting the lipolytic activities of HSL and ATGL (*23, 24*). In contrast, Plin2 has no lipolytic function but can block access of lipases to lipid droplets to limit triglyceride hydrolysis (*25, 26*). In addition, Plin2 binds and sequesters lipids at the lipid droplet surface (*27, 28*) and enhances lipid transport (*29*), suggesting it may act as a regulatory protein, governing the release and deposition of lipids including eicosanoids that are stored in lipid droplets (*9, 11, 30, 31*). Consistent with this, Plin2 has been shown to preferentially bind proinflammatory lipids (*28*) and significantly increase neutral lipid and phospholipid levels when overexpressed in L cells (*17*). Moreover, knockdown of Plin2 in THP-1 macrophages resulted in decreased cellular lipids and lipid droplet size and number, and decreased expression of proinflammatory markers TNFα, IL-6, and COX2 when inflammation was induced by LPS (*12*). Conversely, Plin2 overexpression in LPS-stimulated C2C12 cells resulted in increased expression of IL-1β and caspase-1 (*13*). In mice, global ablation of Plin2 decreased hepatic triglyceride levels and protected against diet-induced obesity, adipose inflammation, and liver steatosis (*32-37*) while reduction of Plin2 by antisense oligonucleotide treatment resulted in decreased hepatic lipid accumulation and enhanced insulin sensitivity (*35, 38*). However, while these data support a role for Plin2

in promoting hepatic steatosis, relatively little is known if the protein contributes to the pathogenesis of inflammation-related NASH.

To investigate this further, we challenged Plin2 liver-specific knockout (L-KO) mice with a methionine and choline-deficient (MCD) diet to produce the NASH phenotype of increased hepatic lipid accumulation, inflammation, and fibrosis. A tissue-specific conditional knockout model was employed to bypass the limitations of traditional constitutive knockout models in terms of compensatory mechanisms and complex phenotypes. Our results suggest that hepatic ablation of Plin2 activates a mechanism that involves phospholipid remodeling enzymes, proinflammatory proteins, and ER stress markers. Taken together, the data herein provide novel insights into the physiological role of Plin2 and suggest that Plin2 plays an important role in hepatic function.

MATERIALS AND METHODS

MICE

Plin2 liver-specific KO mice were created using a LoxP-Cre approach (*39*) to allow conditional targeting of the Plin2 allele. Briefly, Plin2 global KO mice (*Plin2*$^{-/-}$) carrying the Plin2$^{tm1a(EUCOMM)Wtsi}$ in a C57BL/6NTac background were generated by the European Conditional Mouse Mutagenesis Program (EUCOMM). Heterozygous mice (*Plin2*$^{+/-}$) carrying the Plin2 targeted allele were purchased from Welcome Trust Sanger Institute, (UK) and were bred together to obtain mice globally null in Plin2 (*Plin2*$^{-/-}$ mice). To derive Plin2 liver-specific KO mice (*Plin2*$^{L-/-}$*),* the floxed mouse (*Plin2*$^{fl/fl}$) was generated by breeding *Plin2*$^{-/-}$ mice with mouse strain B6.29S4-Gt(ROSA)26Sor$^{tm1(FLP1)Dym}$ (Jackson Laboratory, Bar Harbor, ME) to create a floxed allele and restored Plin2 expression. Mice

heterozygous for the floxed allele were bred together to obtain *Plin2*$^{fl/fl}$ mice that served as WT controls since neither the presence of the LoxP sites or the remaining FRT site altered the expression of Plin2 or the phenotype. *Plin2*$^{fl/fl}$ mice with then bred with mouse strain FVB.Cg-Tg(Alb1-cre)1Dlr/J (Jackson Laboratory, Bar Harbor, ME), a liver-specific *Cre* recombinase-expressing mouse model to generate *Plin2*$^{L+/-}$ mice. Mice containing the liver-specific allele were then bred to homozygosity to produce *Plin2*$^{L-/-}$ mice, hereafter known as L-KO mice. All animal protocols were approved by the Institutional Animal Care and Use Committee at Michigan State University according to criteria outlined in *Guide for the Care and Use of Laboratory Animals* prepared by the National Academy of Sciences and published by the National Institutes of Health (NIH publication 86-23 revised 1985).

DIETARY EXPERIMENTS

One week before the start of the feeding experiments, age-matched WT and L-KO male mice (7-8 weeks old) were placed on a control diet containing 10% fat (Research Diets, Inc., #A02082003B). After one week, half of the mice in each group remained on the control diet, while the rest were switched to an isocaloric methionine/choline deficient (MCD) diet, chemically defined to match the control diet (Research Diets, Inc., #A02082002B). Mice were fed *ad libitum* for 15 days. Body weights and food intake of each mouse were monitored every two days. At the beginning and the end of the feeding study, the percent fat tissue mass and lean tissue mass of each mouse were determined *in vivo* using a TD-NMR based Bruker Minispec LF50 body composition analyzer (Billerica, MA). At the end of the study, non-fasted mice were euthanized by CO_2 asphyxiation and cervical dislocation. In keeping with other work (*40, 41*) and due to the severe weight loss the mice experienced on the MCD diet, we did not fast the mice at the end of the feeding study. Blood was

collected and livers harvested and weighed. Portions of the liver were collected for histological examination. Remaining portions were snap frozen on dry ice and stored at -80°C.

LIVER HISTOLOGY

Liver samples (25 to 75 mm^3 segments) were fixed in a 10% buffered formalin solution at room temperature overnight, then stored in alcohol until embedded in paraffin, sectioned (4-6 m thickness), and stained with hematoxylin and eosin (H&E) or Masson's Trichrome for histological evaluation. Sections were imaged with a Nikon LTX light microscope with a 40X objective. Portions of the liver were frozen in O.C.T. compound (Tissue-Tek; Sakura Finetek USA) for Oil red O staining. Morphometric analysis was performed using MetaMorph software (Sunnyvale, CA) to analyze the number and size of lipid droplets. Histological processing was done at the histopathology lab at Michigan State University.

LIPID ANALYSIS

Lipids were extracted from mouse liver homogenates and resolved into individual lipid classes using thin-layer chromatography as described previously (*42, 43*). Levels of total cholesterol, free fatty acids, triacylglycerol, cholesteryl esters, and total phospholipids were determined by TLC and densitometry following the method of Marzo (*44*). Protein concentration from the dried protein extract residue was digested overnight in 0.2 M KOH

and analyzed using Bradford reagent (*45*). All lipid classes were identified by comparison to known TLC standards.

MASS SPECTROMETRY BASED LIPID ANALYSIS

Prior to performing high resolution/accurate mass spectrometry and tandem mass spectrometry, liver homogenates, spiked with synthetic PC (14:0/14:0), PE (14:0/14:0), and PS (14:0/14:0) as internal standards were subjected to monophasic lipid extraction with methanol: chloroform: water (2:1:0.74, v:v:v) and amine group modification as previously described (*46, 47*). Briefly, extracts (10 μl) were aspirated and directly infused at approximately 250 nL/ minute by nanoelectrospray ionization (nESI) into a high resolution / accurate mass Thermo Scientific model LTQ Orbitrap Velos mass spectrometer (San Jose, CA) using an Advion Triversa Nanomate nESI source (Advion, Ithaca, NY) with a spray voltage of 1.4 kV and a gas pressure of 0.3 psi. High resolution mass spectra were acquired in positive-ion mode from derivatized lipid extracts, and in negative-ion mode from underivatized lipid extracts, using the FT analyzer operating at 100,000 mass resolving power. The mass spectrum signal was averaged for 2 minutes over the range of *m/z* 200-2000. HCD-MS/MS product ion spectra were acquired to verify the identities of selected lipid ions of interest using the FT analyzer operating at 100,000 mass resolving power and default activation times. HCD-MS/MS collision energies were individually optimized for each lipid class of interest using commercially available lipid standards whenever possible. Lipids were identified using the Lipid Mass Spectrum Analysis (LIMSA) v.1.0 software linear fit algorithm, in conjunction with a user-defined

database of hypothetical lipid compounds for automated peak finding and correction of ^{13}C isotope effects. Relative quantification of the abundances of lipid molecular species between samples was performed by normalization of target lipid ion peak areas to the internal standards as previously described (*48*). Data were processed using mean-centering and Pareto-scaling prior to multivariate statistical analysis. The principal component analysis (PCA) was performed using EZinfo software (Umetrics). Partial least-squares-discriminant analysis (PLS-DA) was carried out (EZ Info, Umetrics) to identify the differentially expressed phospholipids responsible for the separation of WT, L-KO, MCD diet fed WT, and MCD diet fed L-KO. The heat map was generated using Cluster 2.0 from the Eisen Lab modified by Michiel de Hoon (http://bonsai.hgc.jp/~mdehoon/software/cluster/). Java Tree Viewer was used to view and color the heat map.

SERUM LIPIDS, LIPOPROTEINS, AND LIPOLYSIS

Total and free cholesterol, triacylglycerol, and non-esterified fatty acid levels in serum from non-fasted mice were determined using Wako Chemicals lipid assay systems (Wako Diagnostics, Richmond, VA). Levels of cholesteryl esters were determined by subtracting free cholesterol from total. Concentrations of cholesterol in high-density lipoprotein (HDL) and low-density (LDL)/very-low-density (VLDL) lipoproteins were quantified using a PEG precipitation using the EnzyChrom HDL and LDL/VLDL kit from BioAssay Systems (Hayward, CA). To measure lipolysis in hepatic tissue, glycerol release was quantified using EnzyChrom Adipolysis Assay Kit, from BioAssay Systems (Hayward, CA). Colorimetric analysis of lipids, lipoprotein, and lipolysis were measured at 570 nm on an Omega FLOUstar 96-well plate reader from BMG labtech (Ortenberg, Germany).

SERUM β-HYDROXYBUTYRATE MEASUREMENT

To measure acetyl CoA production from fatty acid oxidation, serum levels of the ketone body β-hydroxybutyrate were determined using the Wako Chemicals β-hydroxybutyrate kit (Wako Diagnostics, Richmond, VA). Levels were measured with high sensitivity and specificity according to the manufacturer's directions by measuring the rate of Thio-NADH (β-thionicotinamide adenine dinucleotide) production spectrophotometrically at 405nm upon oxidation of β-hydroxybutyrate.

WESTERN BLOT ANALYSIS

Expression levels of Plin1, Plin2, Plin3, and Plin5, and PLA_2 were assessed by Western blot analysis as previously described previously (*17, 42*). Rabbit polyclonal antibodies were purchased from the following sources: anti-Plin1, anti-Plin3, and anti-Plin5 from Thermo Scientific (Rockland, IL) and anti-PLA_2 from Cell Signaling (Danvers, MA). Rabbit polyclonal antibodies against Plin2 were developed in house (*17*). Western blot analysis was performed on tissue (liver, WAT, heart, kidney, and brain) homogenates (20-40 µg) resolved on tricine gels (10%). Proteins were transferred to nitrocellulose membranes and blots were stained with Ponceau S to confirm protein transfer and constant protein loading (*49*) before blocking in 7% non-fat milk in TBST (10 mM Tris-HCl, pH 8, 100mM NaCl, 0.05% Tween-20) overnight. Blots were incubated with specific polyclonal rabbit antibodies and were developed with IRDye 800CW anti-mouse (LI-COR) secondary antibodies. Blots were scanned using the LI-COR Odyssey imaging system (Lincoln, NE) to visualize the bands of interest. Protein bands were quantitated by

densitometric analysis after image acquisition using NIH Scion Image to obtain relative protein levels expressed as integrated density values normalized to GAPDH expression.

QUANTITATIVE REAL-TIME PCR

Total RNA was isolated from liver using Trizol (Qiagen, Valencia, CA) in accordance with the manufacturer's protocol. Total RNA (1 μg) from each liver sample was converted into first strand cDNA using ABI high capacity cDNA reverse transcription kit (Gand Island, NY). Expression levels of IL-1β, IL-6, TNFα, COX2, CHOP, PERK, CCT, SMS, PEMT, GNMT, ACOX1, ACC, ACS, CPT1α, FASN, SCD1, MGAT1, DGAT1, DGAT2, MTTP, HSL, and ATGL were analyzed by SYBR Green technologies using commercially available primers from IDT (Coralville, IA) on a StepOne plus Real Time PCR system (LifeTechnologies, CA, USA). Relative expression was calculated using the comparative $2^{-\Delta\Delta CT}$ method (*50*). Data were expressed as fold difference compared to WT mice on control diet.

STATISTICAL ANALYSIS

Values were expressed as the means ± S.E. Statistical analyses were performed using two-way ANOVA with Newman Keuls post-hoc test (Sigma Plot, San Jose, CA) to determine statistical significance. Values with $P < 0.05$ or less were considered significant.

RESULTS

LIVER-SPECIFIC DELETION OF PLIN2

Conditional targeting of the mouse Plin2 gene was achieved as depicted in Figure 16. Genotyping was confirmed by PCR to detect the presence or absence of the WT allele (850 bp), FRT site (204 bp), exon 4 (1 Kb), and the *Cre* gene (233 bp) in Plin2 floxed (Fig. 16B) and L-KO (Fig. 16C) mice. Western blot analysis showed ablation of Plin2 from liver homogenates but not from white adipose tissue (WAT), heart, brain, or kidney homogenates derived from WT and L-KO mice (Fig. 16D). For the experiments described, age-matched mice containing the floxed allele were designated as wild type (WT) since pilot studies indicated neither the presence of the LoxP or FRT site altered Plin2 expression or phenotype.

HEPATIC PLIN2 ABLATION ALLEVIATES MCD DIET-INDUCED LIPID ACCUMULATION, INFLAMMATION, AND FIBROSIS

To study the role of Plin2 in hepatic function, we challenged Plin2 liver-specific knockout mice with a MCD diet to induce a NASH phenotype of increased hepatic lipid accumulation, inflammation, and fibrosis (*51, 52*). Unlike high fat or high fat/high fructose diets, the MCD diet produces the NASH phenotype of hepatic inflammation and fibrosis in mice rapidly. The MCD diet however, does not generate the obese, insulin resistant phenotype associated with the human NASH phenotype. In contrast, high-fat and high fat/high fructose diets will give rise to an obese, insulin resistant state, yet these diets generally do not result in liver fibrosis and only mildly produce steatosis and inflammation

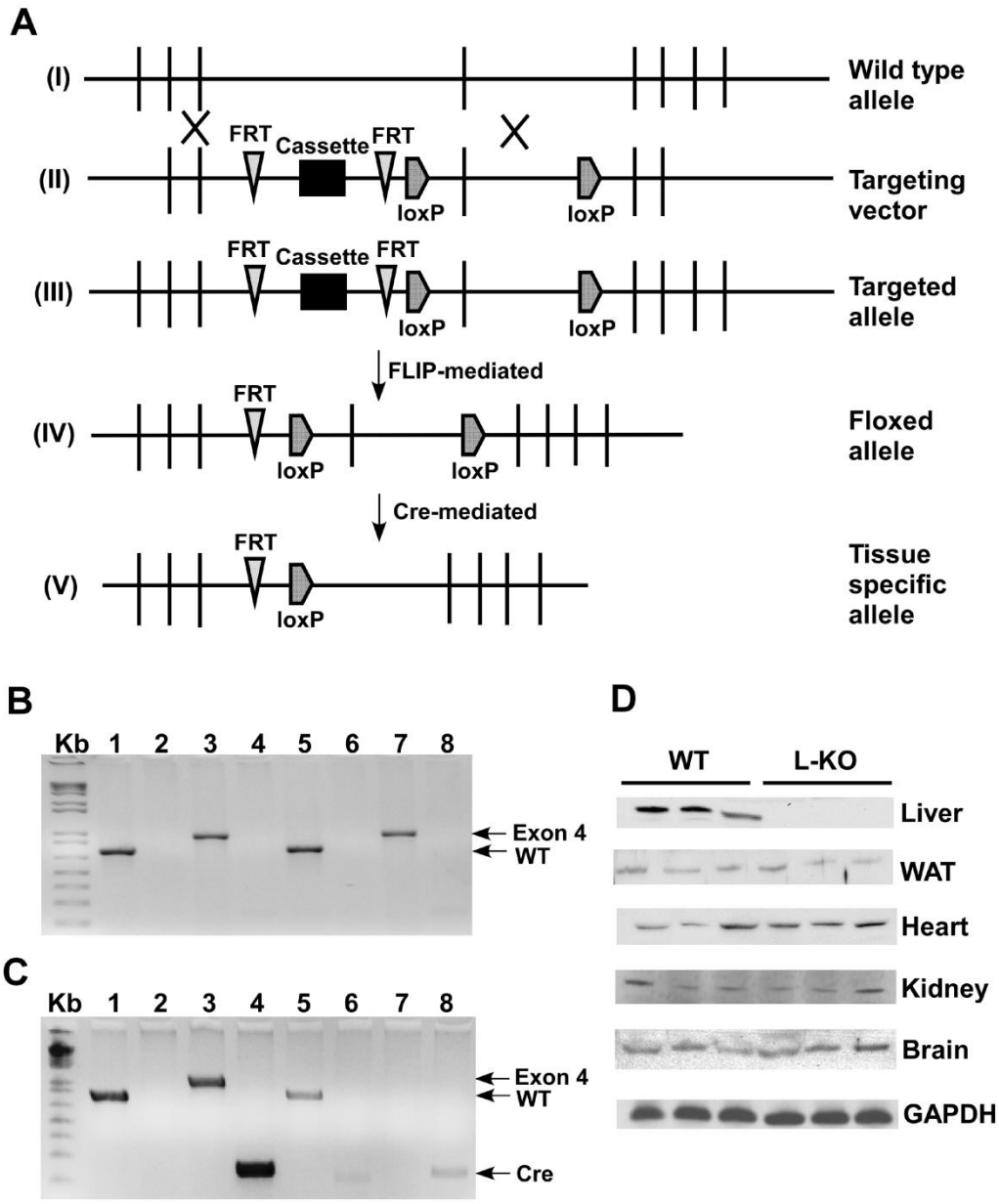

Figure. 16. Conditional targeting of the Plin2 allele allows for liver-specific deletion. (A) Targeting strategy of generating Plin2 L-KO mice. (I) Wild-type allele, (II) targeting vector, (III) targeted allele, (IV) floxed allele, and (V) tissue specific allele. (B) PCR screening of WT mice. Primers were designed to detect the presence or absence of the WT allele (lane 1, 850 bp), FRT site (lane 2, 204 bp), Exon 4 (lane 3, 1Kb), and the Cre gene (lane 4, 233 bp) in tail (lanes 1-4) and liver (lanes 5-8) samples. Mice containing the floxed allele are positive for the WT gene (lane 1) and exon 4 (lane 3), but lack bands corresponding to the FRT site (lane 2) and Cre gene (lane 4). (C) PCR screening of L-KO mice. Tail DNA (lanes 1-4) from L-KO mice show bands corresponding to the WT gene (lane 1), Exon 4 (Lane 3), and the Cre gene (Lane 4). L-KO liver DNA (lanes 5-8) is positive for the WT gene (lane 5) and the Cre gene (lane 8), but exon 4 is not detected (lane 7), indicating tissue-specific deletion. (D) Western blot analysis of Plin2 protein expression in liver, white adipose tissue (WAT), heart, kidney, and brain using GAPDH as a loading control.

(*40, 53-56*). Moreover, lack of methionine-choline in the diet limits PC synthesis and VLDL secretion, resulting in weight loss. To keep the weight loss to less than 25% of body weight, the MCD diet was limited to15 days. Both WT and age-matched L-KO mice lost body weight on the MCD diet, but L-KO mice were significantly less responsive, losing 19% less of their body weight (Fig. 17A, $P<0.03$). The MCD diet significantly decreased liver weights of WT mice (37%, $P<0.002$), but similarly fed L-KO mice showed little to no change (Fig. 17B). A substantial loss in percent fat tissue mass was observed in both L-KO mice and WT mice on the MCD diet (68% and 85%, respectively), but this effect was significantly reduced 20% in L-KO mice (Fig. 17C). The percent lean tissue mass was not affected by genotype in mice fed the control or MCD diets (Fig. 17D). Taken together, these findings suggest the effects of the MCD diet on whole body phenotype are minimized in L-KO mice. We next investigated the effect of hepatic Plin2 deletion and the MCD diet on hepatic lipid accumulation. Liver sections stained with Oil red O showed decreased lipid content in L-KO livers when compared to WT controls (Fig. 18A). Morphometric analysis revealed lipid droplet size and number were respectively decreased 46% and 40% (Fig. 18B, panels 1 and 2). Consistent with this, lipid analysis revealed neutral lipid content decreased 47% in L-KO livers (Fig. 18B, panel 3). The MCD challenge resulted in enhanced Oil red O staining and neutral lipid accumulation in both L-KO and WT livers, but significantly less with L-KO samples. H&E staining revealed marked histopathological lesions including single-cell necrosis, increased vacuolization, and cell body inclusions in MCD WT livers, suggesting increased hepatic steatosis and inflammation (Fig. 18C). These lesions were not observed in livers from control-fed WT or L-KO mice and were

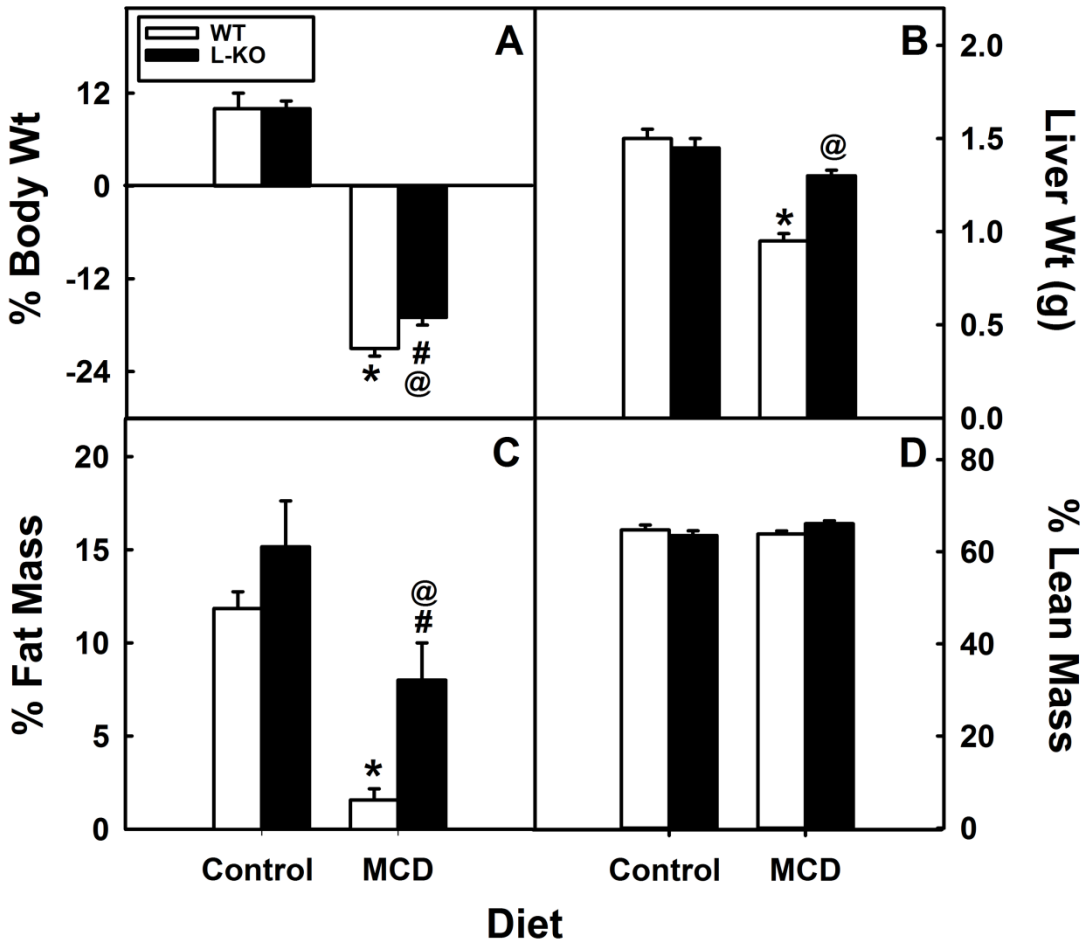

Figure. 17. Effect of hepatic Plin2 ablation and MCD diet on body weight, liver weight, and fat mass. The percent change in body weight (A), liver weight (B), fat tissue mass (C), and lean tissue mass (D) was determined in WT and L-KO mice fed a control and MCD diet for 15 days. Values represent mean ± SEM, n= 4-5. *p<0.05 vs. WT mice on the control diet. @P<0.05 vs. WT mice on the MCD diet. #P<0.05 vs. L-KO mice on the control diet.

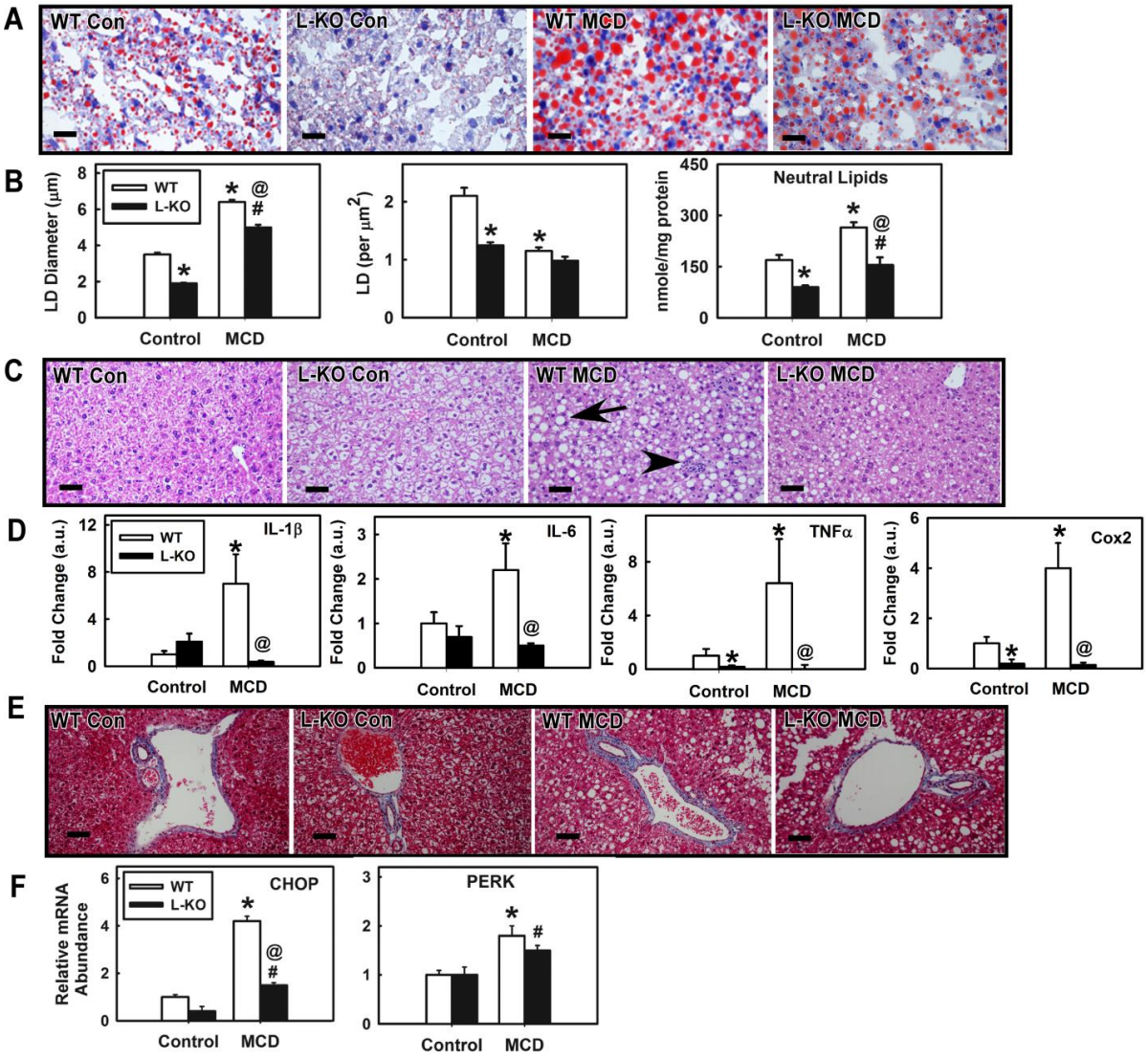

Figure. 18. Liver-specific ablation of Plin2 blunts MCD diet effects on hepatic lipid accumulation, inflammation and fibrosis. (A) Oil red O stained images of liver sections from WT and L-KO mice on control or MCD diets. (B) Morphometric analysis of hepatic lipid droplet size/number and neutral lipid content. (C) Representative H&E stained images. (D) Gene expression of pro-inflammatory markers. (E) Representative Masson Trichrome stained images. (F) Gene expression of pro-fibrotic markers. Values represent mean ± SEM, n= 4-5. *p<0.05 vs. WT mice on the control diet. @P<0.05 vs. WT mice on the MCD diet. #P<0.05 vs. L-KO mice on the control diet. Bars, 20μm.

significantly diminished in the livers from MCD diet-fed L-KO mice. Consistent with this, hepatic expression of genes associated with inflammation (IL-1β, IL-6,TNFα, COX2) were increased in livers from WT mice on the MCD diet but decreased in similarly fed L-KO samples (Fig. 18D). Since steatosis has been identified as a risk factor for liver fibrosis, liver sections were also stained with Masson's Trichrome to visually determine increased collagen levels associated with diet-induced fibrosis (blue coloration, Fig. 18E). Although no genotype effect was observed in control fed mice, the MCD diet significantly increased levels of fibrotic staining in WT, but not L-KO livers, near and around the arterial triad. Hepatic expression of CHOP and PERK, two enzymes involved in fibrosis and ER stress (*57, 58*), were increased 4.2- and 1.8-fold, respectively in livers from MCD diet-fed WT mice, a response blunted in L-KO mice where levels of PERK increased 1.5-fold and CHOP increased 1.6-fold (Fig. 18F). Plin2 ablation and the MCD diet had little effect on levels of TLR4 (Fig. 19A), the receptor responsible for activation of PERK under steatotic conditions (*58*). However, pro-caspase-1 was decreased in livers from both WT and L-KO mice, but less so in L-KO mice. The ratio of caspase-1 to pro-caspase-1 was also determined to assess levels of active caspase-1 (Fig. 19B). The ratio in WT mice fed the MCD diet was increased 6-fold when compared to control fed mice, but L-KO mice showed only a 2.6-fold increase. Taken together, these results suggest that Plin2 ablation may protect against diet-induced ER stress and fibrosis.

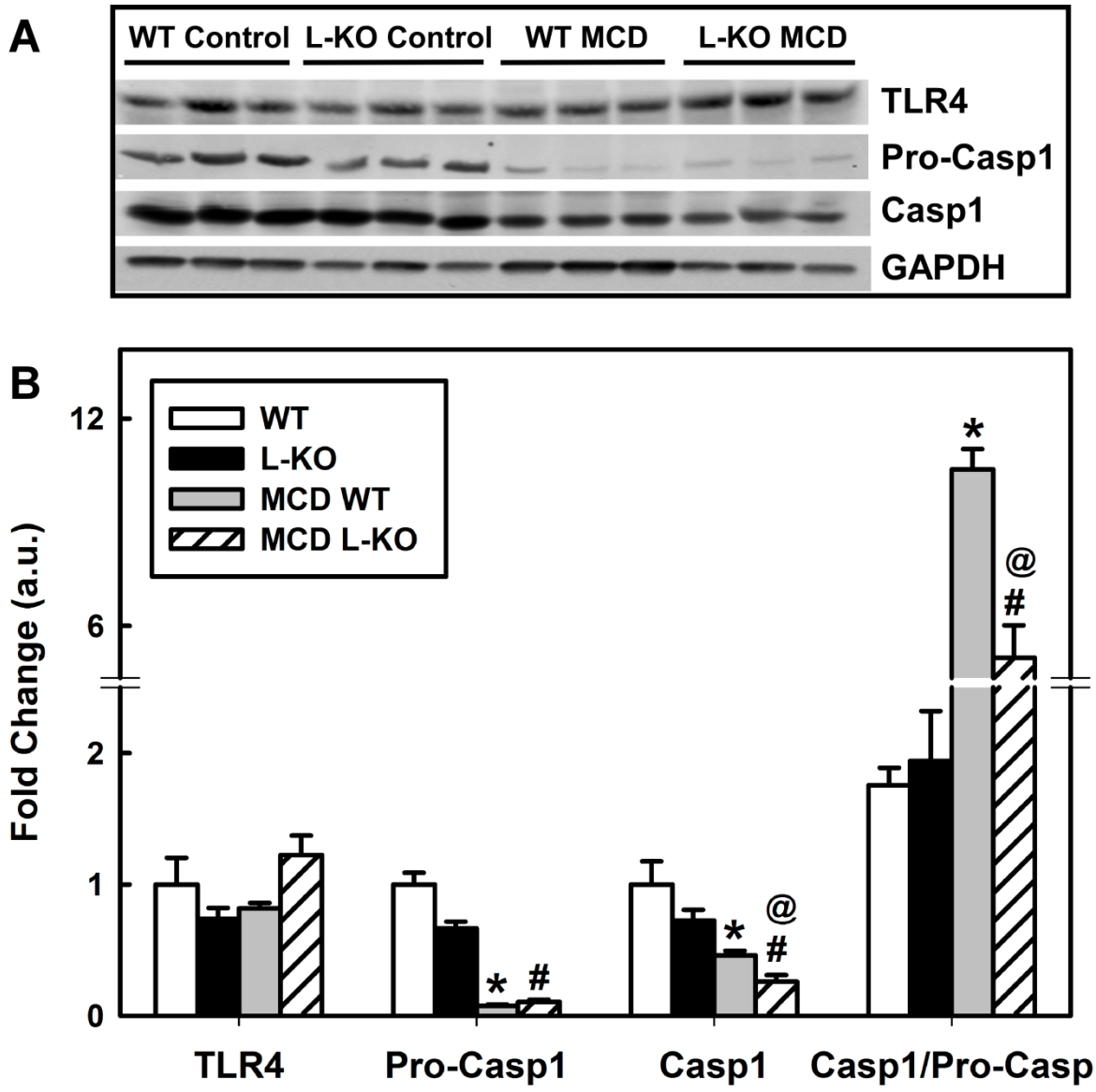

Figure. 19. Ablation of hepatic Plin2 alleviates MCD diet-induced effects on TLR4 and caspase-1. (A). Western blot analysis of TLR4, pro-caspase1, and cleaved caspase-1 levels in hepatic tissue derived from L-KO and WT mice fed the control and MCD diet. (B) Relative protein expression levels were quantified by densitometric analysis. L-KO mice exhibited decreased levels of pro-caspase-1. The MCD diet increased the ratio of cleaved caspase-1/pro-caspase-1 in WT, an effect that was blunted in similarly fed L-KO mice. Values represent mean ± SEM, n= 4-5. *p<0.05 vs. control diet fed WT mice. @P<0.05 vs. MCD diet fed WT mice. #P<0.05 vs. control diet fed L-KO mice.

HEPATIC PLIN2 ABLATION BLUNTS MCD DIET EFFECTS ON LIPOLYSIS, LIPOPROTEIN AND LIPID LEVELS IN SERUM

Since the MCD diet increases neutral lipid production and inhibits VLDL secretion (*51, 59-61*), we investigated the effects of the diet and hepatic Plin2 deletion on lipolysis and levels of serum lipoproteins and lipids. Lipolysis was not affected by Plin2 hepatic ablation in control diet fed mice. However, the MCD diet significantly decreased lipolytic activity in WT mice, a response not observed with similarly fed L-KO mice (Fig. 20A). Serum levels of β-hydroxybutyrate, a product of acetyl CoA produced by β-oxidation, were measured to assess fatty acid oxidation in WT and L-KO mice (*62*). Liver-specific ablation of Plin2 significantly increased β-hydroxybutyrate levels 1.4-fold in control fed mice (Fig. 20B), indicating increased fatty acid oxidation. In contrast, the MCD diet challenge decreased β-hydroxybutyrate levels 3.1- and 2.7-fold, respectively in WT and L-KO mice, suggesting the effects of the diet were to limit oxidation. Levels of total serum lipoproteins, HDL, and LDL/VLDL were significantly decreased 26%, 25%, and 34%, respectively when Plin2 was ablated (Fig. 20C, $P<0.05$). The MCD diet challenge resulted in significantly reduced levels of total serum lipoproteins and HDL in WT and L-KO mice, but levels of LDL/VLDL were restored in L-KO mice. Similar decreases in serum levels of total cholesterol, cholesteryl esters, triglycerides, and free fatty acids in both WT and L-KO mice (Fig. 20D) were observed. Overall, these results suggested that lipolysis and LDL/VLDL production were protected against MCD insult in L-KO mice.

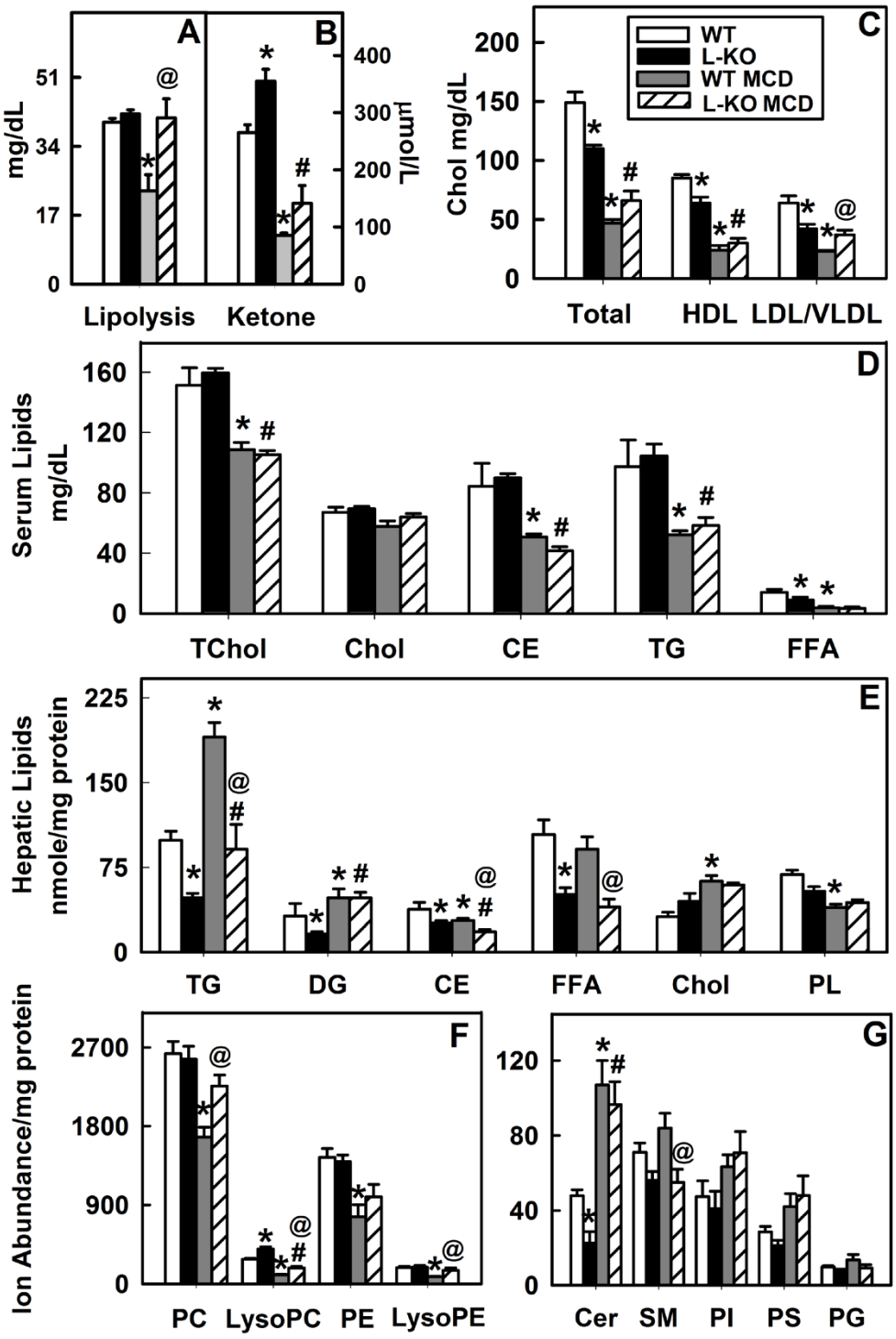

Figure. 20. Hepatic Plin2 ablation and MCD diet alter lipid and lipoprotein profiles. (A, B) Lipolytic activity and ketone body levels in liver samples from WT and L-KO mice on control or MCD diets. (C) Serum lipoproteins levels. (D) Serum lipid levels. (E) Hepatic lipid levels. (F, G) Ion abundance of individual phospholipid classes with high and low abundance in liver. Values represent mean ± SEM, n= 4-5. *p<0.05 vs. WT mice on the control diet. @P<0.05 vs. WT mice on the MCD diet. #P<0.05 vs. L-KO mice on the control diet.

PLIN2 LIVER-SPECIFIC ABLATION REDUCES MCD DIET EFFECTS ON HEPATIC TRIGLYCERIDE AND PHOSPHOLIPID LEVELS

Consistent with results from Oil red O staining (Fig. 18A), hepatic levels of triglycerides, diglycerides, cholesteryl esters, and free fatty acids were significantly reduced in L-KO mice when compared to WT mice (Fig. 20E). The MCD diet increased hepatic levels of triglycerides in both WT and L-KO mice, but the response was significantly reduced in L-KO mice. In contrast, hepatic levels of total phospholipids were significantly decreased in WT mice on the MCD diet, but this effect was not observed with similarly fed L-KO mice. To investigate this further, a phospholipid lipidomic profile was generated. Liver-specific ablation of Plin2 increased levels of lyso-PC 1.5-fold and decreased ceramide levels 2.1-fold (Figs. 20F, G). The MCD diet significantly decreased hepatic levels of PC and PE a respective 1.6- and 1.7-fold in WT, but not L-KO, mice (Fig. 20F). Similar decreases were observed with lyso-PC and lyso-PE levels. In contrast, ceramide levels were significantly increased in both WT and L-KO mice on the MCD diet (Fig. 20F, $P<0.05$). In summary, the MCD diet challenge increased hepatic neutral lipid accumulation and decreased PC and PE levels in WT mice. The response of L-KO mice to the diet was less pronounced and, as shown with PC and PE levels, negligible.

NASH SIGNATURE-BASED ON LIPIDOMIC DATA

Despite the lack of methionine-choline in the MCD diet, L-KO mice did not exhibit decreased levels of hepatic PC or other phospholipid classes including PE, Lyso-PE, sphingomyelin (SM), phosphatidylserine (PS), and phosphatidylinositol (PI). To investigate further, a lipidomic profile of individual phospholipid species was generated

and subjected to principal component analysis (Fig. 21A). Lipidomic data were projected onto a plane depicting the two components representing greatest variance in the data set. Changes in the lipidomic profile were also visually observed in a heat map that presented the data in terms of fold change relative to control diet-fed WT mice (Fig. 21B). Analysis of individual phospholipid species revealed changes across the classes in C16- and C18 fatty acid-containing phospholipid species, in addition to C20 and C22 species (Fig. 21C). Specifically, the effect of Plin2 liver-specific ablation on mice fed the control diet was to decrease levels of Cer 22:2 and SM 22:0 while increasing levels of PC 38:3 (18.1/20:2 Lyso-PC 20:4, Lyso-PC 22:6, and Cer 22:0 (Fig 6C). On the MCD diet, WT mice exhibited significantly decreased levels of PC 34:3, PC 34:2 (16:1/18:1), Lyso-PC 16:0, Lyso-PC 22:6, PE 36:4 (16:0/20:4), PE 38:4 (18:0/20:4), Lyso-PE 18:2, Lyso-PE 18:1, Lyso-PE 20:4, PG 30:3, PI 40:7, PI 36:4, and PS 22:2, reflecting decreased levels of PC, Lyso-PC, PE, and Lyso-PE (Fig. 20F). Results were mixed with L-KO mice, but yielded no net effect.

We next examined the impact of hepatic Plin2 ablation and the MCD diet on levels of phospholipid fatty acid (FA) classes including unsaturated FA (UNSAT), saturated FA (SAT), polyunsaturated FA (PUFA), and monounsaturated FA (MUFA). The MCD diet decreased levels of UNSAT, PUFA and MUFA in WT mice 1.7-fold, 1.5-fold, and 3.1-fold respectively (Fig. 21C, lower right panel), consistent with previous reports of mice on MCD diets (*51, 63*). In L-KO mice, levels of MUFA, but not UNSAT or PUFA,

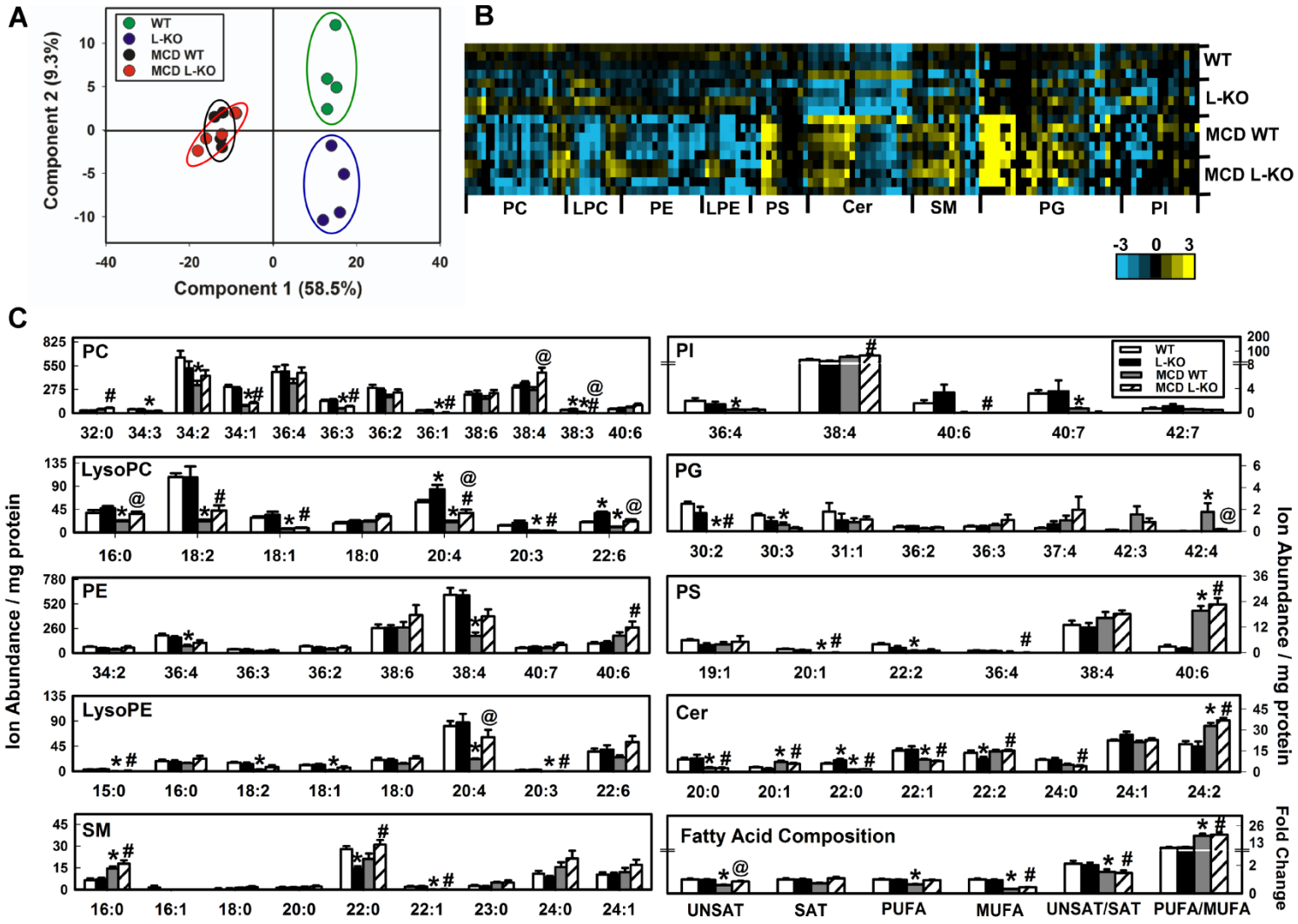

Figure. 21. High resolution/accurate-tandem MS of individual phospholipid classes. (A) Principal component analysis of targeted lipidomics. (B) Heat map representing fold-change of each lipid class relative to the mean in control-fed WT mice. (C) Ion abundance of individual phospholipid species and fatty acid composition. Lipid signals were normalized to synthetic internal standards PC(14:0/14:0), PE(14:0/14:0), and PS(14:0/14:0). Values represent mean ± SEM, n= 4-5. *p<0.05 vs. WT mice on the control diet. @P<0.05 vs. WT mice on the MCD diet. #P<0.05 vs. L-KO mice on the control diet.

decreased 2.1-fold on the MCD diet. Moreover, SAT levels in both WT and L-KO mice did not change, but the ratio of UNSAT to SAT decreased, reflecting higher SAT levels when mice were fed the MCD diet. These findings are consistent with NASH in humans where increased SAT levels in hepatic phospholipid pools is often observed (*63*).

PHOSPHOLIPID REMODELING DIRECTS HEPATIC PC BIOSYNTHESIS IN MCD FED L-KO MICE

The MCD diet inhibited hepatic accumulation of PC and PE in WT, but not L-KO, mice. To investigate this further, expression levels of several phospholipid remodeling enzymes including phosphate cytidyltransferase 1 (CCT), sphingomyelin synthase (SMS), PEMT, and glycine N-methyltransferase (GNMT) were determined. Levels of CCT, rate-limiting enzyme converting dietary choline and diglycerides to PC (*64, 65*), were increased 3.1-fold in L-KO mice, but no further effect was observed when mice were fed the MCD diet (Fig. 22A). In contrast, PEMT, a transferase that converts PE to PC, was down-regulated 8.3-fold in L-KO mice when compared to WT controls. The MCD diet increased PEMT expression 10- and 42-fold in WT and L-KO mice, respectively. In addition, expression levels of two enzymes that use a PC substrate, SM synthase and phospholipase A2 (PLA_2), were decreased 3.8- and 11.3- fold respectively in MCD fed L-KO mice (Figs. 22A, B). Taken together, these results suggest L-KO mice can increase production and limit catabolism of PC when choline and methionine are deficient through compensatory regulation of phospholipid remodeling enzymes.

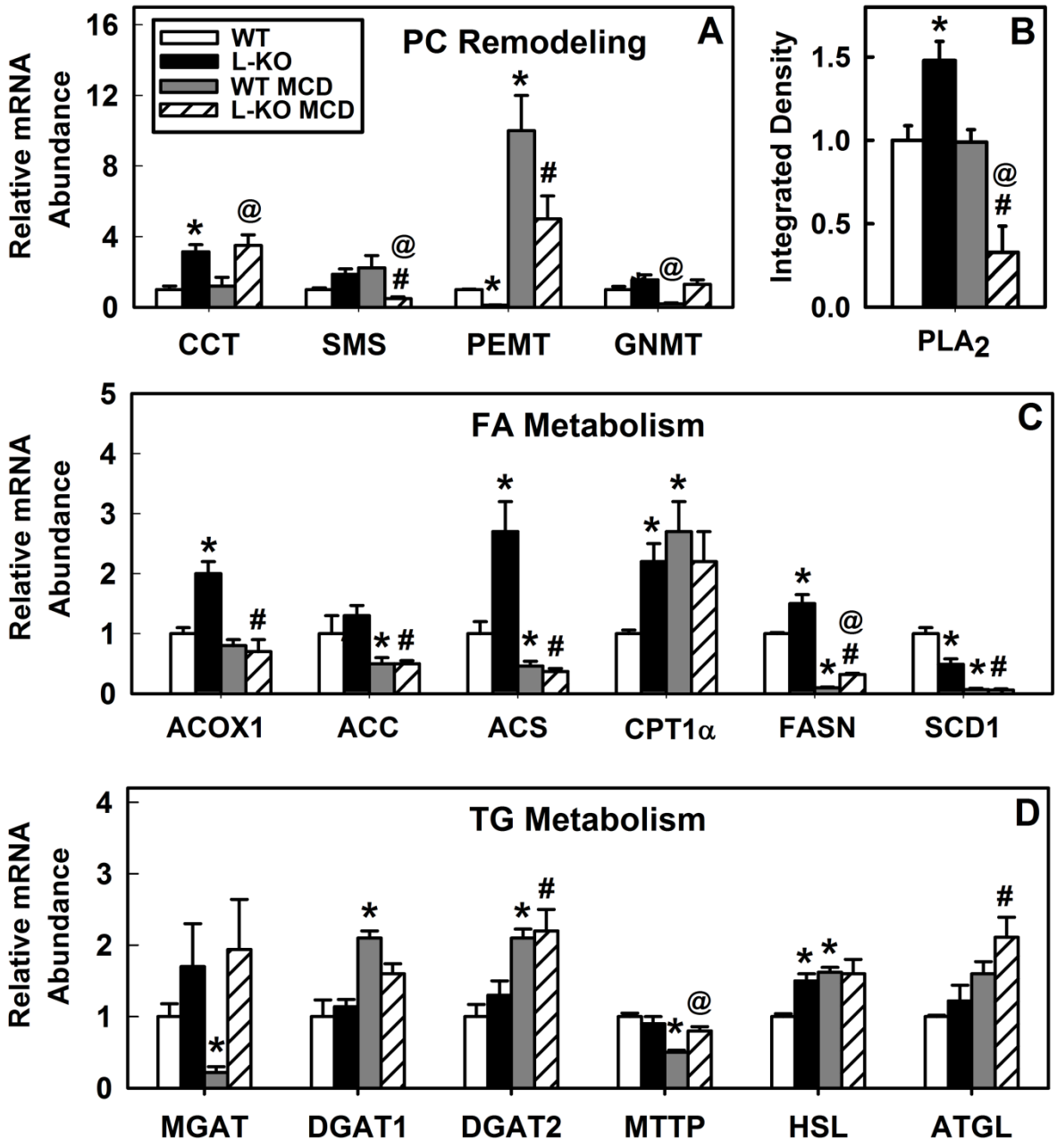

Figure. 22. Plin2 liver-specific ablation reduces MCD diet effects on phospholipid, FA, and triglyceride metabolism. (A) Gene expression of PC remodeling proteins. (B) Western blot analysis of PLA2. (C) Gene expression of proteins involved in FA metabolism. (D) Gene expression of proteins involved in triglyceride metabolism. Values represent mean ± SEM, n= 4-5. *p<0.05 vs. control diet fed WT mice. @P<0.05 vs. MCD diet fed WT mice. #P<0.05 vs. control diet fed L-KO mice.

HEPATIC PLIN2 ABLATION BLUNTS MCD DIET EFFECTS ON FATTY ACID AND TRIGLYCERIDE METABOLISM

To better understand the effect of hepatic Plin2 ablation on lipid metabolism, expression levels of genes involved in FA and triglyceride metabolism were examined. Acyl-coenzyme A oxidase 1 (ACOX1) and carnitine palmitoyltransferase 1 α (CPT1α) were significantly up-regulated 2.0- and 2.2-fold, respectively in control fed L-KO mice (Fig. 22C). Likewise, FA synthase (FASN) and acyl-coenzyme A synthase (ACS) were significantly up-regulated 1.5- and 2.7-fold, respectively. In contrast, sterol-coenzyme A desaturase (SCD1), an enzyme that converts SAT to MUFA,(*52*) was decreased 2-fold. However, no genotype effect was observed in mice fed the control diet (Fig. 22D) with regard to genes involved in triglyceride metabolism including monoacylglycerol acyltransferase (MGAT), diacylglycerol acyltransferase (DGAT1), DGAT2, microsomal triglyceride transfer protein (MTTP), or adipose triglyceride lipase (ATGL). These findings reflect observations of decreased hepatic lipid levels and decreased lipid droplet number/size in livers of L-KO mice. The MCD diet significantly decreased expression of hepatic genes involved in FA oxidation including FASN (10-fold), SCD1 (14.3-fold), acyl-coenzyme A carboxylase (ACC) (2-fold), and ACS (2.2-fold) in WT mice. In similarly fed L-KO mice, expression levels of these genes decreased, but significantly less so with FASN (4.7-fold) and SCD (8.2-fold) expression. With genes related to triglyceride metabolism, the MCD challenge increased expression of DGAT1 (2.1-fold) and DGAT2 (2.2-fold), while decreasing levels of MGAT (4.5-fold) and MTTP (2.0-fold) in WT mice. Plin2 ablation blunted effects on MGAT, DGAT1, and MTTP in LKO mice. Taken together, these findings indicate Plin2 ablation diminishes the

influence of the MCD diet by alleviating the lipid oxidative and steatotic effects associated with the MCD diet.

Expression levels of Plin2 and other lipid droplet proteins including Plin1, Plin3 and Plin5 were also determined in liver, WAT, brain, and heart (Fig. 23). There was no genotype effect observed in hepatic expression of Plin1, Plin3, or Plin5 in control fed mice. In contrast, levels of Plin5 in WAT was significantly decreased 2.5-fold while in brain, Plin2 was decreased 1.7-fold in L-KO mice as compared to WT mice fed the control diet. The MCD diet increased and decreased, respectively the hepatic expression of Plin1 (1.5-fold), and Plin3 (2-fold) in L-KO mice, while similarly fed WT mice exhibited a decrease in hepatic Plin5. In WAT, the MCD diet increased expression of Plin2 in WT animals 6.6-fold while L-KO mice exhibited a respective 2.2- and 2-fold increase in Plin3 and Plin5. In brain and heart tissue, Plin2 expression was significantly decreased in WT mice but no change was observed in L-KO mice. These findings indicate that WAT is most responsive to Plin2 ablation and challenge with the MCD diet.

DISCUSSION

This study resolves a previously unknown role of Plin2 in the progression of NASH using a conditional Plin2 knockout mouse model that selectively deletes Plin2 in hepatocytes. We demonstrate for the first time the physiological importance of hepatic Plin2 on whole body lipid homeostasis and provide compelling evidence that hepatic ablation of Plin2 blunts the effects of diet-induced NASH related to hepatic lipid accumulation, inflammation, and fibrosis.

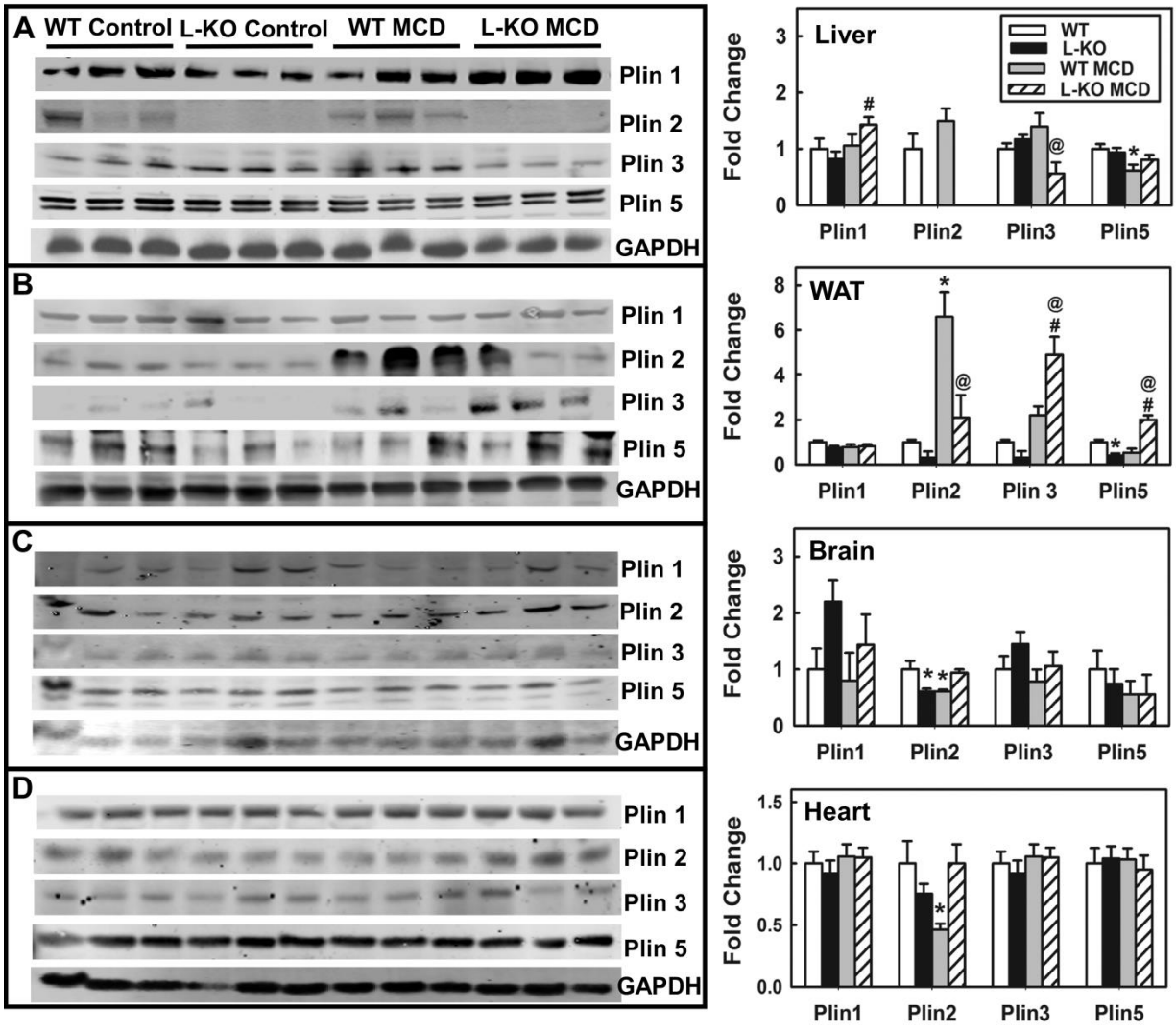

Figure. 23. Plin2 deletion and the MCD diet alter lipid droplet protein expression. Relative protein expression levels of Plin1, Plin2, Plin3 and Plin5 in liver (A), WAT (B), brain (C) and heart (D) tissue from WT mice and L-KO mice fed the control and MCD diets were determined by Western blotting and quantified by densitometric analysis. Values represent mean ± SEM, n= 4-5. *p<0.05 vs. control diet fed WT mice. @P<0.05 vs. MCD diet fed WT mice. #P<0.05 vs. control diet fed L-KO mice.

In terms of development, fertility, viability, and adiposity, hepatic Plin2 ablation had little effect on phenotype. Tissues were of normal size and weight. Analysis of hepatic lipid levels showed neutral lipids were decreased several fold in L-KO mice, in line with previous studies with Plin2 global knockout mice (*32, 33, 37, 61*) and mice treated with Plin2 antisense oligonucleotides (ASO) (*35, 36, 38*). These findings were explained in part by the L-KO mice exhibiting increased hepatic expression of genes involved in fatty acid oxidation including ACOX1 and CPT1α, suggesting increased oxidation of lipids occurred, especially since little to no change was observed in expression levels of lipogenic enzymes MGAT, DGAT1, and DGAT2. In addition to increased hepatic expression of genes involved in fatty acid oxidation, levels of serum β-hydroxybutyrate were increased in L-KO mice, suggesting that fatty acid oxidation was increased in these mice. In support of these findings, recent studies have demonstrated that Hsc-70 targets Plin2 and Plin3 for chaperone-mediated autophagy and degradation, leading to increased lipolysis and fatty acid oxidation of lipids derived from lipid droplets (*66*). We also found that hepatic Plin2 ablation had little effect on expression of MTTP, a triglyceride transfer protein involved in the rate limiting step of VLDL assembly. However, a decrease in total lipoprotein, HDL and VLDL levels was observed in the serum. This was of interest since findings in literature are mixed with regard to VLDL levels and secretion in Plin2 null models. Global Plin2 KO mice exhibited similar VLDL secretion and lipid uptake/utilization as that of WT mice but showed increased expression of MTTP (*32*). In contrast, Plin2 knockdown in mice resulted in decreased hepatic VLDL secretion and production of MTTP (*38*). Interestingly, ablation of both Plin2 and GNMT, an enzyme involved in hepatic SAMe degradation, resulted in a

mouse model with decreased lipogenesis and increased VLDL secretion (*60, 61*). Taken together, these findings demonstrated the differences and similarities between the different Plin2 deletion models and highlighted the importance of examining each mouse in the background of Plin2 deficiency-partial (ASO-treated), global, double ($GNMT^{-/-}/Plin2^{-/-}$) or liver-specific.

To investigate the effect of hepatic Plin2 ablation in the context of NASH, L-KO mice were placed on a MCD diet. Methionine-choline deficiency increases hepatic steatosis by a mechanism that inhibits VLDL secretion and PC synthesis derived from either the CDP-choline pathway involving the enzyme CCT (Kennedy pathway) (*64*) or by sequential methylation of PE by PEMT using methionine-derived substrates (SAMe) (*67*). We found that the effects of the MCD diet were blunted in L-KO mice. Levels of PC and VLDL were unchanged and hepatic steatosis was reduced. These results were due, in part, to an increase in remodeling of PE to PC via the enzyme PEMT where a 10- and 42-fold increase in PEMT expression was observed in MCD fed WT and L-KO mice, respectively. The MCD diet did not change levels of CCT in WT or L-KO mice, but expression of enzymes involved in PC catabolism were reduced when Plin2 was ablated, further bolstering PC levels in L-KO mice. These findings were consistent with the increased PE to PC flux observed in the GNMT/Plin2 knockout mouse model, giving rise to increased PC- and triglyceride-rich VLDL secreted from the liver that helped alleviate hepatic steatosis (*61*). It should be noted that overexpression of Plin2 in mammalian cells increased PC levels via a CCT-mediated mechanism, that did not involve PEMT (*17*). In the current study however, levels of CCT were unchanged in the presence of diet-induced NASH, despite that fact that CCT has been shown to target

lipid droplets and to expand the phospholipid monolayer under conditions of lipid excess (*65, 68*). Based on our findings, we posit that hepatic Plin2 ablation blunts effects from the MCD diet through a mechanism that promotes PC synthesis, not at the lipid droplet surface as directed by the enzyme CCT (*65*), but by a PEMT-mediated mechanism. This hypothesis is consistent with our findings that hepatic Plin2 ablation alleviates diet-induced steatosis while maintaining PC and VLDL levels. In order to summarize the observed findings, a diagram illustrating the proposed mechanism is provided in Figure 24.

Our investigations also demonstrated that hepatic Plin2 ablation reduced diet-induced inflammation and fibrosis. Signs of histopathological lesions and evidence of collagen were diminished in Plin2 null livers when mice were fed the MCD diet. In addition, expression levels of pro-inflammatory markers (IL-1β, TNFα, IL-6, and COX2) were significantly decreased and diet-induced effects on ER stress markers (CHOP and PERK) and proteins induced by CHOP (pro-caspase-1 and caspase-1) were blunted. These findings were consistent with other work showing decreased gene expression and secretion of TNFα, IL-6, and MCP-1 when Plin2 was knocked down in THP-1 macrophages (*12*). Conversely, increased expression of IL-1β and caspase-1 was observed in LPS-stimulated C2C12 cells overexpressing Plin2 (*13*). These findings were significant since TLR4 activation of caspase-1 and NLRP3 links ER stress to inflammation and cell death, two cellular responses that ultimately lead to the onset of hepatic fibrosis and cirrhosis (*57*). In support of these findings, global ablation of Plin2 was found to protect against adipose inflammation in high fat diet fed mice (*37*). Plin2 deficiency reduced adipose inflammatory foci and macrophage invasion in visceral

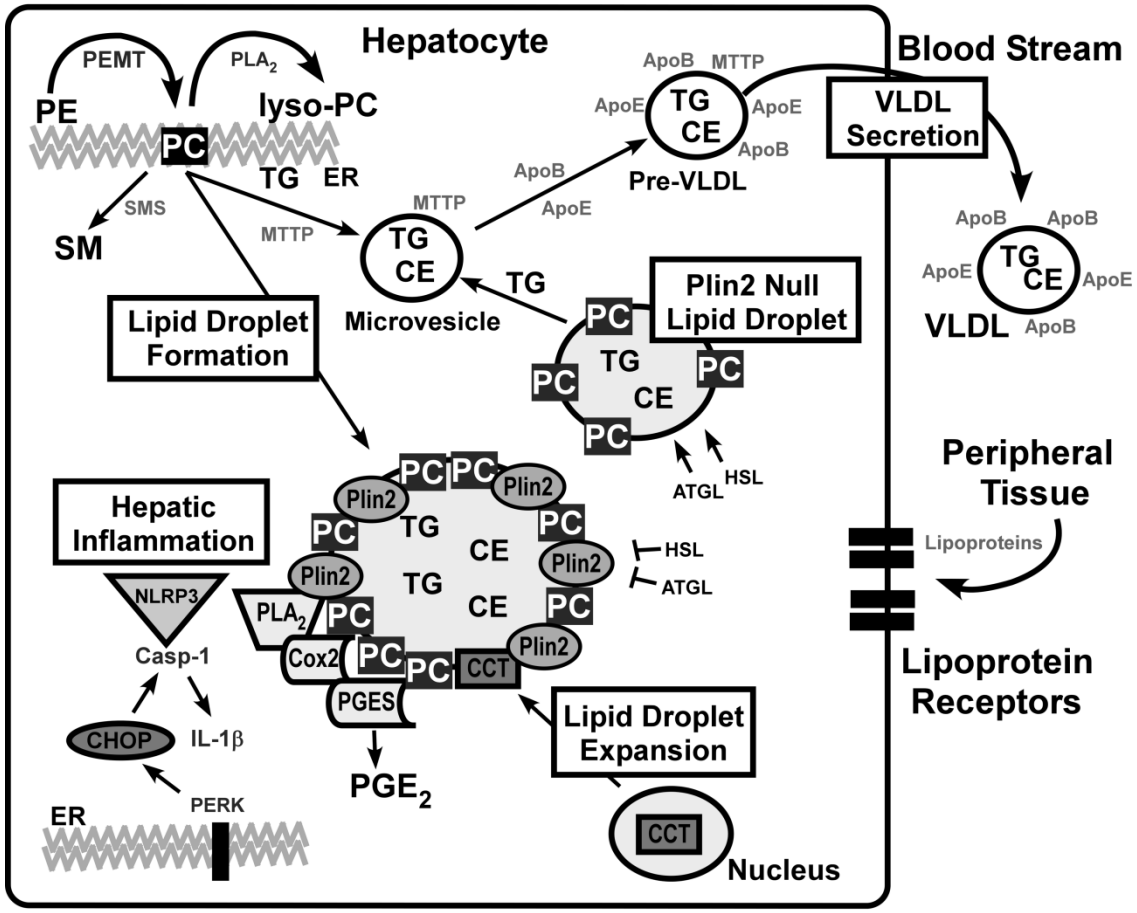

Figure. 24. Schematic diagram illustrating lipid droplet formation, VLDL secretion, and pathways involving hepatic inflammation. Lipid droplet formation: Phospholipids and triglycerides synthesized at the ER form naïve lipid droplets. Hepatic ablation of Plin2 decreases lipid droplet size and number. The MCD diet induces lipid accumulation, resulting in increased lipid droplet size, an effect blunted in L-KO mice. Plin2 null lipid droplets: Lack of Plin2 results in formation of smaller lipid droplets and production of MTTP-rich microsomes that are precursors of pre-VLDL and VLDL particles. VLDL secretion: Partially lipidated ApoB100 containing microsomes constitute naive VLDL particles in the ER. MTTP transfers triglycerides and phospholipids to the nascent VLDL to form pre-VLDL that are stabilized by ApoE. The MCD diet inhibited PC synthesis in WT mice leading to decreased levels of VLDL and increased hepatic steatosis. Lipid droplet expansion: CCT translocates to the lipid droplet surface and begins production of PC to expand the lipid monolayer (37). The lack of choline in the MCD diet favors PC synthesis via the PEMT pathway over CCT-mediated production. Plin2 may block lipase activity of HSL and ATGL. Hepatic inflammation: NLRP3 inflammasomes mediate caspase-1 activation of pro-inflammatory cytokine IL-1β. PERK, an ER stress marker, induces increased expression of CHOP, which then up-regulates pro-caspase-1 which is cleaved by NLRP3 to generate the active form, caspase-1. Several pro-inflammatory markers target lipid droplets including COX2 and PGES. L-KO mice fed the MCD diet, exhibit decreased expression of CHOP, resulting in decreased activation of caspase-1 and IL-1β.

adipose, however no hepatic inflammation or fibrosis was observed in WT or global knockout mice, possibly due to the limitations of the high-fat diet. In other work, Plin2 ASO treated mice fed a high fat diet exhibited signs of fibrosis and increased expression of type 1α collage, but no change in expression of inflammation markers such as TNF-α or macrophage infiltration was observed (*69*). In all, we demonstrated that while the MCD diet increased hepatic inflammation and fibrosis in WT mice yielding conditions consistent with a NASH phenotype, hepatic Plin2 ablation alleviated these effects and protected the liver from obvious signs of injury.

In conclusion, our findings present compelling evidence that lack of hepatic Plin2 alleviates lipid accumulation, inflammation, and fibrosis in the liver. Results support a PEMT-mediated mechanism that involves compensatory changes in proteins involved in PC remodeling, inflammation, and ER stress that work to alleviate diet-induced NASH. Overall, these findings support a role for Plin2 as a target for NASH therapy.

REFERENCES

REFERENCES

1. Harrison, S. A., Torgerson, S., and Hayashi, P. H. (2003) The natural history of nonalcoholic fatty liver disease: a clinical histopathological study., *Am J Gastroenterol 98*, 2042-2047.

2. Ong, J. P., Elariny, H. C., Collantes, R., Younoszai, A., Chandhoke, V., Reines, H. D., Goodman, Z., and Younossi, Z. M. (2005) Predictors of nonalcoholic steatohepatitis and advance fibrosis in morbidly obese patients., *Obes Surg 15*, 310-315.

3. Anderson, N., and Borlak, J. (2008) Molecular mechanism and therapeutic targets in steatosis and steatohepatitis, *Pharm Rev 60*, 311-357.

4. Day, C. P., and James, O. F. (1998) Steatohepatitis: a tale of two 'hits'?, *Gastroenterology 114*, 842-845.

5. Anstee, Q. M., Targher, G., and Day, C. P. (2013) Progression of NAFLD to diabetes mellitus, cardiovascular disease or cirrhosis, *Natl Rev Gastroenterol Hepatol 10* 330-344.

6. Esterbauer, H., Schaur, R., and Zollner, H. (1991) Chemistry and biochemistry of 4-hydroxynonenal, malonaldehyde and related aldehydes., *Free Radic Biol Med 11*, 81-128.

7. Yamauchi, T. e. a. (2003) Globular adiponectin protected ob/ob mice from diabetes and ApoE-deficient mice from atherosclerosis, *J Biol Chem 278*, 2461-2468.

8. Morris, E., Rector, R., Thyfault, J., and Ibdah, J. (2011) Mitochondria and redox signaling in steatohepatitis, *Antioxid Redox Signal 15*, 485-504.

9. Weibel, G. L., Joshi, M. R., Wei, C., Bates, S. R., Blair, I. A., and Rothblat, G. H. (2009) Lipoxygenase-1 associates with neutral lipid droplets in macrophage foam cells: evidence of lipid droplet metabolism, *J Lipid Res 50*, 2371-2376.

10. Melo, R. C. N., and Weller, P. F. (2014) Unraveling the complexity of lipid body organelles in human eosinophils, *J Leukoc 96*, 703-712.

11. Accioly, M. T., Pacheco, P., Maya-Monterio, C. M., Carrossini, N., Robbs, B. K., Oliveira, S. S., Kaufmann, C., Morgado-Diaz, J. A., Bozza, P. T., and Viola, J. P. (2008) Lipid bodies are reservoirs of cyclooxygenase-2 and sites of prostaglandin-E2 synthesis in colon cancer cells., *Cancer Res 68*, 1732-1740.

12. Chen, F. L., Yang, Z. H., Wang, X. C., Liu, Y., Yang, Y. H., Li, L. X., Liang, W. C., Zhou, W. B., and Hu, R. M. (2010) Adipophilin affects the expression of TNFα, MCP-1, and IL-6 in THP-1 macrophages, *Mol Cell Biochem 337*, 193-199.

13. Cho, K., and Kang, P. B. (2015) Plin2 inhibits insulin-induced glucose uptake in myoblasts through the activation of the NLRP3 inflammasome, *Intern J Mol Med 36*, 839-844.

14. Fujii, H., Ikura, Y., Arimoto, J., Sugioka, K., Lezzoni, J. C., Park, S. H., Naruko, T., Itabe, H., Kawada, N., Caldwell, S. H., and Ueda, M. (2009) Expression of Perilipin and Adipohilin in Nonalcoholic Fatty Liver Disease; Relevance to Oxidative Injury and Hepatocyte Ballooning., *J Atheroscler Thromb 16*, 1893-1901.

15. Fukushima, M., Enjoji, M., Kohjima, M., Sugimoto, R., Ohta, S., Kotoh, K., Kuniyoshi, M., Kobayashi, K., Imamura, M., Inoguchi, T., Nakamuta, M., and Nawata, H. (2005) Adipose differentiation related protein induces lipid accumulation and lipid droplet formation in hepatic stellate cells, *In Vitro Cell Dev Biol Anim 41*, 321-324.

16. Larigauderie, G., Cuaz-Perolin, C., Younes, A. B., Furman, C., Lasselin, C., Copin, C., Jaye, M., Fuchart, J. C., and Rouis, M. (2006) Adipophilin increases triglyceride storage in human macrophages by simulation of biosynthesis and inhibition of beta-oxidation, *FEBS J 273*, 3498-3510.

17. McIntosh AL, Senthivinayagam S, Moon KC, Gupta S, Lwande JS, Murphy CC, Storey S, and Atshaves BP. (2012) Direct interaction of ADRP with lipids on the surface of lipid droplets: A live cell FRET analysis., *Am J Physiol Cell Physiol 303*, C728-742.

18. Greenberg, A. S., Coleman, R. A., Kraemer, F. B., McManaman, J. L., Obin, M. S., Puri, V., Yan, Q. W., Miyoshi, H., and Mashek, D. G. (2011) The role of lipid droplets in metabolic disease in rodents and humans, *J Clin Invest 121*, 2102-2110.

19. Wolins, N. E., Quaynor, B. K., Skinner, J. R., Schoenfish, M. J., Tzekov, A., and Bickel, P. E. (2005) S3-12, adipophilin and TIP47 package lipid in adipocytes, *J Biol Chem 280*, 19146-19155.

20. Londos, C., Brasaemle, D. L., Schultz, C. J., Segrest, J. P., and Kimmel, A. R. (1999) Perilipins, ADRP, and other proteins that associate with intracellular neutral lipid droplets in animal cells, *Cell Dev Biol 10*, 51-58.

21. Wolins, N., Quaynor, B., Skinner, J., Tzekov, A., Croce, M., Gropler, M., Varma, V., Yao-Borengasser, A., Rasouli, N., Kern, P., Finck, B., and Bickel, P. (2006)

OXPAT/PAT-1 is a PPAR-induced lipid droplet protein that promotes fatty acid utilization, *Diabetes 55*, 3418-3428.

22. Brasaemle, D. L., Barber, T., Wolins, N., Serrero, G., Blanchette-Mackie, E. J., and Londos, C. (1997) Adipose differentiation-related protein is an ubiquitously expressed lipid storage droplet-associated protein, *J Lipid Res 38*, 2249-2263.

23. Brasaemle, D. L., Levin, D. M., Adler-Wailes, D. C., and Londos, C. (2000) The lipolytic stimulation of 3T3-L1 adipocytes promotes the translocation of hormone-sensitive lipase to the surfaces of lipid droplets, *Biochim.Biophy.Acta 1483*, 251-262.

24. Subramanian, V., Rothenberg, A., Gomez, C., Cohen, A., Garcia, A., Bhattacharyya, S., Shapiro, L., Dolios, G., Wang, R., Lisanti, M., and Brasaemle, D. (2004) Perilipin A mediates the reversible binding of CGI-58 to lipid droplets in 3T3-L1 adipocytes, *J Biol Chem 279*, 42062-42071.

25. Listenberger, L. L., Ostermeyer-Fay, A. G., Goldberg, E. B., Brown, W. J., and Brown, D. A. (2007) Adipocyte differentiation-related protein reduces the lipid droplet association of adipose triglyceride lipase and slows triacyglycerol turnover, *J Lipid Res 48*, 2751-2761.

26. Bell, M., Wang, H., Chen, H., McLenithan, J. C., Gong, D. W., Yang, R. Z., Yu, D., Fried, S. K., Quon, M. J., Londos, C., and Sztalryd, C. (2008) Consequences of lipid droplet coat protein downregulation in liver cells: abnormal lipid droplet metabolism and induction of insulin resistance, *Diabetes 57*, 2037-2045.

27. McIntosh, A. L., Gallegos, A. M., Atshaves, B. P., Storey, S. M., Kannoju, D., and Schroeder, F. (2003) Fluorescence and multiphoton imaging resolve unique structural forms of sterol in membrane of living cells, *J Biol Chem 278*, 6384-6403.

28. Najt, C. P., Lwande, J. S., McIntosh, A. L., Senthivinayagam, S., Gupta, S., Kuhn, L. A., and Atshaves, B. P. (2014) Structural and Functional Assessment of Perilipin2 Lipid Binding Domains., *Biochemistry 53*, 315-321.

29. Gao, J., and Serrero, G. (1999) Adipose differentiation related protein (ADRP) expressed in transfected COS-7 cells selectively stimulates long chain fatty acid uptake, *J Biol Chem 274*, 16825-16830.

30. Bozza, P. T., Yu, W., Penrose, J. F., Morgan, E. S., Dvorak, A. M., and Weller, P. F. (1997) Eosinophil lipid bodies: specific, inducible intracellular sites for enhanced eicosanoid formation., *J Exp Med 186*, 909-920.

31. Wan, H. C., Melo, R. C., Dvorak, A. M., and Weller, P. F. (2007) Roles and origins of leukocyte lipid bodies:proteomic and ultrastructural studies, *FASEB J 21*, 167-178.

32. Chang, B. H., Li, L., Paul, A., Taniguchi, S., Nannegari, V., Heird, W. C., and Chan, L. (2006) Protection against fatty liver but normal adipogenesis in mice lacking adipose differentiation-related protein, *Mol Cell Biol 26*, 1063-1076.

33. Chang, B. H., Li, L., Saha, P., and Chan, L. (2010) Absence of adipose differentiation related protein upregulates hepatic VLDL secretion, relieves hepatosteatosis, and improves whole body insulin resistance in leptin-deficient mice, *J Lipid Res 51*, 2132-2142.

34. Paul, A., Chang, B., Li, L., Yechoor, V., and Chan, L. (2008) Deficiency of adipose differentiation-related protein impairs foam cell formation and protects against atherosclerosis, *Circ Res 102*, 1492-1501.

35. Imai, Y., Varela, G. M., Jackson, M. B., Graham, M. J., Crook, R. M., and Ahima, R. S. (2007) Reduction of hepatosteatosis and lipid levels by an adipose differentiation-related protein antisense oligonuceotide, *Am J Physiol Gastro Liver Physiol 295*, G621-G628.

36. Carr, R. M., Peralta, G., Yin, X., and Ahima, R. S. (2014) Absence of perilipin 2 prevents hepatic steatosis, glucose intolerance and ceramide accumulation in alcohol-fed mice., *PLoS ONE 9*, e97118.

37. McManaman, J. L., Bales, E. S., Orlicky, D. J., Jackson, M. B., MacLean, P. S., Cain, S., Crunk, A. E., Mansur, A., Graham, C. E., Bowman, T. A., and Greenberg, A. S. (2013) Perilipin-2 null mice are protected against diet-induced obesity, adipose inflammation and fatty liver disease, *J Lipid Res 54*, 1346-1359.

38. Varela, G. M., Antwi, D. A., Dhir, R., Yin, X., Singhal, N. S., Graham, M. J., Crook, R. M., and Ahima, R. S. (2008) Inhibition of ADRP prevents diet-induced insulin resistance, *Am J Physiol Gastro Liver Physiol 295*, G621-G628.

39. Kos, C. (2004) Cre/loxP system for generating tissue-specific knockout mouse models., *Nutr Rev 62*, 243-246.

40. Kirsch, R., Clarkson, V., Shepard, E., Marais, D., Jaffer, M., Woodburne, V., Kirsch, R., and Hall, P. (2003) Rodent nutritional model of non-alcoholic steatohepatitis: species, strain and sex difference studies., *J Gastroenterol Hepatol 18*, 1272-1282.

41. Bartneck, M., Fech, V., Ehling, J., Govaere, O., Warzecha, T., Hittatiya, K., Vucur, M., Gautheron, J., Luedde, T., Trautwein, C., Lammers, T., Roskams, T., Jahnen-Dechent, W., and Tacke, F. (2015) Histidine-rich glycoprotein promotes macrophage activation and inflammation in chronic liver disease, *Hepatology* , 63, *1310-1324*.

42. Atshaves, B. P., McIntosh, A. L., Martin, G. G., Landrock, D., Payne, H. R., Bhuvanendran, S., Landrock, K. K., Lyuksyutova, O. I., Johnson, J. D., Marfarlane, R. D., Kier, A. B., and Schroeder, F. (2009) Overexpression of sterol carrier protein-2 differentially alters hepatic cholesterol accumulation in cholesterol-fed mice, *J Lipid Res 50*, 1429-1447.

43. Atshaves, B. P., Gallegos, A., McIntosh, A. L., Kier, A. B., and Schroeder, F. (2003) Sterol carrier protein-2 selectively alters lipid composition and cholesterol dynamics of caveolae/lipid raft vs non-raft domains in L-cell fibroblast plasma membranes, *Biochemistry 42*, 14583-14598.

44. Marzo, A., Ghirardi, P., Sardini, D., and Meroni, G. (1971) Simplified measurement of monoglycerides, diglycerides, triglycerides, and free fatty acids in biological samples, *Clin Chem 17*, 145-147.

45. Bradford, M. (1976) A rapid and sensitive method for the quantitation of microgram quantities of protein utilizing the principle of protein dye binding, *Anal Biochem 72*, 248-254.

46. Lydic, T. A., Busick, J. V., and Reid, G. E. (2014) A monophasic extraction strategy for the simultaneous lipidome analysis of polar and nonpolar retina lipids, *Journal of Lipid Research*, 1797-1809.

47. Fhaner, C. J., Liu, S., Zhou, X., and Reid, G. E. (2013) Functional group selective derivatization and gas-phase fragmentation reactions of plasmalogen glycerophospholipids, *Adv. Mass Spectrom 2*, S0015.

48. Fhaner, C. J., Liu, S., Ji, H., Simpson, R. J., and Reid, G. E. (2012) Comprehensive lipidome profiling of primary and metastatic colon adenocarcinoma cell lines., *Anal Chem 84*, 8917-8926.

49. Romero-Calvo, I., Ocon, B., Martinez-Moya, P., Suarez, M. D., Zarzuelo, A., Martinez-Augustin, O., and Sanchez de Medina, F. (2010) Reversible Ponceau staining as a loading control alternative to actin in Western blots, *Analytical Biochemistry 401*, 318-320.

50. Livak, K., and Schmittgen, T. (2001) Analysis of relative gene expression data using real-time quantitative PCR and the $2^{-\Delta\Delta CT}$ method., *Methods 25*, 402-408.

51. Lee, G. S., Yan, J. S., Ng, R. K., Kakar, S., and Maher, J. J. (2007) Polyunsaturated fat in the methionine-choline-deficient diet influences hepatic inflammation but not hepatocellular injury., *J Lipid Res 48*, 1885-1896.

52. Rizki, G., Arnaboldi, L., Gabrielli, B., Yan, J. S., Lee, G., Ng, R. K., Turner, S. M., Badger, T. M., Pitas, R. E., and Maher, J. J. (2006) Mice fed a lipogenic

methionine-choline-deficient diet develop hypermetabolism conincident with hepatic suppresion of SCD-1, *J Lipid Res 47*, 2280-2290.

53. Anstee, Q., and Goldin, R. (2006) Mouse models in non-alcoholic fatty liver disease and steatohepatitis research., *Int J Exp Pathol 87*, 1-16.

54. Gauthier, M., Favier, R., and Lavoie, F. (2006) Time course of the development of non-alcholic hepatic steatosis in response to high-fat diet-induced obesity in rats., *British J Nutr 95*, 273-281.

55. Romestaing, C., Piquet, M., Bedu, E., Rouleau, V., Dautresme, M., Hourmand-Ollivier, I., Filippi, C., Duchamp, C., and Sibille, B. (2007) Long term highly saturated fat diet does not induce NASH in Wistar rats., *Nutr Metab 4*, 4.

56. Rinella, M., and Green, R. (2004) The methionine-choline deficient dietary model of steatohepatitis does not exhibit insulin resistance., *J Hepatol 40*, 47-51.

57. Verfaillie, T., Rubio, N., Garg, A. D., Bultynck, G., Rizzuto, R., Decuypere, J. P., Piette, J., Linehan, C., Gupta, S., Samali, A., and Agostinis, P. (2012) PERK is required at the ER-mitochondrial contact sites to convey apoptosis after ROS-based ER stress., *Cell Death Differ 19*, 1880-1891.

58. Lebeaupin, C., Proics, E., de Bieville, C. H., Rousseau, D., Bonnafous, S., Patouraux, S., Adam, G., Lavallard, V. J., Rovere, C., Le Thuc, O., Saint-Paul, M. C., Anty, R., Schneck, A. S., Iannelli, A., Gugenheim, J., Tran, A., Gual, P., and Bailly-Maitre, B. (2015) ER stress induces NLRP3 inflammasome activation and hepatocyte death., *Cell Death Dis 6*, e1879.

59. Fujita, K., Y, N., Wada, K., Yoneda, M., Fujimoto, Y., Fujitake, M., Endo, H., Takahashi, H., Inamori, M., Kobayashi, N., Kirikoshi, H., Kubota, K., Saito, S., and Nakajima, A. (2009) Dysfunctional very-low-density lipoprotein synthesis and release is a key factor in nonalcoholic steatohepatitis pathogenesis, *Hepatology 50*, 772-780.

60. Martinez-Una, M., Varela-Rey, M., Cano, A., Fernandez-Ares, L., Beraza, N., Aurrekoetxea, I., Martinez-Arranz, I., Garcia-Rodriguez, J. L., Buque, X., Mestre, D., Luka, Z., Wagner, C., Alonso, C., Finnell, R. H., Lu, S. C., Martinez-Chantar, M. L., Aspichueta, P., and Mato, J. M. (2013) Excess S-adenosylmethionine reroutes phosphatidylethanolamine towards phosphatidylcholine and triglyceride synthesis., *Hepatology 58*, 1296-1305.

61. Martinez-Una, M., Varela-Rey, M., Mestre, D., Fernandez-Ares, L., Fresnedo, O., Fernandez-Ramos, D., Gutierrez-de Juan, V., Martin-Guerrero, I., Garcia-Orad, A., Luka, Z., Wagner, C., Lu, S., Garcia-Monzon, C., Finnell, R. H., Aurrekoetxea, I., Buque, X., Martinez-Chantar, M. L., Mato, J. M., and Aspichueta, P. (2015) S-

Adenosylmethionine increases circulating ver-low-density lipoprotein clearance in non-alcoholic fatty liver disease, *J Hepatol 62*, 673-681.

62. Atshaves, B. P., McIntosh, A. L., Storey, S. M., Landrock, K. K., Kier, A. B., and Schroeder, F. (2010) High dietary fat exacerbates weight gain and obesity in female liver fatty acid binding protein gene-ablated mice, *Lipids 45*, 97-110. PMCID: PMC2831749.

63. Jump, D. B., Depner, C. M., Tripathy, S., and Lytle, K. A. (2015) Impact of dietary fat on the development of non-alcoholic fatty liver disease in $Ldlr^{-/-}$ mice., *Proc Nutr Soc*, 75, 1-9.

64. Pol, A., Gross, S. P., and Parton, R. G. (2014) Review: biogenesis of the multifunctional lipid droplet: lipids, proteins, and sites, *J Cell Biol 204*, 635-646.

65. Krahmer, N., Guo, Y., Wilfling, F., Hilger, M., Lingrell, S., Heger, K., Newman, H., Schmidt-Supprian, M., Vance, D., Mann, M., Farese, R., and Walther, T. (2011) Phosphatidylcholine synthesis for lipid droplet expansion is mediated by localized activation of CTP:Phosphocholine cytidylyltransferease, *Cell Metab 14*, 504-515.

66. Kaushik, S., and Cuervo, A. (2015) Degradation of lipid droplet-associated proteins by chaperone-mediated autophagy facilitates lipolysis., *Nature Cell Biol 17*, 759-770.

67. Horl, G., Wagner, A., Cole, L., Malli, R., Reicher, H., Kotzbeck, P., Kofeler, H., Hofler, G., Frank, S., Bogner-Strauss, J., Sattler, W., Vance, D., and Steyrer, E. (2011) Sequential synthesis and methylation of phosphatidylethanolamine promote lipid droplet biosynthesis and stability in tissue culture and in vivo, *J Biol Chem 286*, 17338-17350.

68. Payne, F., Lim, K., Girousse, A., Brown, R., Kory, N., Robbins, A., Xue, Y., Sleigh, A., Cochran, E., Adams, C., Dev Borman, A., Russel-Jones, D., BGorden, P., Semple, R., Saudek, V., O'Rahilly, S., Walther, T., Barroso, I., and Savage, D. (2014) Mutations disrupting the Kennedy phophatidylcholine pathway in humans with congenital lipodystrophy and fatty liver disease., *PNAS 111*, 8901-8906.

69. Imai, Y., Boyle, S., Varela, G., Caron, E., Yin, X., Dhir, R., Dhir, R., Graham, M., and Ahima, R. (2012) Effects of perilipin 2 antisense oligonucleotide treatment on hepatic lipid metabolism and gene expression, *Physiol Genomics 44*, 1125-1131.

CHAPTER 5:

PLIN2 DRIVES COX-MEDIATED INFLAMMATION THROUGH REGULATION OF MICRORNAS-1894 AND -711

ABSTRACT

Lipid accumulation in lipid droplets plays a key role in production of pro-inflammatory eicosanoids which propagate inflammation. Lipid droplet protein Plin2 promotes lipid storage and has been shown to protect against adipose and hepatic inflammation when ablated. Other work has identified several miRNAs involved in the regulation of inflammation through mechanisms that include lipid droplets but which lipid droplet protein is involved remains unclear. To investigate this further we examined the effect of Plin2 ablation on the miRNA-biome. In Plin2 null livers, 6 miRNAs were significantly increased 3-fold or more. Two of these miRNAs (miRNAs -1894 and -711) were predicted to target genes associated with eicosanoid biosynthesis and inflammation. Luciferase reporter assays and Western blotting demonstrated that miRNAs-1894 and -711 directly target the 3'-UTR sites of COX1, COX2, and human PTGIS and inhibit protein expression of the target genes. In response to LPS-induced inflammation, levels of miRNA-711 decreased and COX2 significantly increased, an effect exacerbated when Plin2 was overexpressed. Conversely, levels of miRNA-1894 increased, negatively affecting the expression of COX1. The extent of targeting of COX1 and COX2 to Plin2-coated lipid droplets was determined by Co-IP and FRET to show increase partitioning of COX2 when inflammation was present. Meta-analysis of ChIP-seq data revealed PPAR, RXR, and p65 response elements within promoter regions of Plin2, COX1, COX2, and miRNAs-1894 and -711, suggesting possible regulation of the target genes. In summary, Plin2 exerts a significant role in COX-mediated inflammation through a miRNA directed mechanism that may involve PPARs and p65.

INTRODUCTION

Lipid droplets are recognized as metabolically active organelles with diverse functions that involve lipid storage, cell signaling, and membrane trafficking (23, 58, 69). In addition, recent work has demonstrated that pathologic conditions where inflammation is present increases the size and number of lipid droplets regardless of cell or tissue type (17, 32, 33, 50), suggesting a role for lipid droplets and associated proteins in the inflammation response. Notably, murine fibroblasts and human monocytes, mast cells, and neutrophils contain prostaglandin hydroperoxide (PGH) synthase on lipid bodies (2, 5, 15) and cytosolic phospholipase A2 ($cPLA_2$) in the lipid droplets of macrophages and mast cells (18, 25, 65). In addition, eicosanoid generating enzymes such as 5-LO, 15-LO, FLAP, LTC_4, PGE_2 synthase, and COX2 target lipid droplets (2, 42), suggesting that eicosanoid intermediates are actively recruited to the lipid droplet surface. In keeping with this, feeding fatty acids to macrophages and monocytes stimulated production of leukotrienes and prostaglandins found on lipid droplets (46) while inhibiting transcription factors NFκB or AP1 prevented lipid droplet formation (32). Taken together, these findings suggest that lipid droplets may function as specialized intracellular sites of signaling within cells engaged in inflammatory processes however, it is unclear how lipid droplet associated proteins are involved.

Recently, liver-specific ablation of Perilipin 2 (Plin2) was shown to alleviate hepatic inflammation and decrease levels of COX2, TNF-α, IL-1β, and IL-6 when mice were fed a methionine choline deficient diet to induce inflammation (52). Conversely, knockdown of Plin2 in macrophages decreased lipid accumulation, and the expression of TNF-α, IL-

6 and MCP-1 (32). In other work, Plin2 augmented inflammation in macrophages (15) and was observed in ballooned hepatocytes from livers of NASH patients (22). In addition, studies with keratinocytes demonstrated that cross talk occurs between PPARs and the p65-subunit of NFκB, resulting in increased lipid accumulation and increased expression of Plin2 and other inflammation genes when cells were treated with TNF-α (1). Taken together, these results suggest a role for Plin2 in inflammation process however, the mechanism of action remains unclear. Recently, several miRNAs have been identified as key mediators in the regulation of the innate immune response and the onset of inflammation through mechanisms that may involve lipid droplets and associated proteins (7). In macrophages, miRNA-155 was shown to increase lipid loading, leading to the formation of lipid droplet-derived foam cells (54). In primary mouse hepatocytes, overexpression of miRNAs -215, -96, -124, -122, and -489 led to increased Plin2 levels and increased lipid droplet size and number (72). Conversely, cells overexpressing miRNAs –let7d, let7e, let7g, and -148a exhibited decreased Plin2 levels and cellular triglyceride content (72). In monocytes treated with LPS to induce inflammation, inhibition of PPARδ by miRNA-9 led to upregulation of Plin2, STAT1, and TNF–α (67). In the current work, several miRNAs including miRNAs-711, -1894, -1224, -574, --494, and -149 that were predicted to target genes associated with inflammation were found up-regulated 3-fold or more by Plin2 ablation. Predicted gene targets of miRNA-711 include *Ptgs2, Ptgis Sp1, Nnfa, Plcd,* and *Akt* (Table 4). Recent work revealed miRNA-711 directly targets AKT (61) and HSP-70 (68) and influences PGI_2 synthesis (51). Less is known regarding miRNA-1894, but a recent study suggests a role in breast cancer (78). Predicted gene targets for miRNA-1894 include *Ptgs1, Pges,*

Pla2, Erk, and Akt. miRNA-1224 was shown to directly target SP-1 and inhibit production of TNF-α (55). Other potential gene targets for miRNA-1224 include *Tnfa, Il-24, Tlr-8, and Il-11*. miRNA-574 was upregulated in patients with end stage sepsis (8). In addition, miRNA-574 was shown to target APP/PS1, resulting in decreased cognitive impairment through regulation of neuritin (35). Other predicted targets for miRNA-574 include *Tgfb and Il-6.* With regard to miRNA-494, predicted gene targets include *Nfkb, Hlf, and cMyc*. In cells treated with TNF-α to induce inflammation, miRNA-494 was up-regulated leading to suppressed insulin action and down-regulation of GSK-3a/b, AS16, and p70S6K phosphorylation (34). In other work, gene target MyD88 was inhibited by miRNA -149 which led to decreased production of inflammatory mediators NFκB, TNF-α, and IL-6 (75). Together, miRNAs-149 and -494 were up-regulated in individuals with glioma and hepatic cancers (63, 74, 77). Predicted gene targets of miRNA-149 include *Akt* and *Torc2*. Based on these findings, we propose that up-regulation of these 6 miRNAs when Plin2 is ablated will inhibit expression of the target genes and as a result, limit production of their pro-inflammatory products. To investigate this further, we focused our study on two of the highest expressing miRNAs in Plin2 KO livers (-1894 and -711) that were predicted to target COX1 and COX2, respectively, to explore the mechanism by which Plin2 ablation and miRNA regulation affects the COX-mediated inflammation response.

In the present work, we examine the inflammatory effect of Plin2 using miRNA microarrays to identify several miRNAs involved in eicosanoid biosynthesis that were up-regulated by Plin2 ablation. To investigate these results further, we performed a serious of luciferase reporter, Western blot, qPCR, co-IP, and FRET experiments to

determine Plin2's role in COX-mediated inflammation and how miRNAs regulate the process.

MATERIALS AND METHODS

MATERIALS

Murine fibroblast and macrophage cell lines, L-Cell (ATCC® CRL-2648) and RAW 264.7 (ATCC® TIB-71) were purchased from American Type Culture Collection (Manassas, VA). DMEM, Lipofectamine 2000, and Opti-MEM were purchased from Life Technologies-Invitrogen (Carlsbad, CA). Lipopolysaacharides (from E.coli 0111:B4) were purchased from Sigma Aldrich Corporation (St. Louis, MO). Rabbit polyclonal COX2, COX1, and PGES antibodies used in LPS treatment experiments were purchased from Cayman Chemical (Ann Arbor, MI). Rabbit polyclonal PLA2, AKT, TLR4, and mTOR2 antibodies were purchased from Cell Signaling (Danvers, MS). Anti-mouse monoclonal antibodies for COX1 and COX2 used in Co-IP experiments were purchased from Santa-Cruz biotechnologies (Santa-Cruz, CA); anti-rabbit polyclonal anti-serum to Plin2 was developed in house (4). The Cy3-labeled anti-mouse and Cy5-labeled anti-rabbit secondary antibodies used for FRET studies were from Life Technologies-Invitrogen (Carlsbad, CA). All other reagents and solvents used were of the highest grade available and were cell culture tested.

CELLS IN CULTURE

L-cells, RAW 264.7 macrophages, and primary mouse hepatocytes were maintained in high glucose DMEM containing 5% FBS and antibiotics (100 units/ml penicillin and 100 units/ml streptomycin) under 5% CO_2 at 37^{o}C. L-cells overexpressing Plin2 were generated previously (47). Mouse hepatocytes were prepared according to White et al. (71). For LPS treatment experiments, cells were plated at a density of 9 x 10^6/dish and serum-starved overnight before treatment with lipopolysaacharides (1-2µg/ml) for 24 hours. Fluorescence imaging and FRET experiments were performed with cells seeded at a density of 50,000 cells/chamber on Lab-Tek chambered coverglass slides (Nunc, Naperville, IL) and cultured overnight before use.

ANIMALS

All animal protocols were approved by the Institutional Animal Care and Use Committee (IACUC) at Michigan State University. Male (6 week old, 20-30 g) inbred C57BL/6NCr mice were obtained from the National Cancer Institute (Frederick Cancer Research and Developmental Center, Maryland). Plin2 null mice were generated as described in the section below. Unless utilized for the dietary studies, all mice were maintained on a standard rodent chow mix (5% calories from fat) and were kept under a 12 hr light/dark cycle in a temperature-controlled facility (25°C) with access to food and water *ad libitum.* Animals in the facility were monitored quarterly for infectious diseases.

PLIN2 KNOCKOUT MICE

Disruption of the murine *Plin2* locus and creation of knockout (KO) mice carrying the *Plin2*$^{tm1a(EUCOMM)Wtsi}$ allele on a C57BL/6NTac background was carried out by the European Conditional Mouse Mutagenesis Program (EUCOMM) consortium. Heterozygous (*Plin2* $^{+/-}$) mice were purchased from the Welcome Trust Sanger Institute and were bred together to establish homozygous mice that were globally null in Plin2 (hereafter known as Plin2 KO mice). The following primer pairs were for genotyping: P1forward-5' CTA GAC TCT CCA AAT CTC TCC AAA AAC 3' and P2backward-5' ATA GGT ATT GGC AAC CGC AAC 3' to amplify the wild type (WT) allele and primers P1forward and P3backward 5' TCG TGG TAT CGT TAT GCG CC 3' to amplify the mutant allele. The presence of the mutant allele was also confirmed by detecting the presence of the lacZ gene using the primers P4forward 5' ATC ACG ACG CGC TGT ATC 3' and P5backward 5' ACA TCG GGC AAA TAA TAT CG 3'. Lack of Plin2 protein expression was confirmed by Western blot analysis.

MICRORNA MICROARRAY

Total liver RNA was extracted from three WT and three Plin2 KO mice using TRIzol and Qiagen miRNA isolation kits. The quality of the RNA was determined in-house with a RNA Pico 6000 analyzer from Agilent Technologies (Santa Clara, CA). RNA samples with RNA integrity index scores of $\geq$ 9 were used in microarray and qPCR analyses. OneArray miRNA expression profiling was performed by Phalanx Biotech Company (Hsinchu, Taiwan). Differentially expressed miRNAs isolated from Plin2 null livers were identified following normalization to internal controls. The microarray data were

deposited at the National Center for Biotechnology Institute Gene Expression Omnibus (GEO) repository.

HEAT MAP AND VOLCANO PLOT ANALYSIS

The miRNA microarray data were processed using mean-centering and Pareto-scaling prior to multivariate statistical analysis. The heat map was generated using Cluster 2.0 from the Eisen Lab modified by Michiel de Hoon (http://bonsai.hgc.jp/~mdehoon/software/cluster/). Java Tree Viewer was used to view and color the heat map. The volcano plot was generated by plotting log10 transposed significance versus log 2 transposed fold change.

GENERATION AND DIRECT TARGETING OF COX1 AND COX2 LUCIFERASE REPORTERS

To perform the luciferase reporter assays, COX2 3'-UTR DNA was purchased from GeneCopoeia (Rockville, MD) and cloned into the pEZX-MT01 dual luciferase reporter construct. The COX1 3'-UTR was generated from mouse genomic DNA by PCR and then cloned into the pEZX-MT01 vector. The Dual luciferase reporter assays were performed as described previously (*48*) and in accordance with manufactures specifications. Relative luciferase activity was calculated as the ratio of firefly luciferase activity divided by the *Renilla* luciferase activity.

CO-IMMUNOPRECIPITATION STUDIES

The Novex system from Life Technologies (Carlsbad, CA) was used for co-immunoprecipitation (co-IP) experiments following the manufacturers' protocol. Briefly, lipid droplets were isolated from L-cell control and Plin2 overexpression cells treated with LPS as described previously (*64*). Lipid droplet fractions were incubated overnight with kit reagents and anti-bodies (anti-Plin2 with anti-COX2 or anti-COX1) at 4^0C with shaking. The next day, unbound fractions were separated by centrifugation, followed by washing and elution of the bound complex. Eluate proteins were analyzed by Western blotting. A parallel co-IP with the lysates using anti-rabbit IgG was performed to assess nonspecific binding (negative control).

LIVE CELL LIPID DROPLET IMAGING

L-cells and Plin2 overexpressing cells were grown on Lab-Tek chambered coverglass slides (Nunc, Naperville, IL) and cultured overnight before use. The next day, cells were washed with PBS and then incubated with Nile red for 30 min at room temperature. Before imaging, cells were washed in PBS. Cell images were acquired on an Olympus FluoView 1000 Laser Scanning Confocal Microscope using the 568 nm diode laser line to acquire images of the cells by sequential excitation. Nile red fluorescence emission was collected through a HQ598/40 nm filter. Image analysis was performed using MetaMorph 7.5 (Molecular Devices, Sunnyvale, CA).

EICOSACELL ASSAY

The EicosaCell assay was performed following the procedure of Bandeira-Melo et al. (*5*). In brief, LPS-treated primary mouse hepatocytes were permeabilized and fixed in 1% EDAC for 30 minutes at 37C. The cells were washed with HBSS and blocked with 2% FBS in HBSS for 1 hour before incubation with primary antibodies [mouse anti-PGE2 at 1:100 dilution and rabbit anti-Plin2 at 1:50 dilution] for 1 hr at room temperature. After extensive washing with HBSS, Cy3 or Cy5 labeled secondary antibodies (at 1:100 dilutions) in PBS was added to each set and incubated for 1 hr at room temperature. Cells were then washed with HBSS and mounted with cover slips using fluorogel mounting medium (Electron Microscopy Science, Hatfield, PA). Cells were stained with Cy3 and Cy5 alone in the absence of primary antibodies to serve as background controls. LPS treated cells fixed in 4% paraformaldehyde and permeabilised with 0.1% saponin served as negative controls for EDAC-mediated entrapment of PGE2 at sites of synthesis. Cell images were sequentially acquired on an Olympus FluoView 1000 Laser Scanning Confocal Microscope using 559 nm excitation, 575/50 filter (green channel) to view the Cy3 emission and 635 nm excitation, 725/30 filter (red channel) for the Cy5 emission. Co-localization of the Cy3- and Cy-5 signals were obtained using the Olympus Fluoview software where the confocal images from the green and red channels were merged and appeared yellow where superimposition occurred (red and green are additive and yield yellow to orange in RGB color space).

COLOCALIZATION AND FLUORESCENCE RESONANCE ENERGY TRANSFER (FRET) IMAGING

Colocalization and FRET imaging studies were performed following procedures described earlier (*62*). Briefly, mouse primary hepatocytes were fixed in cold acetone/ethanol (70:30 v/v) and washed with PBS. The cells were blocked with 2% BSA and then incubated with either mouse anti-COX1 (1:10) or mouse anti-COX2 (1:25) and then rabbit anti-Plin2 (1:50)] for 1 hr at room temperature. After extensive washing with PBST (0.05% Tween100 in PBS), a mixture of secondary reagents consisting of Cy3 or Cy5 labeled secondary antibodies (at 1:100 dilution) in PBS were added to each set and incubated for 1 hr at room temperature. Cells were then washed with PBS and mounted with cover slips using fluorogel mounting medium. Cells stained with Cy3 and Cy5 alone in the absence of primary antibodies served as background controls. Cell images were sequentially acquired and analyzed on an Olympus FluoView 1000 Laser Scanning Confocal Microscope as described in the previous section. Acceptor photobleaching FRET experiments were performed to measure the increase in donor (Cy3) emission upon photobleaching of the acceptor (Cy5) as described elsewhere (47,62). To calculate the FRET efficiency (*E*), representing the efficiency of energy transfer between donor and acceptor, the following equation was used: $E = 1-(I_{DA}/I_D)$ where I_{DA} is donor fluorescence intensity before acceptor photobleaching and I_D is the donor fluorescence intensity after acceptor photobleaching. An average *E* value was calculated from Cy3 fluorescence emission increase after photobleaching. The intermolecular distance *R* between Plin2 and COX2 or Plin2 and COX1 was calculated from the equation $E = 1/(1-(R/R_o)^6)$, where *E* is experimentally determined and R_o is the Foster radius for the Cy3-Cy5 FRET pair, previously determined as 51 Å. For the FRET efficiency images,

analysis was performed in MetaMorph 7.5 (Molecular Devices, Sunnyvale, CA). Images were filtered to remove randomized noise by using a low pass filter. The filtered images of the donor emission before acceptor photobleaching were subtracted from the image after acceptor photobleaching. The resultant image was divided by the image of donor emission after acceptor photobleaching and multiplied by 100 to generate bar-scale FRET efficiencies.

QUANTITATIVE REAL-TIME PCR

Total RNA was isolated from liver using Trizol (Qiagen, Valencia, CA) in accordance with the manufacturer's protocol. Total RNA (1 μg) from each liver sample was converted into first strand cDNA using ABI high capacity cDNA reverse transcription kit (Gand Island, NY). Expression was analyzed by SYBR Green or Taqman microRNA assays using commercially available primers from IDT (Coralville, IA) or Life Technologies (Carlsbad, CA) on a StepOne plus Real Time PCR system. Relative expression was calculated using the comparative $2^{-\Delta\Delta CT}$ method (*39*). Data were expressed as fold difference.

WESTERN BLOT ANALYSIS

Cell lysates (10-20 μg protein) were separated on 10% tricine gels using a Mini-Protean II cell (Bio-Rad lab, Hercules, CA) system at constant amperage (40 mA per gel) for about 2 hrs. Proteins were then transferred onto PVDF membranes at constant voltage (90 V) for 2 hrs. Blots were stained with Ponceau S to confirm uniform protein loading (*3, 73*) before blocking in 3% BSA in TBST (10 mM Tris-HCl, pH 8, 100mM

NaCl, 0.05% Tween-20) for 1 hour. Blots were incubated with specific polyclonal rabbit antibodies overnight and were developed with IRDye 800CW anti-mouse (LI-COR) or IRDye 680RD anti-rabbit (LI-COR) secondary antibodies. To visualize the bands of interest, blots were scanned using the LI-COR Odyssey imaging system (Lincoln, NE). Protein bands were quantitated by densitometric analysis after image acquisition using NIH Scion Image to obtain relative protein levels expressed as integrated density. All values were normalized to GAPDH or β-actin expression.

RNA INTERFERENCE (SIRNA)

Plin2 siRNA (sense-5′-AACGUCUGUCUGGACCGAAUA-3′ and the corresponding antisense) sequences were synthesized from Dharmacon (Lafayette, CO). A non-targeting control siRNA was purchased from Dharmacon. RAW 264.7 cells were transfected with siRNA using opti-MEM and RNAiMax as per the manufacturer's instructions. Briefly, cells (0.5×10^6 cells/ well) in 6-well plates (Nunc, Naperville, IL) were transfected with either the non-targeting control siRNA (100nM) or the Plin2 siRNA (100nM). Un-transfected control cells plated at the same density were maintained simultaneously. Twenty four hours after transfection, the media was changed to complete growth medium. After 48-hours of transfection, cells were treated with 1 μg/ml LPS for 4 hours. Cells were then harvested and cell lysates stored at -80 C until used for further analyses.

ANALYSIS OF TNF-α AND IL-1β IN PLIN2 KNOCKDOWN CELLS

RAW 264.7 cells transfected with control and Plin2 siRNA were treated with 1μg/mL LPS for 4 hrs. Concentrations of *TNF-α and IL-1β* were determined using ELISA kits from eBioscience (San Diego, CA) according to the manufacturer's instructions. Colorimetric analysis of TNF-α and IL-1β were measured on an Omega FLOUstar 96-well plate reader from BMG labtech (Ortenberg, Germany).

META-ANALYSIS OF CHIP-SEQ DATASETS

ChIP-Seq datasets for hepatic binding of p65 (6), PPARα (9), and RXR (*27*) in mice were obtained from the Gene Expression Omnibus (GEO). BedGraph files were imported as custom tracks into the UCSC Genome Browser (https://genome.ucsc.edu/) using the mouse mm9 GRCm37 genome build in order to visualize transcription factor binding within the promoter regions of Plin2, miR-1894, miR-711, Ptgs1, and Ptgs2.

STATISTICAL ANALYSIS

Values were expressed as the means ± S.E. In comparisons made between two groups, Student's *t* tests were performed using Graphpad Prism (San Diego, CA). When more than two groups were compared, one-way analysis of variance (ANOVA) with Newman Keuls post-hoc test was performed. Values with $p < 0.05$ were considered statistically significant.

RESULTS

GENERATION OF PLIN2 GLOBAL KO MICE

To generate Plin2-null mice, a targeting strategy was designed that involved insertion of a promoterless cassette in the intronic region between exons 3 and 4 to disrupt the WT allele (Fig. 25A). Homozygous mice globally null in Plin2 were generated by breeding together heterozygous mice carrying the Plin2 targeted allele. The mice were genotyped using three PCR assays to identify homozygous (Fig. 25B, lanes 1-3), heterozygous (lanes 4-6) and WT (lanes 7-9) mice. Heterozygous mice were positive for all three PCR assays while homozygous mice contained bands representing the FRT site (204 bp) and the lacZ gene (108 bp). WT mice lacked the FRT site and lacZ gene and were positive only for a 650 bp band representing the WT allele (Fig. 25B). Western blot analysis confirmed ablation of Plin2 in the liver, kidney, heart, white adipose tissue, (WAT), and muscle (Fig. 25C).

PROFILE OF THE MIRNAS AFFECTED BY PLIN2 ABLATION

Recently, several miRNAs were shown to influence lipid droplet morphology by altering lipid droplet size and lipid content (72). Since Plin2 is also known to affect these parameters, we decided to examine the effect of Plin2 ablation on the miRNA biome by performing a miRNA microarray on Plin2 null liver samples (Phalanx Biotech, San Diego, CA). Out of the 1200 sequences analyzed, 1086 returned a detectable signal. The data was presented as log2 transformed and normalized using the 75% media scaling normalization method (41). A heat map displaying unsupervised hierarchy clustering was developed showing the expression profile of miRNAs on a

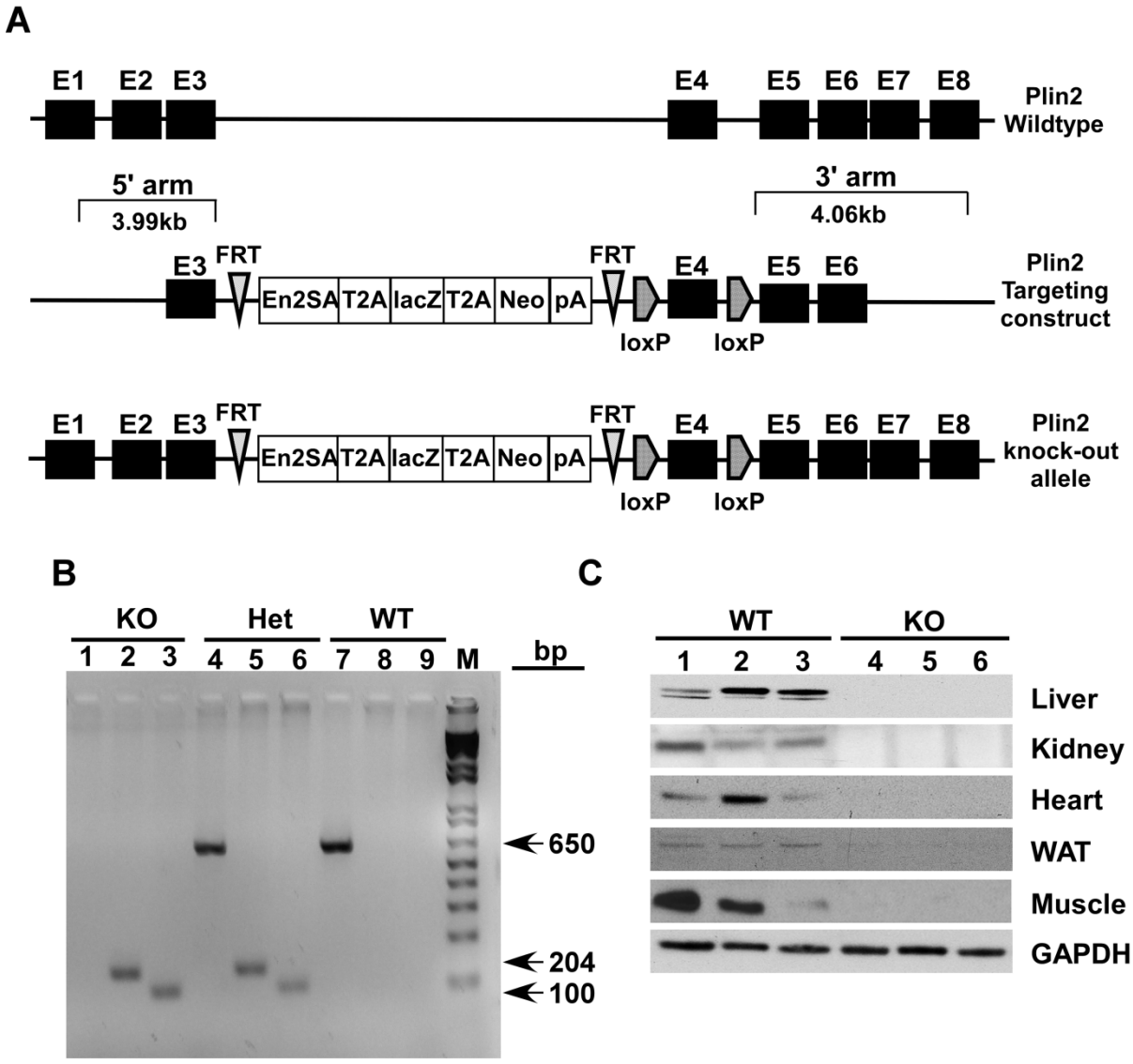

Figure. 25. Generation of Plin2 gene ablated mice. (A) Targeting strategy for generating Plin2 KO mice. (B) PCR screening of Plin2 KO, hetereozygous (Het) and WT mice. Primers were designed to detect the presence or absence of the WT allele (lanes 1, 4, and 7; 650bp), the mutant exon3 site (lanes 2, 5, and 8; 148 bp) and the LacZ insert (lanes 3, 6, and 9; 108 bp). Tail DNA containing the mutant exon 3 site and the LacZ insert were Plin2 KO mice, while samples positive for the WT allele, the mutant exon3 site, and LacZ insert were Plin2 Het mice. WT mice were positive for only the WT allele product. (C) Western blot analysis of Plin2 protein expression in liver, kidney, heart, white adipose tissue (WAT), and muscle for WT (lanes 1-3) and Plin2 KO (lanes 3-6) mice.

green to red scale where green shades indicated reduced relative expression and red indicated increased expression (Fig. 26A). To identify the miRNAs showing replicate reproducibility and greater than a 2-fold change, a Volcano plot was generated (Fig. 26B). The plot described the distribution of differentially expressed probes as a measure of significance (negative logarithm of the P-value) on the y axis against the fold-change (x-axis). In response to Plin2 ablation, 20 miRNAs were up-regulated, and of these, 6 miRNAs (-1894, -494, -711, -1224, -574, and -149) were significantly up-regulated 3-fold or more (Fig. 27A). Microarray results were validated by qPCR and showed significantly increased miRNA levels in Plin2 null samples when compared to controls (Fig. 27B). Several miRNAs downregulated by Plin2 ablation (-5122, -92a, -1907, -146a, -709, and -665) exhibited a minimal reduction (2.3-fold and less) and were not considered further (Fig. 27A). We noticed that several of the miRNAs were predicted to target genes associated with eicosanoid biosynthesis and inflammation as listed in Table 4. In particular, miRNAs -1894 and -711 contained seed sequences with targets to the 3' UTRs of COX1, COX2, PGIS, PGES, PLA2 and AKT. Based on these findings, we propose that up-regulation of miRNAs-1894 and -711 when Plin2 is ablated may inhibit expression of eicosanoid producing target genes and as a result, limit inflammation. To test this hypothesis, we determined the effect of Plin2 ablation on levels of these gene targets (Fig. 28A), along with other markers of inflammation including NFκB, IL-1β, IL-6, and TNF-α (Fig. 28B). Expression levels of COX1, COX2, and PTGIS were decreased 2-, 1.8-, and 2.2-fold, respectively in Plin2 null livers, in keeping with the observed up-regulation of miRNAs-1894 and -711. Inflammation markers IL-1β, IL-6, and TNF-α were also decreased 3.3-, 6.3-, and 4.4-fold,

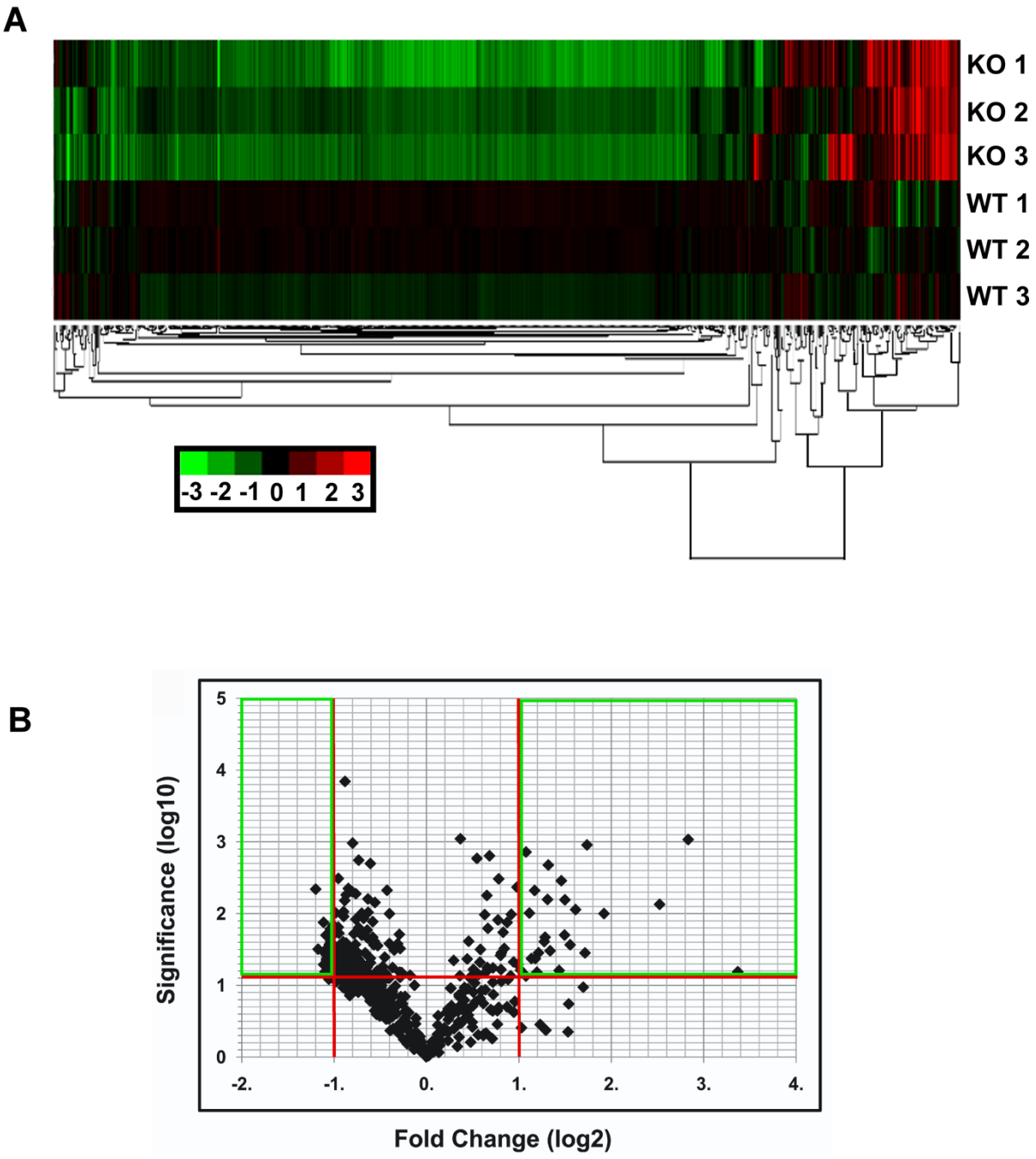

Figure. 26. Heat map and volcano plot on miRNA microarray data. (A) Heat map showing the hepatic miRNAs that are up-regulated (red) and down-regulated (green) in 3 WT and 3 Plin2 KO mice. Unsupervised hierarchy clustering was used to separate distinct miRNA patterns. (B) Volcano plot showing changes in expression of hepatic miRNAs of Plin2 KO versus WT mice. Green boxes contain miRNAs with >2-fold difference compared to WT and P value <0.05.

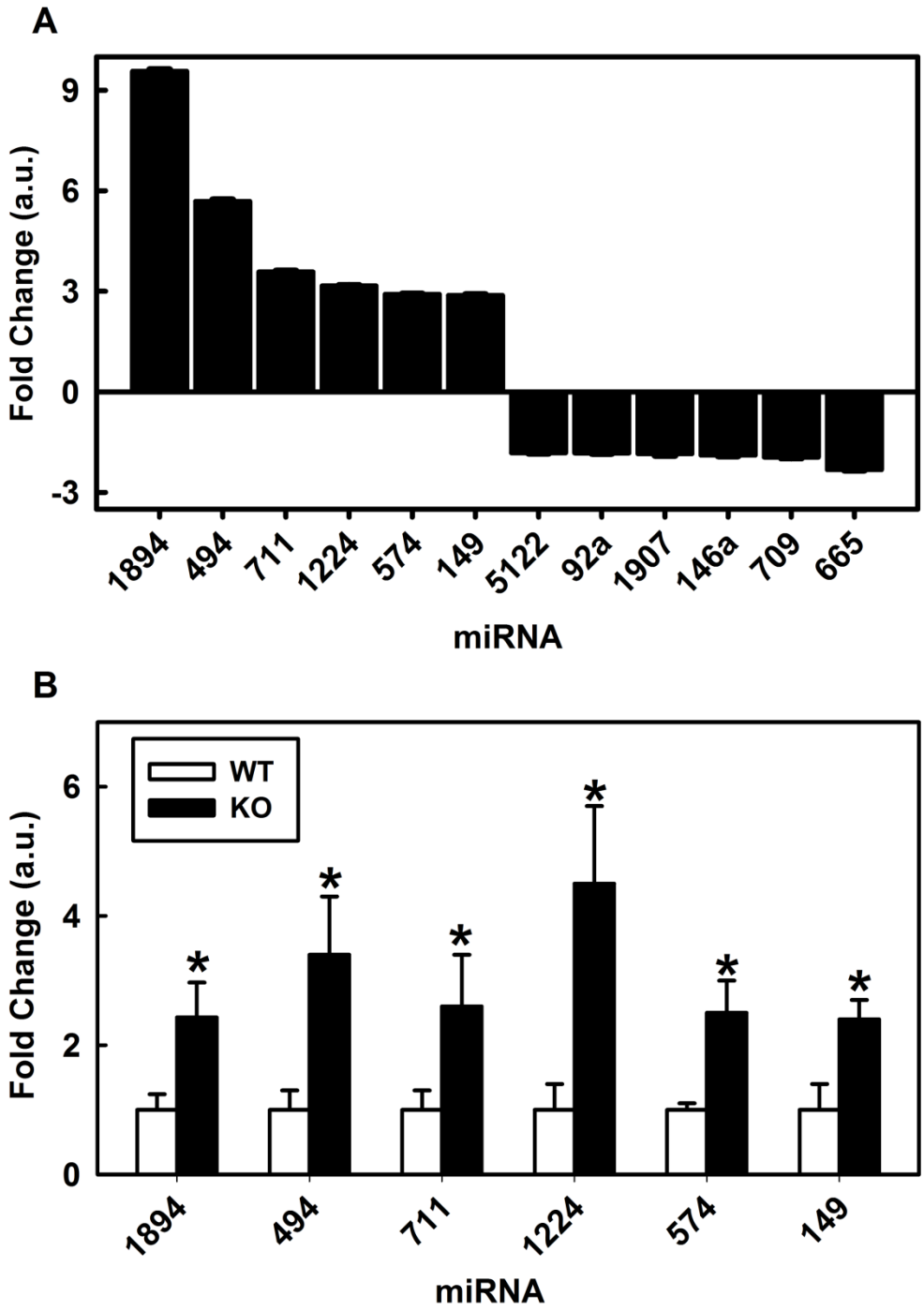

Figure. 27. Relative expression levels of miRNAs altered by Plin2 ablation. (A) Increases and decreases of the top 12 miRNAs altered by Plin2 ablation. (B) Up-regulated miRNAs were validated by qPCR. The mature miRNA sequences were used to determine miRNA expression. Values represent mean ± SEM (n=3). (*) indicates $p < 0.05$ as compared to control.

Table 4. Predicted miRNA targets altered by Plin2 ablation.

MicroRNA	Predicted Gene Targets	Gene Product	Significant Pathways
miR-711	*Ptgs2, Sp1, Tnfa, Plcd, Akt, Ptgis*	COX2, SP1, TNFα, PLCδ, AKT, PTGIS	Inflammation, Fibrosis
miR-1894	*Ptgs1, Pges, Pla2, Erk, Akt*,	COX1, PGES, $cPLA_2$, ERK, AKT	Inflammation, Cancer, CCR
miR-1224	*Tnfa, Sp1, Il-24, Tlr-8, Il-11*	TNFα, SP1, IL-24, TLR-8, IL-11	Inflammation, Hepatocellular carcinoma
miR-574	*Tgfb, Rrxra, Ppara, Ap-1, Il-6*	TGFB, RXRα, PPARα, AP-1, IL-6	Inflammation, Liver cirrhosis, CCR
miR-494	*Nfkb, Hlf, cMyc,*	NFκB, HLF, cMyc,	Inflammation, Cancer
miR-149	*Actin, Akt, Torc2,*	β–actin, AKT, mTOR2,	Inflammation, Fibrosis, Cancer

TargetScan.org and Exiqon.com were used to determine possible targets associated with hepatic inflammation. Significant pathways associated with the predicted targets based on the genes listed and recent findings were also determined. CCR= Cell Cycle Regulation

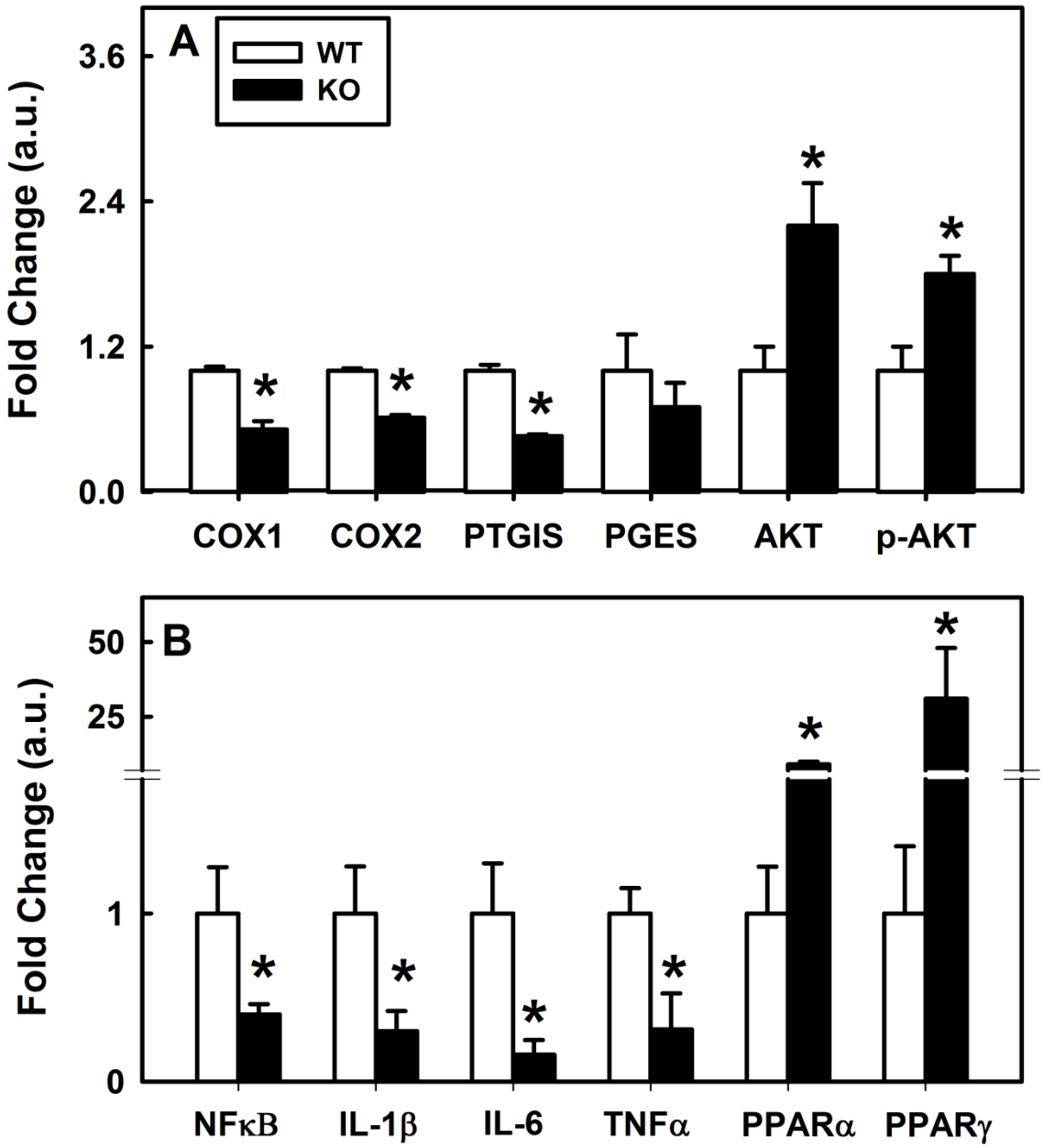

Figure. 28. Relative expression levels of hepatic proteins involved in inflammation and eicosanoid biosynthesis in WT and Plin2 KO. (A) Western blot analysis of predicted targets of miRNAs altered by Plin2 ablation. Expression levels were normalized to the housekeeper gene GAPDH and expressed as fold change relative WT controls. (B) Relative gene expression of cytokines and transcription factors involved in the propagation of the inflammation response were quantified by qPCR. Values represent mean ± SEM (n=3-5). (*) indicates $p < 0.05$ as compared to wild type controls.

respectively (Fig. 28B). In contrast, levels of AKT and p-AKT were upregulated 2.2- and 1.8-fold, while PGES levels were unaffected. Transcription factor NFκB was decreased 2.5-fold, while PPARα and PPARγ were increased 8.9- and 31-fold, respectively (Fig. 28B). Notably, recent studies have shown that PPARs exert a regulatory effect on inflammation genes through interactions with the NFκB pathway (14, 28, 43). Using ChIP-seq data sets that are available through the genome omnibus (GEO), we identified response elements for PPARα, PPARγ, RXR, and the p65 (a subunit of NFκB) in the promoter regions of Plin2, miRNAs-1894 and -711, and their gene targets COX1 and COX2 (Fig. 29). Files were downloaded from previous ChIP-seq studies (6, 9, 27) and available tracks uploaded to UCSC genome browser (https://genome.ucsc.edu/). Transcription factor binding intensities were normalized to show comparative signals for PPARα, PPARγ, RXR, and p65 (X-axis) while the proximal promoter regions for each gene (Y-axis) were scaled to the areas of interest. The Plin2 locus, located on chromosome 4, showed binding of PPARα, PPARγ, RXR, and p65 to within 5 kb of the transcription start site (Fig. 29A). The data showed that PPARα was bound at two locations upstream of Plin2 (Fig. 29A, green box) and overlapped with RXR and PPARγ (blue and green box), suggesting that PPAR-RXR heterodimers may exist at these sites. Increased RXR signal at the region overlapping with PPARα under bexartene (Bexa) stimulation, a potent retinoid RXR agonist (Fig. 29A, blue and green box overlap) and treatment with rosiglitazone (Rosi), a PPAR agonist, supported the existence of PPAR-RXR heterodimers at this location (Fig. 29A, blue box). NFκB -p65 signal was not detected at the Plin2 locus under basal conditions however, stimulation with kdo2-lipid A (KLA), a synthetic TLR4- NFκB agonist, induced a strong p65

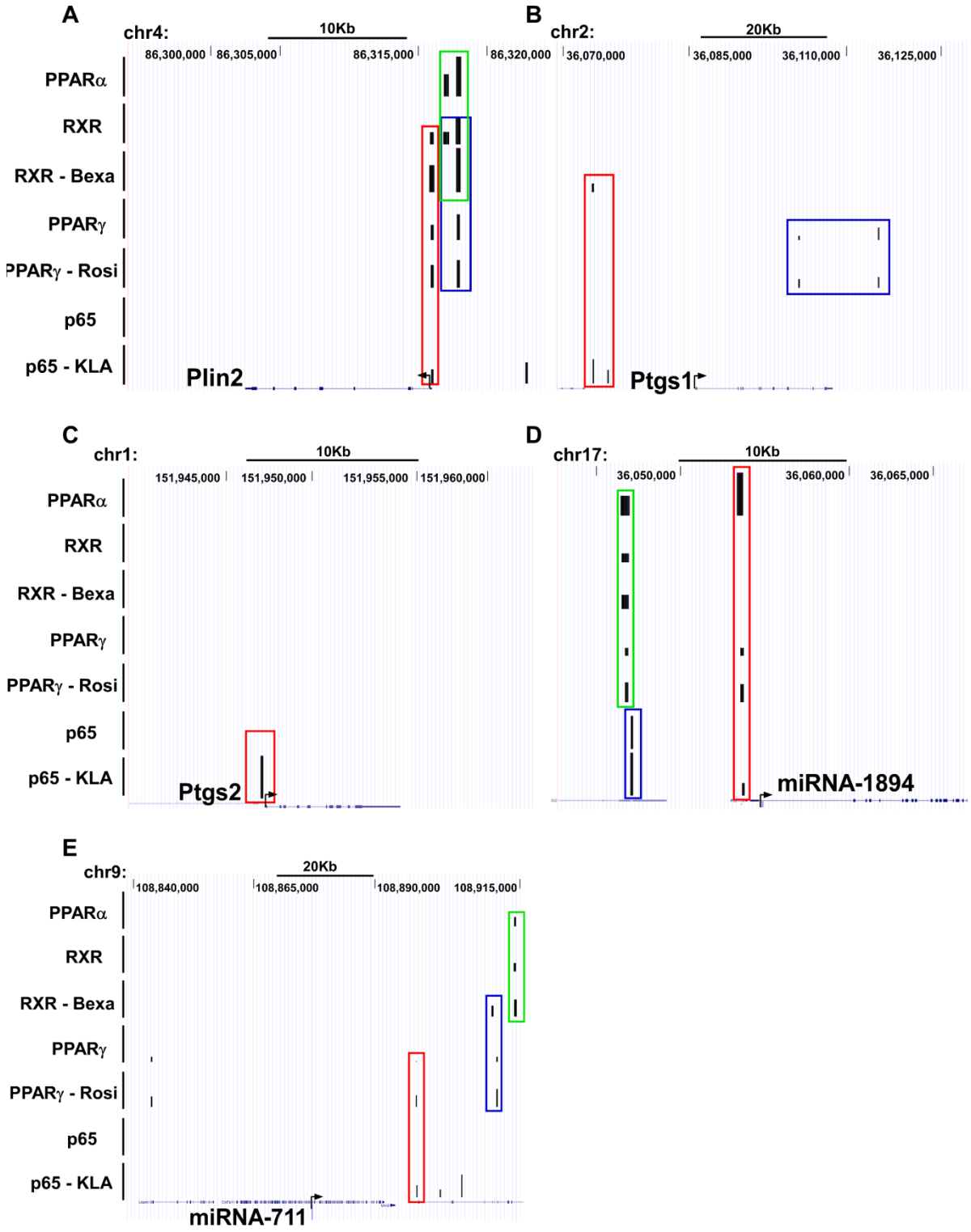

Figure. 29. Chip-Seq data outlining transcription factor binding. PPARα, PPARγ RXR, and p65 are shown binding to the gene loci of Plin2 (A), COX1 (B), COX2 (C), miRNA-1894 (D) and miRNA-711 (E). UCSG Genome Browser tracks were derived from PPARα, PPARγ RXR, and p65 ChIP-Seq data obtained from the GEO omnibus.

response increasing p65 signal directly at the RXR and PPARγ binding site (Fig. 29A, red box). Taken together, these findings suggest that PPARα, PPARγ, RXR, and p65 drive Plin2 expression under basal and LPS-stimulated inflammation,

COX1 (encoded by the *Ptgs1* gene on chromosome 2), showed less PPAR binding than Plin2 (Fig. 29A vs B) however, PPARγ binding was mapped to an intronic and downstream region of COX1. The intronic bound PPARγ peak was enriched under stimulation with Rosi indicating PPARγ may play a role in the post transcriptional regulation or mRNA splicing of COX1 (60) as shown in (Fig 29B, blue box). In addition, COX1 contained a p65 binding site present under KLA induction, one of which overlapped with BEXA-stimulated RXR (Fig 29B Red box). COX2 encoded by the *Ptgs2* gene on chromosome 1, contained a single p65 peak in the proximal promoter region that was strongly induced by KLA (Fig 29C Red box). With regards to transcriptional control of miRNAs, the miRNA-1894 locus, located on chromosome 17, showed that PPARα and PPARγ bound to the promoter region within 5kb of its transcriptional start site. Additional binding sites were observed ~10kb upstream of the start site however, the presence of additional genes indicated that these sites may not be involved in miRNA-1894 regulation (Fig 29D, green and blue boxes). In alignment with the PPARα and PPARγ sites to within 5kb of the transcriptional start site was a p65 signal. Activation of p65 induced overlap with PPARα and PPARγ, supporting cross talk between the two transcription factors (Fig 29D, red box). In contrast to the other genes, miRNA-1894, miRNA-711 did not contain binding of transcription factors in the proximal promoter region (Fig 29E). In place of proximal binding, a p65 binding site was observed 20kb downstream, overlapping with PPARγ binding in the presence of Rosi

(Fig 29E, red box). Further downstream of the p65 site were additional PPARγ, PPARα, and RXR sites that were enriched under BEXA or Rosi treatment (Fig 29E, blue and green boxes). Based on these results, we propose that the downstream binding sites of p65, PPARγ, PPARα, and RXR regulate miRNA-711 expression by looping back on the upstream promoter region, as observed for TNF-α in a similar mechanism (30). Overall, meta-analysis of available Chip-Seq data suggests that expression of Plin2, COX1, and miRNAs-1894 and -711 is controlled via crosstalk between PPARs and p65. COX2 on the other hand, appears to be under the direct control of p65, suggesting that Plin2 may influence COX2 levels post transcriptionally.

MIR-1894 AND -711 DIRECTLY TARGET AND REGULATE COX1 AND COX2 EXPRESSION

To determine whether miRNAs-1894 and -711 directly target their predicted gene targets COX1, COX2, and PTGIS, several 3'-UTR luciferase reporter vectors were generated and dual luciferase reporter assays were performed as described in the Methods section. In cells overexpressing miRNA-1894, luciferase activities were significantly reduced when the COX1 3'-UTR luciferase reporter system was present, indicating miRNA-1894 directly targeted and inhibited expression of COX1 (Fig. 30A). Likewise, luciferase activities were decreased in the presence of the COX2 3'-UTR luciferase reporter system in miRNA-711 overexpression cells, signifying that miRNA-711 directly targets and inhibits COX2 (Fig. 30A). However, no change in luciferase signal was observed in the presence of the 3'-UTR of mmu-PTGIS, indicating that miRNA-711 did not directly target mouse PTGIS. Upon further examination, we found a conserved consensus sequence for hsa-miRNA-711 present in the 3'-UTR of human

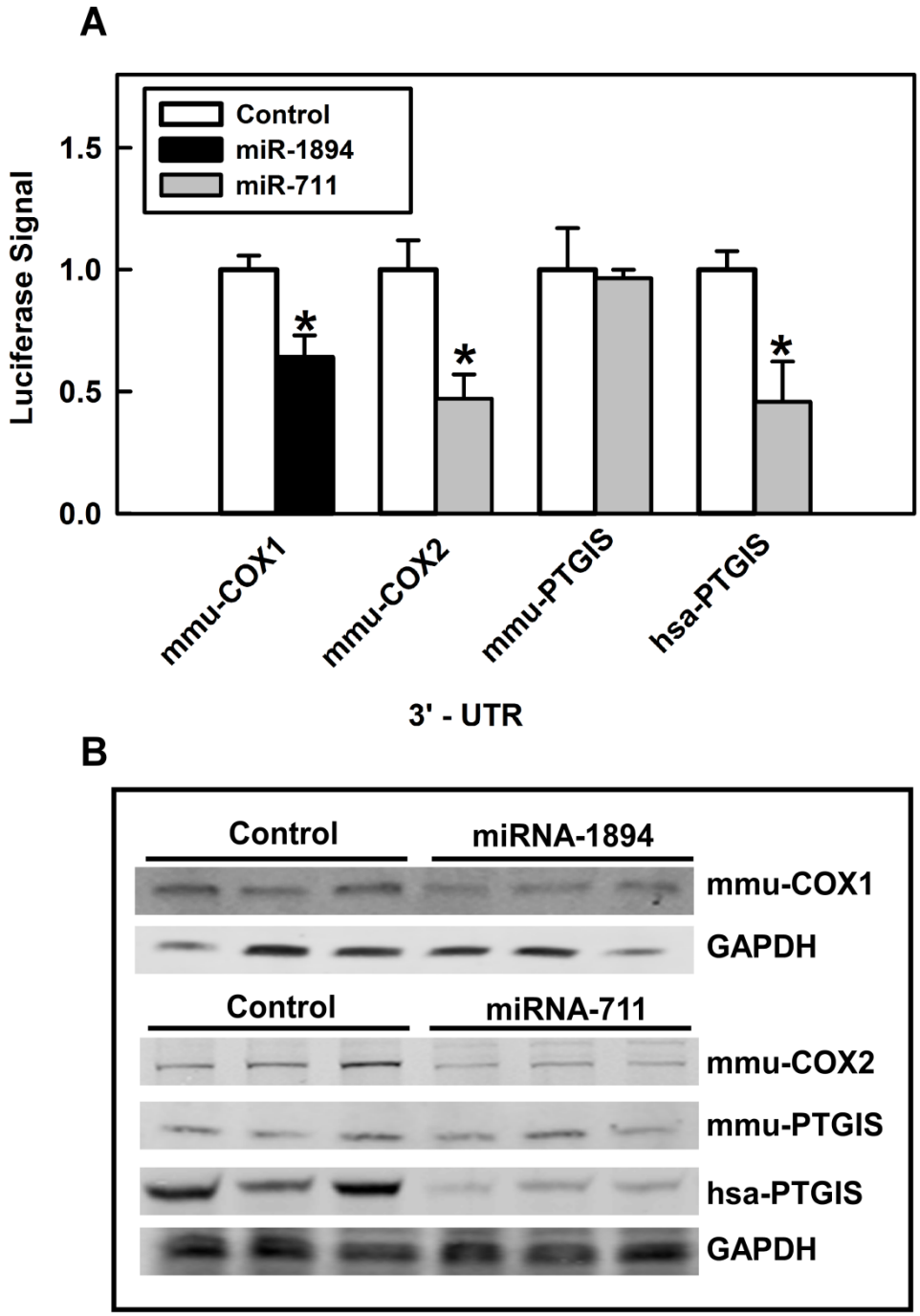

Figure. 30. COX1, COX2, and human PTGIS are direct targets of miRNAs-1894 and -711. (A) Quantification of mouse COX1, COX2, and PTGIS WT vector luciferase reporter activity in control and miRNA-1894 and -711 overexpression cells. The luciferase signal was expressed as fold change as compared to the Firefly luciferase signal in control cells normalized to Renilla luciferase signal. (B) Western blot analysis of COX1, COX2, and PTGIS protein levels in control and miRNA-1894 and -711 overexpression cells. Expression levels were normalized to the housekeeper gene GAPDH and expressed as fold change relative WT controls. Values represent mean ± SEM (n=3-5). (*) indicates $p < 0.05$ as compared to controls.

PTGIS. Therefore, we repeated the luciferase experiments with human hsa-miRNA-711 and human PTGIS 3'-UTR transfected into HepG2 cells. Under similar conditions, we found decreased luciferase activities when hsa-miRNA-711 was overexpressed (Fig. 30A). Taken together, these results indicate that COX1, COX2, and human PTGIS mRNA are post-transcriptionally controlled by miRNAs -1894 and -711, respectively. To verify these results, we examined levels of COX1, COX2, and PTGIS in cells overexpressing their respective miRNAs. In miRNA-1894 overexpression cells, levels of COX1 were significantly decreased 1.5-fold when compared to control cells, indicating miRNA-1894 suppression of COX1 (Fig 30B). Similarly, levels of COX2 were significantly decreased 3.3-fold in miRNA-711 overexpression cells (Fig. 30B). No significant difference was observed with mouse PTGIS levels in mmu-miRNA-711 overexpression cells but a 3.3-fold decrease in human PTGIS levels was observed when hsa-miRNA-711 was overexpressed (Fig. 30B). These results demonstrate that mmu-miRNAs-1894 and -711 directly target and inhibit expression of target mouse genes COX1 and COX2, but not PTGIS. However, human PTGIS is targeted by hsa-miRNA-711, leading to significant decreases in expression when hsa-miRNA-711 is overexpressed. Given the function of the target genes (eicosanoid biosynthesis), these results suggest that miRNAs-1894 and -711 that are up-regulated when Plin2 is ablated may play a key role in regulating the inflammation response.

MIRNA -1894 AND-711 CORRELATE INVERSELY WITH COX1 AND COX2 UNDER CONDITIONS OF LPS-INDUCED INFLAMMATION

To determine the effect of Plin2 and inflammation on levels of miRNAs-1894 and -711 and their gene targets COX1 and COX2, we next examined levels of miRNAs-1894

and -711, COX1 and COX2, along with other inflammation markers (TNF-α, IL-6, and Il-1β) in Plin2 overexpression cells treated with LPS. As expected, increased expression of Plin2 led to decreased levels of miRNAs-1894 and -711 2.5- and 3.3-fold, respectively (Fig. 31A) while levels of COX2, TNF-α, IL-6, and Il-1β increased a respective 1.9-, 2-, 1.8-, and 1.9-fold (Figs. 31B, C). COX1 levels however, remained unchanged (Fig. 31B). These results suggest that Plin2 may mediate the inflammation response by regulating levels of miRNA-711 and its gene target COX2, an enzyme involved in eicosanoid biosynthesis. The fact that COX1 remained unchanged when miRNA-1894 was decreased was unanticipated; however COX1 regulation is complex and may involve other factors (21). When control cells were treated with LPS, levels of miRNA-711 decreased 3.3-fold, concomitant with a 2.9-fold increase in COX2 levels (Fig. 31A, B). Conversely, levels of miRNA-1894 increased 2-fold, producing a 2.5-fold decrease in COX1 expression. In addition, expression of TNF-α, IL-6, and IL-1β increased 2.8-, 2.6-, and 2.4-fold, respectively when inflammation was induced. Upon treatment of Plin2 overexpression cells with LPS, COX2 levels increased 1.9-fold (Fig. 31B). In contrast, levels of miRNA-1894 were increased 1.6-fold, while levels of COX1 decreased 2.4-fold, suggesting that miRNA-1894 and its gene target COX1 are regulated independently of Plin2 under LPS stimulated conditions. With miRNA-711, no further reduction in levels was observed when compared to untreated Plin2

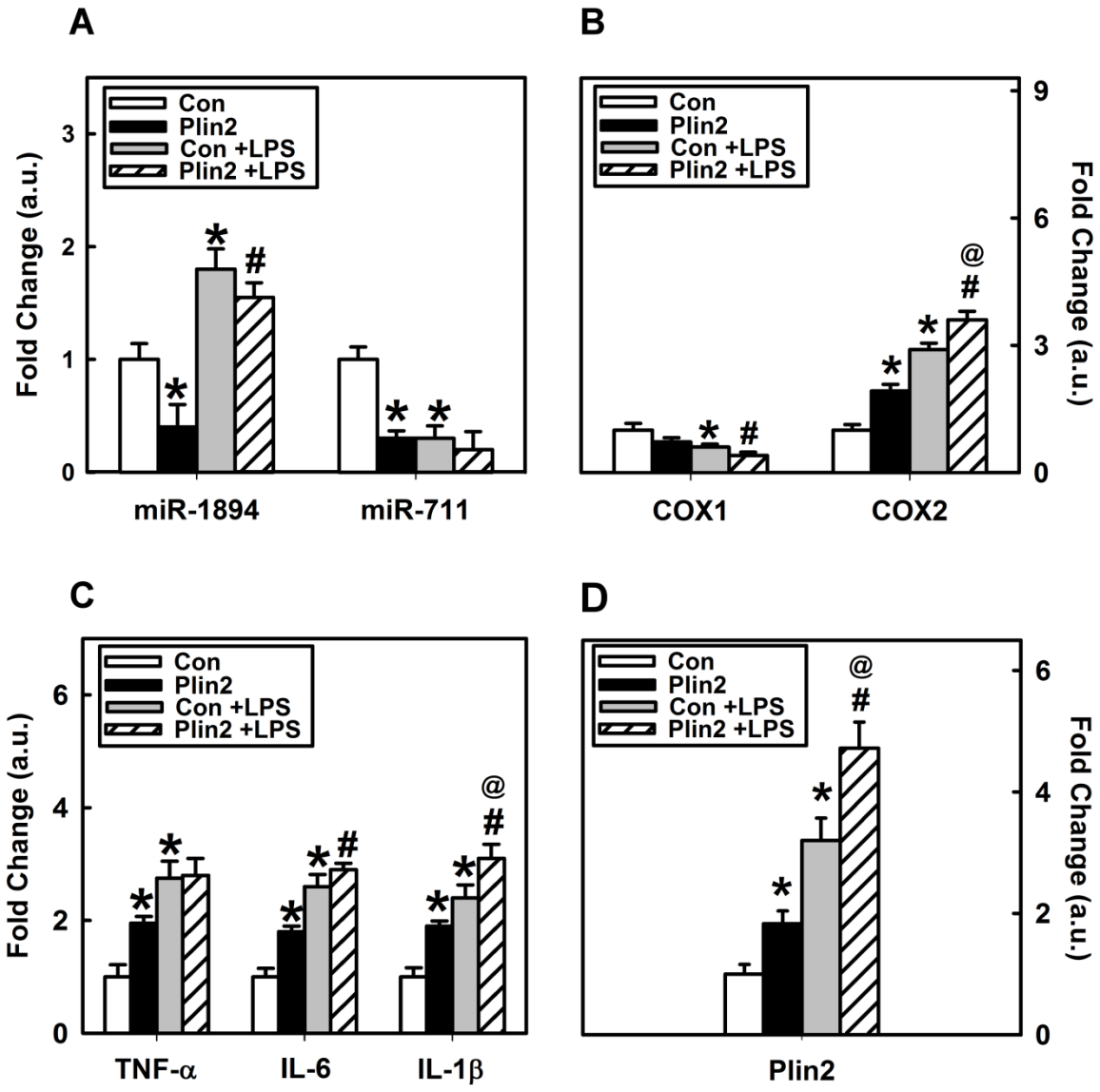

Figure. 31. Effect of LPS-induced inflammation on miRNA and protein expression. (A) Expression levels of miRNAs-1894 and -711 were determined in control and Plin2 overexpression cells in the absence and presence of LPS as described in the Methods section. (B) Western blot analysis of COX1 and COX2 in control and Plin2 overexpression cells in the absence and presence of LPS. (C) Expression levels of pro-inflammatory genes TNF-α, IL-6 and IL-1β were determined by qPCR. (D) Western blot analysis of Plin2 in control and Plin2 overexpressing cells with and without LPS treatment. Expression levels were normalized to the housekeeper gene GAPDH and expressed as fold change relative WT controls. Values represent mean ± SEM (n=3-5). (*) indicates $p < 0.05$. (#) indicates $p < 0.05$ as compared to Plin2 overexpressing cells. (@) indicates $p < 0.05$ as compared to cells treated with LPS.

overexpression cells or LPS-treated control cells, possibly because levels were already substantially reduced (Fig. 31D). We also assessed levels of Plin2 under these conditions and found that LPS treatment in control and Plin2 overexpression cells increased Plin2 levels 3.2- and 2.4-fold, respectively (Fig. 31D). The above effects were reversed in Plin2 knockdown RAW macrophages treated with LPS. Silencing of Plin2 by siRNA knocked down Plin2 by 69% and decreased COX2 levels 2-fold (Fig. 32). LPS treatment increased Plin2, COX2, TNF-α, and IL-1β 1.7-, 1.5, 1.5-, and 1.6-fold in control cells, however in Plin2 knockdown cells, these effects were completely blunted (Fig. 32). A morphological examination of these cells revealed overexpression of Plin2 increased the size and number of lipid droplets (Fig. 33B), as shown in other studies where eicosanoid and prostaglandin synthesis increased at the lipid droplet surface (2, 5, 10). It should be noted that LPS-induced inflammation also increased Plin2 expression (Fig. 31D) and lipid droplet size and number in control cells (Fig. 33C). However, when Plin2 was overexpressed in LPS treated cells, larger, more numerous lipid droplets were observed (Fig. 33D), concomitant with a further increase in COX2 expression (Fig. 31B). Since it has been shown that COX2 targets to lipid droplets (17), these results suggest that the changed morphology of lipid droplets may be the result of increased partitioning of COX2 and other eicosanoid producing enzymes to Plin2-coated lipid droplets when inflammation is present.

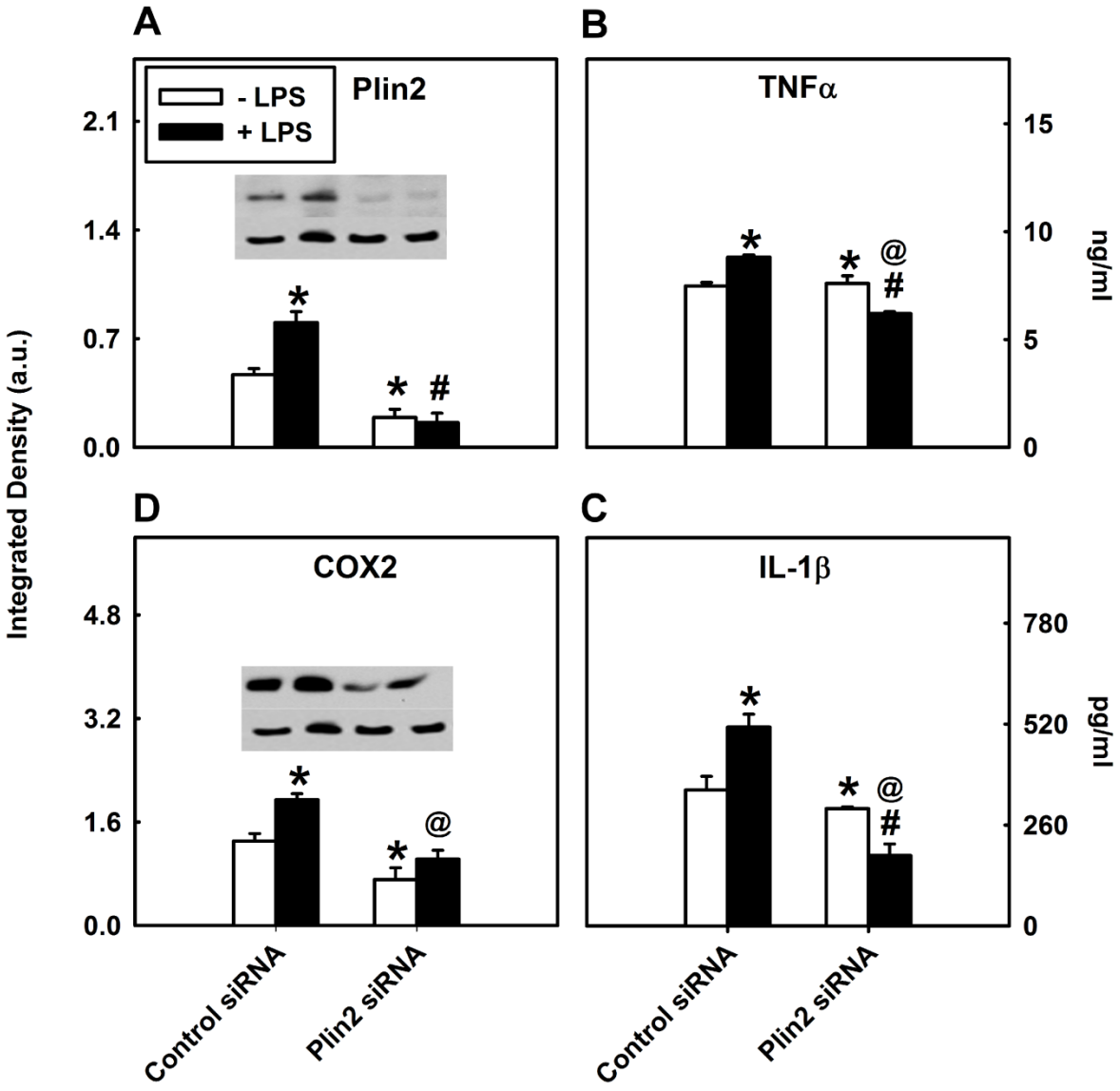

Figure. 32. Knockdown of Plin2 decreases COX2, TNF-α and IL-1β levels under LPS- stimulation. Expression levels of Plin2 (A), TNFα (B), COX2 (C), and IL-1β (D) were quantified by Western blotting (A and C) and Elisa (B and D) in control and Plin2 knockdown cells treated with LPS as described in the Methods section. Inset, representative Western blots. Values represent mean ± SEM (n=3). (*) indicates $p < 0.05$ compared to untreated cell. (#) indicates $p < 0.05$ compared to Plin2 siRNA knockdown cells. (@) indicates $p<0.05$ compared to LPS treated control cells.

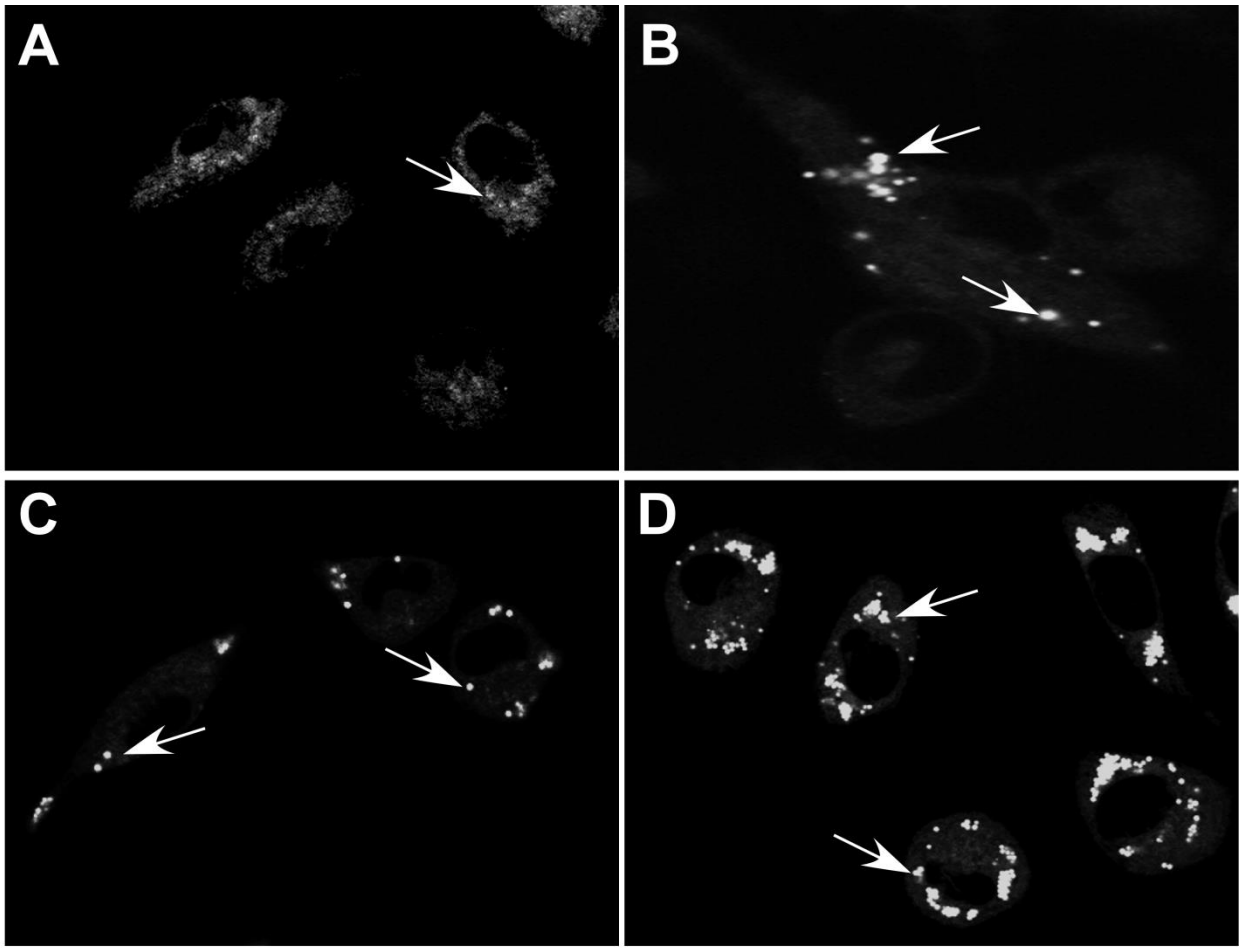

Figure. 33. Plin2 overexpression and LPS treatment induces lipid droplet formation. Control cells (A), Plin2 overexpressing cells (B), LPS-treated control cells (C), and LPS-treated Plin2 overexpressing cells (D) were treated with Nile red and imaged as described in the Methods section. Arrows indicate representative lipid droplets. Images shown are representative of data from n= 4-5 dishes.

LPS-INDUCED INFLAMMATION ALTERS PLIN2-COX INTERACTIONS IN ISOLATED LIPID DROPLET FRACTIONS

To determine whether inflammation promotes increased partitioning of COX2 to lipid droplets, we isolated lipid droplet fractions from control and Plin2 overexpression cells treated with LPS. Plin2, COX2 and PLA_2 were detected in the lipid droplet fractions as expected (Fig. 34A Lane 5). When Plin2 was overexpressed, levels of COX2 were increased 2.5-fold (Fig. 34B). LPS treatment further increased COX2 levels 2- and 1.8-fold, respectively in lipid droplets isolated from control and Plin2 overexpression cells (Fig. 34B). To determine if Plin2 interacts with COX2 (or COX1) in lipid droplets, Co-IP assays were performed (Figs. 34C-F). Lipid droplet fractions were immunoprecipitated with COX1 and COX2 antibodies in control cells (Fig. 34C, lane 2), cells treated with LPS (Fig. 34C; lane 3), and LPS-treated Plin2 overexpression cells (Fig. 34B, lane 4). Samples were immunoblotted with anti-Plin2 to show interactions between Plin2-COX1 and Plin2-COX2. Control cells precipitated with anti-COX1 and anti-COX2 pulled down Plin2 indicating that Plin2-COX1 and Plin2-COX2 complexes formed in lipid droplet fractions. In cells treated with LPS, interactions between Plin2 and COX1 decreased by 2.4-fold (Fig. 34D). Conversely, interactions between Plin2 and COX2 increased 2.8-fold. Plin2 overexpression attenuated this effect, increasing Plin2-COX2 complexation an additional 1.7-fold (Fig. 34D). Lipid droplet fractions were also immunoblotted with the COX2 antibody to show that levels of COX2 immunoprecipitated in the assay were similar (Fig. 34C). Plin2 was next immunoprecipitated from control cells (Fig. 34E, lane 2), cells treated with LPS (Fig. 34E; lane 3), and LPS-treated Plin2 overexpression cells (Fig. 34E, lane 4). LPS-treated control cells precipitated with Plin2 showed a 1.9-fold

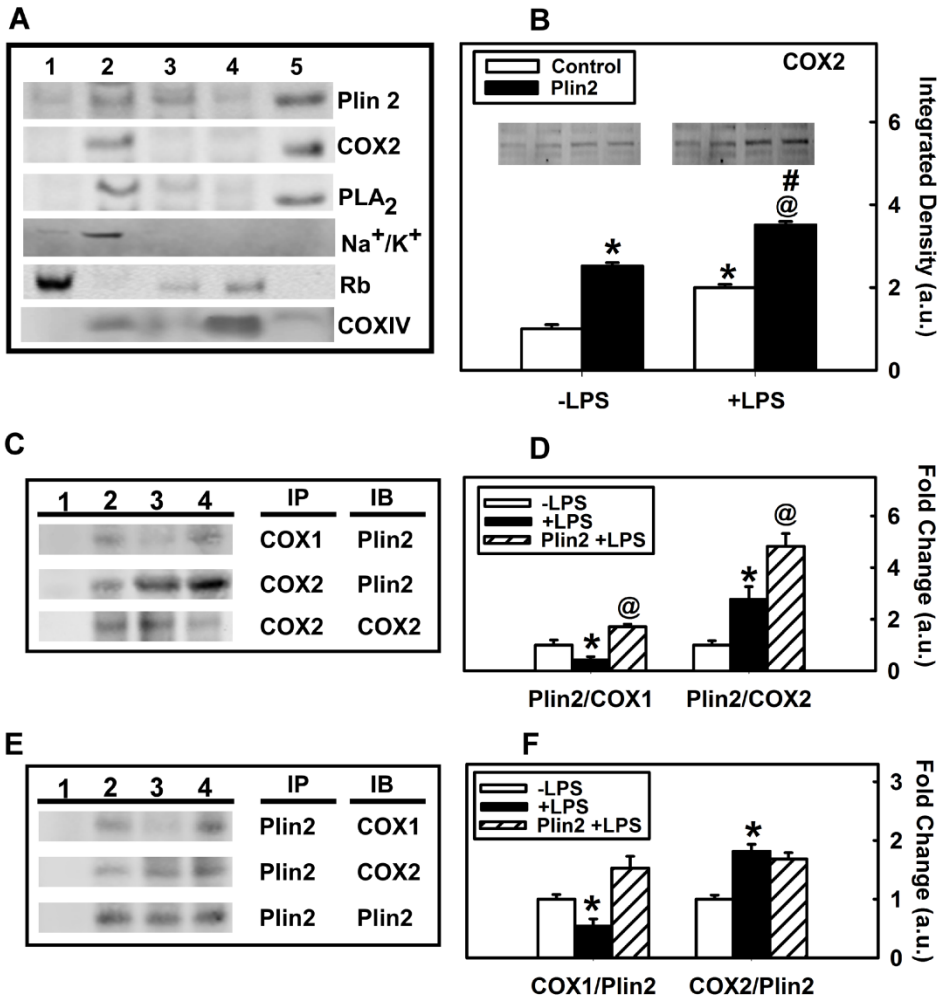

Figure. 34. LPS-induced inflammation increases COX2 partitioning to lipid droplets. (A) Representative Western blots of cellular fractions isolated from control and Plin2 overexpressing cells: lane 1, nucleus; lane 2, plasma membrane; lane 3, cytosol; lane 4, mitochondria; and lane 5, lipid droplets. Blots were probed with antibodies against Plin2, COX2, PLA2, Na+/K+, Rb, and COXIV to verify the purity of the cellular fractions. (B) Relative enrichment of COX2 in lipid droplets isolated from control and Plin2 overexpression cells, with and without LPS treatment was determined by Western blot analysis. (C) Co-immunoprecipitation of COX1 and COX2 in lipid droplet fractions. Levels of Plin2 in the immunoprecipitate from lipid droplets isolated from control cells (lane 2), control cells treated with LPS (lane 3), and Plin2 overexpressing cells treated with LPS (lane 4) were analyzed by immunoblotting with anti-Plin2. Equal immunoprecipitation of COX2 was verified by immunoblotting with anti-COX2 (blot 3) to normalize COX2 levels within samples. (D) The ratios of Plin2 to COX1 and Plin2 to COX2 were calculated from the integrated density values from the Western blots. (E) Reverse immunoprecipitation experiments were also performed. Plin2 was immunoprecipitated with anti-Plin2 and levels of COX1 and COX2 in the immunoprecipitate were analyzed by immunoblotting with anti-COX1 or anti-COX2, respectively. Equal immunoprecipitation of Plin2 was verified by immunoblotting with anti-Plin2 (blot 3) to normalize Plin2 levels within samples. (F) The ratios of COX1 and COX2 to Plin2 were calculated from the integrated density values from the Western blots. Immunoprecipitate obtained using secondary IgG antibodies (lane 1) were used as negative controls for each set. Values represent mean ± SEM (n=3-5). (*) indicates $p < 0.05$ as compared to control. (@) indicates $p < 0.05$ as compared to control cells treated with LPS.

decrease in Plin2-COX1 interactions (Fig. 34F). Plin2 precipitation in LPS-treated control cells resulted in a 1.8-fold increase in Plin2-COX2 interactions (Fig. 34F). However, Plin2-COX2 interactions were not further increased by Plin2 overexpression in LPS treated cells as they were in the COX2 precipitated samples (Fig. 34F). Taken together, these results demonstrated that COX2-Plin2 interactions were enhanced under LPS-induced inflammation conditions but COX1-Plin2 interactions were decreased. To confirm Plin2-COX2 interactions, FRET imaging was performed with Plin2 and COX2 using acceptor photobleaching as described in our previous work [27, 28]. Since FRET allows estimation of intermolecular distances between molecules to within 10-100 Å, this method allowed detection of direct Plin2-COX2 interactions at the molecular level. The mean distance *R* observed between Plin2 and COX2 was calculated as 65$\pm$1 Å (Table 5), indicating close proximity. To visualize where in the cell FRET occurred, co-localization (Fig. 35A) and FRET efficiency (*E*) images (Fig. 35B) were generated. *E* was scaled to visualize regions of lower (black to blue) and higher (green to yellow) FRET. With Cy3- COX2/Cy5-Plin2 labeled cells, areas of high intensity identified by morphology as lipid droplets showed *E* in the range of 45-60% (blue to cyan on the FRET inset color scale), values consistent with efficient overlap of electronic states and direct interaction of Plin2 with COX2 on lipid droplets. Overall, we demonstrate that Plin2 sequesters COX2 to the lipid droplet surface, an effect that is attenuated when inflammation is present. In support of these findings, co-localization experiments in the EicosaCell assay showed entrapped PGE_2 at the surface of Plin2-coated lipid droplets (Fig. 35C) under LPS stimulation. Using a novel anti-PGE_2 antibody (Fig. 35C) we demonstrate a significant amount of PGE_2 covalently cross-links

Table 5. FRET efficiency *E* and distance *R* between Cy3-COX2 and Cy5- Plin2.

FRET PAIR	*E (%)*	*R* (Å)
Plin2-COX2	20 ± 2.1	65 ± 1.4
Plin2-COX1	21 ± 2.5	65 ± 1.8

Interaction between Plin2 and COX1 or COX2 was analyzed by acceptor photobleaching FRET. FRET experiment was performed by measuring the fluorescence emission of the Cy3 donor (COX1 or COX2) through the 575/50 nm filter upon excitation at 559nm before and after photobleaching of the Cy5-acceptor (Plin2) at 633nm. One or two cells in the field of 3-6 cells selected for photobleaching were left unbleached to serve as a negative bleaching control. Values represent the mean ± SE, from n = 20-40 lipid droplets in 20-30 cells.

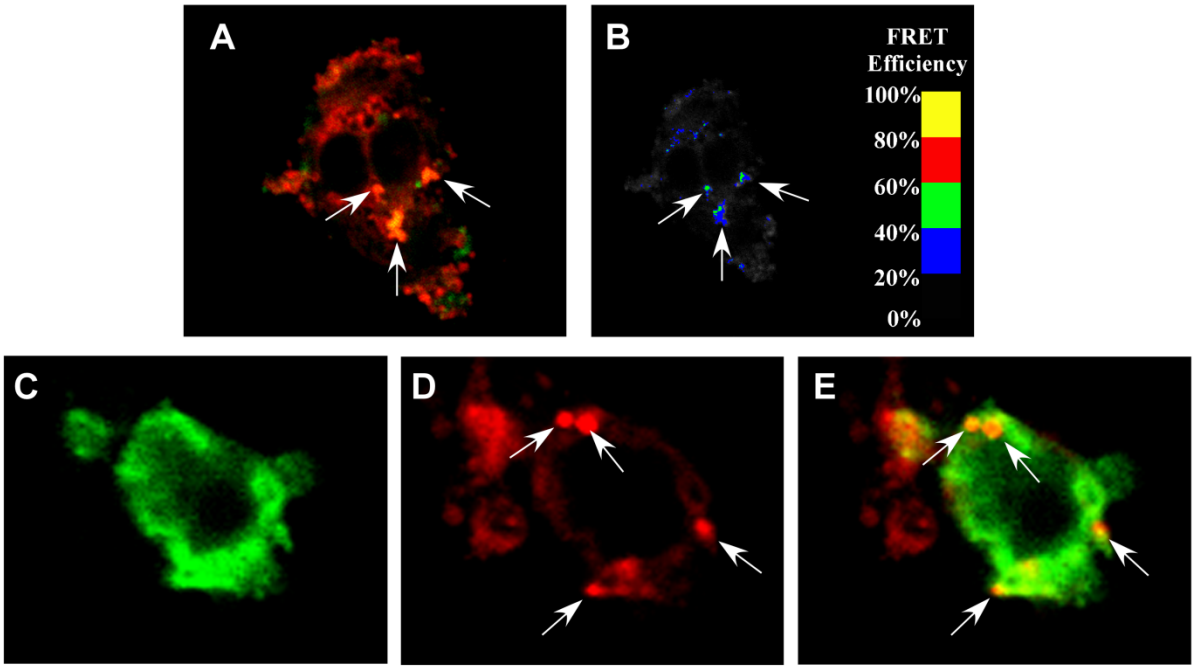

Figure. 35. FRET and EicosaCell assays demonstrate Plin2 directly interacts with COX2 at the lipid droplet surface where PGE2 synthesis occurs. (A) Co-localization of Cy3-labeled COX2 with Cy5-labeled Plin2 in primary mouse hepatocytes revealed yellow-to-orange areas where both probes overlapped. (B) FRET imaging was performed as described in the Methods section. The FRET overlay was pseudo-colored to visualize regions of higher and lower FRET as shown by the inset color scale. Arrows indicate areas of highest FRET efficiencies in lipid droplets. (C) Primary mouse hepatocytes were crosslinked with EDAC to trap PGE2 during synthesis as described in the Methods section. Confocal imaging of Cy3-labeled PGE2 revealed sites of synthesis in the cell. (D) Confocal image of Cy5-Plin2 labeled cells showed lipid droplets. (E) Co-localization of Cy3-PGE2 (green) with Cy5-Plin2 (red) showed yellow-to-orange areas where synthesis of PGE2 occurs on lipid droplets. Arrows indicate Plin2-coated lipid droplets where co-localization is the greatest.

to Plin2 coated lipid droplets (Fig. 35D; arrows). The overlay indicated the greatest amount of co-localization occurred at the lipid droplet surface, providing support that lipid droplets not only contain eicosanoid producing enzymes, but that they are active sites of eicosanoid synthesis. Taken together, these results indicate that lipid droplets compartmentalize the enzymatic machinery necessary for eicosanoid synthesis under inflammatory conditions and that Plin2 plays an active role in the recruitment of COX1 and COX2 to the lipid droplet surface.

DISCUSSION

The current study resolves a previously unknown role of Plin2 in hepatic miRNA regulation. Using a combination of Plin2 global knockout and overexpression models we demonstrate for the first time the effects of hepatic Plin2 ablation on the miRNA-biome and provide compelling evidence that Plin2 and two miRNAs, -1894 and -711, play key roles in regulating the inflammation response.

Perturbations in lipid droplet function have been implicated in promoting several diseases including type 2 diabetes, atherosclerosis, and cardiovascular disease (26), yet few studies have focused on the role of lipid droplets and associated proteins in the regulation of inflammation. Lipid droplet protein Plin2 has been shown to promote lipid accumulation (24, 37, 47), to augment inflammation in macrophages (15), and was observed in ballooned hepatocytes from livers of NASH patients (22). Plin2 was also significantly upregulated in both monocytes and macrophages after exposure to oxLDL (40, 57, 70), suggesting that Plin2 may play a key role in the formation of foam cells and initiation of atherosclerosis. Global ablation of Plin2 protected against diet-induced obesity, adipose inflammation, and liver steatosis, but effects on hepatic inflammation

were not determined (11-13, 29, 49, 57). This was addressed in recent work where liver-specific ablation of Plin2 alleviated diet-induced hepatic steatosis, inflammation, and fibrosis (52). Notably, pro-inflammatory markers COX2, TNF-□, IL-6, and IL-1□ were significantly decreased in these mice when inflammation was induced by a methionine and choline deficient diet. Consistent with these findings, studies with Plin2-GNMT double KO mice showed that the hepatic steatosis and inflammation that occurred in the single GNMT KO mouse model were relieved when both Plin2 and GNMT were ablated (44, 45). In other work, Plin2 knockdown in THP1 macrophages resulted in decreased expression of several pro-inflammatory markers including TNF-□, IL-6, and MCP-1 (15). Conversely, Plin2 overexpression in LPS-treated cells led to increased levels of IL-1β and caspase-1 in a mechanism proposed to include NLRP3 and Plin2 (16). Taken together, these studies based on mice and cell models of altered Plin2 expression indicate a key role for Plin2 in regulating the inflammation response.

Other studies have identified miRNA-mediated mechanisms involving lipid droplets, and in one case Plin2 in the onset of inflammation. For example, inhibition of PPARδ by miRNA-9 in monocytes led to upregulation of Plin2, STAT1, and TNF-α when cells were treated with LPS to induce inflammation (67). In other work, miRNA-155 was shown to modify the inflammatory capacity of macrophages by increasing lipid loading and promoting the formation of lipid droplet derived foam cells, the hallmark of atherosclerosis (53). THP-1 macrophages stimulated with oxLDL showed increased expression of miRNA-150, along with increased lipid loading and atherosclerosis (36). This work was followed by challenging miRNA-150 knockout mice with a high fat diet. The mice exhibited increased fat accumulation and decreased glucose tolerance and

insulin sensitivity, along with increased expression of pro-inflammatory cytokines in adipose tissue (76). Studies with miRNA-21 showed increased expression when macrophages were treated with LPS to induce inflammation (20). When miRNA-21 was overexpressed by transfection increased lipid accumulation and formation of lipid-laden foam cells was observed which was reversed when expression of miRNA-21 was silenced (20). Plin2 was not measured in these studies, however the close association of Plin2 with foam cell formation has been extensively reported (40, 57, 66, 70) and was likely part of the process. In the present work we found that Plin2 ablation led to up-regulation of several miRNAs. Notably, two of the highest expressing miRNAs, miRNAs-1894 and -711, were predicted to target eicosanoid-producing gene products COX1, COX2, and human PTGIS and were selected for further study. We demonstrate herein that miRNA-1894 directly targets COX1 while miRNA-711 directly targets COX2 and human PTGIS. In keeping with this, levels of the target gene products COX1, COX2 and human PTGIS are decreased in miRNA-1894 and -711 overexpression cells. Given the function of the target genes (eicosanoid biosynthesis), these results suggest that miRNAs-1894 and -711 likely play a role in regulating COX-mediated inflammation. Consistent with this, cells overexpressing a hybrid COX1-PTGIS enzyme exhibited increased miRNA-711 levels which was proposed to play a negative feedback role in PGI_2 production (51). We found that cells treated with LPS to induce inflammation had decreased expression of miRNA-711 and a concomitant increase in COX2 levels. Conversely, levels of miRNA-1894 were increased, negatively affecting the expression of COX1. These results are not surprising since COX2 is activated by inflammation and synthesizes prostaglandins to activate the inflammatory process (21) whereas COX1

responds to mostly physiological stimuli and releases prostaglandins under basal conditions (21, 38). Intriguingly, a morphological examination of LPS-treated cells revealed that lipid droplet size and number were increased upon LPS treatment, an effect exacerbated by Plin2 overexpression. These results were consistent with studies with microglia where LPS treatment resulted in accumulation of lipid droplets, up-regulation of Plin2, and recruitment of PGES and phospholipase A_2 to lipid droplets in a JNK/MAPK-dependent manner (19, 32). In the current work, we show that Plin2 co-localizes with PGE_2 on lipid droplets. Results from our co-IP experiments and FRET imaging show that Plin2 directly interacts and sequesters COX2 to the lipid droplet surface, an effect that is increased when inflammation is present. These results suggest that Plin2 actively recruits COX2, promoting lipid droplet involvement in inflammation progression.

Several lines of evidence suggest that transcription factors such as PPARs and p65, a subunit of transcription factor NFκB, are involved in the onset of inflammation inflammation (1, 14, 28). To determine the relationship between these transcription factors that are known to regulate lipid droplet proteins and COX-mediated inflammation, we turned to ChIP-Seq studies that mapped response elements across the genome (Fig. 29). After screening the available data, we identified putative response elements for PPARα, PPARγ, RXR, and p65 in the promoter regions of Plin2, COX1, COX2, miRNA-1894, and miRNA-711. These findings were significant because overlap of PPAR-RXR heterodimers with p65 in the promoter region has been shown to foster cross talk between the transcription factors (1, 28). For example, direct interactions of PPARγ with the p65 RelA region caused p65 to undergo ubiquitination and degradation,

resulting in termination of NFκB signaling (1, 14, 28). In addition, displacement of PPARγ by p65 promoted increased expression of Plin2 (19, 32, 56), COX2 (21), and TNFα (31, 59) under inflammation conditions. Consistent with this, mice injected with LPS exhibited increased hepatic lipid accumulation and expression of Plin2 while expression of PPARα, RXR, and PPARγ were decreased (56). Moreover, enzymes involved in fatty acid synthesis and oxidation including fatty acid synthase, enoyl-CoA hydratase, stearoylCoA desaturase, acyl-CoA dehydrogenase, acetyl-CoA carboxylase, and carnitine palmitoyl-transferase 1 that are direct targets of PPARα, RXR, and PPARγ were also decreased following LPS-induced inflammation (56). In other work, activation of p65 and AP-1 in macrophages led to increased expression of Plin2 whereas inhibition of p65 or AP-1 blunted development of hepatic steatosis (32, 56). A closer examination of the cross talk between PPARs and p65 in keratinocytes demonstrated *in vivo* that p65/RelA repression of PPARδ in TNF-α stimulated cells increased lipid accumulation, Plin2, and cytokine expression through a mechanism involving histone deacetylases (1). A schematic overview detailing the roles of Plin2, miRNAs-1894 and -711, along with PPARs and p65 is presented in Figure 36 to illustrate the overall mechanisms involved.

In summary, we investigated the effect of Plin2 ablation on the microRNA-microbiome. In Plin2 null livers, 6 miRNAs were significantly increased 3-fold or more. Two miRNAs (-1894 and -711) were predicted to target genes associated with eicosanoid biosynthesis and inflammation. Luciferase reporter assays and Western blotting demonstrated that miRNAs-1894 and -711 directly target the 3'-UTR sites of COX1, COX2, and human PTGIS and inhibit protein expression of the target genes. In

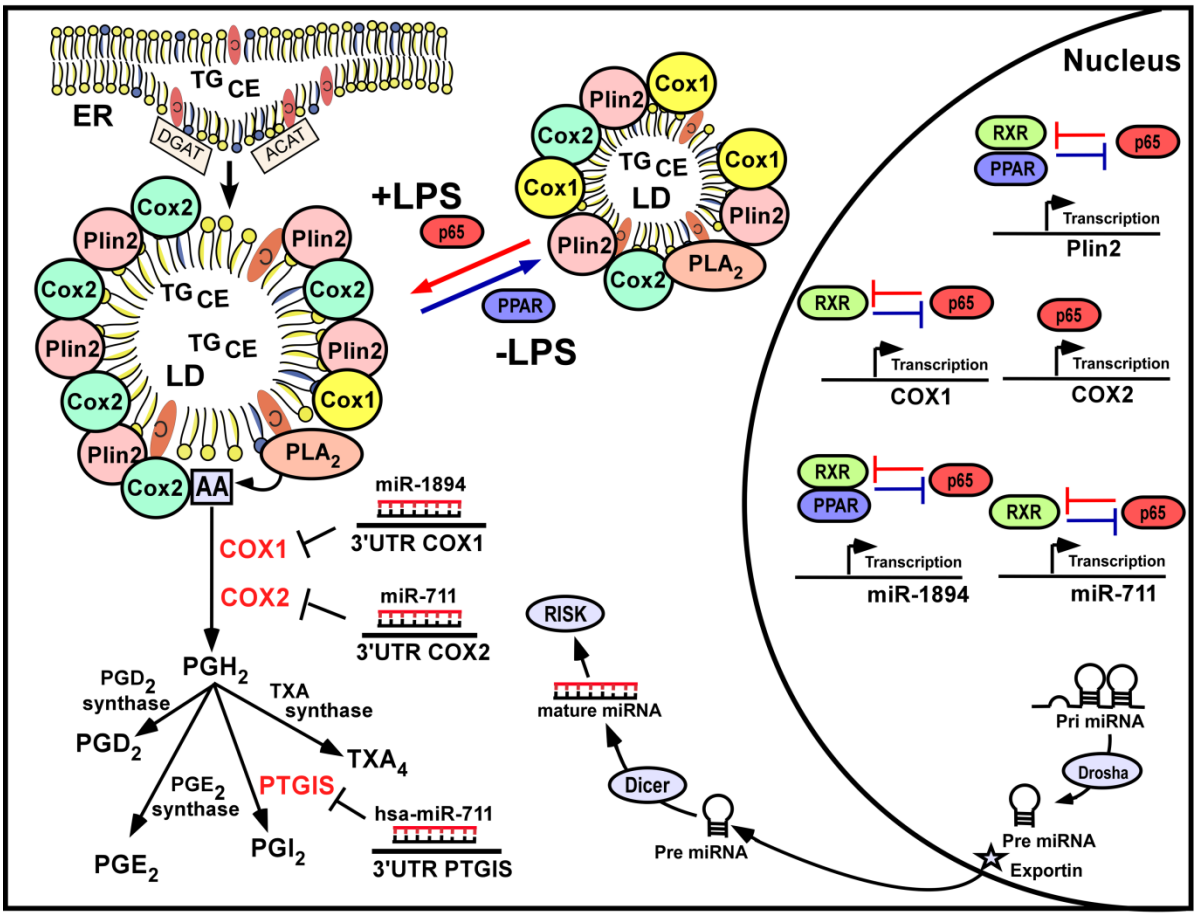

Figure. 36. Schematic diagram illustrating roles of Plin2 and miRNAs-1894 and -711 in COX-mediated inflammation. Phospholipids and triglycerides synthesized at the ER are deposited between the bilayer leaflets to form naïve lipid droplets. Increased expression of Plin2 leads to increased lipid droplet size and number, while decreased Plin2 leads to smaller, less numerous lipid droplets. LPS treatment in control cells increases activation of p65 (red arrow), leading to elevated expression of Plin2 and COX2, concomitant with decreased levels of miRNA-711. Under similar conditions, levels of miRNA-1894 are increased, resulting in decreased COX1. In Plin2 overexpression cells treated with LPS, levels of COX2 are further increased. Without LPS treatment (blue arrow), displacement of p65 by PPAR promotes increased fatty acid oxidation and altered expression of COX1, COX2, Plin2, and miRNAs-1894 and -711, resulting in smaller lipid droplets.

response to LPS-induced inflammation, levels of miRNA-711 decreased and COX2 significantly increased, an effect exacerbated when Plin2 was overexpressed. Conversely, levels of miRNA-1894 increased, negatively affecting the expression of COX1. Co-IP assays and FRET imaging showed that Plin2 sequestered COX2 to the lipid droplet surface, an effect that was increased when inflammation was present. Meta-analysis of ChIP-seq data revealed PPAR, RXR, and p65 response elements within promoter regions of Plin2, COX1, COX2, and miRNAs-1894 and -711, suggesting possible regulation of the target genes. Collectively, we demonstrate lipid droplets are the site of eicosanoid production and propagate the inflammation response. Plin2 impacts this process by actively recruiting COX enzymes to the lipid droplet surface altering their expression post-transcriptionally via miRNAs-1894 and -711.

REFERENCES

REFERENCES

1. Aarenstrup L, Noerregaard Flindt E, Otkjaer K, Kirkegaard M, Skorstensgaard Andersen J, and Kristiansen K. HDAC activity is required for p65/RelA-dependent repression of PPARg-mediated transactivation in human keratinocytes. *J Invest Dermatology* 128: 2008.

2. Accioly MT, Pacheco P, Maya-Monterio CM, Carrossini N, Robbs BK, Oliveira SS, Kaufmann C, Morgado-Diaz JA, Bozza PT, and Viola JP. Lipid bodies are reservoirs of cyclooxygenase-2 and sites of prostaglandin-E2 synthesis in colon cancer cells. *Cancer Res* 68: 1732-1740, 2008.

3. Aldridge GM, Podrebarac DM, Greenough WT, and Weiler IJ. The use of total protein stains as loading controls: An alternative to high-abundance single-protein controls in semi-quantitative immunoblotting. *J Neuroscience Methods* 172: 250-254, 2008.

4. Atshaves BP, Petrescu AD, Starodub O, Roths JB, Kier AB, and Schroeder F. Expression and intracellular processing of the 58 KDa SCP-x/3-oxoacyl-CoA thiolase in transfected mouse L cells. *J Lipid Res* 40: 610-622, 1999.

5. Bandeira-Melo C, Weller PF, and Bozza PT. Identifying intracellular sites of eicosanoid lipid mediator synthesis with EicosaCell assays. *Methods Mol Biol* 717: 277-289, 2011.

6. Barish GD, Yu R, Karunasiri M, Ocampo CB, Dixon J, Benner C, Dent AL, Tangirala RK, and Evans RM. Bcl-6 and NFkB cistromes mediate opposing regulation of the innate immune response. *Genes and Development* 24: 2760-2765, 2010.

7. Bartel D. MicroRNAs:genomics, biogenesis, mechanism, and function. *Cell* 116: 281-297, 2004.

8. Benz F, Roy S, Trautwein C, Roderburg C, and Luedde T. Circulation microRNAs as biomarkers for Sepsis. *In J Mol Sci* 9: E78, 2016.

9. Boergesen M, Pedersen TA, Gross B, van Heeringen SJ, Hagenbeek D, Bindesboll C, Caron S, Lalloyer F, Steffensen KR, Nebb HL, Gustafsson JA, Stunnenberg HG, Staels B, and Mandrup S. Genome-wide profiling of Liver X Receptor, Retinoid X Receptor, and Persoxisome Proliferator-Activated Receptor a in mouse liver reveals extensive sharing of binding sites. *Mol Cell Biol* 32: 852-867, 2011.

10. Bozza PT, Baker-Abreu I, Navarro-Xavier RA, and Bandeira-Melo C. Lipid body function in eicosanoid synthesis: an update. *Prostaglandins Leukot Essent Fatty Acids* 85: 205-213, 2011.

11. Carr RM, Peralta G, Yin X, and Ahima RS. Absence of perilipin 2 prevents hepatic steatosis, glucose intolerance and ceramide accumulation in alcohol-fed mice. *PLoS ONE* 9: e97118, 2014.

12. Chang BH, Li L, Paul A, Taniguchi S, Nannegari V, Heird WC, and Chan L. Protection against fatty liver but normal adipogenesis in mice lacking adipose differentiation-related protein. *Mol Cell Biol* 26: 1063-1076, 2006.

13. Chang BH, Li L, Saha P, and Chan L. Absence of adipose differentiation related protein upregulates hepatic VLDL secretion, relieves hepatosteatosis, and improves whole body insulin resistance in leptin-deficient mice. *J Lipid Res* 51: 2132-2142, 2010.

14. Chen F, Wang M, O'Connor JP, He M, Tripathi T, and Harrison LE. Phosphorylation of PPARg via active ERK1/2 leads to its physical association with p65 and inhibition of NFkB. *J Cell Biochem* 90: 732-744, 2003.

15. Chen FL, Yang ZH, Wang XC, Liu Y, Yang YH, Li LX, Liang WC, Zhou WB, and Hu RM. Adipophilin affects the expression of TNFa, MCP-1, and IL-6 in THP-1 macrophages. *Mol Cell Biochem* 337: 193-199, 2010.

16. Cho K, and Kang PB. Plin2 inhibits insulin-induced glucose uptake in myoblasts through the activation of the NLRP3 inflammasome. *Intern J Mol Med* 36: 839-844, 2015.

17. D'Avila H, Freire-de-Lima CG, Roque NR, Teixeira L, Barj-Fidalgo C, Silva AR, Melo RCN, DosReis GA, Casto-Faria-Neto HC, and Bozza PT. Host cell lipid bodies triggered by Trypanosoma cruzi infection and enhanced by the uptake of apoptotic cells are associated with prostaglandin E_2 generation and increased parasitic growth. *J Infectious Diseases* 204: 951-961, 2011.

18. Dvorak AM, Dvorak HF, Peters SP, Shulman ES, MacGlashan DW, Pyne K, Harvey SV, Galli S, and Lichtenstein LM. Lipid Bodies: cytoplasmic organelles important to arachidonate metabolism in macrophages and mast cells. *J of Immunol* 131: 2965-2976, 1983.

19. Fan B, Ikuyama S, Gu JQ, Oyama J, Wei P, Inoguchi T, and Nishimura J. Oleic acid-induced ADRP expression requires both AP-1 and PPAR response elements, and is reduced by psycnogenol through mRNA degradation in NMuLi liver cells. *Am J Physiol Endocrinol Metab* 297: E112-E123, 2009.

20. Feng J, Li A, Deng J, Yang Y, Dang L, Ye Y, Li Y, and Zhang W. miR-21 attenuates lipopolysaccharide-induced lipid accumulation and inflammatory response: potential role in cerebrovascular disease. *Lipids Health Dis* 13: 27, 2014.

21. Font-Nieves M, Sans-Fons MG, Gorina R, Bonfill-Teixidor E, Salas-Perdomao A, Marquez-Kisinousky L, Santalucia T, and Planas AM. Induction of COX-2 enzyme and down-regulation of COX-1 expression by lipopolysaccharide (LPS) controls prostaglandin E_2 production in astrocytes. *J Biol Chem* 287: 6454-6468, 2012.

22. Fujii H, Ikura Y, Arimoto J, Sugioka K, Lezzoni JC, Park SH, Naruko T, Itabe H, Kawada N, Caldwell SH, and Ueda M. Expression of Perilipin and Adipohilin in Nonalcoholic Fatty Liver Disease; Relevance to Oxidative Injury and Hepatocyte Ballooning. *J Atheroscler Thromb* 16: 1893-1901, 2009.

23. Fujimoto T, and Parton RG. Not just fat: The structure and function of the lipid droplet. *Cold Spring Harb Perspect Biol* 3: a004838, 2011.

24. Fukushima M, Enjoji M, Kohjima M, Sugimoto R, Ohta S, Kotoh K, Kuniyoshi M, Kobayashi K, Imamura M, Inoguchi T, Nakamuta M, and Nawata H. Adipose differentiation related protein induces lipid accumulation and lipid droplet formation in hepatic stellate cells. *In Vitro Cell Dev Biol Anim* 41: 321-324, 2005.

25. Giannotti KC, Leiguez E, Moreira V, Nascimento N, Lomonte B, Gutierrez JM, De Melo RL, and Teixeira C. A Lys49 phopholipase A2, isolated from Bothrops asper snake venom, induces lipid droplet formation in macrophages which depends on distinct signaling pathways and the C-terminal region. *Biomed Res Int* 2013: 807982, 2013.

26. Greenberg AS, Coleman RA, Kraemer FB, McManaman JL, Obin MS, Puri V, Yan QW, Miyoshi H, and Mashek DG. The role of lipid droplets in metabolic disease in rodents and humans. *J Clin Invest* 121: 2102-2110, 2011.

27. Haakonsson AK, Madsen MS, Nielsen R, Sandelin A, and Mandrup S. Acute genome-wide effects of rosiglitazone on PPARg transcriptional networks in adipocytes. *Mol Endocrinol* 27: 1536-1549, 2013.

28. Hou Y, Moreau F, and Chadee K. PPARg is an E3 ligase that induces the degradation of NFkB/65. *Nat Commun* 3: 1300, 2012.

29. Imai Y, Varela GM, Jackson MB, Graham MJ, Crook RM, and Ahima RS. Reduction of hepatosteatosis and lipid levels by an adipose differentiation-related protein antisense oligonuceotide. *Am J Physiol Gastro Liver Physiol* 295: G621-G628, 2007.

30. Jin DY, Teramoto H, Giam CZ, Chun RF, Gutkind JS, and Jeang KT. A human suppressor of c-Jun N-terminal kinase 1 activation by tumor necrosis factor alpha. *J Biol Chem* 272: 25816-25823, 1997.

31. Kauppinen A, Suuronen T, Ojala J, Kaarniranta K, and Salminen A. Antagonistic crosstalk between NFkB and SIRT1 in the regulation of inflammation and metabolic disorders. *Cell Signal* 25: 1939-1948, 2013.

32. Khatchadourian A, Bourque S, Richard V, Titorenko V, and Maysinger D. Dynamics and regulation of lipid droplet formation in lipopolysaccharide (LPS)-stimulated microglia. *Biochimica et Biophysica Acta* 1821: 607-617, 2012.

33. Larigauderie G, Cuaz-Perolin C, Younes AB, Furman C, Lasselin C, Copin C, Jaye M, Fuchart JC, and Rouis M. Adipophilin increases triglyceride storage in human macrophages by simulation of biosynthesis and inhibition of beta-oxidation. *FEBS J* 273: 3498-3510, 2006.

34. Lee H, Jee Y, Hong K, Hwang GS, and Chun KH. MicroRNA-494, upregulated by tumor necrosis factor-a, desensitizes insulin effect in C2C12 muscle cells. *PLoS ONE* 11: e83471, 2013.

35. Li F, Wei G, Bai Y, Li Y, Huang F, Lin J, Hou Q, Deng R, Zhou JH, Zhang SX, and Chen DF. MicroRNA-574 is involved in cognitive impairment in 5-month-old AAP/PS1 mice through regulation of neuritin. *Brain Res* 1627: 177=188, 2015.

36. Li J, and Zhang S. microRNA-150 inhibits the formation of macrophage foam cells through targeting adiponectin receptor 2. *Biochem Biophys Res Comm* In press: 2016.

37. Listenberger LL, Ostermeyer-Fay AG, Goldberg EB, Brown WJ, and Brown DA. Adipocyte differentiation-related protein reduces the lipid droplet association of adipose triglyceride lipase and slows triacyglycerol turnover. *J Lipid Res* 48: 2751-2761, 2007.

38. Liu SF, Newton R, Evans TW, and Barnes PJ. Differential regulation of cyclo-oxygenase-1 and cyclo-oxygenase-2 gene expression by lipopolysaccaride treatment in vivo in the rat. *Clinical Sci* 90: 301-306, 1996.

39. Livak K, and Schmittgen T. Analysis of relative gene expression data using real-time quantitative PCR and the $2^{-\Delta DCT}$ method. *Methods* 25: 402-408, 2001.

40. Llorent-Cortes V, Royo T, Juan-Babot O, and Badimon L. Adipocyte differentiation-related protein is induced by LRP1-mediated aggregated LDL internalization in human vascular smooth muscle cells and macrophages. *J Lipid Res* 48: 2133-2140, 2007.

41. Lopez-Romero P, Gonzalez MA, Callejas S, Dopazo A, and Irizarry RA. Processing of Agilent microRNA array data. *BMC Research Notes* 3: 18, 2010.

42. Luna-Gomes T, Magalhaes KG, Mesquita-Santos FP, Bakker-Abreu I, Samico RF, Molinaro R, Calheiros AS, Diaz BL, Bozza PT, Weller PF, and Bandeira-Melo C. Eosinophils as a novel cell source of prostaglandin D2: Autocrine role in allergic inflammation. *J Immunol* 187: 6518-6526, 2011.

43. Luo H, Wang J, Qiao C, Ma N, Liu D, and Zhang W. Pycnogenol attenuates atherosclerosis by regulating lipid metabolism through the TLR4-NFkB pathway. *Expt & Mol Med* 47: e191 2015.

44. Martinez-Una M, Varela-Rey M, Cano A, Fernandez-Ares L, Beraza N, Aurrekoetxea I, Martinez-Arranz I, Garcia-Rodriguez JL, Buque X, Mestre D, Luka Z, Wagner C, Alonso C, Finnell RH, Lu SC, Martinez-Chantar ML, Aspichueta P, and Mato JM. Excess S-adenosylmethionine reroutes phosphatidylethanolamine towards phosphatidylcholine and triglyceride synthesis. *Hepatology* 58: 1296-1305, 2013.

45. Martinez-Una M, Varela-Rey M, Mestre D, Fernandez-Ares L, Fresnedo O, Fernandez-Ramos D, Gutierrez-de Juan V, Martin-Guerrero I, Garcia-Orad A, Luka Z, Wagner C, Lu S, Garcia-Monzon C, Finnell RH, Aurrekoetxea I, Buque X, Martinez-Chantar ML, Mato JM, and Aspichueta P. S-Adenosylmethionine increases circulating ver-low-density lipoprotein clearance in non-alcoholic fatty liver disease. *J Hepatol* 62: 673-681, 2015.

46. Masoodi M, Mir AA, Petasis NA, Serhan CN, and Nicolaou A. Simultaneous lipidomic analysis of three families of bioactive lipid mediators leukotrienes, resolvins, protectins, and related hydroxy-fatty acids by liquid chromatography/electrospray ionisation tandem mass spectrometry. *Rapid Commun Mass Spectrom* 22: 75-83, 2008.

47. McIntosh AL, Senthivinayagam S, Moon KC, Gupta S, Lwande JS, Murphy CC, Storey S, and Atshaves BP. Direct interaction of ADRP with lipids on the surface of lipid droplets: A live cell FRET analysis. *Am J Physiol Cell Physiol* 303: C728-742, 2012.

48. McIntosh AL, Atshaves BP, Hostetler HA, Huang H, Davis J, Lyuksyutova OI, Landrock D, Kier AB, and Schroeder F. Liver type fatty acid binding protein (L-FABP) gene ablation reduces nuclear ligand distribution and peroxisome proliferator-activated receptor alpha activity in cultured primary hepatocytes. *Arch Biochem Biophys* 485: 160-173, 2009.

49. McManaman JL, Bales ES, Orlicky DJ, Jackson MB, MacLean PS, Cain S, Crunk AE, Mansur A, Graham CE, Bowman TA, and Greenberg AS. Perilipin-2 null

mice are protected against diet-induced obesity, adipose inflammation and fatty liver disease. *J Lipid Res* 54: 1346-1359, 2013.

50. Melo RCN, and Weller PF. Lipid bodies in leukocytes: Organelles linked to inflammatory responses. *Exp Cell Res* 340: 2016.

51. Mohite A, Chillar A, So S, Cervantes V, and Ruan K. Novel mechanism of the vascular protector prostacyclin: Regulating microRNA expression. *Biochemistry* 50: 1691-1699, 2011.

52. Najt CP, S S, Aljazi M, Fader K, Olenic S, Brock J, Lydic TA, Jones AD, and Atshaves B. Liver-specific loss of Perilipin 2 alleviates diet-induced hepatic steatosis, inflammation, and fibrosis. *Am J Physiol Gastro Liver Physiol* 310: G726-G738, 2016.

53. Nazari-Jahantigh M, Wei Y, Noels H, Akhtar S, Zhou Z, Koenen RR, Heyll K, Gremse F, Keiessling F, Grommes J, Weber C, and Schober A. MicroRNA-155 promotes atherosclerosis by repressing Bcl6 in macrophages. *J Clin Invest* 122: 190-202, 2012.

54. Nazari-Jahantigh M, Wei Y, Noels H, Akhtar S, Zhou ZK, R R, Heyll K, Gremse F, Keiessling F, Grommes J, Weber C, and Schober A. MicroRNA-155 promotes atherosclerosis by repressing Bcl6 in macrophages. *J Clin Invest* 122: 190-202, 2012.

55. Niu Y, Mo D, Qin L, Wang C, Li A, Zhao X, Wang XB, Xiao S, Wang Q, Xie Y, He Z, Cong P, and Cheng Y. Lipopolysaccharide-induced miR-1224 negatively regulates tumour necrosis factor-a gene expression by modulating SP1. *Immunology* 133: 8-20, 2011.

56. Ohhira M, Motomura W, Fukuda M, Yoshizaki T, Takahashi N, Tanno S, Wakamiya N, Kohgo Y, Kumei S, and Okumura T. Lipopolysaccharide induces adipose differentiation-related protein expression and lipid accumulation in the liver through inhibition of fatty acid oxidation in mice. *J Gastroenterol* 42: 969-978, 2007.

57. Paul A, Chang B, Li L, Yechoor V, and Chan L. Deficiency of adipose differentiation-related protein impairs foam cell formation and protects against atherosclerosis. *Circ Res* 102: 1492-1501, 2008.

58. Pol A, Gross SP, and Parton RG. Review: biogenesis of the multifunctional lipid droplet: lipids, proteins, and sites. *J Cell Biol* 204: 635-646, 2014.

59. Pozniak PD, White MK, and Khalili K. TNF-a/NFkB signaling in the CNS: possible connection to EPHB2. *J Neuroimmune Pharmacol* 9: 133-141, 2014.

60. Qin N, Zhang SP, Reitz TL, Mei JM, and Flores CM. Cloning, expression, and functional characterization of human cyclooxygenase-1 splicing variants: evidence for intron 1 retention. *J Pharmacol Exp Ther* 315: 1298-1305, 2005.

61. Sabirzhanov B, Stoica BA, Zhao Z, Loane DJ, Wu J, Dorsey SG, and Faden AI. MiR-711 upregulation induces neuronal cell death after traumatic brain injury. *Cell Death Differ* 23: 654-668, 2015.

62. Senthivinayagam S, McIntosh AL, Moon KC, and Atshaves BP. Plin2 inhibitis cellular glucose uptake through interactions with SNAP23, a SNARE complex protein. *PLoS ONE* 8: e73696. doi: 73610.71371/journal.pone.0073696, 2013.

63. Shen X, Li J, Liao W, Wang J, Chen H, Yao Y, Liu H, and Ding K. microRNA-149 targets caspace-2 in glioma progression. *Oncotarget* In press: 2016.

64. Storey SM, McIntosh AL, Senthivinayagam S, Moon KC, and Atshaves BP. The phospholipid monolayer associated with perilipin-enriched lipid droplets is a highly organized rigid membrane structure. *Am J Physiol Endocrinol Metab* 301: E991-E1003. PMCID: PMC3213997, 2011.

65. Suram S, Brown GD, Ghosh M, Gordon S, Loper R, Taylor PR, Akira S, Uematsu S, Williams DL, and Leslie CC. Regulation of cytosolic phospholipase A2 activation and cyclooxygenase 2 expression in macrophages by the beta-glucan receptor. *J Biol Chem* 281: 5506-5514, 2006.

66. Tangirala RK, Jerome WG, Jones NL, Small DM, Johnson WJ, Glick JM, Mahlberg FH, and Rothblat GH. Formation of cholesterol monohydrate crystals in macrophage-derived foam cells. *J Lipid Res* 35: 93-104, 1994.

67. Thulin P, Wei T, Werngren O, Cheung L, Fisher RM, Grander D, Corcoran M, and Ehrenborg E. MicroRNA-9 regulates the expression of peroxisome proliferator-activated receptor d in human monocytes during inflammatory response. *Internatl J Mol Med* 31: 1001-1010, 2013.

68. Tranter M, Helsley R, Paulding W, McGuinness M, Brokamp C, Haar L, Liu Y, Ren X, and Jones W. Coordinated post-transcriptional regulation of Hsp70.3 gene expression by microRNA and alternative polyadenylation. *J Biol Chem* 286: 29828-29837, 2011.

69. Walther TC, and Farese R. Lipid droplets and cellular lipid metabolism. *Annu Rev Biochem* 81: 28.21-28.28, 2012.

70. Weibel GL, Joshi MR, Wei C, Bates SR, Blair IA, and Rothblat GH. Lipoxygenase-1 associates with neutral lipid droplets in macrophage foam cells: evidence of lipid droplet metabolism. *J Lipid Res* 50: 2371-2376, 2009.

71. White AL. Biogenesis of Lp (a) in transgenic mouse hepatocytes. *ClinGenet* 52: 326-337, 1997.

72. Whittaker R, Loy PA, Sisman E, Suyama E, Aza-Blanc P, Ingermanson RS, Price JH, and McDonough PM. Identification of microRNAs that control lipid droplet formation and growth in hepatocytes via high-content screening. *J Biomol Screen* 15: 798-805, 2010.

73. Willenborg M, Schmidt C, Braun P, Landgrebe J, von Figura K, Saftig P, and Eskelinen E-L. Mannose 6-phosphate receptors, Niemann-Pick C2 protein, and lysosomal cholesterol accumulation. *J Lipid Res* 46: 2559-2569, 2005.

74. Xiao J, Ly D, Zhao Y, Chen X, Song M, Liu J, Bei Y, Wang F, Yang W, and Yang C. miR-149 control non-alcoholic fatty liver by targeting FGF-21. *J Cell Mol Med* In press: 2016.

75. Xu G, Zhang Z, Xing Y, Wei J, Ge Z, Liu X, Zhang Y, and Huang X. MicroRNA-149 negatively regulates TLR-triggered inflammatory response in macrophages by targeting MyD88. *J Cell Biochem* 115: 919-927, 2014.

76. Ying W, Tseng A, Chang RC, Wang H, Lin Y-L, Kanameni S, Brehm T, Morin A, Jones B, Splawn T, Criscitiello M, Golding MC, Bazer FW, Safe S, and Zhou B. miR-150 regulates obesity-associated insulin resistance by controlling B cell functions. *Sci Rep* 6: 20178, 2016.

77. Yuan J, Wang K, and Xi M. MiR-494 inhibits epithelial ovarian cancer growth by targeting c-Myc. *Med Sci Monit* 22: 617-624, 2016.

78. Zhang L, Li X, Dong W, Sun C, Guo D, and Zhang L. Mmu-miR-1894-3p inhibits cell proliferation and migration of breast cancer cells by targeting Trim46. *In J Mol Sci* 22: E609, 2016.

CHAPTER 6:

CONCLUSIONS

OVERVIEW

The objective of this thesis was to establish the role lipid droplet protein Plin2 plays in inflammation and inflammation-based metabolic diseases. From our studies we found that Plin2 promotes COX-mediated inflammation through high-affinity interactions with pro-inflammatory lipids and direct interactions with COX2 (Chapter 3 and Chapter 5). Results reported in chapter 4 provide evidence that Plin2 hepatic ablation blunts the onset of hepatic steatosis, inflammation, and fibrosis through a PEMT-mediated mechanism. Plin2 ablation in mice also resulted in decreased inflammation markers COX2, TNFα, IL-1β, and IL-6 and reduced expression of ER stress proteins CHOP and caspase-1. In chapter 5 we show Plin2 ablation alters the miRNA-biome and mitigates COX1 and COX2 expression post-transcriptionally by altering the levels of miRNAs-1894 and -711. Key points from each chapter are highlighted in the sections below.

CHAPTER 3: STRUCTURAL AND FUNCTIONAL ASSESSMENT OF PERILIPIN 2 LIPID BINDING DOMAIN(S)

In chapter 3 we defined the structural regions of Plin2's lipid binding pocket. Major findings in this study indicate that the N-terminal PAT domain, shared by Plin1, Plin2, Plin3 and Plin5, does not bind cholesterol or stearic acid. In addition, Plin2 residues 119−251, containing helix α4, the α−β domain, and part of helix α6 form a Plin3-like cleft, critical for highest affinity lipid binding. Both stearic acid and cholesterol interact favorably with the Plin2 cleft formed by conserved residues in helix α6 and adjacent strands. We also demonstrate that Plin2 preferentially binds the pro-inflammatory lipid arachidonic acid with 2-fold higher affinity than DHA, a lipid known for its anti-inflammatory properties. Thus, the work outlined in Chapter 3 reveals specific domains

responsible for Plin2−lipid interactions that are involved in the protein's lipid binding and targeting functions. It is proposed that lipid binding in the binding pocket allows Plin2 to retain pro-inflammatory lipids on the lipid droplet surface.

CHAPTER 4: LIVER-SPECFICI LOSS OF PERILIPN 2 ALLEVIATES DIET-INDUCED HEPATIC STEATOSIS, INFLAMMATION, AND FIBROSIS

In previous work, global ablation of Plin2 was shown to alleviate dietary-induced hepatic steatosis and adipose inflammation; however its role in the progression of hepatic inflammation remained unknown. To investigate this further, we challenged a novel Plin2 liver-specific knockout mouse and respective wild type controls with a methionine-choline-deficient diet to induce a NASH phenotype of increased hepatic triglyceride levels through impaired phosphatidylcholine synthesis and VLDL secretion. Results detailed in Chapter 4 demonstrated that wild type and liver specific Plin2 knock out mice fed the MCD diet exhibited signs of hepatic steatosis, fibrosis, and inflammation; however Plin2 ablation blunted the effects. Levels of PC and VLDL were unchanged and hepatic steatosis was reduced in Plin2 null mice fed the MCD diet, due in part to an increase in remodeling of PE to PC via the enzyme PEMT. Plin2 knockout mice also exhibited decreased hepatic expression of pro-inflammatory markers including COX2, IL-6, TNFα, IL-1β and reduced expression of ER stress proteins such as CHOP and cleaved caspase-1. Results support a PEMT-mediated mechanism that involves compensatory changes in proteins involved in PC remodeling, inflammation, and ER stress that work to alleviate diet-induced NASH. Overall, these findings support a role for Plin2 as a target for NASH therapy. In the overall context of lipid droplet and Plin2 research, findings from chapter 4 also clarify the mechanism of reduced hepatic TG due to the absence of Plin2, (i.e., increased lipolysis that leads to increased β-oxidation).

CHAPTER 5: PERILIPIN 2 DRIVES COX-MEDIATED INFLAMMATION THROUGH REGULATION OF MICRORNAS-1894 AND -711

Chapter 5 provides evidence that Plin2 ablation affects the miRNA-biome. In Plin2 null livers, 6 miRNAs were significantly increased 3-fold or more. Two of these miRNAs (miRNAs -1894 and -711) were predicted to target genes associated with eicosanoid biosynthesis and inflammation. Luciferase reporter assays and Western blotting demonstrated that miRNAs-1894 and -711 directly target the 3'-UTR sites of COX1, COX2, and human PTGIS, respectively. LPS-induced inflammation decreased levels of miRNA-711 and significantly increased COX2. Conversely, levels of miRNA-1894 increased, negatively affecting the expression of COX1. Co-IP assays and FRET imaging showed that Plin2 sequestered COX2 to the lipid droplet surface, an effect that was increased when inflammation was present. Collectively, in this study we demonstrate that lipid droplets are the site of eicosanoid production which can lead to propagation of the inflammation response. Plin2 impacts this process by actively recruiting COX enzymes to the lipid droplet surface, altering their expression post-transcriptionally via miRNAs-1894 and -711.

FUTURE WORK

The work embodied in this dissertation presents a new model for hepatic lipid droplet protein Plin2 in the development and progression of lipid-based inflammation. While the results outlined in this dissertation characterize the underlying mechanisms of Plin2 in hepatic steatosis and inflammation, future work will be needed to full understand the process. Work will focus on elucidating the following three main points.

First, the steps outlining VLDL assembly in the absence of Plin2 need to be investigated. Specifically, what drives the steps between TG storage in Plin2 null lipid droplets and the creation of naïve VLDL particles should be explored. Little is known if the ablation of Plin2 creates smaller lipid droplets that are then targeted by VLDL assembly enzymes or if additional lipid droplet associated proteins are required to transform the lipid droplet into VLDL particles. In addition to VLDL assembly, the cross-talk between Plin2 ablated hepatic tissue and WAT containing Plin2 needs to be examined. It is proposed that the increased secretion of VLDL particles observed in Plin2 null mice fed the MCD diet contribute to the blunted fat mass loss, however without an examination of the tissue cross-talk, minimal conclusions can be drawn.

The second major area is the characterization of Plin2-COX2 interactions. It is unknown which domains are responsible for Plin2-COX2 interactions, and how removal of one or multiple domains will affect the complex. Moreover, recent evidence suggests Plin2 undergoes post-translational modification during lipolytic stimulation (*1, 2*). It is proposed that under inflammation conditions, a similar post-translation modification may be present that activates the protein to recruit and stabilize Plin2-COX2 interactions. This last point however, is speculative as this aspect of Plin2 mediated inflammation was not investigated in the present study.

Finally, the lipid droplet proteome of Plin2 null lipid droplets should be characterized. The absence of Plin2 has been associated with blunted inflammation and increased lipolysis, yet it is unknown which proteins are lost or are increased on the lipid droplet surface when Plin2 is absent. A characterization of the Plin2 null lipid droplet proteome

may provide valuable insights into the VLDL assembly in the absences of Plin2, and the anti-inflammatory nature of Plin2 ablation.

REFERENCES

REFERENCES

1. Kaushik, S., and Cuervo, A. (2015) Degradation of lipid droplet-associated proteins by chaperone-mediated autophagy facilitates lipolysis., *Nature Cell Biol 17*, 759-770.

2. Kaushik, S., and Cuervo, A. M. (2016) AMPK-dependent phosphorylation of lipid droplet protein PLIN2 triggers its degradation by CMA, *Autophagy 12*, 432-438.